Estudios Geol., 57: 175-273 (2001)

GEOLOGY AND VOLCANOLOGY OF LA PALMA AND EL HIERRO, WESTERN CANARIES

J. C. Carracedo[1], E. R. Badiola[2], H. Guillou[3], J. de la Nuez[4] and F. J. Pérez Torrado[5]

Dedicamos este trabajo a la memoria de José María Fúster Casas. El profesor Fúster dirigió en la década de los 60 del pasado siglo el primer estudio geológico moderno y detallado de las Islas Canarias, a las que dedicó, hasta su fallecimiento, la mayor parte de su investigación. Los autores de este artículo, que fuimos inicialmente sus alumnos y posteriormente sus colaboradores y amigos, intentamos seguir sus pasos y su ejemplo.

SUMMARY

The western Canaries, relatively little studied until a few years ago from the geological point of view, have however provided decisive data for understanding many of the most important geological problems of the Archipelago, which would probably have been dilucidated earlier, had the study begun with the most recent islands, as occurs in similar chains of oceanic volcanic islands in other parts of the world.

To summarize the main geological features and evolutionary characteristics of both islands we emphasize the following stages of development:

During the Pliocene, a submarine volcanic edifice or seamount formed in the island of La Palma, made up of pillow lavas, pillow breccias and hyaloclastites, intruded by trachytic domes, plugs of gabbros, and a highly dense dyke swarm. The intense magmatic and dyke intrusion uplifted the seamount up to 1,500 m, tilting it 45-50° to the SW. This intrusive phase was followed by a period of quiescence and erosion of the emerged submarine edifice. The definitive consolidation and progression of the construction of the island continued from at least 1.77 ma in angular and erosive discordance over the submarine basement. The subaerial volcanic reactivation, in which explosive volcanism predominated during the initial stages, producing abundant volcanoclastic and phreatomagmatic materials at the base of the subaerial edifice, persisted in a highly continuous manner until at least 0.41 ma. This initial subaerial stage shaped the northern volcanic shield, formed by the accumulation of several superimposed volcanoes, approximately concentric in relation to one another and the submarine basement.

The initial stage of the northern volcanic shield lasted between 1.77 and 1.20 ma, during which period the Garafía volcano was built to a height of 2,500-3,000 m, with steeply sloping flanks, formed predominantly by alkaline basalts with abundant pahoehoe lavas. The rapid growth and progressive instability of the Garafía volcano culminated some 1.20 ma ago in a gravitational landslide of the south flank of the volcanic edifice. The eruptive activity that followed the collapse built the Taburiente volcano, that rests upon a clear angular discordance caused by the landslide. The landslide depression was filled completely some 0.89 ma ago, as shown by the age of the first lavas to overflow the collapse embayment. The filling-in of the depression by the Taburiente volcano lavas finally formed a sequence of horizontal lavas, predominantly alkaline basalts, that ponded against the headwall of the landslide scarp forming a plateau in the centre of the volcanic shield.

[1] Estación Volcanológica de Canarias, IPNA-CSIC, Tenerife, Spain «jcarracedo@ipna.csic.es».
[2] Museo Nacional de Ciencias Naturales, CSIC, Madrid, Spain.
[3] Laboratoire des Sciences du Climat et de l'Environnement, CEA-CNRS, Gif-sur-Yvette, France.
[4] University of La Laguna, Tenerife, Spain.
[5] University of Las Palmas de Gran Canaria, Spain.

Coinciding approximately with the Matuyama-Brunhes boundary (0.78 ma) an important reorganisation of the Taburiente volcano took place, the dispersed emission centres of which progressively concentrated in three increasingly defined rifts (NW, NE and N-S) and subsequently in a central edifice situated at the geometrical centre of the volcanic shield. The abundant emissions of this final stage covered the earlier formations with sequences of lava flows up to 1,000 m thick in places, with the exception of a part of the alignments of cones of the rifts. The basaltic lavas evolved towards more differentiated phonolitic and trachytic terms at the terminal phases of construction of the volcano. One of these rifts, the southern or Cumbre Nueva rift, developed more than the others, possibly because the volcanism already began to migrate southwards, forming a N-S trending dorsal ridge over 2,500 m high. The progressive instability of the Cumbre Nueva rift, due to overgrowth, triggered the gravitational landslide of the western flank, in a process that took place about 560 ka ago, involving the detachment of some 180-200 km^3 and the formation of a wide depression (the Valle de Aridane) and the beginning of the formation, by incision and retrogressive erosion, of the Caldera de Taburiente.

The activity subsequent to the collapse in the northern shield was preferentially concentrated in the interior of the new collapse basin, quickly building the Bejenado stratovolcano. This activity was coetaneous with that of other residual centres dispersed over the flanks of the shield. The initially basanite lavas of Bejenado volcano evolved to mafic tephrites in differentiated lateral and terminal vents. The activity of the volcanic shield ceased definitively some 0.4 ma ago. After a transition period with a certain degree of activity associated with Bejenado late peripheral vents, volcanism was definitively located until the present in the new Cumbre Vieja volcano, at the south of the island. The oldest Cumbre Vieja lavas have been dated in 123 ka, although the first eruptions of the volcano may be considerably older. During this last stage of volcanism in La Palma a N-S trending rift has been formed, with predominantly basanitic, tephritic and tephri-phonolitic lavas, and intrusions of domes of tephri-phonolites and phonolites, frequently associated with eruptive vents. Numerous submarine eruptive vents, several of which are apparently very recent, have recently been observed and sampled at the prolongation of the Cumbre Vieja rift southwards in the ocean.

The foreseeable geological evolution of this rift is similar to that of its Cumbre Nueva predecessor, towards a progressive development and increasing instability, although changes may take place that may modify it towards more stable configurations, fundamentally the submarine progression of the southern tip of the rift, that could redistribute the volume of emitted materials, reduce the aspect ratio of the volcano and, consequently, its instability. The en echelon faults generated during the 1949 eruption have been interpreted as a possible detachment of the western flank of the volcano, although a more favourable hypothesis would be that such faults are surficial and contribute to accommodating the volcano by reducing its instability. A noteworthy aspect is the important role played by the mobility of the general feeding system of the volcanism in shaping the form and structure of the island. If the volcanism had not continually migrated southward since the final stages of construction of the northern shield, the island of La Palma would probably have taken on a similar configuration to that of the islands of El Hierro or Tenerife, in the shape of a triangular pyramid, with triple-armed rifts and landslide lobes between the rifts. The southward migration of volcanism in La Palma left the northern shield extinct, the rifts incomplete and finally configured an island lengthened in a N-S direction. Another point of interest is that the islands of La Palma and El Hierro are the first of the Canaries to form simultaneously, with possibly alternating eruptive activity, at least in the most recent period. This separation in a «dual line» of islands and the greater depth of its oceanic basement account for the long time they have required to emerge since the formation of the prior island of La Gomera.

The island of El Hierro is geologically somewhat younger than La Palma and, because it formed over a stationary source of magma, it presents, in comparison, a perfect, concentric development, with superimposed volcanoes and a regular three-armed rift geometry. The activity of the subaerial volcanism began in El Hierro with the development of Tiñor volcano on the NE flank of the island (approximately from 1.12 to 0.88 ma), with the emission of massive typical basalts. The volcano developed quickly, with different stages of growth, the eruption of Ventejís volcano being the terminal explosive stage, and probably the precursor of the collapse of the NW flank of the edifice some 882 ka ago. The emissions of the new volcano —El Golfo, approximately 545 to 176.000 ka— totally filled the depression of the lateral collapse of Tiñor volcano, the lava flows of which then spilled over the flanks of the earlier volcano. The beginning of the construction of the El Golfo volcano seems to have taken place after a relatively long

period of activity, probably coinciding with the maximum development of the Cumbre Nueva rift on La Palma. The initial subaerial activity at El Golfo was characterised by basaltic lavas that evolved to trachybasalts and trachytes, and finally towards more differentiated eruptive episodes indicative of the terminal state of the volcanic activity of the El Golfo volcano. The excessive growth of this volcano triggered the failure of its north flank, generating the spectacular scarp and present El Golfo depression. Subsequent volcanism, from emission vents arranged in a three-armed rift system (rift volcanism, with ages ranging from 145 ka to 2,500 years, with probably prehistoric eruptions), implies the much more moderate continuation of the earlier predominantly basanitic-tephritic volcanic activity. This period may correspond to that of maximum development of the Cumbre Vieja rift, in the island of La Palma.

RESUMEN

Las Canarias occidentales, relativamente poco estudiadas hasta hace unos años desde el punto de vista geológico, han aportado sin embargo datos decisivos para la comprensión de muchos de los problemas geológicos más importantes del archipiélago, que posiblemente se hubieran dilucidado más prontamente si su estudio se hubiese comenzado, como en la mayoría de las cadenas de islas volcánicas oceánicas, por su extremo más reciente.

Como resumen de sus principales rasgos geológicos evolutivos de ambas islas destacamos las siguientes etapas de desarrollo:

Durante el Plioceno se levanta en el extremo occidental del Archipiélago, en la isla de La Palma, un edificio o monte submarino constituido por pillow lavas, pillow brechas e hialoclastitas de composición basáltica, intruido por domos traquíticos, plutones de gabros y una densísima red de diques. Por el efecto de la intensa intrusión magmática y filoniana el edificio submarino sufrió un levantamiento hasta cotas de 1.500 m y basculamiento de 45-50° al SO, seguido de un período de quiescencia y erosión del edificio submarino emergido. La consolidación definitiva y progresión de la construcción de la isla se hace en discordancia angular y erosiva sobre el basamento submarino a partir de al menos unos 1,77 millones de años. La reactivación volcánica subaérea, con predominio de volcanismo explosivo en las fases iniciales con producción de abundantes materiales volcanoclásticos y freatomagmáticos en la base del edificio subaéreo, persistió de forma muy continua hasta al menos 0,41 millones de años. Esta fase subaérea inicial configura el Escudo Volcánico Norte, formado por la superposición de varios edificios volcánicos superpuestos y aproximadamente concéntricos entre sí y con el basamento submarino.

El Escudo Volcánico Norte tiene una primera etapa, desde 1,77 a 1,20 ma, en la que se construye el edificio volcánico Garafía, formado por lavas predominantemente basálticas alcalinas poco diferenciadas y abundancia de lavas «pahoe-hoe», que alcanza una altura de 2.500-3.000 m, con flancos de acusadas pendientes. El rápido crecimiento y progresiva inestabilidad del edificio Garafía culminó hace unos 1,20 millones de años en un deslizamiento gravitatorio del flanco meridional del edificio. La actividad eruptiva que siguió al colapso comienza rellenando la depresión de deslizamiento, levantando un nuevo edificio volcánico —el edificio volcánico Taburiente—, que se apoya sobre una clara discordancia angular producto del deslizamiento. La depresión se rellenó completamente hace unos 0,89 ma, edad de las primeras lavas en desbordarla. El relleno de la depresión por las lavas del Taburiente acaba conformando un apilamiento de coladas horizontales —predominantemente basaltos alcalinos— que se remansan contra la cabecera del escarpe de deslizamiento formando una meseta colgada en el centro del escudo volcánico. Coincidiendo aproximadamente con el límite Matuyama/Brunhes (0,78 ma) se produce una importante reorganización del edificio volcánico Taburiente, cuyos centros de emisión se concentran progresivamente en tres rifts (NO, NE y N-S) cada vez más definidos, y posteriormente en un aparato central situado en el centro geométrico del escudo volcánico. Las abundantes emisiones de esta etapa final recubren las formaciones anteriores, excepto parte de las alineaciones de conos de los rifts. Las lavas se diferencian hacia términos fonolíticos y traquíticos.

El rift meridional (Cumbre Nueva) se desarrolla más que los otros, posiblemente por el comienzo de la migración hacia el sur del volcanismo, formando una dorsal con más de 2.500 m de altura y con el eje mayor en dirección N-S. La progresiva inestabilidad del rift de Cumbre Nueva, por un crecimiento excesivo, provoca el deslizamiento gravitatorio del flanco occidental, proceso que ocurrió hace unos 560 ka y supuso el desgarro de unos 180-200 km^3 y la formación de una amplia depresión (el Valle de Aridane) y el inicio de la formación —por encajamiento y erosión remontante— de la Caldera de Tabu-

riente. La actividad posterior al colapso en el escudo norte se concentra preferentemente en el interior de la cuenca de deslizamiento, construyendo rápidamente el estratovolcán Bejenado. Esta actividad es coetánea con la de otros centros residuales y dispersos en los flancos del escudo. Las lavas inicialmente basaníticas del edificio Bejenado evolucionaron hacia tefritas máficas en centros laterales y terminales diferenciados. La actividad del escudo volcánico terminó definitivamente hace unos 0,4 millones de años. Tras un periodo de transición en que hay cierta actividad asociada a centros periféricos del Bejenado, el volcanismo se localiza de forma definitiva y hasta el presente en un nuevo edificio —Cumbre Vieja—, que prolonga la isla hacia el sur. Las lavas más antiguas han sido datadas en 123 Ka, aunque las primeras erupciones del edificio volcánico Cumbre Vieja deben ser bastante más antiguas. En esta última fase del volcanismo de La Palma se ha configurado un rift progresivamente estructurado en la dirección N-S, con lavas predominantemente basaníticas, tefritas y tefri-fonolitas, e intrusiones en forma de domos y coladas de tefri-fonolitas y fonolitas, asociados a episodios eruptivos que se continúan hasta la actualidad. Recientemente se han observado y muestreado numerosos centros eruptivos submarinos que prolongan el rift de Cumbre Vieja hacia el sur en el océano, algunos de éstos aparentemente muy recientes.

La previsible evolución geológica de este rift es similar a la de su antecesor de Cumbre Nueva, hacia un progresivo desarrollo y creciente inestabilidad, aunque pueden originarse cambios que la modifiquen hacia configuraciones más estables, fundamentalmente la progresión submarina del extremo sur del rift, que podría redistribuir el volumen de productos emitidos, rebajar la relación de aspecto del edificio volcánico y, en consecuencia, su inestabilidad. Las fallas escalonadas generadas en la erupción de 1949 han sido interpretadas como un posible desgarre del flanco occidental del edificio volcánico, aunque una hipótesis más favorable sería la de que tales fallas son superficiales y contribuyen a acomodar el edificio volcánico reduciendo su inestabilidad. Un aspecto a destacar es el importante papel que ha jugado la movilidad del sistema general de alimentación del volcanismo en la forma y estructura de la isla. De no haberse producido una emigración continua del volcanismo desde las fases finales de construcción del escudo norte, la isla de La Palma posiblemente hubiera adquirido una configuración similar a la de las islas de El Hierro o Tenerife, con forma de pirámide triangular, dorsales triples y lóbulos de deslizamiento entre las dorsales. La emigración del volcanismo hacia el sur en La Palma dejó el escudo norte extinguido, los rifts inacabados y configuró finalmente una isla alargada en dirección N-S. Otro interesante aspecto es que las islas de La Palma y El Hierro son las primeras de las Canarias que se están formando de forma simultánea, con una posible alternancia de la actividad eruptiva entre ambas islas, al menos en el período más reciente. Esta «doble» alineación de islas y la mayor profundidad de su asentamiento explican el largo tiempo que han necesitado para emerger desde la emersión de La Gomera, la anterior isla en formarse.

La Isla de El Hierro es geológicamente algo más joven que La Palma y, por haberse formado sobre una fuente magmática estacionaria, ofrece en comparación un perfecto desarrollo concéntrico, con edificios superpuestos y un sistema regular de dorsales triples. La actividad del volcanismo subaéreo se inicia en El Hierro con el desarrollo del edificio Tiñor en la zona NE de la isla desde aproximadamente 1,12 a 0,88 Ma, con emisión de típicos basaltos masivos poco diferenciados. El edificio se desarrolla rápidamente con diferentes estadios de crecimiento, siendo la erupción del centro eruptivo del Ventejís del estadio explosivo terminal, probablemente precursor del colapso del flanco NO del edificio volcánico hace unos 0,88 Ma. Las emisiones del nuevo edificio volcánico —El Golfo, aproximadamente 545 a 176 Ka— rellenan totalmente la depresión originada por el colapso lateral del edificio Tiñor, con coladas que acaban vertiendo por los flancos del edificio anterior. El comienzo de la construcción del edificio volcánico de El Golfo parece haberse producido tras un periodo relativamente largo de inactividad, probablemente coincidente con el máximo desarrollo del rift de Cumbre Nueva en la isla de La Palma. La actividad subaérea inicial de El Golfo se caracteriza por la emisión de lavas basálticas, que evolucionan hacia traquibasaltos y traquitas hacia la parte alta del edificio, y finalmente hacia episodios eruptivos más diferenciados e indicativos del estadio terminal de la actividad volcánica del edificio El Golfo. El excesivo crecimiento de este edificio volcánico provocó el deslizamiento de su flanco norte, generando el espectacular escarpe y depresión actual de El Golfo, proceso que tuvo lugar entre 21 y 133 Ka. El volcanismo posterior, a partir de centros agrupados formando un rift triple (volcanismo de Rift, con edades comprendidas entre los 145 Ka y 2.500 años, con probables erupciones prehistóricas), supone la continuación, mucho más moderada, de la actividad volcánica, predominantemente de basanitas y tefritas. Este periodo de menor actividad eruptiva relativa podría corresponderse con el máximo desarrollo del rift de Cumbre Vieja, en la isla de La Palma.

LA PALMA AND EL HIERRO IN THE GEOLOGICAL CONTEXT OF THE CANARIAN ARCHIPELAGO

Regional geological framework

La Palma and El Hierro, located at the western edge of the 450-km-long Canarian archipelago, are the last islands to form and the most active in the Quaternary.

The Canaries rest on old (Jurassic) oceanic lithosphere, La Palma and El Hierro lying along the magnetic anomaly M25 (about 156 ma, according to Klitgord and Schouten, 1986). Each island forms an independent edifice, except Fuerteventura and Lanzarote (Fig. 1 B and C). These edifices developed on increasingly deep ocean floor, reaching a maximum of -4 km in La Palma and El Hierro (Fig. 1 A). Their relative topographic heights and submarine/subaerial volume ratios reflect their stage of development. The island of Tenerife is clearly at its peak of volcanic growth, whereas La Palma and El Hierro are still in the juvenile stage of development, while La Gomera and the eastern islands of Gran Canaria and Fuerteventura–Lanzarote are already deeply eroded (Fig. 1).

The magmatic processes that generated the Canaries are related to a hotspot either spreading westward beneath the lithosphere or fixed under a plate slowly progressing eastward (Carracedo, 1979, 1999; Hoernle and Schmincke, 1993; Carracedo et al., 1998). According to some authors, the Canarian hotspot would be a part of a superplume responsible for the volcanism extending from the Cape Verde islands to eastern Europe (Hoernle et al., 1995; Oyarzun et al., 1997).

Geldmacher et al. (2001) dated the Madeira and Selvagem Islands and modelled three parallel hotspot pathways in the eastern North Atlantic, the Madeira, Canaries and Sahara tracks. The Canarian hotspot track extended from the Lars Seamount, to the north, to the island of El Hierro, in about 70 ma. Any relationship of the Canaries with the Atlas tectonics seems, therefore, out of place, since these tracks are parallel and congruent with the rotation of the African plate defined by Morgan (1983). Only the Canaries are located in the prolongation of the Atlas system, which may merely represent a geographical coincidence.

Radiometric dating of the oldest subaerial volcanism (Guillou et al., 1996, 1998, and 2001) and new ages from La Gomera and Tenerife (work in progress) show that the islands have developed in agreement with the continuous westward progression expected from the hotspot activity. La Palma and El Hierro are the only islands of the archipelago at present in the juvenile shield stage and the remainder of the Canaries are already in the posterosional stage (Fig. 2).

An important change occurred after the formation of La Gomera, apparently splitting the E-W trending, single line, Canarian volcanic belt into a N-S trending dual line, perpendicular to the general trend of the archipelago (see Fig. 3). Large-scale distribution and age progression in most oceanic island chains are well explained by the steady movement of lithospheric plates over fixed mantle plumes, yielding chains of consecutive discrete volcanoes. In this model, a new island starts to form when the bulk of the previous one has already developed, the inter-island distance governed by lithospheric thickness and rigidity (Voght, 1974; ten Brink, 1991). In the Canaries, however, the western islands have developed contemporaneously (Fig. 3). This important change in style may also account for the time interval of about 7-8 ma between the emergence of La Gomera and the western Canaries. This is considerably longer than the time gap between the formation of the single-line islands, decreasing from about 5 ma between Fuerteventura and Gran Canaria, to <3 ma between Tenerife and La Gomera (Figs. 2 and 3).

Dual-line volcanoes, such as the Kea and Loa trends in the Hawaiian Islands, have been associated with changes in plate motion, resulting in the location of a volcanic load off the hotspot axis. In this model of Hieronymus and Bercovici (1999) compressive stresses related to the off-axis volcano block the formation of the next island and split the single line of volcanoes into a dual line of alternating positions of volcanoes. However, the association of the dual line in the Canarian chain with a change in direction of the African plate is not clear (Carracedo et al., 1998; Carracedo, 1999).

This feature may finally explain the distribution of recent (Quaternary) volcanism in the western Canaries. Extensive radiometric dating and magnetic stratigraphy indicate that main phases of eruptive activity alternate in both islands, at least in the last 500 ka, as discussed later (see section III.1 and Fig. 72). This feature may be related to changes in the regional stress fields associated with giant gravitational collapses of the unstable volcanoes at their peak of development. This may also account for the lack of historical eruptions (last 500 years) in El Hierro while most of the historical volcanism of the Canarian archipelago has been located in La Palma.

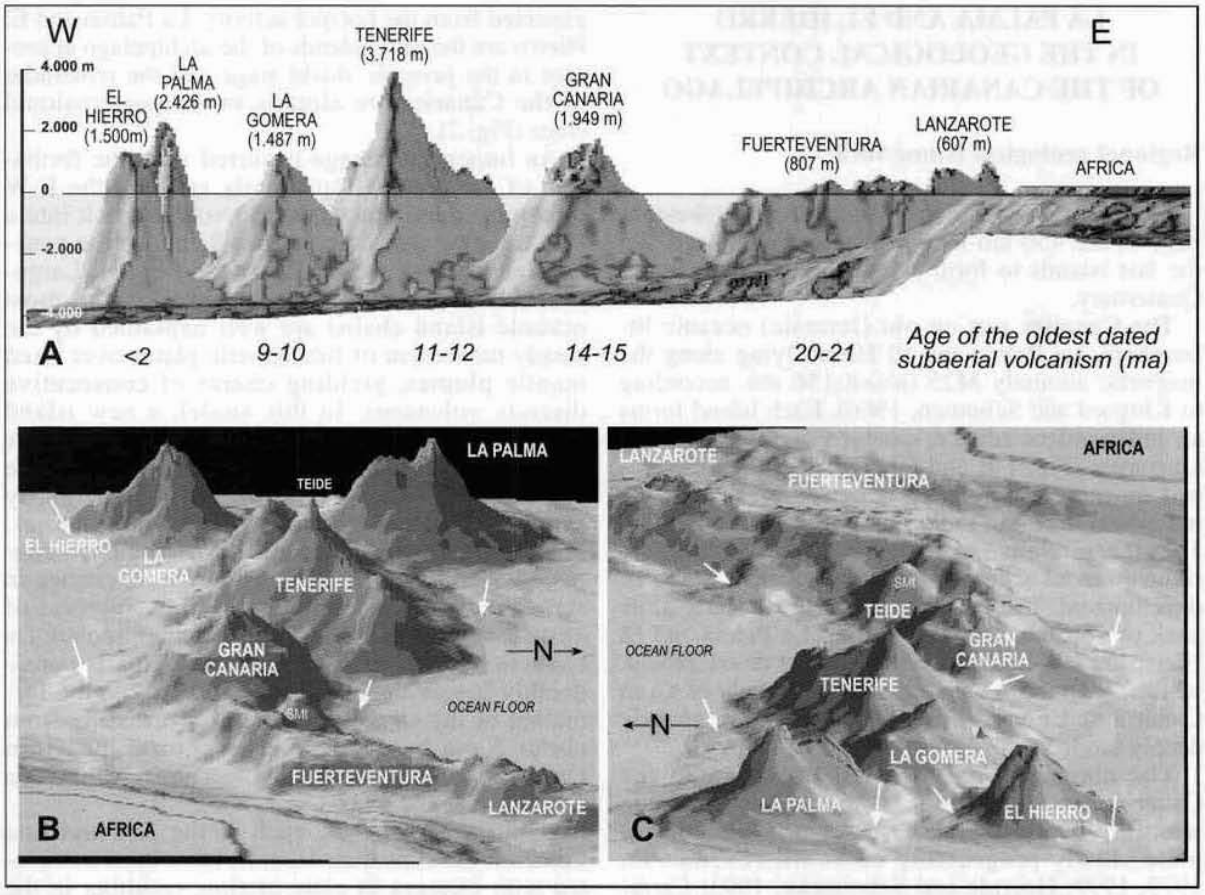

Fig. 1.—Computer-generated 3-D images of the Canary Islands (bathymetry from Hunter et al., 1983) A) Cross section showing age vs. height of the different islands. B) Views from the E and W of the archipelago. The progressive decrease in volume of the island towards the continent due to mass wasting is clearly observed, as well as the change from single to dual line after La Gomera.

Development of concepts of the geological history of the western Canaries

Fúster and coworkers (1968 a-d) initiated the first modern and comprehensive geological study of the Canaries in the island of Lanzarote. This apparently irrelevant fact may have imposed important difficulties on understanding key geological features of the Canary Islands. The volcanostratigraphic units defined in the eastern, posterosional islands, proved unfeasible in the western Canaries. The definition of 'Old' and 'Recent' Series led to considerable confusion, since the 'Old' Series of La Palma or El Hierro were found to be considerably younger than the 'Recent' Series of Fuerteventura, Lanzarote or Gran Canaria. This circumstance may explain why the knowledge of the geology of the western Canaries was at best scant until a few years ago, lacking even a basic geological map. Concurrently, the insufficient geological knowledge of the juvenile islands hindered the earlier understanding of the role of rift zones, gravitational collapses, etc., as key features in the evolution of the Canaries and oceanic islands in general, as well as the definition of volcanostratigraphic units applicable to the entire archipelago. Furthermore, this approach accounted for the difficulties in defining a model for the genesis and evolution of the Canary Islands that would most probably have been avoided, had the study of the Canaries started, as in the Hawaiian Islands, in the youngest part of the volcanic belt. The persistence of concepts such as the connection of the Canarian magmatism to fractures associated with the Atlas tectonics, or the apparently contrasting structural features in the eastern and western Canaries, would probably have been identified much earlier as lacking geological support or reflecting the different stages of evolution of the islands (Carracedo et al., 1998; Carracedo, 1999).

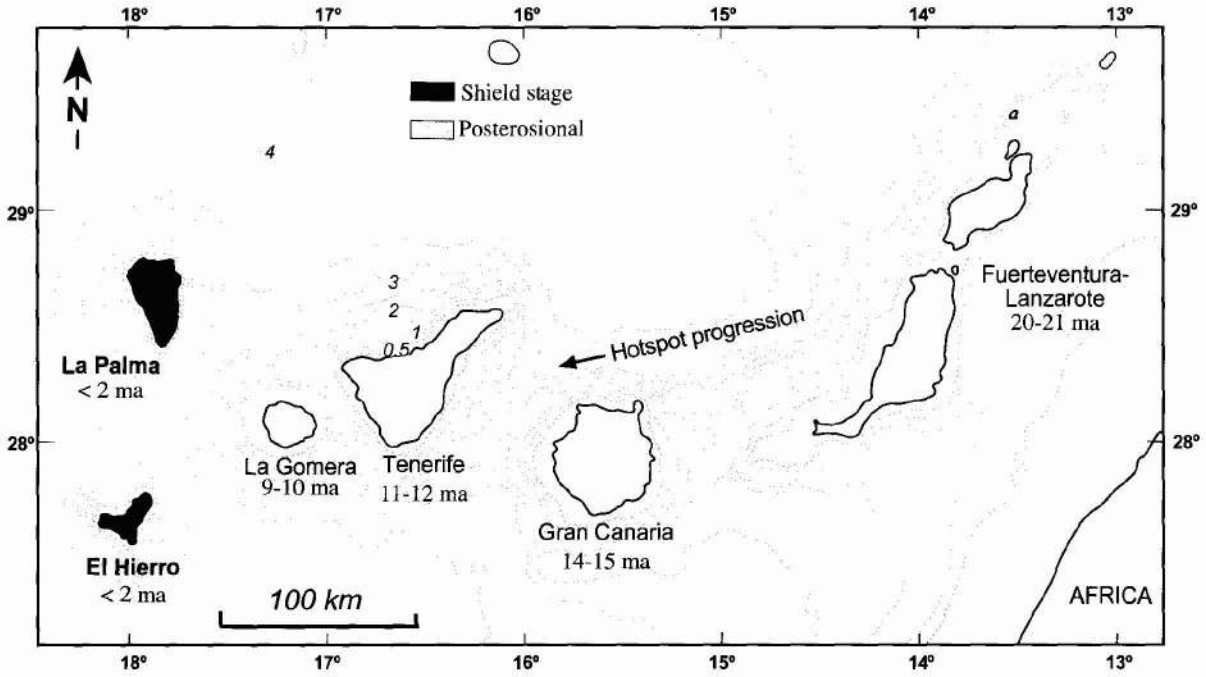

Fig. 2.—Revised oldest ages obtained for the emerged volcanism (work in progress). One of the main inconsistencies of the Canarian hotspot model disappears as the island of Tenerife and La Gomera fit in the general age progression scheme (new ages of Tenerife and La Gomera in work in progress). Note the extended period of time elapsed between the emergence of La Gomera and La Palma-El Hierro dual-line islands.

Several important concepts have been revised following the work carried out in the western Canaries. The structure and composition of the submarine part of the islands was poorly understood prior to the study carried out in La Palma by Staudigel (1981) and Staudigel and Schmincke (1984). In the islands of Fuerteventura, La Gomera and La Palma, the products of shield volcanism rest upon variably deformed and uplifted sequences of submarine sediments, volcanic rocks, dyke swarms and plutonic intrusions which form the cores of these islands. These formations, named 'Basal Complex' by Bravo in 1964, are consistently separated from the subaerial volcanism by a major unconformity. Early interpretations relating these formations to uplifted blocks of 'oceanic basement' in the pre-plate tectonic sense (Hausen, 1958; Fúster et al., 1968 a, b) proved to be inconsistent since the igneous rocks are younger than the oceanic sedimentary sequences (Robertson and Stillman, 1979 a, b). The studies by Staudigel (1981) and Staudigel and Schmincke (1984) demonstrated that the majority of the formations of the 'basal complexes' represent the seamount stage of the growth of these islands. Similar conclusions had been reached for the 'basal complex' of Fuerteventura (Stillman, 1987). Detailed geological mapping inside the Caldera de Taburiente (Carracedo et al., 2001 a, b) showed that several formations previously included in the 'basal complex' of La Palma could be assigned to younger subaerial stratigraphic units. When these units were excluded, the remaining formations conformed to the seamount described by Staudigel (1981) and Staudigel and Schmincke (1984), making the use of the term 'basal complex' unnecessary and confusing, except probably in the island of Fuerteventura, where this formation includes uplifted oceanic sediments.

Caldera-type depressions in the Canaries were incorrectly believed to be originated by erosive, collapse or explosive processes (Fúster et al., 1968 d; Araña, 1971). Some authors had tentatively related these depressions to slumps or gravitational collapses (Hausen, 1956, 1961; Bravo, 1962; Machado, 1963; Navarro and Coello, 1989; Holcomb and Searle, 1991). On-shore and off-shore studies in the western Canaries provided clear evidence that many of these features were initiated by gravitational flank failures of steep, unstable volcanoes, including the prototypical erosion Caldera de Taburiente (Machado, 1963; Ancochea et al., 1994; Carracedo, 1994; Masson, 1996; Urgeles et al.,

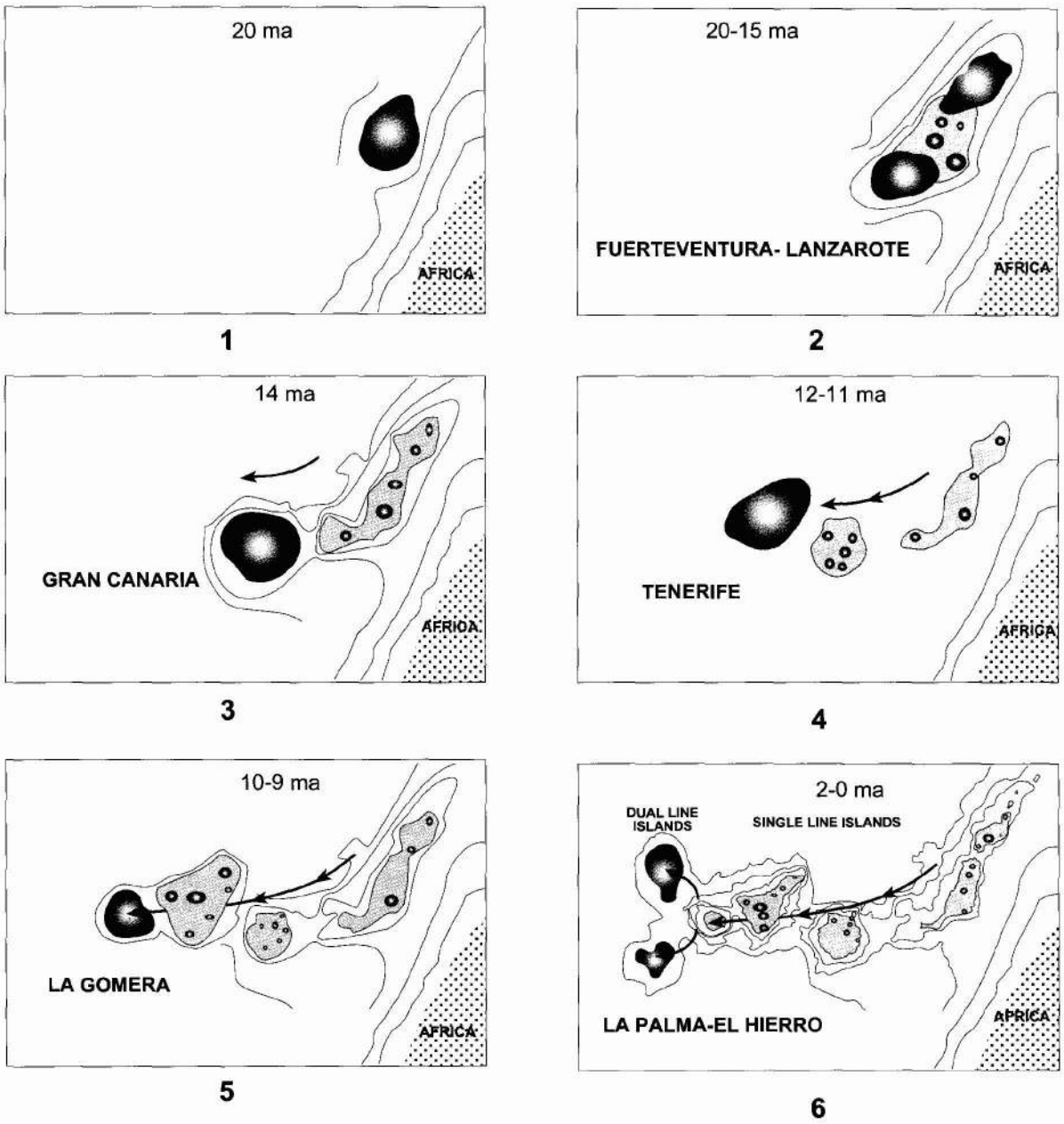

Fig. 3.—Sequential surfacing of the Canary Islands. New ages of Tenerife and La Gomera (work in progress).

1997, 1999; Carracedo et al., 1999 a, b; Masson et al., 2002).

The geological and geochronological study of the western Canaries evidenced the advantages of using the volcano-stratigraphic units defined in the Hawaiian Islands (MacDonald and Abbot, 1970; Walker 1990): the *shield stage* and the *posterosional or rejuvenated stage*. These units were applied to the Canaries (Carracedo et al., 1998; Carracedo, 1999) instead of volcanic series or cycles (Fúster et al., 1968 a-d; Schmincke, 1982). The studies carried out in the western Canaries and in the Madeira and Selvagem islands greatly contributed to show the Canaries not as a singular volcanic archipelago related to the Atlas tectonics, but as a part of the numerous hotspot island chains in the eastern North

Atlantic, strikingly similar to the Hawaiian group and, in general, to oceanic volcanic islands (Carracedo, 1979, 1999 a; Carracedo et al., 1998; Geldmacher et al., 2001). However, the Canaries preserve important peculiarities, such as the lack of significant subsidence (Schmincke et al., 1997; Carracedo et al., 1998; Carracedo, 1999 a) and other features summarized by Schmincke (1994).

GEOLOGY AND VOLCANOLOGY OF THE ISLAND OF LA PALMA

Geomorphological features

The island of La Palma is the fifth in extension (706 km^2) of the Canaries and the second in elevation (2.423 m asl), after Tenerife. The island is elongated in a N-S trend and is made up of two main polygenetic stratovolcanoes separated by a saddle (the Valle de Aridane depression): the conical northern shield and the elongated Cumbre Vieja volcano at the southern part of the island (Fig. 4). Both volcanoes reach considerable heights (2.430 and 1.990 m asl, respectively).

Rainfall is relatively high (up to 900 mm in the summit areas) because of the altitude and the island's location within the Atlantic. High erosion rates have originated deep, Oahu-type barrancos in the northern shield, whereas the younger Cumbre Vieja volcano is barely incised. Perched ice sheets seem to have formed on the summit of the northern shield, particularly during glaciations, accounting for the periglacial features observed. Rainfall is, however, much lower than in most tropical oceanic islands (Hawaii, Réunion, etc.). Consequently, the island is less vegetated and rock outcrops are abundant and fresh. The demand for water by farming prompted the perforation of several hundred kilometres of horizontal wells or *galerías* to mine groundwater, providing a unique mode of access to the deep structure of the island volcanoes.

Steep slopes are frequent in the island, being mainly structural in the flanks of the Cumbre Vieja volcano, and structural and erosive in the northern shield. The main depressions of the island, the Valle de Aridane and the Caldera de Taburiente, the latter formerly considered to be the prototypical erosion caldera after Lyell's report in 1864, were initiated by gravitational landslides (Machado, 1963; Ancochea et al., 1994; Carracedo, 1994; Carracedo et al., 1999 a, b).

High coastal cliffs are frequent in the northern shield, where rockfalls favour the rapid regression of the coastline. Conversely, the cliffs of the Cumbre Vieja volcano are lower and the verticality frequently smoothed by lava flows and coastal platforms that fossilize the cliffs and retard the progression of coastal erosion. Beaches are sparse and made up of basaltic blocks, pebbles and sand. Beachrocks have formed and are in progress in several beaches of the western coast of the Cumbre Vieja volcano (Calvet et al., in press).

Swath bathymetry coverage around La Palma (Masson et al., 2002) shows important features related to the constructional and destructive events of the submarine part of the island. The shaded relief images obtained by these authors (Fig. 5) clearly outline the debris avalanche deposits originated in gravitational slope failures (DAD in Fig. 5) and the submarine extension of the main rift zones (SSR in Fig. 5).

Age of volcanism

About 118 radiometric ages (K/Ar, ^{40}Ar-^{39}Ar and ^{14}C) of volcanics of La Palma have been published since the first ages obtained by Abdel Monem and co-workers in 1972. However, the increase in the number of ages can hinder rather than contribute to the precise reconstruction of the geochronology and volcanic history of the islands, because of the absence in some cases of stringent controls in the selection of rock samples and inter-laboratory cross-checking. Contrarily to geochemical analyses, dating methods lack precise controls of the accuracy and reliability of the results (ages). Argon loss or excess in rock samples can result in erroneous ages that nevertheless are usually published and generally accepted. As the number of ages increases the errors also increase and, if all the ages are equally considered, the stages of volcanic history of the islands tend to be artificially enlarged and confusing, as illustrated in Fig. 6.

The precision of these ages has been greatly improved by: 1) using both K/Ar and ^{40}Ar-^{39}Ar methods, 2) using replicate age determinations, 3) collecting samples in stratigraphic sequences, 4) separating out microcrystalline groundmass for K and Ar analysis, 5) using an unspiked K-Ar technique (Cassignol et al., 1978) to determine the isotopic composition of Ar and Ar content with a precision of 0.4% (± 2s), 6) cross-correlating the ages and their polarities with the magnetostratigraphy defined by field and laboratory measurements and with the established geomagnetic and astronomic polarity time scales (GPTS and APTS) (Carracedo, 1975; Carracedo and Soler, 1995; Guillou et al., 1996, 1998, 2001).

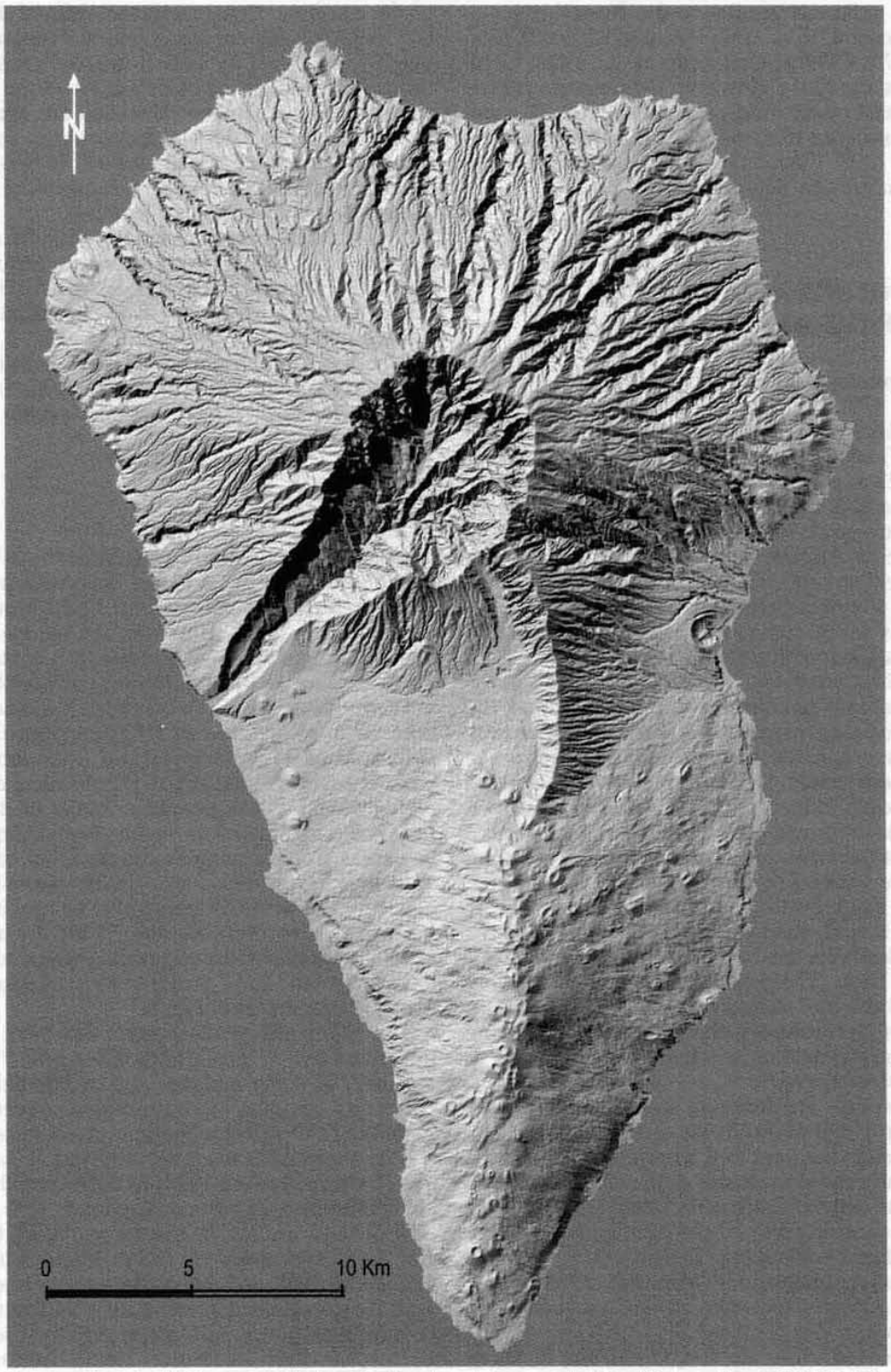

Fig. 4.—Shaded relief image of La Palma showing the main geomorphological features (image GRAFCAN).

The island of La Palma is probably a prime scenario to study the duration of each volcanic stage of an oceanic volcano and to check the consistency of the radiometric ages obtained. The rapid and continued growth of the island and the homogeneity of the volcanic formations make the combination of geological mapping, magnetostratigraphy and radiometric dating extremely useful to individualize each unit stratigraphically and temporally. This provides a framework for further control of the reliability of the ages and to cross-examine the results obtained by the different methods. Preliminary works in La Palma by Abdel Monem et al. (1972), Staudigel et al. (1986) and Ancochea et al. (1994) established an age interval from about 2 ma to present for the volcanic activity of La Palma (B, C and D in Fig. 6). Another 85 unspiked K/Ar and ^{40}Ar-^{39}Ar ages from La Palma (Fig. 7 and Table 1) have been published by Guillou and co-workers (1998, 2001) and Carracedo and co-workers (2001 a, b). Moreover, some of these flows recorded reversals of the earth's magnetic field and/or magnetic events (Abdel-Monem et al., 1972; Carracedo, 1979; Quidelleur and Valet, 1994; Guillou et al., 1998, 2001; Carracedo et al., 2001 a, b; Singer et al., 2002). Nevertheless, only recently has an extensive comparison been attempted between the radiometric ages and the geomagnetic and astronomical polarity time scales (GPTS and APTS) in order to test the geological significance of the published K-Ar ages for the western Canaries (Guillou et al., 2001; Carracedo et al., 2001 a, b).

Detailed geological and palaeomagnetic polarity mapping of the islands of Tenerife, La Palma and El Hierro allowed the sampling of rocks for dating after defining their relative stratigraphic position and geomagnetic polarity (Carracedo, 1979; Guillou et al., 1996, 2001; Carracedo et al., 2001 a, b). In La Palma, two dating techniques from different laboratories, the unspiked K-Ar (Guillou et al., 1996) and ^{40}Ar-^{39}Ar (Guillou et al., 2001) methods, were combined to ensure the overall geological significance of the ages. Samples of the same volcanic units were dated using both techniques for comparison purposes. The magnetic polarity of each unit was established on the field using a portable magnetometer (fluxgate) and confirmed by laboratory measurements. Radiometric ages were confronted to polarity ages and, when possible, dated samples were collected within well-established stratigraphic sections in lava sequences, and at the lower and upper limits of the main volcanic sequences and geomagnetic polarity units. The results of this restrictive multidisciplinary approach for dating the island of La Palma are shown in Figs. 7 and 8 and Table 1. These ages show that two separate volcanoes, corresponding to the northern shield and the Cumbre Vieja volcano, form the subaerial part of the island. The apparent gap separating the development of these volcanoes (see Figs. 6 and 8) may correspond either to a period of volcanic quiescence, or to incomplete sampling of the earlier, inaccessible sequences of the initial stages of Cumbre Vieja volcano.

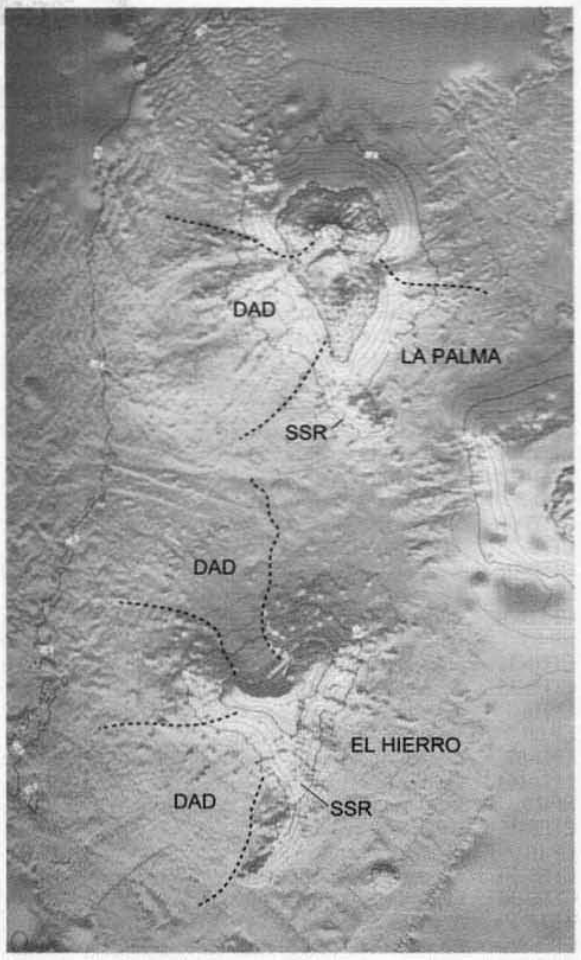

Fig. 5.—Shaded relief image of La Palma and El Hierro with indication of the main features of the submarine flanks: submarine rifts (SSR in the figure) and debris avalanche deposits from gravitational flank collapses (DAD). Images from Masson et al., 2002.

Several features of Fig. 6 are worthy of analysis. Since the ages reported by the different groups are taken from the same volcanic formations they should be consistent within some error margin. However, as indicated in Fig. 6, there is a clear disparity in the ages and duration of the Cumbre Vieja and Bejenado volcanoes. New (25) radiometric ages

Table 1.—**Location, type of rock, geomagnetic polarity and age of volcanics from La Palma (Ages from Guillou et al., 1998, 2001)**

Sample	Locality	Type of rock	UTM	Pol	Method	Age mean value
CILP 62	Galería Cuevitas, 2,600 m	Basalt	2245/31906	R	K/Ar	1.72 ± 0.02 ma
LPD-159	Galería Los Hombres, 1,500 m	Basalt	2197/31882	R	$^{40}Ar/^{39}Ar$	1.65 ± 0.08 ma
LPD-155	Galería Los Hombres, 2,100 m	Basalt	2197/31882	R	$^{40}Ar/^{39}Ar$	1.61 ± 0.12 ma
LPD-119	Bco. El Agua, 1,365 m	Basalt	2235/31856	R	$^{40}Ar/^{39}Ar$	1.52 ± 0.10 ma
CITB-21	Bco. Las Grajas, 1,630 m	Basalt	2165/31865	R	K/Ar	1.49 ± 0.22 ma
CITB -06	Bco. Gallegos, 455 m	Basalt	2236/31907	R	K/Ar	1.44 ± 0.02 ma
CITB -05	Bco. El Agua, 485 m	Basalt	2262/31879	R	K/Ar	1.44 ± 0.03 ma
LPD-118	Bco. El Agua, 1,465 m	Basalt	2235/31854	R	$^{40}Ar/^{39}Ar$	1.38 ± 0.14 ma
CITB-22	Bco. Franceses, 415 m	Basalt	2222/31910	R	K/Ar	1.37 ± 0.02 ma
CILP-63	Galería Cuevitas, 1,600 m	Basalt	2245/31906	N	K/Ar	1.27 ± 0.01 ma
LPD-376	Bco. Los Hombres, 115 m	Basalt	2195/31923	R	$^{40}Ar/^{39}Ar$	1.23 ± 0.09 ma
CITB-19	Bco. Gallegos, 470 m	Basalt	2238/31909	R	K/Ar	1.20 ± 0.02 ma
LPD-372	Bco. Jieque, 1,400 m	Basalt	2146/31809	N	$^{40}Ar/^{39}Ar$	1.20 ± 0.05 ma
LPD-160	Galería Los Hombres, 1,400 m	Basalt	2197/31882	N	$^{40}Ar/^{39}Ar$	1.12 ± 0.20 ma
LPD-100	Tamagantera trail, 2,160 m	Basalt	2204/31854	LI	$^{40}Ar/^{39}Ar$	1.08 ± 0.04 ma
LPD-106	Tamagantera trail, 1,920 m	Basalt	2204/31859	N	$^{40}Ar/^{39}Ar$	1.02 ± 0.08 ma
LPD-366	La Cumbrecita, 1,400 m	Basalt	2213/31781	N	$^{40}Ar/^{39}Ar$	1.02 ± 0.04 ma
CITB-09	Bco. de Los Hombres, 245 m	Basalt	2201/31925	N	K/Ar	948 ± 14 ka
CITB-23	Bco. Franceses, road east of barranco, 440 m	Basalt	2219/31912	R	K/Ar	936 ± 14 ka
CITB-08	Bco. de Los Hombres, 15 m	Basalt	2207/31931	R	K/Ar	932 ± 14 ka
LPD-93	Lomo del Caballo, 1,860 m	Basalt	2220/31877	R	$^{40}Ar/^{39}Ar$	890 ± 160 ka
CI TB-38	Bco. Gallegos, road east of barranco, 515 m	Basalt	2238/31908	R	K/Ar	886 ± 14 ka
LP-05	Bco. Las Angustias, 45 m	Basalt	2126/31735	R	K/Ar	853 ± 10 ka
CITB-31	Hacienda del Cura, 1,080 m	Basalt	2160/31793	R	K/Ar	836 ± 14 ka
CITB-35	Barranco de Los Hombres, 60 m	Basalt	2196/31927	R	K/Ar	833 ± 14 ka
LP-18	Road to Los Llanos-Sta. Cruz, Km 18.5	Basalt	2232/31721	R	K/Ar	834 ± 12 ka
LP 06	Bco. Las Angustias, 445 m	Basalt	2127/31776	R	K/Ar	833 ± 11 ka
LPD-87	Bco. El Agua, trail to Marcos-Cordero, 360 m	Basalt	2248/31851	N	$^{40}Ar/^{39}Ar$	770 ± 90 ka
LPD-164	Galería Los Hombres, 675 m	Basalt	2197/31882	N	$^{40}Ar/^{39}Ar$	770 ± 40 ka
LP-19	Road to Los Llanos-Sta. Cruz, Km 18.3	Basalt	2233/31722	N	K/Ar	770 ± 11 ka
CITB-15	Bco. Seco, 270 m	Basalt	2309/31805	N	K/Ar	737 ± 12 ka
LP-07	El Time, 465 m	Basalt	2127/31747	N	K/Ar	734 ± 8 ka
CITB-36	Road to La Fajana Los Hombres, 280 m	Basalt	2202/31992	R	K/Ar	731 ± 11 ka
CITB-30	La Cumbrecita, dyke, 1,395 m	Basalt	2213/31781	LI	K/Ar	726 ± 12 ka
BEJ-02	Borehole S-01 315 m	Basalt	2168/31738	N	K/Ar	710 ± 11 ka
CITB-20	Bco. del Cedro, 1,850 m (sobre discordancia)	Basalt	2179/31861	N	K/Ar	681 ± 10 ka
CITB-32	Barranco Jieque, 1,460 m	Basalt	2151/31812	N	K/Ar	660 ± 11 ka
LP-22	Camino Ermita La Peña, 1,247 m	Basalt	2233/31745	N	K/Ar	659 ± 11 ka
LP-21	Camino Ermita La Peña, 1,310 m	Basalt	2234/31745	N	K/Ar	647 ± 10 ka
LP-20	Camino Ermita La Peña, 1,370 m	Basalt	2236/31746	N	K/Ar	621 ± 9 ka
CITB-39	Bco. Franceses, road east of barranco, 470 m	Basalt	2219/31913	N	K/Ar	620 ± 9 ka
LPD-91	Lava from Mña. de La Yedra	Basalt	2197/31735	N	$^{40}Ar/^{39}Ar$	590 ± 40 ka
CITB-27	Road El Roque to the coast, 635 m	Basalt	2085/31846	N	K/Ar	585 ± 10 ka
LPD-91B	Lava from Mña. de La Yedra	Tephrite	2197/31735	N	$^{40}Ar/^{39}Ar$	580 ± 30 ka
CITB-37	Road to La Fajana de Los Hombres, 330 m	Basalt	2202/31926	N	K/Ar	575 ± 9 ka
CITB-07	Bco. Gallegos, 520 m	Basalt	2238/31913	N	K/Ar	567 ± 8 ka
LP-04	Ermita de La Peña trail, 1,400 m	Basalt	2238/31744	N	K/Ar	566 ± 8 ka
CITB-03	Punta Gorda harbour cliff, 125 m	Basalt	2066/31847	N	K/Ar	563 ± 8 ka
CITB-28	Bco. del Roque, 560 m	Basalt	2089/31841	N	K/Ar	560 ± 9 ka
CITB-12	Coast of Puntallana (Pta. Salinas), 90 m	Basalt	2334/31822	N	K/Ar	560 ± 8 ka
CITB-17	Coast of La Fajana de Barlovento, 0 m	Basalt	2276/31938	N	K/Ar	549 ± 8 ka
BEJ-01B	Lava from Bejenado, borehole S-01, 73 m	Basalt	2168/31738	N	K/Ar	549 ± 12 ka
BEJ-01	Lava from Bejenado, borehole S-01, 73 m	Basalt	2168/31738	N	K/Ar	537 ± 8 ka
CITB-11	Bco. El Jurado, 500 m	Basalt	2116/31789	N	K/Ar	533 ± 8 ka
CITB-01	Lava Mña. Negra, Pta. Gutiérrez, 360 m	Basalt	2085/31884	N	K/Ar	531 ± 9 ka
LPD-165	Galería Los Hombres, 220 m	Basalt	2197/31882	N	$^{40}Ar/^{39}Ar$	530 ± 70 ka
MLP-358	Morro Pinos Gachos (western rim of the Caldera)	Phonolite	2166/31817	N	K/Ar	525 ± 8 ka
CITB-24	Coast of Juan Adalid, 250 m	Basalt	2168/31942	N	K/Ar	507 ± 8 ka
MLP-419	Piedra Llana (NE. Caldera)	Phonolite	2229/31828	N	K/Ar	499 ± 7 ka
LPD-137	Top of Bejenado, 1,580 m	Basalt	2206/31773	N	$^{40}Ar/^{39}Ar$	490 ± 60 ka

Table 1.—**Location, type of rock, geomagnetic polarity and age of volcanics from La Palma (Ages from Guillou et al., 1998, 2001)** *(continued)*

Sample	Locality	Type of rock	UTM	Pol	Method	Age mean value
CITB-33	Tamagantera, trail 2,210 m	Basalt	2206/31853	N	K/Ar	440 ± 8 ka
LPD-42	Cliff of Playa de La Veta, 250 m	Basalt	2092/31843	N	$^{40}Ar/^{39}Ar$	410 ± 80 ka
LP 10	Cliff of Playa Nueva	Basalt	2161/31683	N	K/Ar	123 ± 3 ka
LP 12	Cliff of Puerto Naos	Basalt	2158/31658	N	K/Ar	121 ± 2 ka
LP 183	Cliff of Puerto Tazacorte	Basalt	2124/31723	N	K/Ar	120 ± 3 ka
LP 11	Cliff of Puerto Naos	Basalt	2157/31661	N	K/Ar	95 ± 4 ka
LP 08	Cliff of Playa Nueva	Basalt	2164/31679	N	K/Ar	100 ± 4 ka
LP 13	Cliff of Puerto Naos	Basalt	2172/31636	N	K/Ar	90 ± 3 ka
LP 25	Roque Teneguía	Phonolite	2203/31537	N	K/Ar	56 ± 2 ka
CV 154	La Fajana., Lava from V. Fuego (W)	Tephrite	2209/31555	N	K/Ar	36 ± 1 ka
LP 14	C-832 Km 39. Dome of Dña. María	Phonolite	2187/31642	N	K/Ar	34 ± 1 ka
CV 151	Cliff of Puerto Tigalate	Tephri-Phonolite	2265/31590	N	K/Ar	27 ± 1 ka
LP 16	Lava dome of Mendo	Traqui-Phonolite	2195/31622	N	K/Ar	26 ± 1 ka
CV 150	Tiguerorte. Bco. La Lava	Tephrite	2274/31629	N	K/Ar	25 ± 2 ka
CV 163	Las Salineras	Basanita	2297/31635	N	K/Ar	21 ± 2 ka
CV 152	Cliff of Puerto Tigalate (80 m)	Tephrite-Trachybas	2262/31586	N	K/Ar	20 ± 2 ka
LP 01	C-832 Km 39 Km 34	Tephri-Phonolite	2196/31596	N	K/Ar	18 ± 2 ka
LP 02	C-832 Km 39 Km 35.5	Tephri-Phonolite	2194/31613	N	K/Ar	15 ± 2 ka
LP 09	Cliff of Playa Nueva	Basalt	2164/31678	N	K/Ar	8 ± 2 ka
CV 165	Road to airport, Km 1.2	Basalt	2301/31718	N	K/Ar	8 ± 1 ka
LP95SD14	Charcoal in phreatomag. ash, Bco. Llanos del Agua	Charcoal	2212/31656	N	C14	7.99 ± 0.08 ka
LP95SD11	Barranco Los Llanos del Agua	Charcoal	2206/31657	N	C14	6.85 ± 0.06 ka
LP 03	Birigoyo, northern flank	Tephrite	2216/31678	N	K/Ar	6 ± 2 ka
CV 156	C-832 Km 25.5. Lava from V. Fuego (E)	Tephri-Phonolite	2234/31569	N	K/Ar	4 ± 2 ka
CV 155	Las Indias. Lava from V. La Fajana	Tephrite	2197/31561	N	K/Ar	3 ± 2 ka
LPC14-01	La Fajana	Charcoal	2234/31569	N	C14	3.2 ± 0.01 ka
LP94SD7	Crater of El Fraile cone	Charcoal	2227/31655	N	C14	2.31 ± 0.05 ka
LPC14-03	Nambroque, SE flank.	Charcoal	2246/31643	N	C14	1.04 ± 0.09 ka
LPC14-04	Lava from Mña. Goteras volcano	Human bones	2298/31657	N	C14	1.09 ± 0.05 ka

obtained by Guillou et al. (1998, 2001 and this work) from these volcanoes, many of them in stratigraphic sections, show the lava outcrops of the Cumbre Vieja constrained to the last 123 ka. Contrarily, the ages of Abdel Monem et al. (1972) and Ancochea et al. (1994) for the same volcanic sequences are significantly older, many of them from intrusions that are dated as older than the lavas they intrude. As discussed below, the Bejenado volcano developed unconformably on the debris avalanche deposits of the Cumbre Nueva flank collapse at about 560 ka (Carracedo et al., 1999 a, b) and should, therefore, be younger than this age. However, most of the ages reported by Ancochea et al. (1994) predate the collapse and, accordingly, this volcano should be anterior and not the filling of the collapse embayment. Finally, the apparently important gap between the Taburiente and Garafía volcanoes (Lower and Upper Old Series of Ancochea et al., 1994) merely reflects incomplete sampling, as in the ages from Abdel Monem et al. (1972) and Staudigel et al. (1986).

These differences are relevant to the definition of the volcanic stratigraphy and history of La Palma, and stress the convenience of interlaboratory cross-checking.

Main stratigraphic units and volcanoes

The two main stages of the development of oceanic volcanoes, the *submarine* and *subaerial* stages, outcrop in La Palma, after the former was uplifted to about 1 km asl.

The main volcanic stratigraphy units of La Palma were defined from the ages and the magnetic stratigraphy shown in Fig. 8. Two different overlapping volcanoes, the Garafía and Taburiente volcanoes, were defined in the northern shield, notwithstanding the fact that the eruptive activity has been substantially uninterrupted. This separation was feasible because of the presence a regional angular discordance, the result of the lateral collapse of the Garafía volcano at about 1.2 ma, as already pointed out by Ancochea et al. (1994). As discussed below in detail, a change in eruptive style allowed the definition of two phases –Lower and Upper– in the Taburiente volcano. Another general discordance related to a

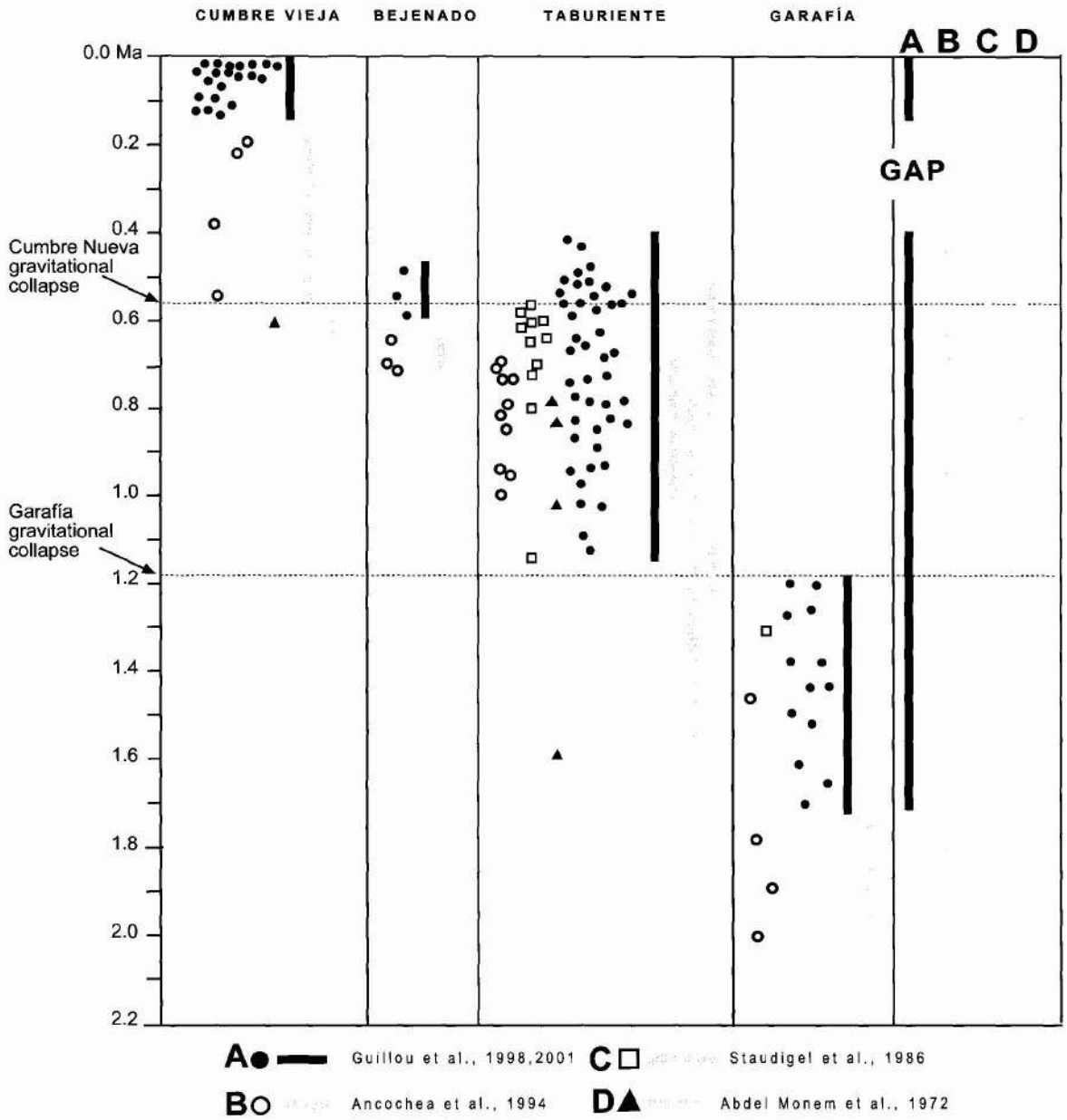

Fig. 6.—Comparison of the ages published from volcanics and intrusives of La Palma.

major gravitational collapse made the separation of the Bejenado volcano possible. All these volcanoes overlap to form the northern shield of La Palma, whereas the Cumbre Vieja forms a clearly independent feature (see Figs. 4, 6, 7 and 8).

Sections in different localities of the Taburiente and Garafía volcanoes, shown in Fig. 9, give a clear indication of the consistency of the ages obtained and their correlation with the established geomagnetic time scale. Similar agreement was attained with the palaeomagnetic and volcanostratigraphic units defined in water tunnels or *galerías* of the northern shield (Fig. 10). These stratigraphic units were, therefore, used in volcanostratigraphic corre-

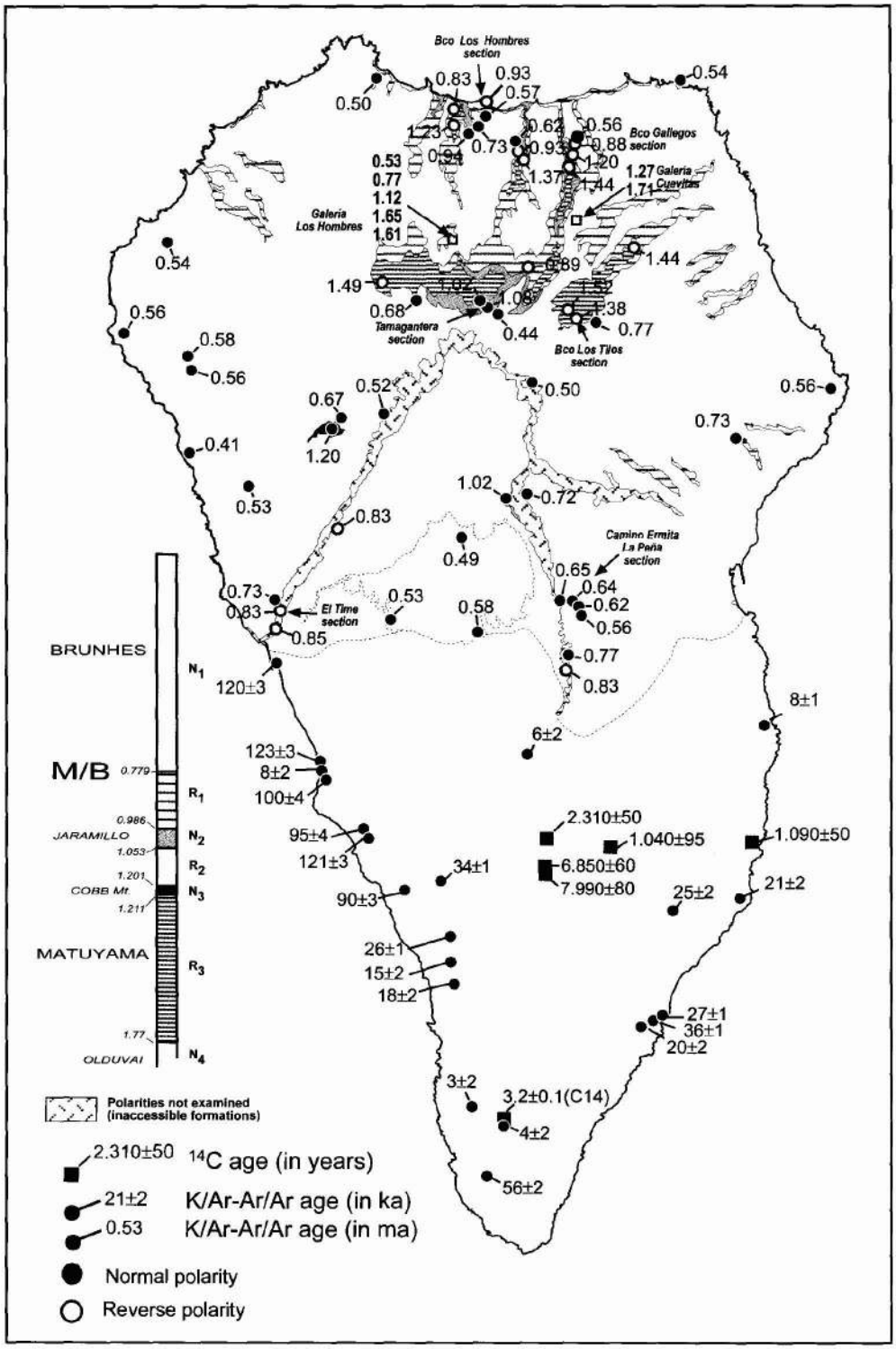

Fig. 7.—Ages and magnetozones of La Palma (ages from Guillou et al., 1998, 2001 and Carracedo et al., 2001 a, b).

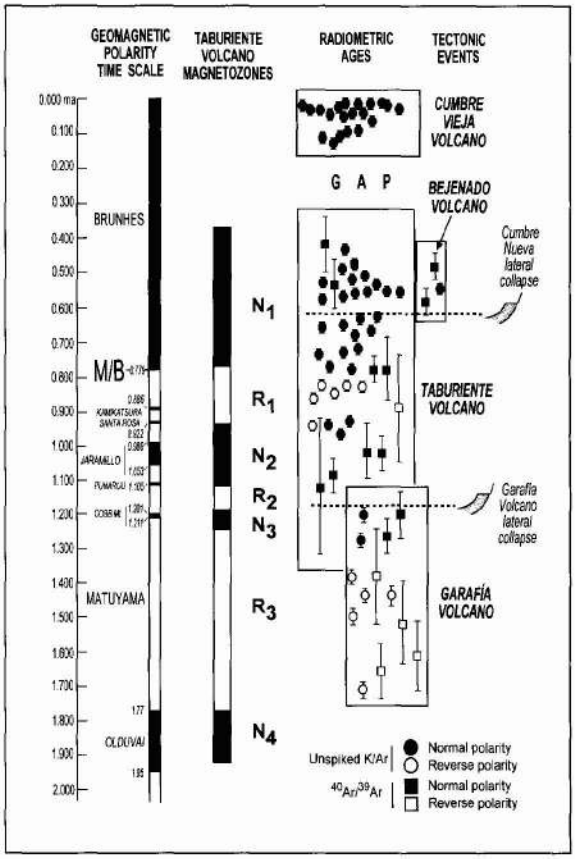

Fig. 8.—Definition of the main volcanostratigraphic units and constructive and destructive events of La Palma from the ages (Guillou et al., 1998, 2001 and Carracedo et al., 2001 a, b) and magnetostratigraphy. N: Normal polarity, R: Reverse polarity.

lation and geological mapping in the island of La Palma, as described below.

Geological and volcanological description of the stratigraphic units and volcanoes

The Pliocene Seamount

Staudigel (1981) and Staudigel and Schmincke (1984) interpreted the submarine and plutonic complex exposed in the walls and floor of the Caldera de Taburiente as an uplifted seamount. The Seamount Series of La Palma is a sequence of submarine volcanic and associated intrusive rocks outcropping to a maximum altitude of about 1 km above sea level, and separated from the overlying subaerial volcanic rocks of the Taburiente volcano by a distinct angular and erosive unconformity. Plutonic intrusions and a large number of dykes, which represent feeders to the subaerial volcanic sequence, cut Seamount Series rocks deep inside the Caldera.

As described in detail by Staudigel (1981) and Staudigel and Schmincke (1984), the Seamount Series outcropping in the bottom of the Barranco de Las Angustias represents a complete, 3.6-km-thick cross-section through a seamount. Similar formations are exposed in La Gomera (Bravo, 1964; Cendrero, 1971) and Fuerteventura (Fúster et al., 1968 b; Stillman and Robertson, 1977; Stillman, 1987). A comparable suite of rocks also occurs in Maio in the Cape Verde archipelago (Stillman et al., 1982). The original interpretation of these (Fúster et al., 1968 b), dating back to the pre-Plate Tectonic era, was that they represent uplifted blocks of a region-wide basement complex; a later modification was to interpret them as uplifted blocks of ophiolitic oceanic crust although palaeontological and radiometric work showed them to be much younger than the adjacent sections of the Atlantic ocean lithosphere. These «basal complexes» have most or all of the following features in their exposed sections:

— Uplifted and strongly deformed sequences of oceanic sediments, substantially older than other parts of the «basal complexes» as shown by palaeontological and radiometric evidence.

— Thick sequences of submarine volcanic rock (mainly pillow basalts, with shallow-water and littoral hyaloclastites present in the higher parts of the sections, indicating emergence).

— Intense basaltic dyke swarms, attaining, for example, over 80% of the outcrop in parts of Fuerteventura (Stillman, 1987).

— Substantial plutonic intrusive complexes, cutting and cut by different components of the dyke swarms.

— Moderately intense deformation of the dyke swarms and intrusive complexes, involving, variously, tilting (Staudigel and Schmincke, 1984), block faulting (Stillman, 1987), and radial thrusting (Stillman et al., 1982). This is generally related to emplacement of the plutonic intrusive complexes.

— Hydrothermal metamorphism, rising from zeolite to albite —epidote— hornfels facies, affecting all of the above components (Staudigel and Schmincke, 1984; Schiffman and Staudigel, 1994, 1995); localized high-grade thermal contact metamorphism and anatexis may be present around several of the plutonic complexes (Stillman, 1987).

— Late intrusive complexes (dykes, plugs, occasional ring complexes and other large plutons, which are inferred to be feeders to overlying rocks of the subaerial volcanic complexes).

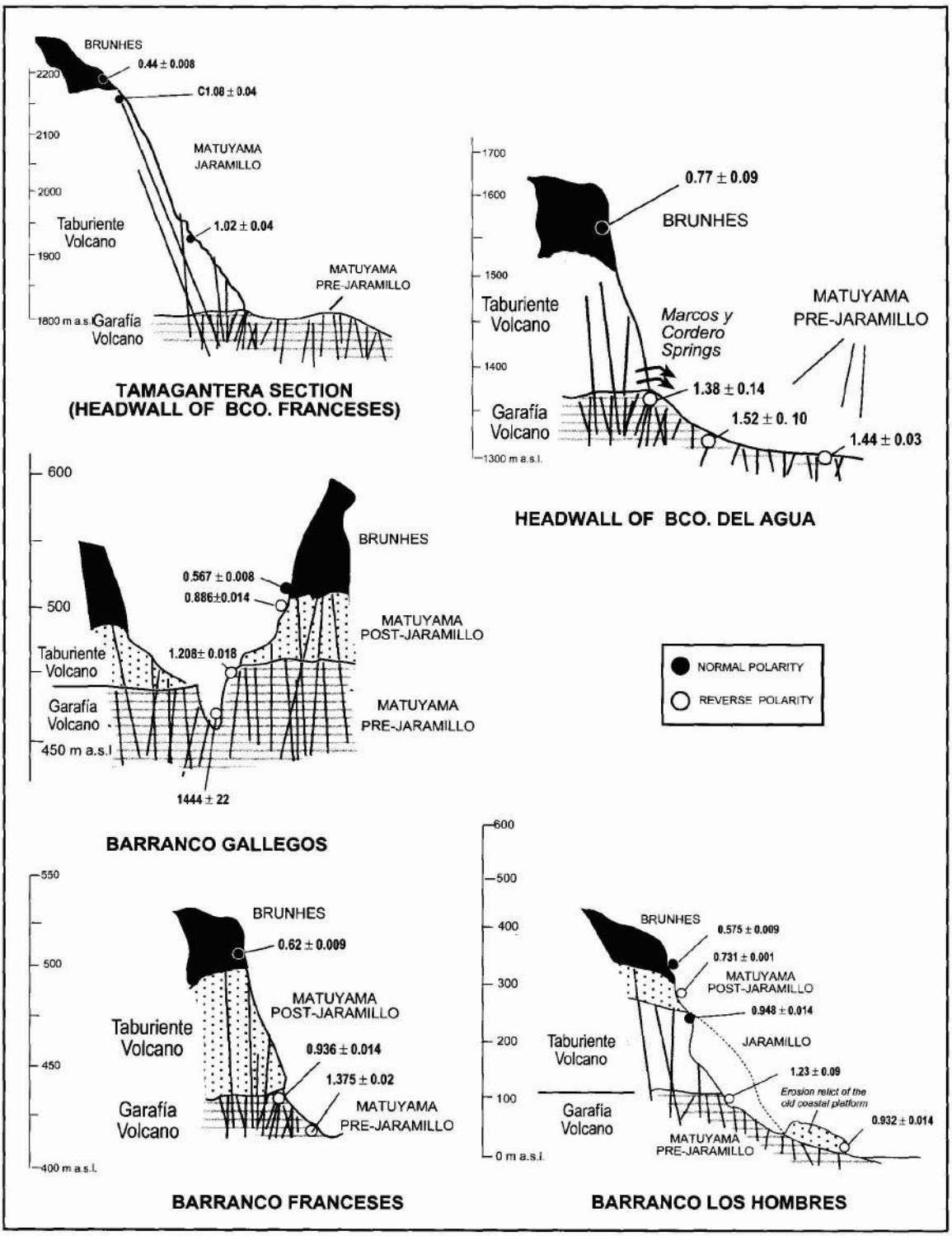

Fig. 9.—Representative cross sections in the northern shield showing the main volcanostratigraphic and magnetostratigraphic units.

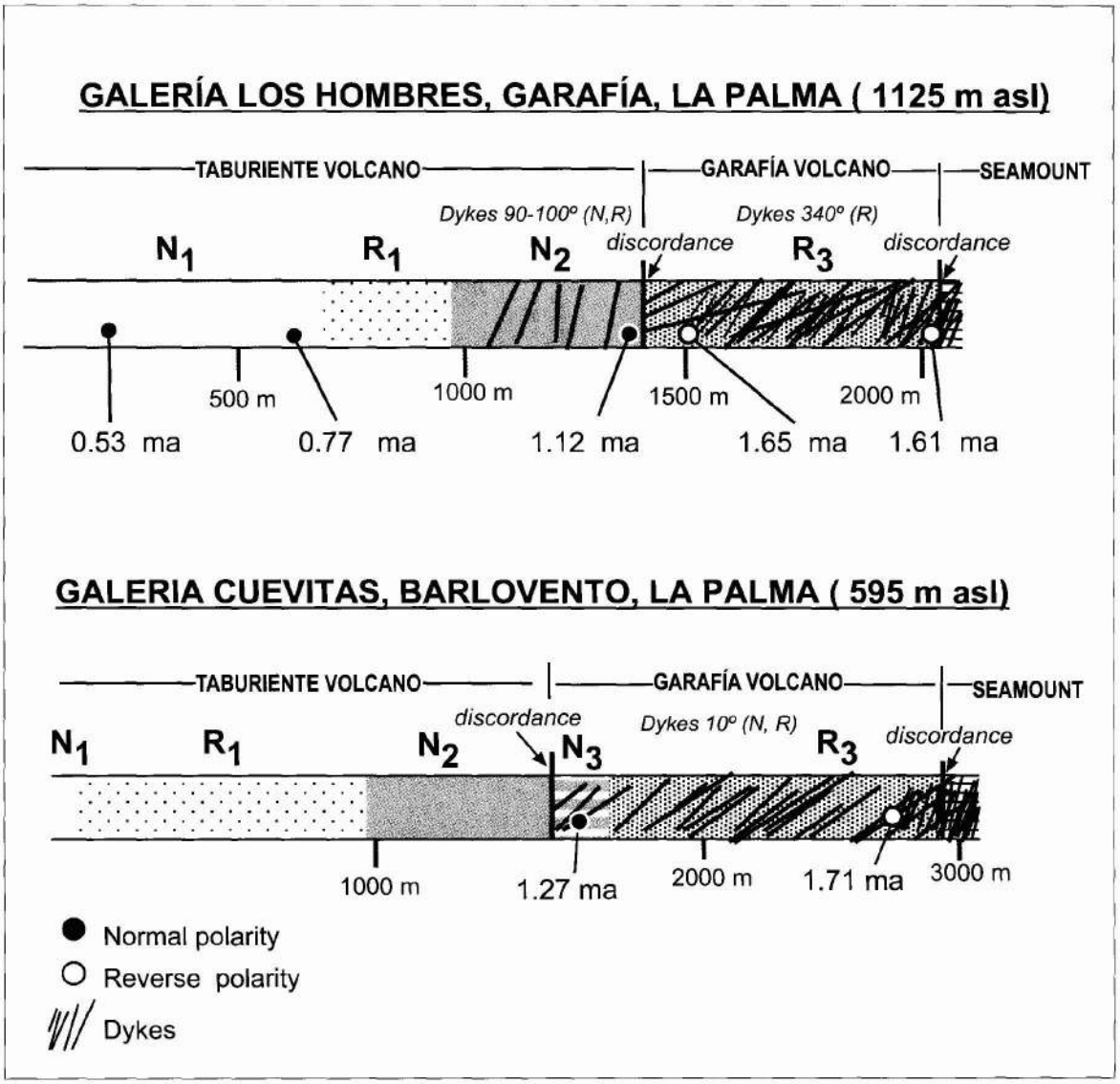

Fig. 10.—Disposition and extension of the main magnetozones defined in the northern shield in the Los Hombres and Cuevitas *galerías*. N: Normal polarity, R: Reverse polarity.

— Substantial terrestrial unconformities, with significant topography, which mark erosion down to the level of the dyke swarms and, in some cases, the plutonic complexes. In other places, however, transitional sequences with only moderate dyke swarm densities and, typically, littoral volcanic facies are present.

Radiometric data for the «basal complexes» are commonly in contradiction to field evidence, particularly in regard to their relationships to the overlying subaerial volcanic rocks. This most probably reflects the widespread use of dating techniques on unsuited, altered rocks. The Seamount Series of La Palma has been approximately dated as Pliocene (3-4 ma) using foraminifera (*Globorotalia crassaformis, Neogloboquadrina humerosa, Globoquadrina altispira* and *Globorotalia puncticulata)* found in hyaloclastites interbedded in the submarine lavas (Staudigel, 1981, 1997).

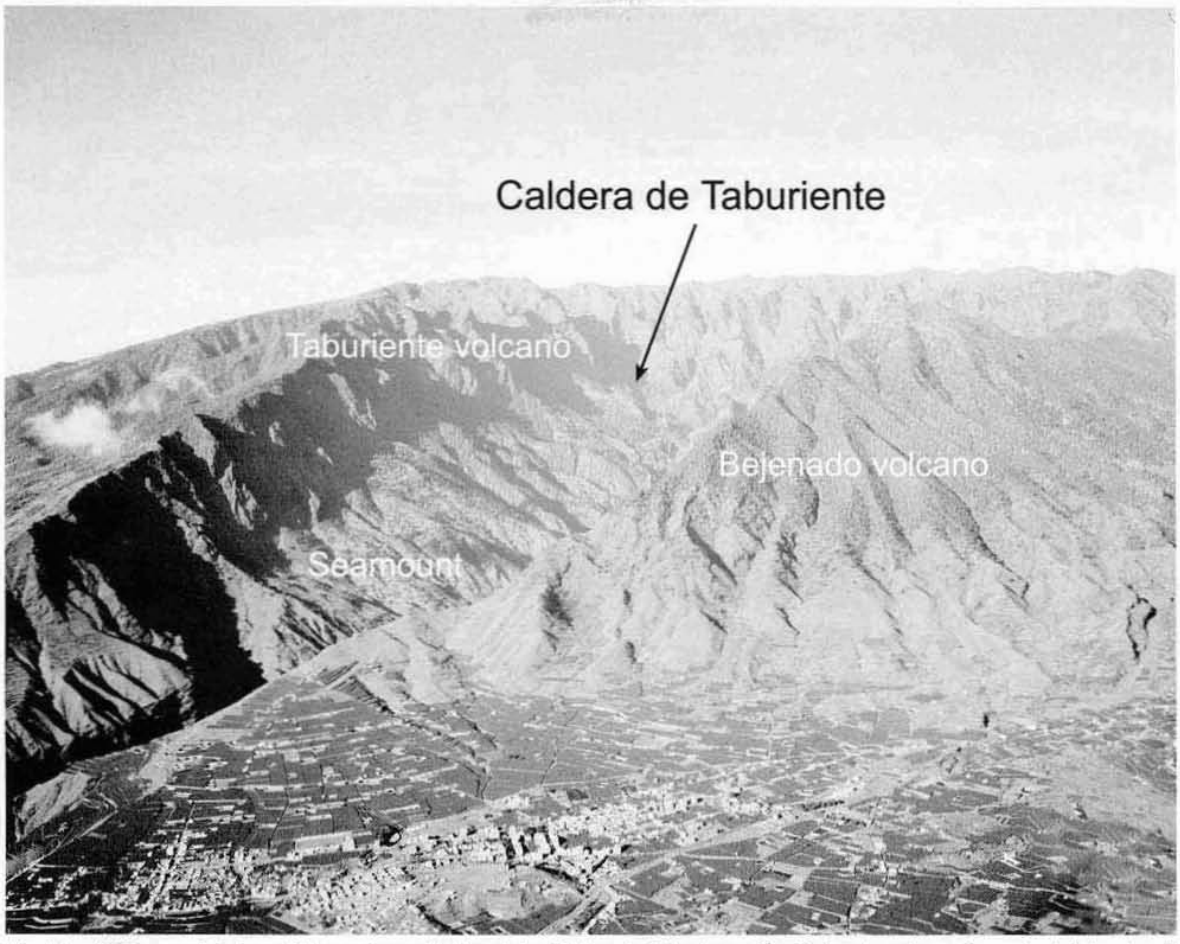

Fig. 11.—Oblique aerial view of the northern shield and the Caldera de Taburiente. The Bejenado volcano forms the left-hand wall of the Caldera.

The Seamount Series of La Palma only outcrops inside the Caldera de Taburiente (Fig. 11), exposed by the deep incision originated by a large gravitational collapse and subsequent erosion. However, it forms the deep core of the northern shield, where its extension and disposition have been determined by Coello (1987) through observation in *galerías* (Fig. 12). It consists of two main units, an extrusive sequence of layered lavas and an intrusive (plutonic) sequence. However, according to Staudigel (1981), both series grade progressively from shallow water lavas (see Fig. 13 A, B) to a plutonic core (Fig. 13 C).

The extrusive Seamount Series

Staudigel (1981, 1997) and Staudigel and Schmincke (1984) have described this Series in detail. The outcrop of the Barranco de Las Angustias consists of a layered sequence of pillow lavas and volcaniclastics grading to a sheeted dyke swarm (Figs. 13 and 14). Two sections have been separated by these authors (Fig. 14): a shallow-water and a deep-water facies, the deepest outcropping inside the Caldera at El Carbón (365 m asl), and the shallowest at La Viña (145 m asl). These represent a 1.8-km section at the flank of the seamount. The layered sequence of the NW-SE-trending submarine lavas and volcaniclastics are tilted 50° to the SW, parallel to the axis of the barranco, caused by endogenous growth and intrusion. The shallow-water facies include a large fraction of volcaniclastics, whereas the deep-water facies are predominantly made of thick pillow lavas, similar to deep abyssal hills on the ocean floor (Staudigel, 1981, 1997).

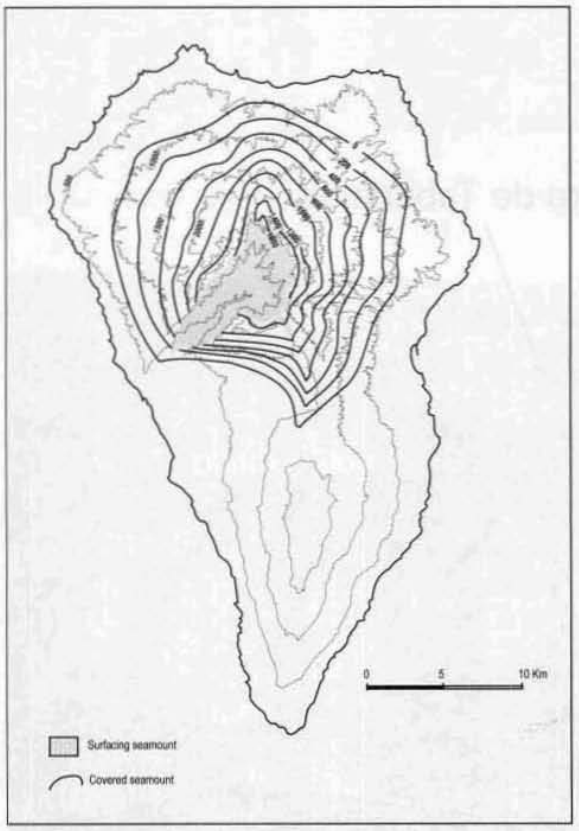

Fig. 12.—Disposition and approximate extension (from Coello, 1987) of the seamount. Contours of the subaerial volcanoes and the underlying seamount are indicated for comparison.

An interesting feature of the extrusive Seamount Series is the continuous prograde hydrothermal metamorphism. First described by Hernández Pacheco and Santín (1974) and later by Staudigel (1981), metamorphism grades from low (<10 °C) alteration at the top of the formation to medium-grade metamorphism (greenschist facies metamorphism) near the base (Hernández Pacheco and Fernández Santín, 1974; Staudigel and Schmincke, 1984; Schiffman and Staudigel, 1994, 1995). For these last authors, the paragenesis and mineralogical zonation observed imply a metamorphic gradient of 200-300 °C/km and the circulation of a high rate of fluids over a long period, that has almost completely altered the original igneous minerals of these rocks. Hydrothermal alteration has likewise contributed to erase the original magnetization of the rocks (Gee et al., 1993) and has led to significant variations in the concentration of certain elements such as Re and Os (Marcantonio et al., 1995).

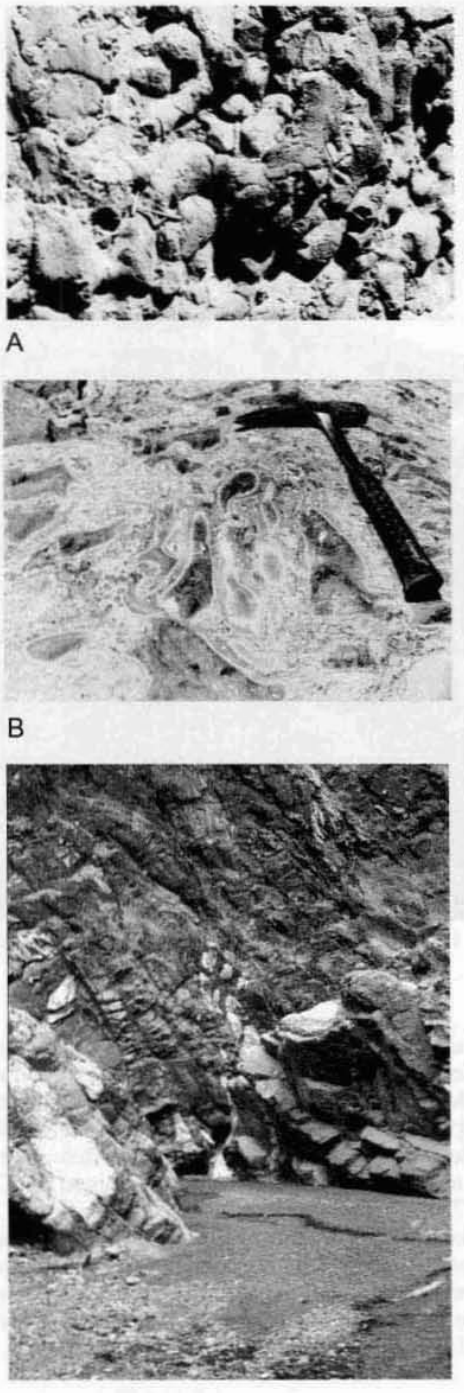

Fig. 13.—View of increasingly deeper facies of the seamount in the bed of Bco. de Las Angustias. A) Shallow pillow lavas. B) Hyaloclastite breccias. C) Dyke swarm intruding the submarine formations.

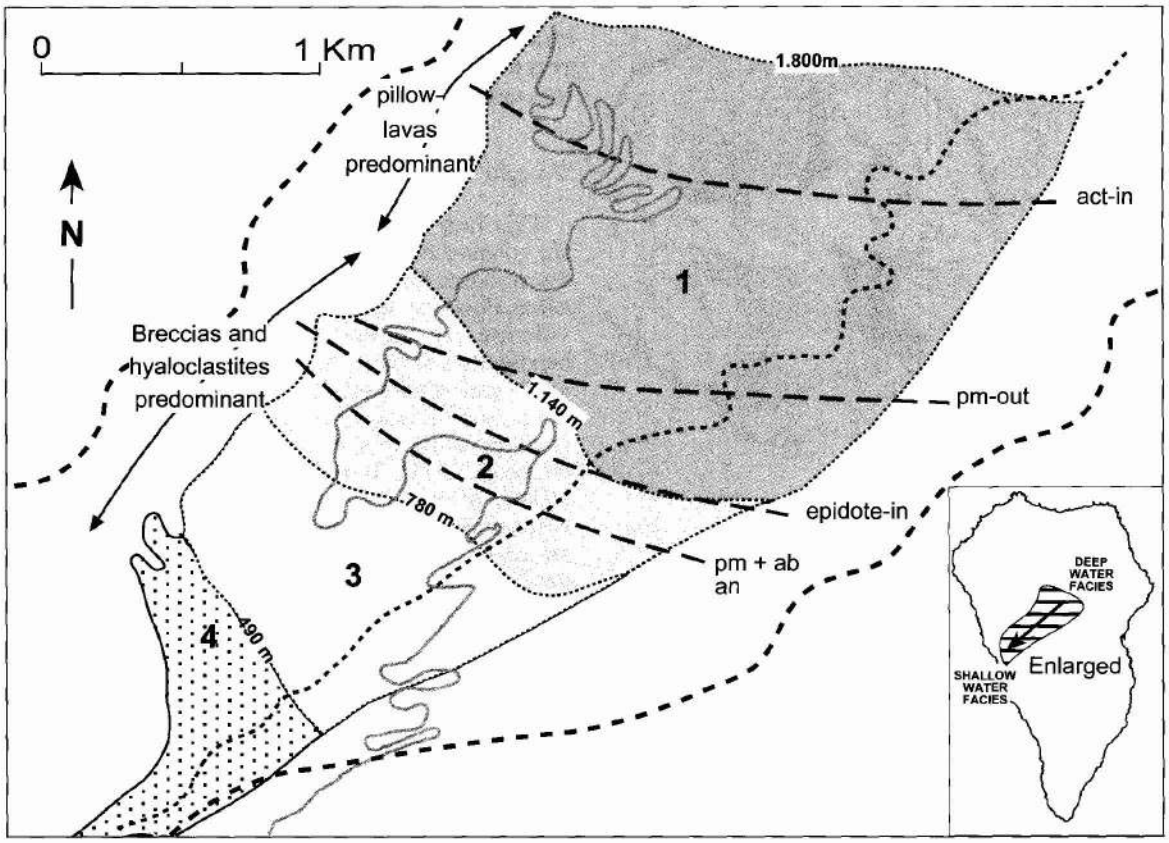

Fig. 14.—Submarine extrusive sequence in the Caldera de Taburiente (modified from Staudigel and Schmincke, 1984). 1 to 4 indicate different facies of increasing water depth.

The intrusive Seamount Series

Intrusions inside the Caldera correspond to the seamount and the subsequent subaerial volcanism, and can be separated into three main groups:

1. *Trachytic-phonolitic domes of Dos Aguas.* This unit outcrops in an arc between the Barranco de Taburiente, Dos Aguas, El Carbón and Los Brecitos and extends approximately over some 2 km^2. These materials have previously been interpreted as salic rocks (Hernández Pacheco and Fernández Santín, 1974), and keratophyres or metatrachytes (Staudigel and Schmincke, 1984). In any case, they remain considerably indeterminate, due, on the one part, to the fact that they appear as metric-sized fragments between the dense dyke swarm and, on the other, to their high degree of compositional and textural alteration.

De la Nuez recognized two main types of facies (1984), a coarse-to-medium-grain breccia and a massive facies. The breccias are preferentially localized close to the contact with the submarine volcanic formation, while the massive facies are located towards the centre of the formation. Clasts of pillow lavas of a trachytic composition are observed in the breccias, indicating that they were probably formed in a marine environment. Relict flow structures and some fragments that seem to correspond to pyroclastic products have been detected in the massive facies. This trachytic and phonolitic formation, probably corresponding to one or several domes intruding the basaltic submarine formation in the deepest sequences, appear crossed by a dense dyke swarm and by several plutonic bodies several tens to hundreds of metres thick.

2. *Intrusive plutonic rocks.* Numerous plutonic bodies, tens to hundreds of metres thick, outcrop at the bottom of the Caldera de Taburiente over an area of several km^2. They correspond to multiple intrusions associated to submarine and subaerial eruptions,

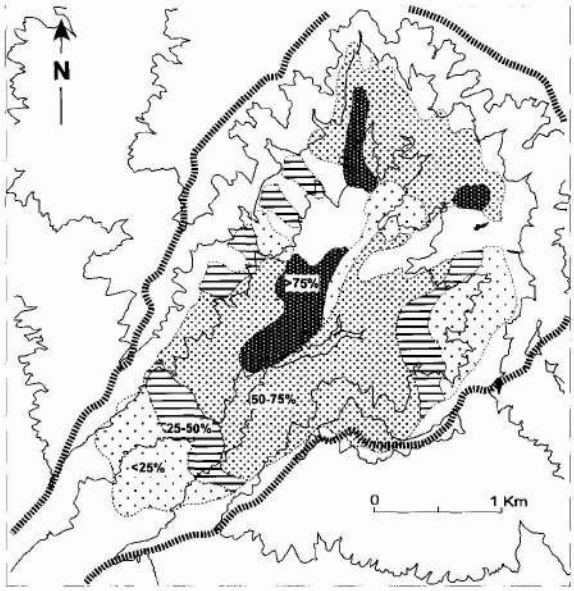

Fig. 15.—Percentage of dykes and sills in the Caldera de Taburiente.

reaching, in places 75% of the rock (Fig. 15). However, it is very difficult to individualize plutonic bodies or separate those belonging to the seamount from those corresponding to the subaerial Garafía, Taburiente and Bejenado volcanoes.

Three main groups of gabbros have been separated (see geological map), the first two corresponding to the submarine edifice, and the third to intrusions related to the subaerial volcanism (Carracedo et al., 2001 a, b). The oldest gabbros outcrop in the northern half of the Caldera, the most probable location of the submarine emission centres. The most recent gabbro intrusives are located to the south, probably related to the emission centres of the Taburiente and Bejenado volcanoes.

3. *Dyke swarms.* The dyke network is highly developed throughout the submarine edifice, with a maximum density at the centre of the Caldera de Taburiente and along the Barranco de Las Angustias, decreasing gradually towards the edges and downwards. The maximum intrusion can make up as much as 100% of the rock (always more than 75%) in the barrancos of Taburiente, Verduras de Alfonso and Los Cantos, while down at La Viña dykes constitute less than 10% of the rock (Fig. 15).

Staudigel and coworkers (1986) separated three groups of dykes with different ages and general orientation. The two older groups are rotated due to the tectonic uplift of the seamount prior to the emergence of the island and, therefore, feed the submarine formation. The third group, more recent and unrotated, is related to the subaerial volcanoes.

Garafía Volcano

This first subaerial volcanism formed the Garafía volcano overlying in clear angular and erosive discordance and entirely mantling the uplifted and tilted Pliocene seamount. Outcrops of the Garafía volcano are limited to erosive windows at the headwalls and beds of the deepest barrancos of the north and southwest flanks of the northern shield (Fig. 16). These outcrops were interpreted as corresponding to the Basal Complex (Hernández Pacheco, 1974), Taburiente I (Navarro and Coello, 1994), or as Lower Old Series (Coello, 1987; Ancochea and coworkers, 1994). However, there are reasons for separating this volcano as an independent unit. The radiometric and palaeomagnetic data indicate that this volcano formed between 1.722 and 1.208 ma, the period corresponding to the Matuyama post-Olduvai and the Cobb Mt event (see Figs. 7, 8 and 16 and Table 1). The lower limit of this volcano can be set at 1.77 ma, since the normal polarity lavas of the Olduvai event (see Fig. 8) have not been found at the basal sequences of the volcano, even at the discordant contact with the underlying seamount formations, as occurs in the *galerías* Los Hombres and Cuevitas (Fig. 10).

The volcanic activity in the northern shield continued without significant interruptions until about 0.4 ma (see Fig. 8). The separation of the Garafía and the subsequent Taburiente volcanoes has been feasible because in many areas their contact is an angular and/or erosive discordance, originated by the afore-mentioned gravitational collapse of the south flank of the former volcano approximately 1.2 ma ago. The large collapsed portion of the volcano, and the superposition of about 1.000 m of lavas of the subsequent Taburiente volcano made the approximate reconstruction of the extension and configuration of the Garafía volcano difficult. However, its distribution in the subsoil has been approximately defined by means of the numerous *galerías* excavated for groundwater mining in the northern shield (Coello, 1987; Carracedo et al., 2001 a, b). These observations indicate that the Garafía volcano developed as a steep cone, with lava flows consistently exceeding 20°, frequently 30-35°, and closely centred over the seamount (see Fig. 16). The mean thickness of the formation (some 400 m)

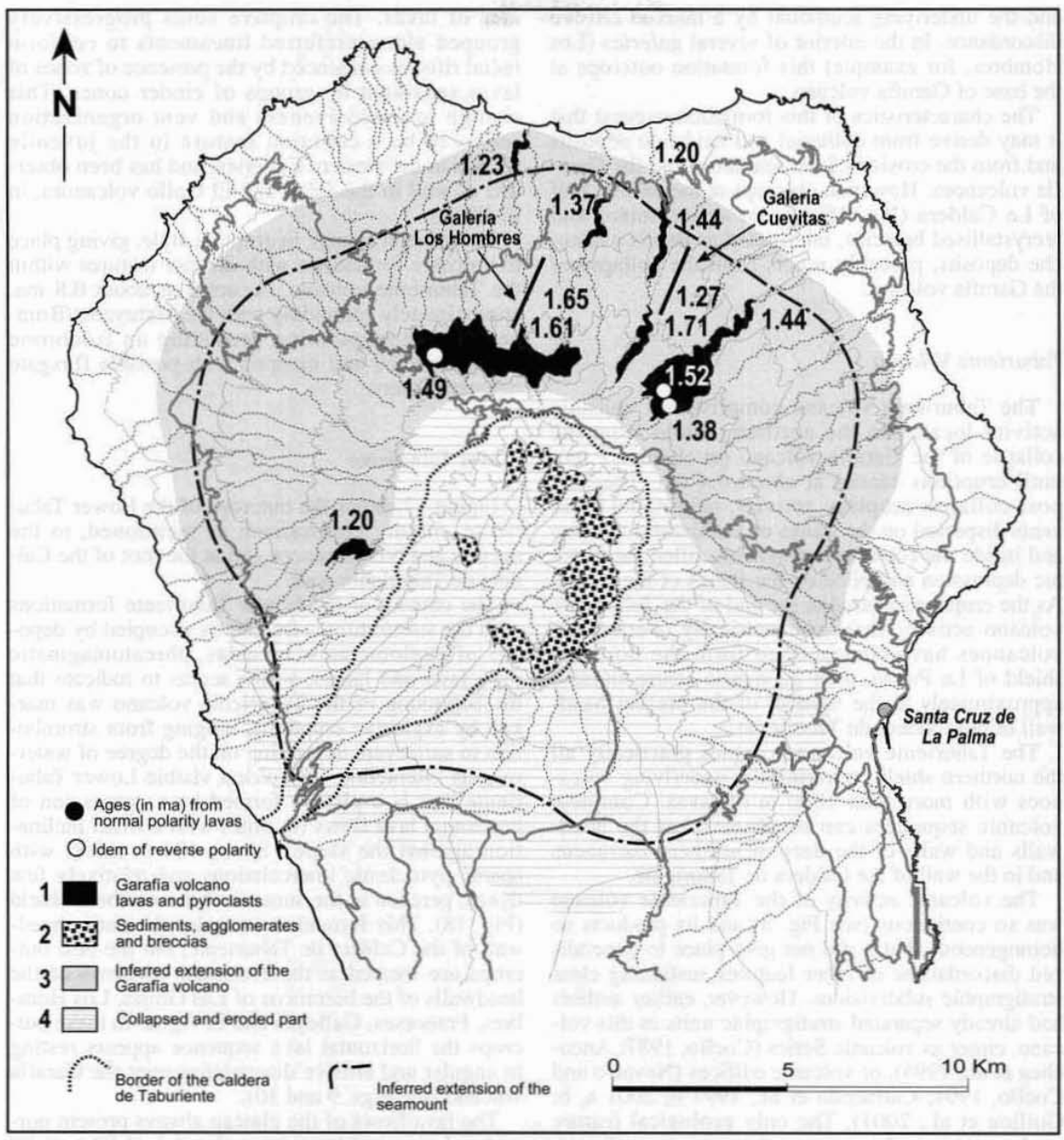

Fig. 16.—Outcrops of the Garafía volcano. The approximate extension of this volcano and the underlying seamount are indicated for comparison.

points to a volcanic edifice at least 2.000 m high and around 25 kms in diameter, with a volume of about 160 km^3 (after subtracting the volume of the seamount, of about 166 km^3). The corresponding eruptive and growth rates near 0.3 km^3/ka and 0.8 mm/y, respectively.

Sediments, agglomerates and breccias in the interior of the Caldera de Taburiente. A several hundred metres-thick sequence of sediments, agglomerates and breccias outcrops in the Caldera de Taburiente (Fig. 16 and geological map), at the base of the Taburiente volcano and is separated from this

and the underlying seamount by a marked erosive discordance. In the interior of several *galerías* (Los Hombres, for example) this formation outcrops at the base of Garafía volcano.

The characteristics of this formation suggest that it may derive from colluvial and landslide deposits and from the erosion of the seamount and the Garafía volcanoes. However, outcrops at the eastern half of La Caldera (Fig. 16) appear as tectonised and recrystallised breccias, interpreted as debris avalanche deposits, probably relicts from the collapse of the Garafía volcano.

Taburiente Volcano

The Taburiente volcano comprises de volcanic activity located in the northern shield from the collapse of the Garafía volcano (at about 1.2 ma) until eruptions ceased at about 0.4 ma. The first post-collapse eruptive activity, originated from vents dispersed on the flanks of the Garafía volcano and inside the collapse embayment, filled the tectonic depression and piled on the flanks of the shield. As the eruptions ceased at the end of the Taburiente volcano activity, three concentrically overlapping volcanoes have coalesced to form the northern shield of La Palma, their geometric centre situated approximately at the vertical of the present headwall of the Caldera de Taburiente.

The Taburiente volcano occupies practically all the northern shield, covering the underlying volcanoes with more than 1000 m of lavas. Complete volcanic sequences can be observed at the headwalls and walls of the deepest northern barrancos and in the wall of the Caldera de Taburiente.

The volcanic activity of the Taburiente volcano was so continuous (see Fig. 8) and its products so homogeneous that it did not give place to generalized discordances or other features sustaining clear stratigraphic subdivisions. However, earlier authors had already separated stratigraphic units in this volcano, either as volcanic Series (Coello, 1987; Ancochea et al., 1994), or volcanic edifices (Navarro and Coello, 1994; Carracedo et al., 1997 b, 2001 a, b; Guillou et al., 2001). The only geological feature we have observed to support the separation of units in this volcano is based on a change in eruptive style. The lower volcanic sequences outcropping at the headwalls and beds of the deepest barrancos are characterized by the predominance of pyroclastic deposits densely crossed by dykes. These features suggest a wide dispersion of the initial, predominantly explosive eruptive centres. In the advanced stages of the Taburiente volcano the eruptions changed to more effusive, with emission of large volumes of lavas. The eruptive vents progressively grouped along preferred lineaments to conform radial rifts, as evidenced by the presence of zones of lavas separated by groups of cinder cones. This change in explosiveness and vent organization seems to be a common feature in the juvenile shields in the western Canaries, and has been observed as well in the Tiñor and El Golfo volcanoes, in El Hierro.

The general change in eruptive style, giving place to volcanic formations with distinct features within the Taburiente volcano, occurred at about 0.8 ma, approximately coinciding with the Matuyama/Brunhes change of polarity, providing an isochrone easily detected and mapped with portable fluxgate magnetometers.

Lower Taburiente

Figure 17 shows the outcrops of the Lower Taburiente, mainly constrained, as mentioned, to the deep N and NE barrancos and at the foot of the Caldera de Taburiente wall.

The contact of the Lower Taburiente formations with the substratum is frequently occupied by deposits of agglomerates, breccias, phreatomagmatic pyroclasts and lahars, which seems to indicate that the beginning of the Taburiente volcano was marked by explosive eruptions, ranging from strombolian to surtseyan, depending on the degree of water-magma interaction. The oldest visible Lower Taburiente unit is a plateau formed by a succession of horizontal lava flows (at times with a small inclination against the slope), about 400 m thick, with sparse pyroclastic intercalations and relatively few dykes, perched at the summit of the northern shield (Fig. 18). This formation encircles the entire headwall of the Caldera de Taburiente, but the best outcrops are located at the erosional windows of the headwalls of the barrancos of Las Grajas, Los Hombres, Franceses, Gallegos and El Agua. In these outcrops the horizontal lava sequence appears resting in angular and erosive discordance over the Garafía volcano (see Figs. 9 and 10).

The lava flows of the plateau always present normal polarity and have been dated in 1.02 to 1.08 ma. They therefore seem to correspond to the Jaramillo normal polarity event (0.996-1.053 ma) and have been apparently emitted at extremely fast rates (>6 mm/y), apparently a common characteristic of post-collapse volcanism, such as the Bejenado, El Golfo, Post-Cañadas, etc. This plateau was first explained by Coello (1987) and Navarro and Coello (1994) as the filling-up with lavas of two large ravines excavated at the contact between Garafía volca-

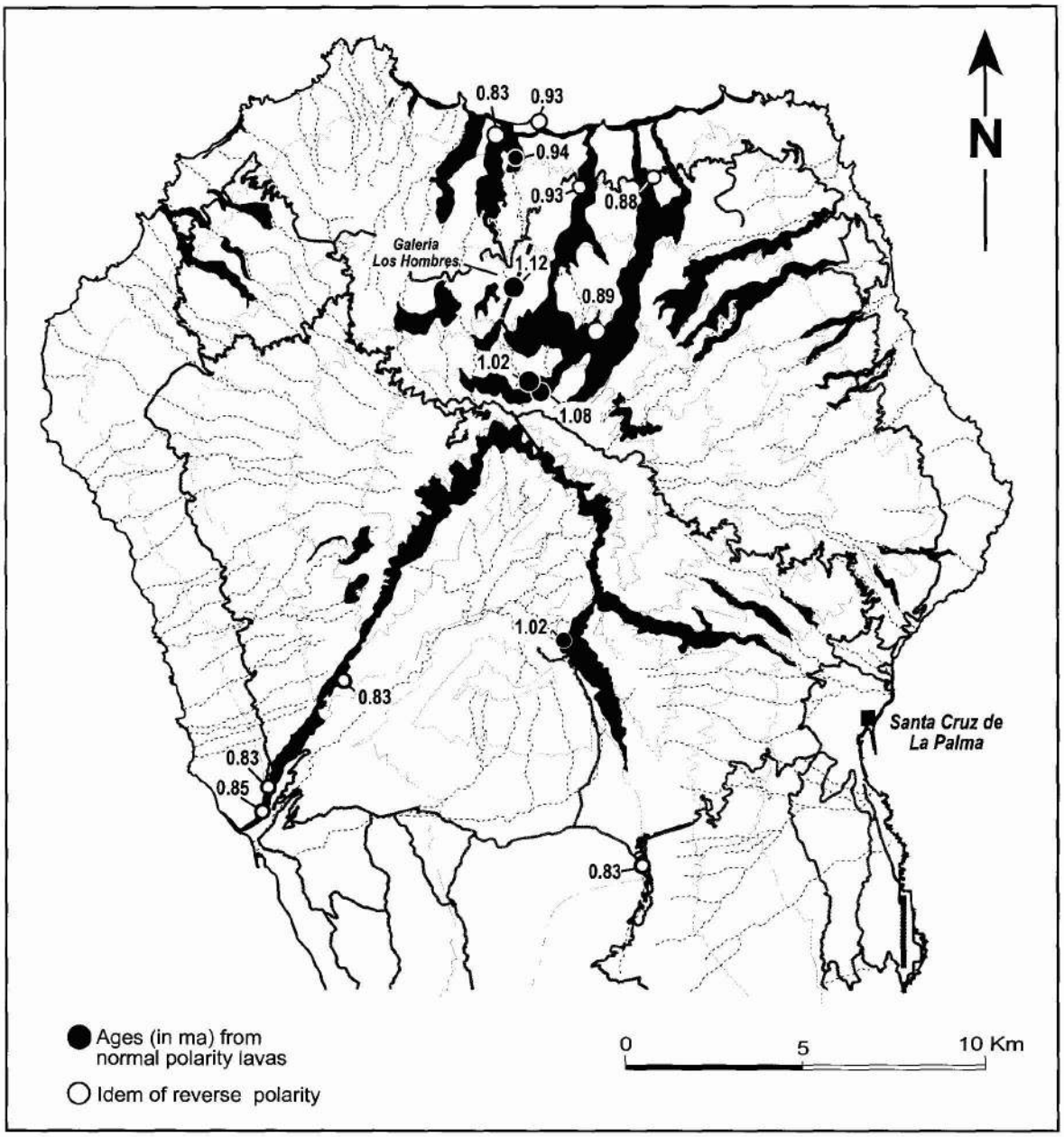

Fig. 17.—Outcrops of the Lower Taburiente volcano.

no (Taburiente I for these authors) and the submarine basement. However, the lack of significant interruptions in the eruptive activity shown by the radiometric ages seems incompatible with the successive incision of several hundreds of metres deep, steep barrancos, their subsequent filling with lavas, and the erosion required to generate the lava plateau by relief inversion. A more plausible explanation, consistent with the geochronological and stratigraphical data, is the filling with lavas of the depression formed in the lateral collapse of the south flank of Garafía volcano already described.

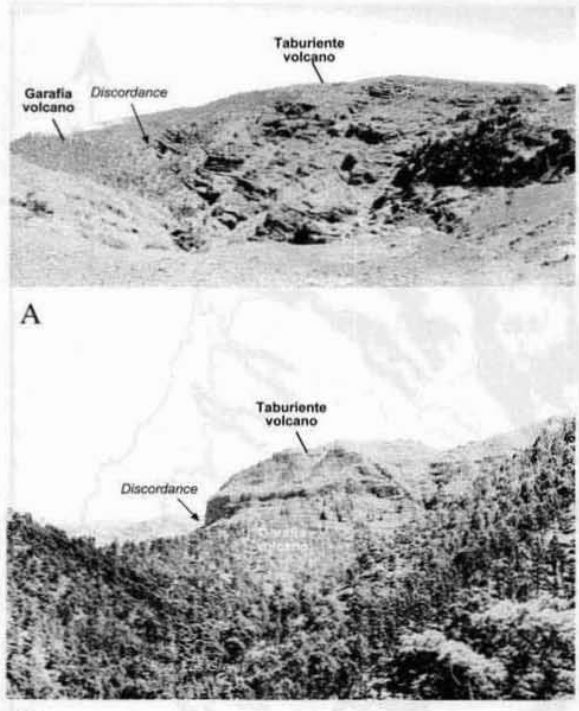

Fig. 18.—Views of the Lower Taburiente horizontal lavas overlying unconformably the Garafía volcano. A) The Tamagantera section. B) View from the NW (from Bco. de Las Grajas).

Upper Taburiente

The Upper Taburiente unit completely mantles the northern shield (Fig. 19), except in the erosional windows at the headwalls of the deep northern barrancos and at the Caldera de Taburiente. Instead of enlarging significantly the extension of the northern shield, this volcanic phase built a progressively higher and steeper volcano. The Upper Taburiente formation corresponds to the culmination of the construction of the northern shield, involving the emission of a sequence of lavas about 1000-m thick, erupted from about 0.8 ma to some 0.4 ma (see Fig. 8).

The Upper Taburiente lavas present great structural and morphological uniformity, appearing in thick sections of basaltic lava flows with sparse pyroclastic beds and dykes, except in the rift zones, where cinder cones are predominant and dykes are abundant (see Figs. 19 and 35). Coastal hydromagmatic cones are relatively abundant, such as the spectacular tuff cone of La Galga, north of Puntallana, with phreatomagmatic eruptions of slightly differentiated magmas that emitted very thick ignimbrites, and the tuff cone of La Caldereta, near Santa Cruz de La Palma.

The final stages of activity of the Upper Taburiente may have formed a central volcano, possibly reaching 2.500-3.000 m asl, with late stages of terminal differentiated lavas and explosive eruptions. Although salic materials have not previously been described from Taburiente volcano, flows of mafic phonolites and trachytes outcrop at the rim of the Caldera de Taburiente, as well as several metres-thick block and ash flow deposits, possibly associated with eruptions that emitted juvenile phonolites (see geological map).

Eruptive activity seems to have started a constant southward migration at the final stages of the Upper Taburiente, finally leaving the northern shield inactive. Eruptions concentrated in the southern part, developing the Cumbre Nueva rift that became progressively steeper and unstable. The collapse of the western flank of the rift formed the southern depression that initiated the Caldera de Taburiente (see Fig. 19). Post-collapse activity in the northern shield mainly concentrated inside the collapse embayment to form the nested Bejenado volcano, although disperse eruptions on the flanks of the shield postdated the Bejenado volcano until 0.4 ma.

The Bejenado volcano

The Bejenado volcano is the continuation of the Upper Taburiente volcanism immediately after the above-mentioned Cumbre Nueva gravitational collapse (see Fig. 8). The separation of this volcano from the remainder of Taburiente is based, similarly to the Garafía volcano, on the occurrence of a gravitational collapse generating a general discordance, over which the Bejenado volcano developed. This volcano illustrates spectacularly the structural and magmatic evolution of post-collapse volcanism, with parallelisms in the cases of Las Cañadas in Tenerife and El Golfo in El Hierro (Ancochea et al., 1990; Guillou et al., 1996).

The construction of this stratovolcano was extremely fast, as shown by the radiometric ages (Figs. 6-8 and Table 1), possibly only a few tens of thousands of years. In this short time the lavas built a very steep volcano, partially dismantled at present by the progression of erosion in the Caldera de Taburiente. The summit of Bejenado reaches 1.864 m asl, but only the top 600 m belong to this volcano, which appears forming the SE wall of the Bco. de Las Angustias, at the exit of the Caldera de Taburiente (see Fig. 11). There is a clear lack of correspondence in the western and eastern walls of the Caldera de Taburiente, as pointed out by Sapper in

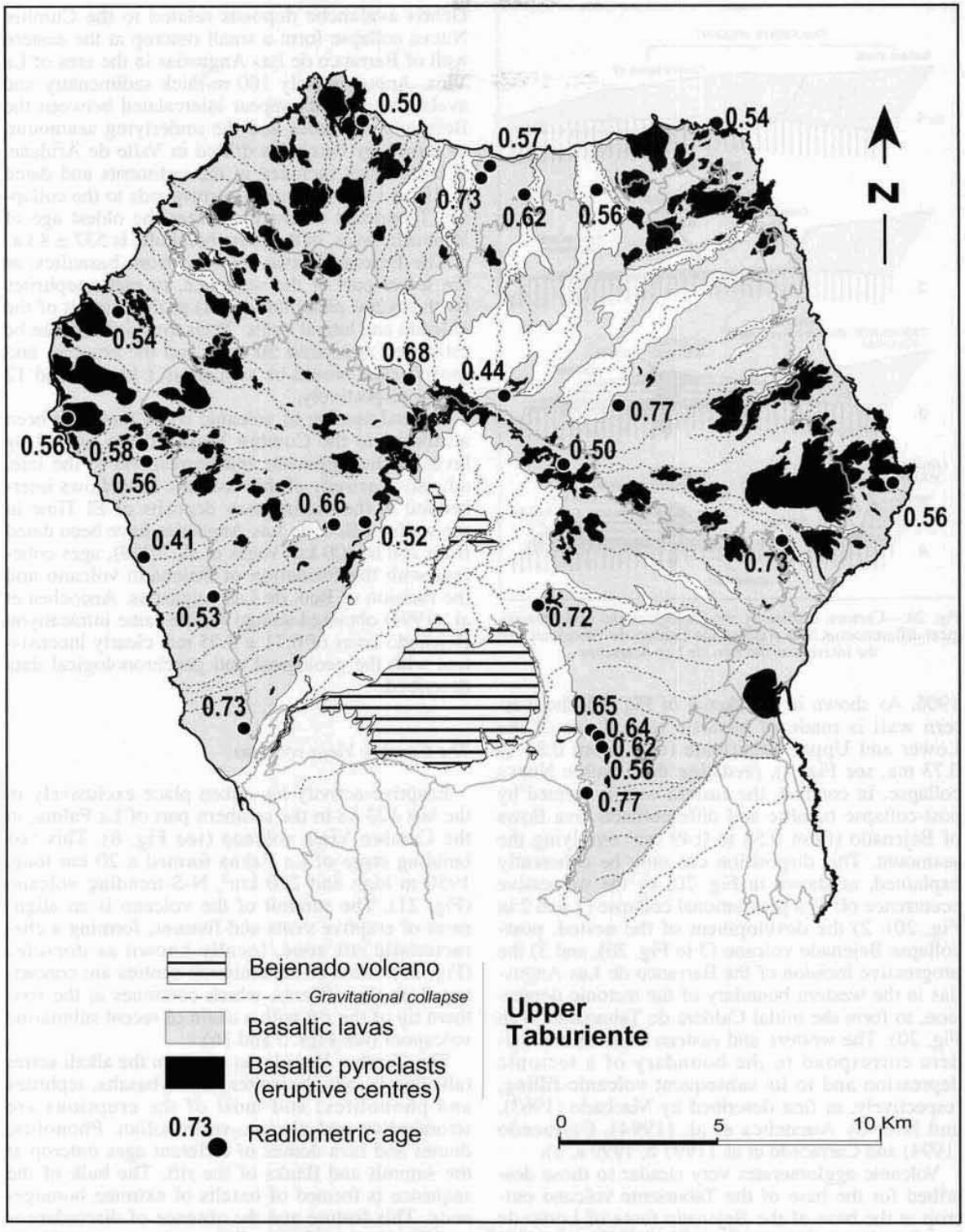

Fig. 19.—Outcrops of the Upper Taburiente and Bejenado volcanoes.

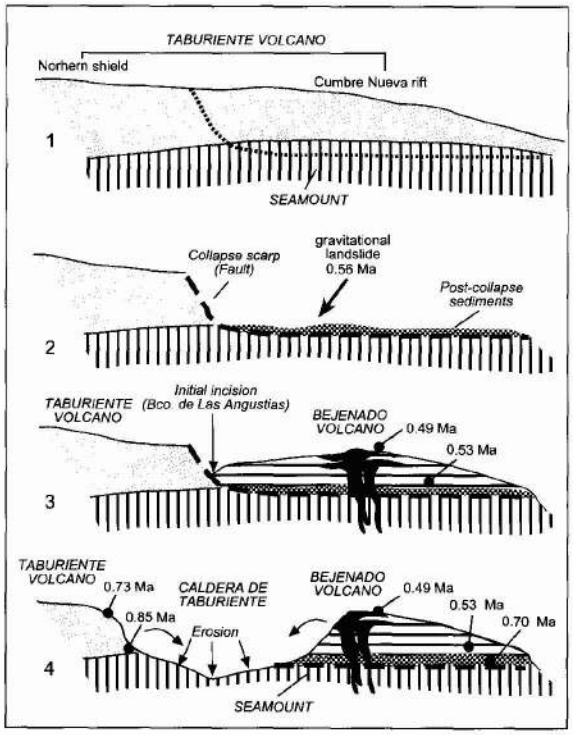

Fig. 20.—Cartoon explaining the geological and geochronological differences at both walls of the Caldera de Taburiente and the incision of the Bco. de Las Angustias

1906. As shown in the sketch of Fig. 20, the western wall is made of basaltic lava flows of the Lower and Upper Taburiente (ages from 0.85 to 0.73 ma, see Fig. 7), predating the Cumbre Nueva collapse. In contrast, the eastern wall is formed by post-collapse basaltic and differentiated lava flows of Bejenado (from 0.58 to 0.49 ma) overlying the seamount. This disposition can only be coherently explained, as shown in Fig. 20, by the successive occurrence of: 1) a gravitational collapse (1 and 2 in Fig. 20), 2) the development of the nested, post-collapse Bejenado volcano (3 in Fig. 20), and 3) the progressive incision of the Barranco de Las Angustias in the western boundary of the tectonic depression, to form the initial Caldera de Taburiente (4 in Fig. 20). The western and eastern walls of the Caldera correspond to the boundary of a tectonic depression and to its subsequent volcanic filling, respectively, as first described by Machado (1963), and later by Ancochea et al. (1994), Carracedo (1994) and Carracedo et al. (1997 b, 1999 a, b).

Volcanic agglomerates very similar to those described for the base of the Taburiente volcano outcrop at the base of the Bejenado (area of Lomo de Los Caballos and along the road to La Cumbrecita). Debris avalanche deposits related to the Cumbre Nueva collapse form a small outcrop at the eastern wall of Barranco de Las Angustias in the area of La Viña. Approximately 100 m-thick sedimentary and avalanche deposits appear intercalated between the Bejenado volcanics and the underlying seamount, as shown by boreholes drilled in Valle de Aridane. A large block included in the sediments and dated in 710 ± 11 ka obviously corresponds to the collapsed Taburiente volcano, whereas the oldest age of Bejenado lavas, in the same borehole, is 537 ± 8 ka.

The Bejenado lavas evolved from basanites, at the lower part of the sequence, to mafic tephrites (with several phonolite dykes) at the summit of the volcano and lateral vents. Their total volume can be estimated at around 50 km^3, and the eruptive and growth rates would be as high as 1 km^3/ka and 12 mm/y, respectively.

A good number of volcanic cones that have been attributed to the Cumbre Vieja rift are topped by lavas of the Bejenado and correspond to the late, adventive activity of this volcano. Lava flows interbedded in the sedimentary deposits of El Time in the walls of Bco. de Las Angustias have been dated from 200 to 400 ka (Vegas et al., 1999), ages coherent with the formation of Bejenado volcano and the incision of Bco. de Las Angustias. Ancochea et al. (1994) obtained an age for the same intracanyon Bejenado lavas of 0.71 ± 0.05 ma, clearly inconsistent with the geological and geochronological data described.

The Cumbre Vieja volcano

Eruptive activity has taken place exclusively in the last 123 ka in the southern part of La Palma, in the Cumbre Vieja volcano (see Fig. 8). This last building stage of La Palma formed a 20 km long, 1950 m high and 220 km^2, N-S-trending volcano (Fig. 21). The summit of the volcano is an alignment of eruptive vents and fissures, forming a characteristic rift zone, locally known as *dorsales* (Fig. 21). Most of the emission centres are concentrated on the rift axis, which continues at the southern tip of the rift with a chain of recent submarine volcanoes (see Figs. 5 and 36).

The Cumbre Vieja lavas are from the alkali series (alkaline basalts, basanites, trachybasalts, tephrites and phonolites) and most of the eruptions are strombolian and phreato-strombolian. Phonolitic domes and lava domes of different ages outcrop at the summit and flanks of the rift. The bulk of the sequence is formed of basalts of extreme homogeneity. This feature and the absence of discordances or other stratigraphic markers make it very difficult

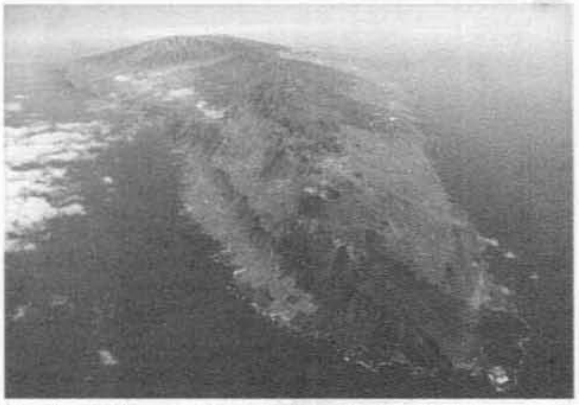

Fig. 21.—Oblique aerial view of the Cumbre Vieja rift volcano (photograph S. Socorro).

to separate volcanostratigraphic units in this volcano. The stratigraphy defined has, therefore, been based significantly on radiometric dating (K/Ar and C^{14}) with a highly restrictive sampling system and a dating technique that has proven useful in lavas only a few thousand years old (Guillou et al., 1996, 1998, 2001). A total of 25 new radiometric ages have been obtained, as indicated in Fig. 7 and Table 1. As discussed above, earlier ages reported for this relatively recent volcano lack the necessary accuracy (see Fig. 6) and only the ages determined by Guillou and co-workers (1998) and Carracedo and co-workers (2001 b) were used to define the volcanostratigraphic units of this volcano. The flanks of Cumbre Vieja, especially the western one, have undergone important marine erosion, giving place to considerably high coastal cliffs. Lava flows from recent eruptions streamed over these cliffs to form coastal platforms (Fig. 22 A). The correlation of the radiometric ages obtained from lavas forming cliffs and those forming coastal platforms indicates that they form distinct chronostratigraphic sequences, the former systematically presenting ages greater than about 20 ka, while the latter yield consistently more recent ages. This feature can be used as an isochrone to define the volcanostratigraphy of the volcano, that coincides with the peak of the last glaciation (Fig. 22 A). The lavas emitted before and during the glacial maximum were eroded to form coastal cliffs, while those emitted subsequently fossilized the cliffs to form coastal lava platforms (Fig. 22 B).

These data and geochronological criteria have allowed the definition in Cumbre Vieja (and in the island of El Hierro, as discussed later) of the volcanostratigraphic units described below, used in the elaboration of the geological map of the island.

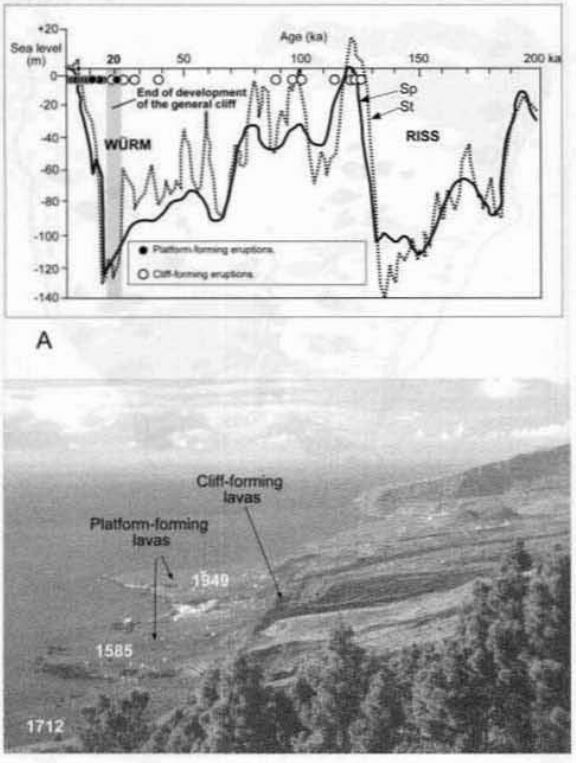

Fig. 22.—A) Correlation of ages of Cumbre Vieja lavas with the low sea level stand in the last glacial maximum and separation of cliff- and platform-forming eruptions. B) View of the western cliff of Cumbre Vieja and the coastal platforms formed by historical (1585, 1712 and 1949) eruptions.

Cliff-forming eruptions

Although these eruptions form the bulk of the Cumbre Vieja volcano, they outcrop mainly in the northwest and eastern flanks, the remainder of the volcano being resurfaced by more recent eruptions. They form a cliff over 100 m high at the NW, decreasing towards the south end of the island and at the eastern flank, correlatively with the progressive decrease in age of the lavas (see Figs. 7 and 21).

The eruptive centres corresponding to this unit are distributed over the entire volcano, forming a scarcely defined multiple rift, with a slight predominance of NW and NE directions from the centre of the rift (Fig. 23). The great part of the emission centres form strombolian cones, but there are relatively abundant phreato-strombolian vents interbedded in the lava sequences at the coastal cliffs, such as the tuff cone of Puerto Naos, on the west coast, and those of Mña. Vento

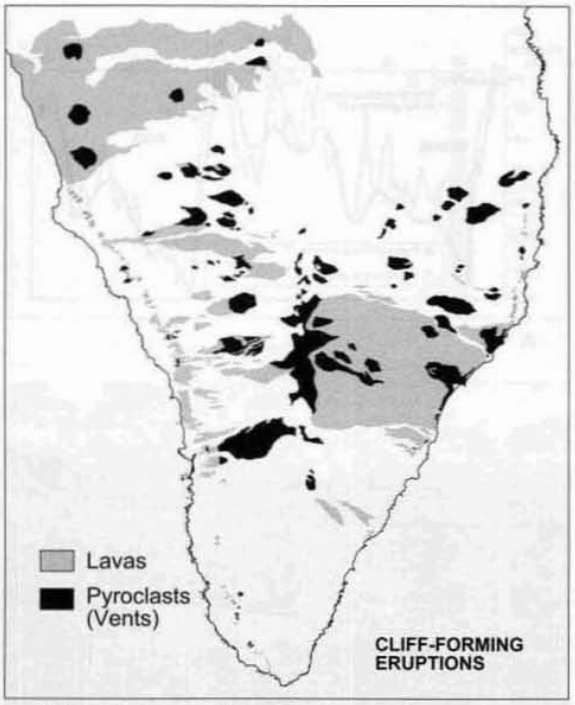

Fig. 23.—Distribution of cliff-forming eruptive vents and lava flows in the Cumbre Vieja volcano.

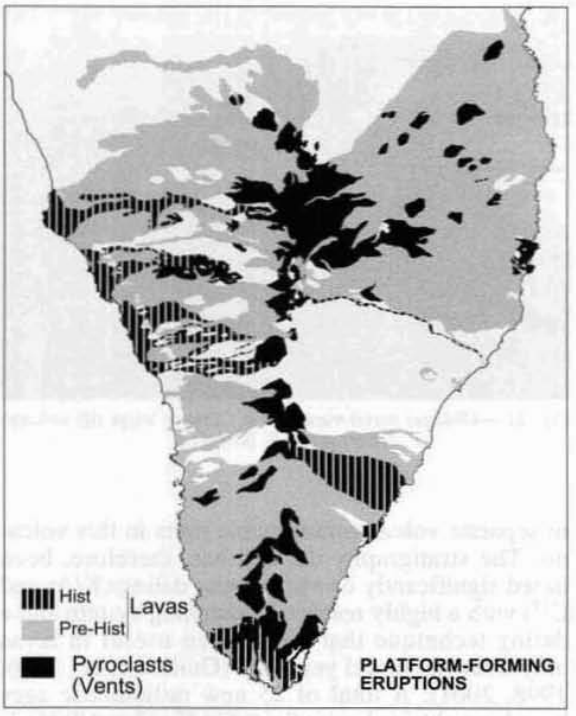

Fig. 24.—Distribution of platform-forming eruptive vents and lava flows in the Cumbre Vieja volcano. Note the reorganization of vents from about 7 ka clustering along the N-S main rift.

and Roque de Guerra to the east. The lavas are basaltic, frequently with high contents of large mafic xenoliths.

Phonolitic domes and lava domes are relatively abundant in Cumbre Vieja, their age ranging from the 56 ka of Roque Teneguía to the 26 ka of Mendo, although others must be considerably older, such as Mña. Enrique, which could not be dated due to the extreme weathering of the rock. The tephri-phonolitic and phonolitic composition of these domes was determined by Hausen (1969) and by Hernández Pacheco and de La Nuez (1983). These last authors interpreted these intrusions to be a single salic Mid-Pleistocene unit forming the basement of the Cumbre Vieja rift. However, the different ages yielded by the intrusions show that they correspond to younger intrusive episodes spread along the whole volcanic history of the Cumbre Vieja rift (see Table 1). Their abundance may reflect, as in Bejenado, the rapid evolution of the magmas of Cumbre Vieja, parallel to their equally fast construction. These salic domes are frequently associated to recent basaltic eruptions, probably because they are highly fractured and provide a pathway for magma to reach the surface.

Platform-forming eruptions

This unit comprises eruptions younger than about 20 ka and was emitted by eruptive centres forming an increasingly concentrated alignment along the N-S axis of Cumbre Vieja (Fig. 24). This reorganization of volcanism in Cumbre Vieja, with a progressive concentration of emission centres in a progressively better-defined rift, is a characteristic feature of the volcanism of La Palma and oceanic volcanic islands in general (Carracedo, 1979, 1984, 1994, 1996, 1999; Walker, 1992), and will be discussed in greater detail in section II.6.

The lava flows of this unit have resurfaced most of the Cumbre Vieja volcano (Fig. 24), frequently forming wide coastal platforms (see Figs. 4 and 22 B). They are predominantly basaltic in composition, although tephrites and phonolitic tephrites abound.

Some groups of volcanoes are noteworthy, such as the tephritic and basaltic-tephritic Mña. Cabrera and Mña. Faro volcanoes built on the summit of the rift 15 and 18 ka ago, respectively. Other interesting volcanoes are the tephritic and phonolitic-tephritic Birigoyo-La Barquita volcanic group, dated in 6±2 ka and forming a pair of volcanoes situated on the

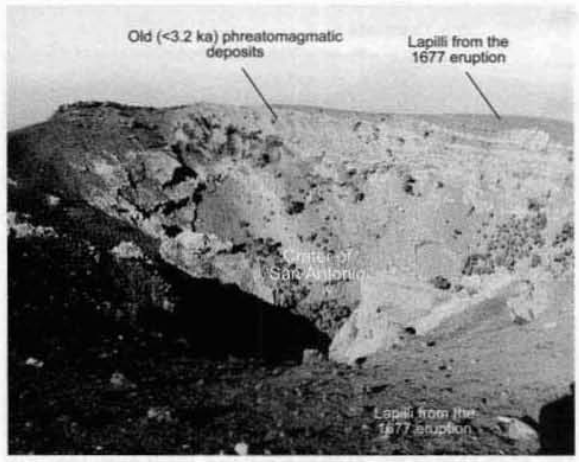

A

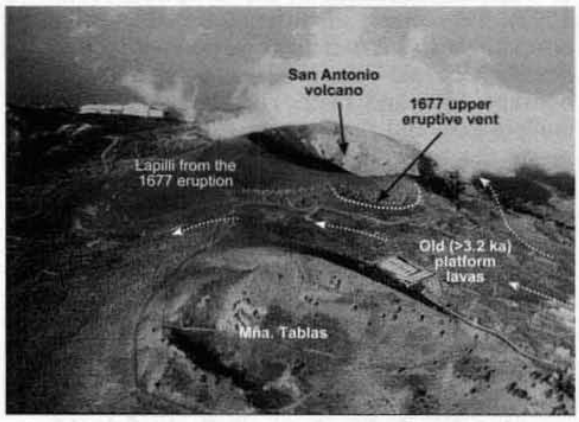

B

Fig. 25.—Views of the prehistorical eruption of San Antonio. A) Crater of the prehistorical San Antonio volcano mantled with pyroclasts of the 1677 Fuencaliente eruption. B) Oblique aerial view of prehistorical lavas older than 3.2 ka encircling the San Antonio volcano.

northern edge of the rift. An especially interesting group is that of the San Antonio-La Caldereta volcanoes, both phreatostrombolian vents located close to the town of Fuencaliente. The San Antonio volcano has been related to the 1677 eruption, although evidence that this eruptive centre, with clear indications of relatively high-energy phreato-strombolian stages, is much earlier than the 1677 eruption, has already been published (Carracedo et al., 1996; Day et al., 2000). This can be synthesized as follows: 1) The cone is surrounded by clearly prehistorical lavas (Fig. 25) dated in 3±2, 4±2 and 3.3±0.1 ka (Guillou et al., 1998); 2) The phreatic stages, with the generation of lateral explosions, must have extended explosive deposits over a wide area around the cone, as can be observed in the La Caldereta vent. However, in the access roadcut to the San Antonio volcano, scarcely 100 m from the cone, the pyroclasts of the 1677 eruption overlie the afore-mentioned prehistorical lavas with no intercalated explosive deposits; 3) Despite the explosivity of the volcano, no important damage to the town, only a few hundred metres distant, is reported in the eye-witness accounts; 4) Remains of an aboriginal settlement have been located on the flanks of the San Antonio volcano (Pais Pais, personal communication); 5) The San Antonio cone appears on a map drawn by Torriani in 1586.

As described later, the true 1677 eruption consists of a small vent resting upon the northern flank of the San Antonio volcano, and several eruptive fissures at the southern base of this volcano, from which abundant lavas were emitted (Carracedo et al., 1996). Pyroclasts from the 1677 and 1971 eruptions covered the San Antonio cone and give it the appearance of a recent volcano. On the other hand, confusion in the identification of eruptions is relatively frequent, even where eye-witness accounts are available (Day et al., 2000). A similar misidentification occurred in La Palma with the 1585 and 1646 eruptions (Hernández Pacheco and Vals, 1982), and part of the 1646 eruption (Carracedo et al., 2001 b).

Dated prehistorical eruptions

Include dated eruptions older than the colonization of the island in 1492 and, therefore, without eye-witness reports, as well as those initially considered to be historical and later found to be earlier (see Table 1).

Malforada-Nambroque. This group of cones and emission centres is situated at the summit of the rift, overlying a large and fractured salic lava dome (Fig. 26 A). Both the Malforada and Nambroque groups are apparently similar in age and composition, although only the Nambroque lavas have been dated, with C^{14}, giving an age of 1045±95 years (Carracedo et al., 1999 a). The lavas of both eruptive centres vary from phonolitic tephrites to phonolites, with very thick, short-reaching lava flows (Fig. 26 B).

An interesting aspect of this eruption is the discovery of a burial site containing human and archaeological remains consisting of pottery and partially carbonized human bone fragments, dated by C^{14} in 1090±50 years, embedded in spatters. An analysis

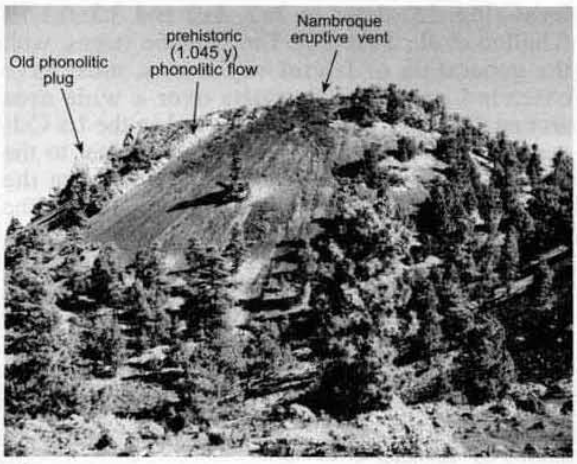

A

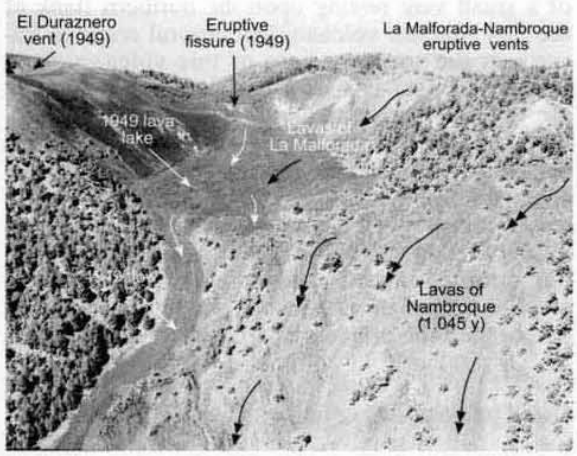

B

Fig. 26.—Views of the prehistorical Nambroque-Malforada volcanic group. A) Main eruptive centre of the Nambroque eruption (916 AD) showing the pre-existing phonolitic plug and the prehistorical vent and lavas. B) Oblique aerial view of the 1949 basaltic lavas cascading over the Malforada and Nambroque phonolite lavas.

of the recent eruptions of Cumbre Vieja pointed to the Nambroque eruption*.

Mña. Quemada-Martín Volcano. The eruption that gave place to the volcanic cone of Mña. Quemada (Fig. 27), very recent in appearance and located at the northern end of the Cumbre Vieja rift, has been mistaken for that of 1585 on the basis of inter-

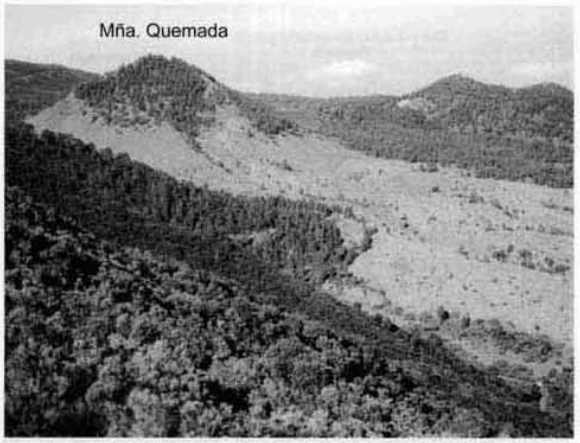

Fig. 27.—View of the prehistorical (circa 1480) Mña. Quemada volcano.

pretation by Santiago (1960) and Machado (1963) of Torriani's account of this eruption (Torriani, 1592). The correct identification of this eruption, also known as Tacande, was carried out by Hernández Pacheco and Vals (1982), who dated it by C^{14} at between 1470 and 1492. The lavas are basaltic in composition and flow towards the north and west inside the Valle de Aridane, stopping about 2 km from the western coast.

A similar confusion seems to have arisen with the 1646 eruption, in which the interpretation of eye-witness accounts led to the inclusion in this eruption of a group of cones and lava flows, the Martín volcano group, that seem to correspond to a prehistorical event. This group of volcanic cones, tightly clustered on the axis of the rift, is topped with phreatostrombolian ash, providing evidence of explosive eruptive episodes. Attached to the south flank of the Martín volcanic group is a lineament of vents and hornitos issuing abundant lavas towards the coast, unambiguously assigned to the 1646 eruption. The reasons for separating the Martín group, as prehistorical, from the 1646 eruption, are based on the fact that only those that are believed to be prehistorical are covered with phreatomagmatic ash related to the final explosive stages of the Martín vents. The lavas are colonised by a relatively well-developed plant association, absent from any of the historical eruptions of La Palma, and prehistorical archaeological remains were found inside lava tubes of this volcanic group (Pais Pais, personal communication).

Historical eruptions

This unit comprises the eruptions that occurred in the last 500 years, the historical period of the

* Studies in progress indicate the phreato-strombolian eruption of Montaña Goteras, close to the burial site and an important prehistorical dwelling, to be of similar composition to the spatter englobing the human bones dated at 866 AD, and therefore the most probable age for this prehistorical eruption.

Canary Islands, and all are documented by eye-witness accounts. They frequently present a number of common features, such as the above-mentioned association with fractured phonolitic domes, that act as favoured paths for the magma, and the presence of multiple eruptive vents in a single eruption, frequently along several kilometres long fissures, several of them oblique to the axis of the rift. These vents are predominantly explosive at the summit area (White and Schmincke, 1999) and effusive at the flanks (Klügel et al., 1999).

The duration and other characteristics of the historical eruptions of La Palma have been summarized in Hernández Pacheco and Vals (1982).

XVIth Century Eruptions. Only one eruption, the Tahuya, Tajuya or Jedey eruption, took place in La Palma during this century. It is described in an account by Torriani (1592), who witnessed it. A detailed study of this eruption appeared in the work of Hernández Pacheco (1990) and Hernández Pacheco and Vals (1982).

The 1585 eruption includes several cones and emission centres situated over an old phonolitic dome (Fig. 28), located above the village of Jedey, on the western flank of Cumbre Vieja rift. The lava flows cascade down the coastal cliffs towards the sea, forming wide coastal platforms at the shoreline (see Fig. 22 B). An interesting feature of this eruption is that juvenile phonolite lavas were emitted along with basaltic flows, the former intruded as domes and cryptodomes because of their extreme viscosity. These phonolites differ from those corresponding to the older dome over which the eruption took place. The pressure of the lava seems to have lifted the old phonolites to form spines, in a process reported by Torriani (1592) as accompanied with strong seismicity. Falling phonolite blocks appear englobed in the 1585 basaltic flows and show magmatic assimilation and dissolution features.

XVIIth Century Eruptions. Two eruptions took place in La Palma in this century, in 1646 and 1677.

The 1646, Tigalate or Martín eruption has eye-witness accounts (Santiago, 1960) reporting two eruptive centres: the upper one at the flank of the prehistorical Martín volcano and the lower vent at the coast (see geological map). Both formed conelets and hornitos and emitted very fluid basaltic lavas.

The 1677 eruption, erroneously associated to the older San Antonio volcano, as already discussed, has been described by Carracedo and co-workers (1996) as having two eruptive vents: the upper, strombolian vent, located at the northern flank of the San Antonio volcanic cone (Fig. 29 A), and the lower vent, which comprises several spatter hornitos along a NW-SE eruptive fissure at the southern

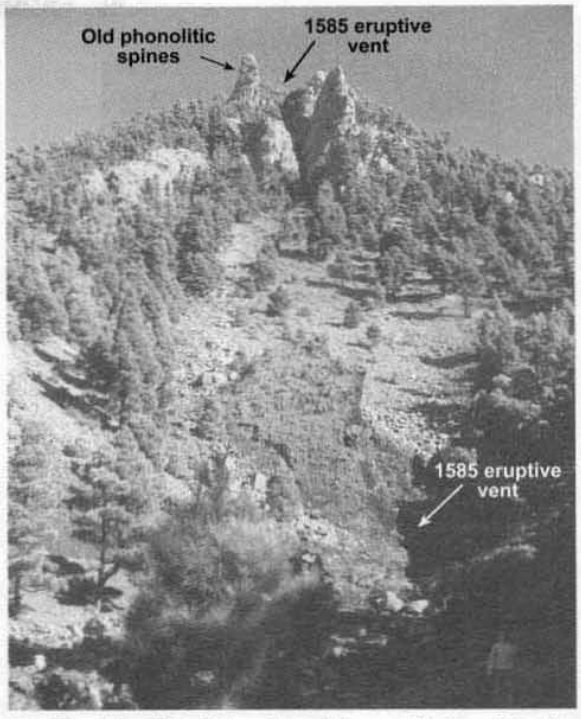

Fig. 28.—The Mña. Jedey, formed by an old phonolitic plug mantled by the vents and lavas of the 1585 eruption.

flank of the San Antonio cone (Fig. 29 B). The latter vent emitted several lava flows that formed an extensive coastal platform. A contemporary picture depicts a recumbent human figure and some livestock lying on the ground (circle in Fig. 29 C), possibly asphyxiated by volcanic gases during the eruption, a rare document illustrating human casualties in relation to volcanic events.

XVIIIth Century Eruptions. Only the 1712 or El Charco eruption occurred in this century. This eruption, poorly documented with eye-witness accounts (Santiago, 1960), comprises a large cinder cone (Mña. Lajiones, Fig. 30 A) and several eruptive vents aligned in a NW-SE, 2.5-km-long eruptive fissure from which several lava flows cascaded down the western cliff to form a wide platform (Fig. 30 B).

XXIth Century Eruptions. The last two eruptive episodes of La Palma, in 1949 and 1971, are the best studied and documented. The 1949 event, which occurred after a very long quiescence period (237 years), has been described by Bonelli Rubio (1950), Romero Ortiz (1950), Benitez Padilla (1951), San Miguel et al. (1952), and Martel San Gil (1960). Recent detailed studies include those of

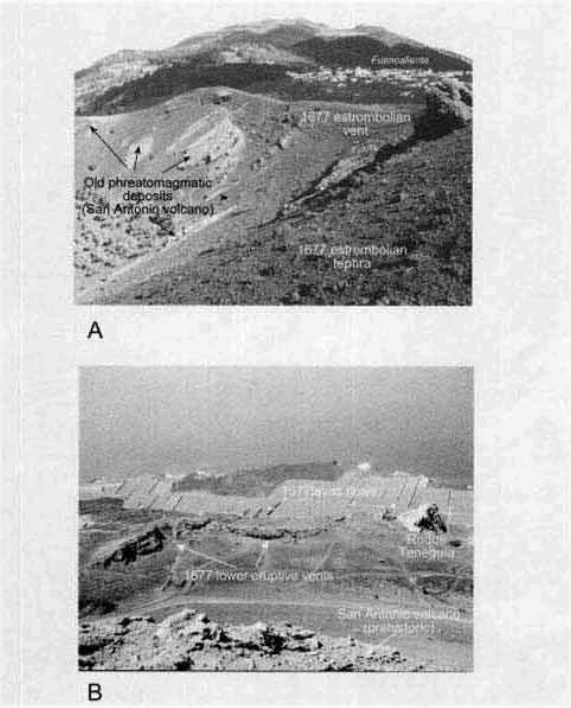

Fig. 29.—View of the southern end of the Cumbre Vieja rift with the upper strombolian vent of the 1677 Fuencaliente volcano mantling the prehistorical San Antonio volcano, the latter showing phreatic surge deposits. B) Lower fissure vents and lava platform of the 1677 eruption. C) Contemporary painting of the 1677 Fuencaliente eruption. Note the recumbent human figure and livestock, indicating casualties (apparently asphyxiated by volcanic gases) in this eruptive event.

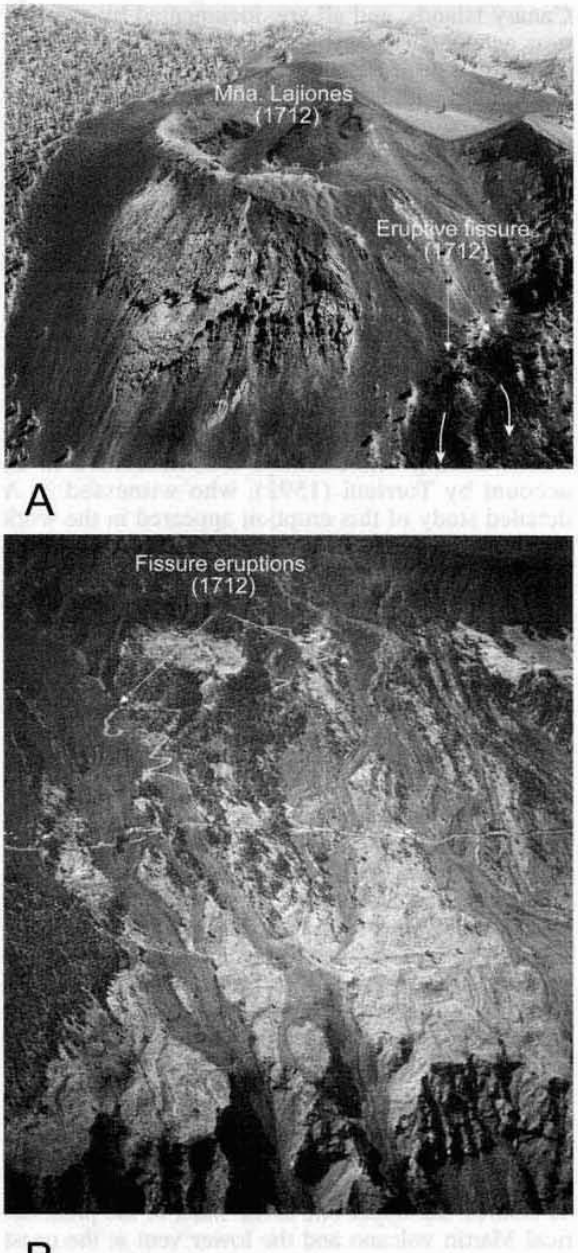

Fig. 30.—Aerial views of the 1712 eruption. A) The main strombolian and phreatostrombolian vent of Mña. Lajiones and the eruptive fissures of 1712. B) Flows from the western eruptive fissures cascading over the cliff at El Remo-Puerto Naos.

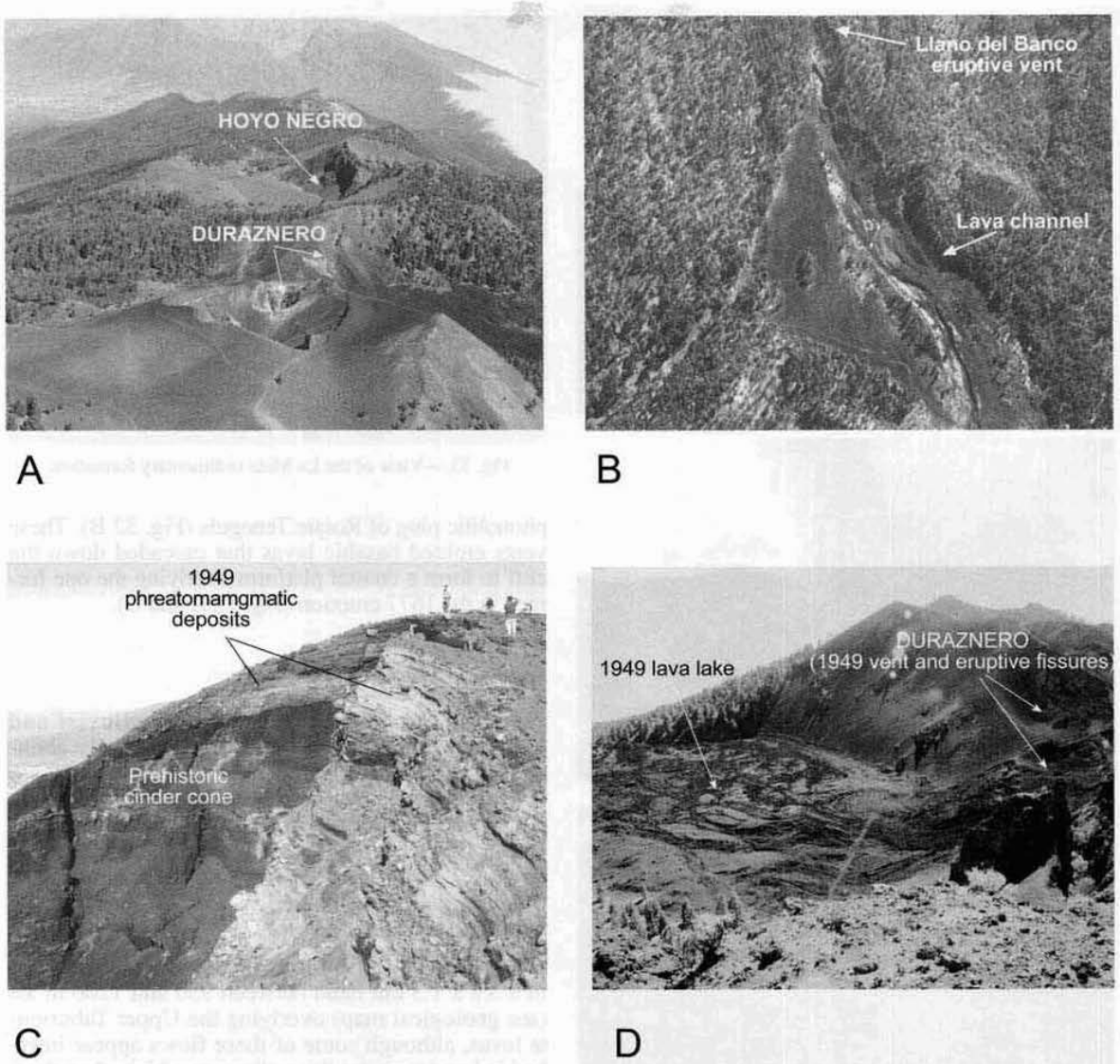

Fig. 31.—Views of the different vents of the 1949 eruption. A) Oblique (from the south) aerial view of the Duraznero and Hoyo Negro 1949 vents. B) Aerial view (from the west) of the Llano del Banco vent and lava flows. C) Phreatomagmatic deposits of the 1949 Hoyo Negro vent mantling a prehistorical strombolian cone. D) Eruptive fissure and lava lake of the 1949 Duraznero emission centre.

Klügel (1998), Klügel et al. (1997, 1999), White and Schmincke (1999), and Day et al. (1999).

Three eruptive vents opened in different phases of this eruption along a 2-km lineation (Klügel et al., 1999). The upper ones, Hoyo Negro and El Duraznero, are located at the summit of the rift in a N-S trend (Fig. 31 A), while the lower one, the Llano del Banco vent opened at 1300 m asl at the western flank (Fig. 31 B). The Hoyo Negro vent was essentially explosive (Fig. 31 C), with several phreatomagmatic phases (White and Schmincke, 1999). Contrarily, the El Duraznero and Llano del Banco vents were predominantly effusive, the former emitting basaltic lavas that formed a lava lake (Fig. 31 D) and descended the eastern flank to a few metres from the coast. The lower vent discharged large volumes of very fluid basaltic lavas that formed a 6 x 3.5-km coastal platform (Fig. 22 B).

The 1971 eruption, the last to occur in La Palma and in the Canaries, has been described in detail in a special volume of Estudios Geológicos (Teneguía volcano, Estudios Geológicos Spec. vol., 1974)

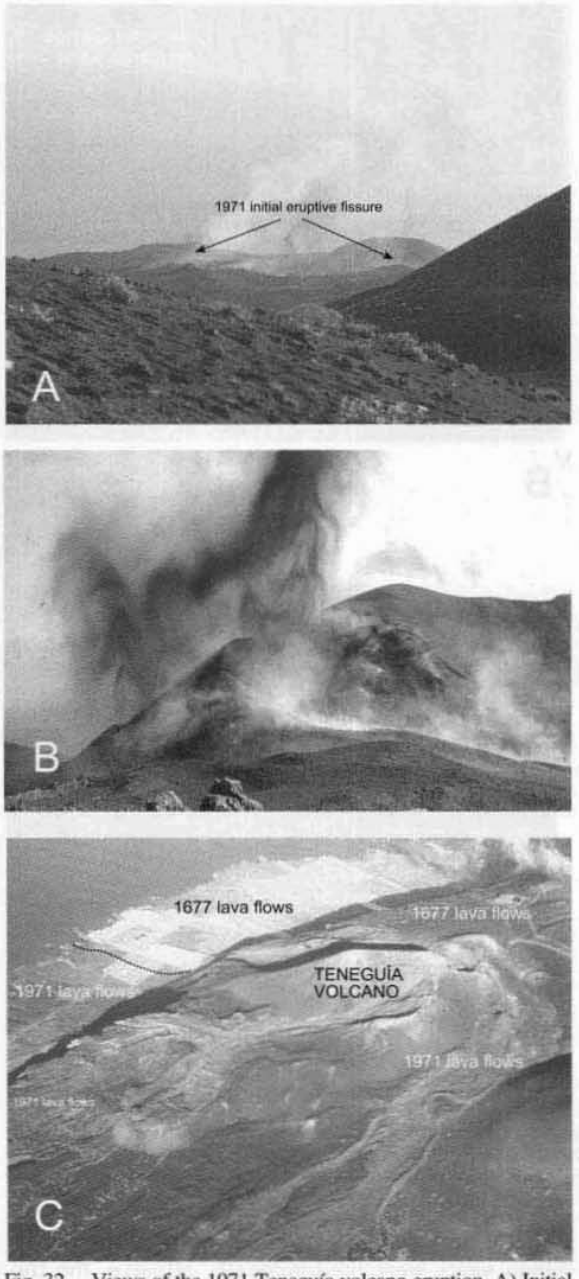

Fig. 32.—Views of the 1971 Teneguía volcano eruption. A) Initial eruptive fissure activity. B) Strombolian vents. C) Oblique aerial view (from the SE) of the group of strombolian cinder cones and lava flows of the 1971 Teneguía volcano eruption. The 1949 coastal platform formed over the previous 1677 coastal lava platform.

Praegel (1986). The eruption started as an eruptive fissure (Fig. 32 A), which progressed to form a group of cinder cones located close to the lower eruptive vents of the 1677 eruption, and both, to the fractured phonolitic plug of Roque Teneguía (Fig. 32 B). These vents emitted basaltic lavas that cascaded down the cliff to form a coastal platform overlying the one formed in the 1677 eruption (Fig. 32 B and C).

Fig. 33.—View of the La Mata sedimentary formation.

Sedimentary formations

Sedimentary formations, such as alluvial and beach deposits, aeolian sands, etc., relatively abundant in the older, posterosional eastern islands, are of little significance in the juvenile islands of La Palma and El Hierro. Interesting exceptions, however, are the thick and extensive sedimentary formations of El Time and La Mata, at the mouth of the Caldera de Taburiente and in the NW flank of the northern shield, respectively.

Sediments of La Mata. This formation outcrops in a 3.5 x 1.5 km band between 950 and 1200 m asl (see geological map) overlying the Upper Taburiente lavas, although some of these flows appear interbedded and capping the sediments which, therefore, can be located in the Pleistocene.

This deposit, which can be observed in cuts of the northern road above La Mata, shows different facies with gradual lateral changes. The most common is a several metres thick matrix supported conglomerate of rounded to subangular clasts, sometimes exceeding 1 m in diameter and predominantly basaltic (Fig. 33). The structure is predominantly massive with poor reverse grading in places and interbedded alluvial layers. The matrix is clay without traces of volcanic ash. These features suggest a complex mix of massive debris-flows and alluvial deposits.

Sediments of El Time. This sedimentary formation is located at the mouth of the Barranco de Las Angus-

tias and extends upriver to the area of La Viña (see geological map). This thick (up to 300 m) succession of poorly sorted conglomerates (Fig. 34 A and B) appears attached discordantly to the Upper and Lower Taburiente lava sequences, and interbedded with the Bejenado volcanics. It was first reported by Lyell (1855) and many other authors thereafter, but the first detailed analysis was carried out by Vegas and co-workers in 1999 and Carracedo and co-workers in 2001. The former authors defined two main units: a volcanic Pyroclastic Unit and a sedimentary Epiclastic Unit. This interpretation has been questioned by the latter authors, who constrain the volcanic pyroclasts to a parasitic vent of the Bejenado volcano, the El Time formation being exclusively made of sediments, as previously generally interpreted.

The genesis of the epiclastic unit is related to *fan delta* deposition (Vegas et al., 1999), prograding in only a few kilometres from the coast to depths of about 4000 m. Subsequent coastal regression favoured the progressive incision of the Bco. de Las Angustias. This process explains why the clasts of the lower part of the sediments are predominantly volcanics of the Taburiente and Bejenado volcanoes, and why clasts corresponding to the submarine lavas and associated intrusives only appear in the upper part of the sequence.

Beachrocks. Beachrocks have been located along the SW coast of La Palma, from Punta Naos to Fuencaliente (Calvet et al., in press). They are formed by sand to gravel size sediments in different stages of carbonate cementation, on the beaches of Punta Naos, Charco Verde, Las Zamoras, Chica and Echentive, developed on platform-forming lavas of the Cumbre Vieja volcano (see geological map).

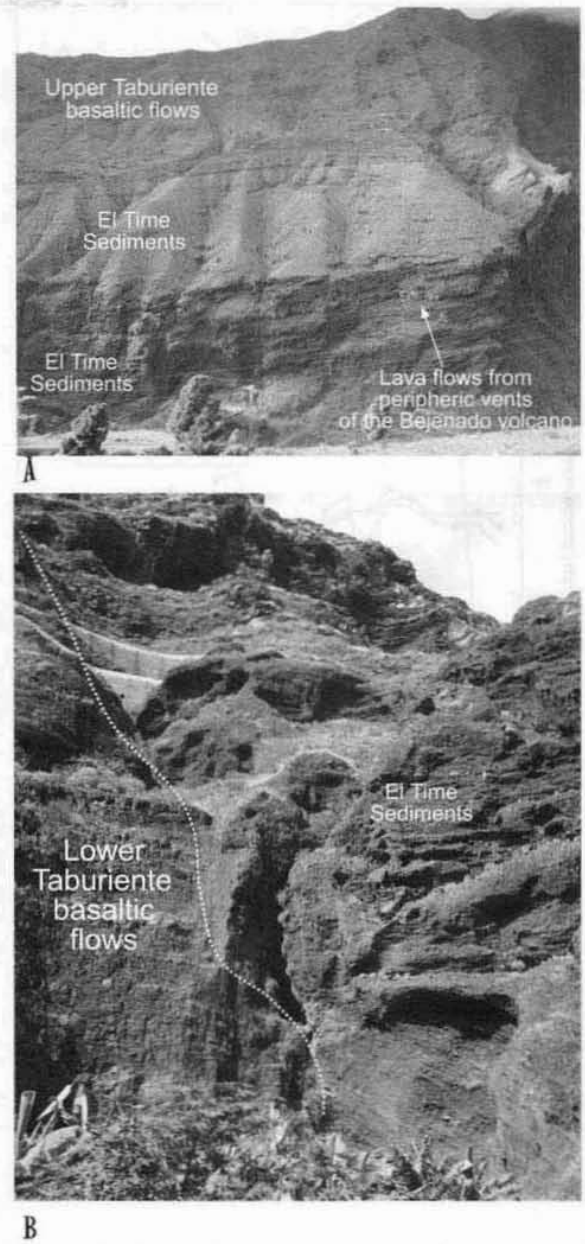

Fig. 34.—Sediments of El Time. A) Epiclastic formations of El Time with interbedded lava flows of the Bejenado volcano outcropping in the western wall of the Caldera de Taburiente. B) Close-up of the sediments of El Time, attached unconformably to the Lower Taburiente volcanic sequence at the western wall of the Caldera de Taburiente.

Petrology and geochemistry

Submarine volcano

The petrographic characteristics of the pillow lavas, pillow breccias and hyaloclastites that form the submarine volcano have been analysed by Hernandez-Pacheco and Fernandez Santín (1974), Staudigel (1981), Staudigel y Schmincke (1984), and in the MAGNA of Northern La Palma (Carracedo et al., 2001a). These lavas comprise different types of basalts, grading from plagioclase basalts to doleritic basalts (oceanites-ankaramites), in relation to the relative content of plagioclase and olivine-pyroxene and textural characteristics (Hernandez-Pacheco and Fernandez Santín, 1974; Staudigel and Schmincke, 1984).

These basalts are strongly altered by metasomatism, giving place to new paragenetic sequences (albite, clorite, epidote, actinolite, andradite, zeolites and calcite), as well as by propylitization, possibly as a result of the different intrusions (Hernandez-Pacheco and Fernandez Santín, 1974; Staudigel, 1981; Staudigel and Schmincke, 1984; De La Iglesia et al., 1996).

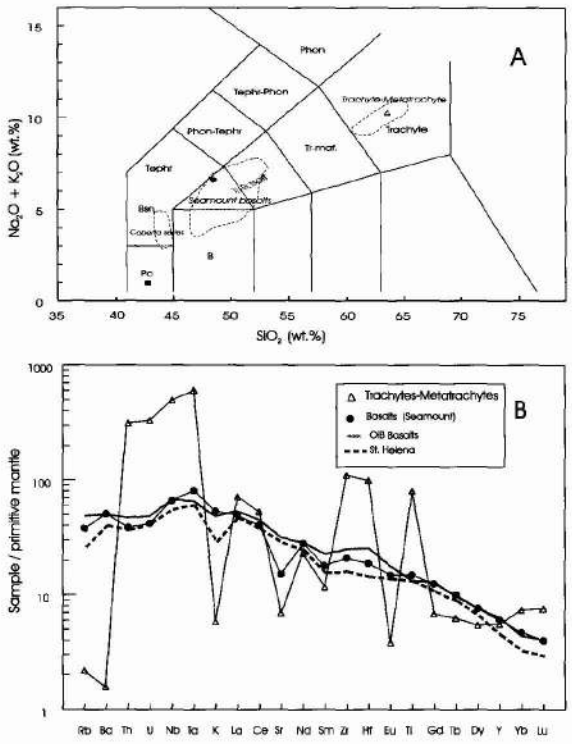

Fig. 35.—A) Total Alkali vs. Silica (TAS) diagram for submarine lavas and trachytic domes. The limits are from Hernández Pacheco and Fernandez Santín (1974), Staudigel and Schmincke (1984). The boundaries are from Le Bas et al. (1986). B) Primitive mantle normalized diagram (Sun and McDonough, 1989), for incompatible trace elements of seamount basalts and trachytes. The OIB data and primitive basalt from St. Helena, are taken from Sun and McDonough (1989).

The pyroxene-plagioclase basalts forming the pillow lavas in the Barranco de Las Angustias (Table 2-1, Sample-95) plot in the TAS diagram of Fig. 35A in the basalt-trachybasalt field, clearly separated from the oceanitic-picritic terms (Hernandez-Pacheco and Fernandez Santín, 1974). Their primitive mantle normalized values are close to the mean values of many other oceanic volcanoes (OIB) and St. Helena HIMU basalt, as proposed by Sun and McDonough, 1989 (Fig. 35B).

Intrusive formations

Trachytic domes and lava domes. Mainly made of breccia fragments with flowage textures (Hernandez-Pacheco and Fernandez Santín, 1974), they were termed as metatrachytes by Staudigel and Schmincke (1984) because they frequently appear altered to albite, biotite, clorite and epidote.

These intrusives (Table 2-1, Sample 105) are grouped in the trachyte field in the TAS diagram of Fig. 35A. However, they show important elemental variations, as shown in Fig. 35B, probably due to metasomatism. Staudigel and Schmincke (1984) emphasized the significant enrichment in incompatible elements, as shown by the low content in Rb and Ba. Another interesting feature is the high positive anomalies (Th, U, Nb, Ta, Zr and Hf), negative anomalies (K, Sr, Eu), and enrichment in heavy rare earth elements (HREE).

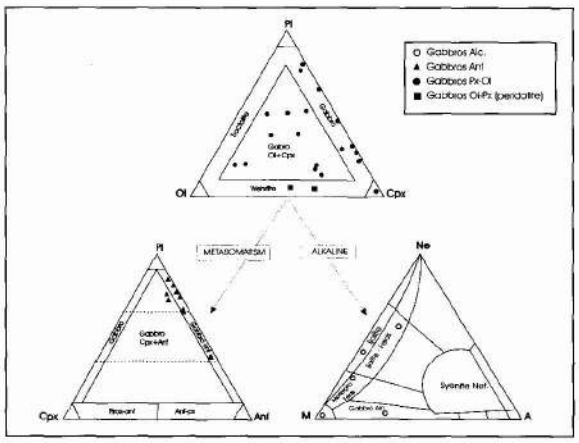

Fig. 36.—Modal composition of intrusive gabbros inside the Caldera de Taburiente. Data from De La Nuez (1984).

Gabbros. De La Nuez (1984) and Carracedo et al. (2001) confirmed the petrological and geochemical variability of the plutonic intrusions inside the Caldera de Taburiente. The former author separated two different groups: «Gabbros» and «Olivine gabbros» (De La Nuez, 1984, Table 7 and Fig. 85). The composition and alteration processes of representative plutonic samples obtained inside the Caldera in the MAGNA of Northern La Palma by Carracedo and co-workers (2001) are shown simplified in Fig. 36.

Gabbro plutonics outcropping inside the Caldera, clearly independent of the seamount and most probably related to the feeding of the subaerial volcanoes (Table 2-1, Samples 103-104-108), have been separated in the MAGNA (Carracedo et al., 2001) and in the geological map from those intruding the seamount (Table 2-1, Samples 96,59,98,109). As shown in the plots of Fig. 37A and 37B, the petrological characteristics are less discriminating than field observations, mainly because of the wide range of compositional variation of the rocks. However, these younger gabbros clearly differ in the lack of significant hydrothermal alteration.

Dyke swarms. The significant petrological and geochemical diversity of the different dyke swarms has been quoted by many authors (Hernández Pacheco, 1975; Staudigel, 1981; Staudigel and Schmincke, 1984, Staudigel et al., 1986; De La Nuez, 1984, 1991; Carra-

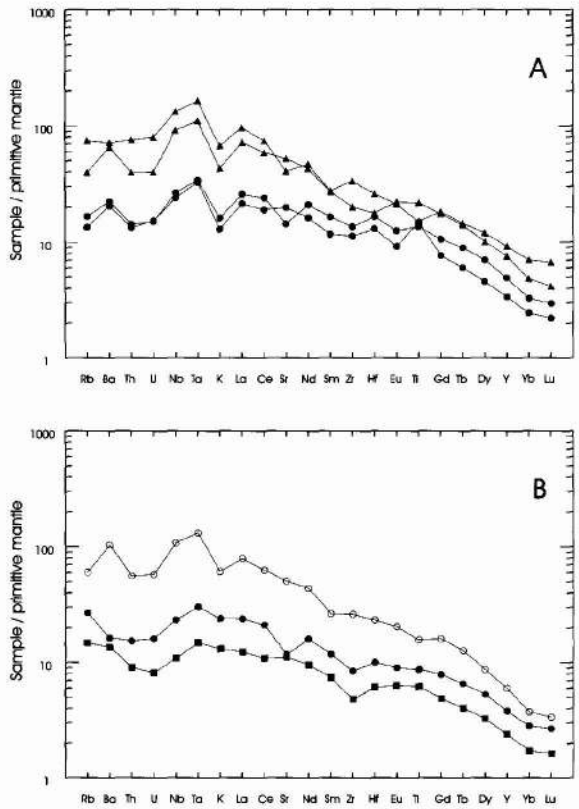

Fig. 37.—A) Primitive mantle normalized diagram (Sun and McDonough, 1989) of incompatible trace elements of intrusive gabbros intruding the seamount. B) Idem from gabbros postdating the seamount and feeding the subaerial volcanoes. The primitive mantle element concentrations are from Sun and McDonough (1989). Symbols as in Fig. 36A.

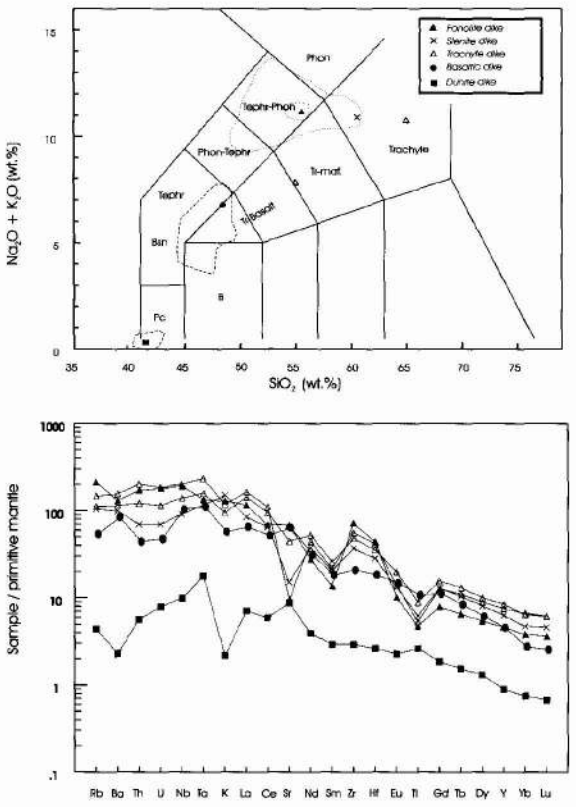

Fig. 38.—A) TAS diagram for intrusive dykes inside the Caldera de Taburiente. The limits are from Hernández Pacheco and Fernández Santín (1974), and Staudigel and Schmincke (1984). The boundaries are from Le Bas et al. (1986). B) Primitive mantle normalized diagram (Sun and McDonough, 1989) for incompatible trace elements from dykes inside the Caldera de Taburiente.

cedo et al., 2001). As shown in the TAS diagram of. 38A, basaltic dykes are predominant with respect to trachytic and phonolitic, with fewer syenite and dunite intrusives (Hernández Pacheco, 1974, 1975).

The geochemical characteristics of representative samples of the different types of dykes are shown in Table 2-1 (samples 102 a 181) and Fig. 38B, where the dunite dykes separate because of the lower elemental content from the other groups of more differentiated intrusives. The latter show significant enrichment in REE and incompatible elements, with Zr and Hf positive anomalies and negative Ti, Sm and Sr, the latter absent in the phonolitic dykes.

The Northern Shield

The Garafia Volcano. Lavas from this volcano are mainly olivine-pyroxene and olivine-pyroxene-plagioclase alkali basalts, the former presenting frequently porphyritic to aphyric (trachytoid) textures and subophitic the later. The olivine-pyroxene-plagioclase basalts form the bulk of the earlier stages of the volcano and outcrop in the headwall of the deep northern barrancos and inside the galería Los Hombres.

Many of the samples (Table 2-2, samples 77, 80, 157, 172) with primary characteristics (Mg#> 60 and Ni > 200-300 ppm) plot in the basaltic field, whereas the more evolved samples plot in the trachybasaltic field (Fig. 39A). The elemental variation diagram of Fig. 39B evidences a progressive increase in elemental content, from the less enriched olivine-pyroxene-plagioclase basalts to the trachybasalts, but with clear subparalle trends. Some significant differences can be observed when the normalized values (Sun and McDonough, 1989) of the primitive basal from St. Helena (Mg# ~ 65) are shown for comparison. The highly incompatible elements presenting uniform subparallel trends, with progressive increments and marked positive (Rb, Ba, Th and U) anomalies

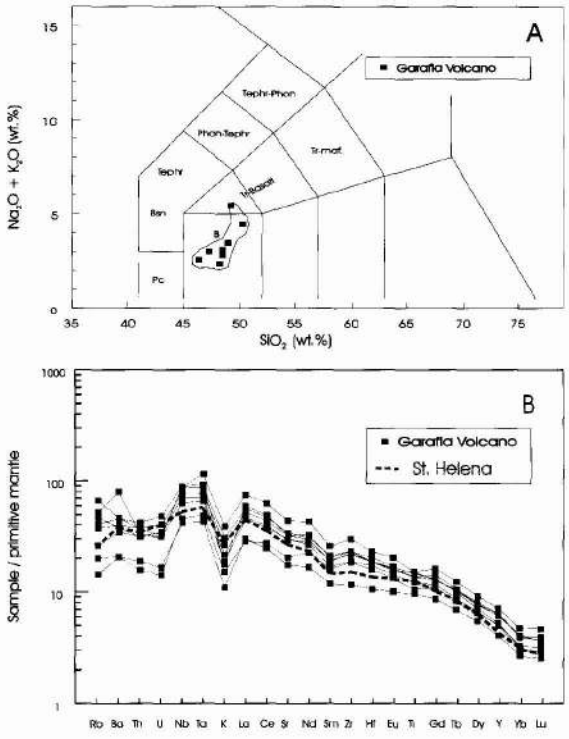

Fig. 39.—A) TAS diagram from basaltic lavas of the Garafía volcano. Boundaries from Le Bas et al. (1986). B) Primitive mantle normalized diagram (Sun and McDonough, 1989), for incompatible trace elements from basaltic lavas of the Garafía volcano. The data of a primitive basalt from St. Helena, are taken from Sun and McDonough (1989).

towards the more differentiated terms. Similarly, light rare earth element (LREE) and Zr enrichment is progressive from the ol-px basalts to trachybasalts, with K and Sm showing negative anomalies. The lesser importance of feldspars is evidenced by the normal values of Eu. Analogous HREE progressive enrichment can be observed, trends with similar subparallel coinciding with St. Helena values.

Elemental variations are shown in the plots of Fig. 40. Variations of major elements in the Garafía volcano lavas are constrained by MgO content, with minor increment of SiO_2, Fe_2O_3t, TiO_2 y P_2O_5, and a better definition of decrements in CaO/Al_2O_3 towards the more differentiated terms (MgO < 8%). Decrement patterns in compatible elements Ni, Cr, Co and Sc may be in relation to the fractionation of ferromagnesian components.

The Taburiente volcano. The entire Taburiente volcano presents similar compositional trends, with prevalent alkali basalt to trachybasalt lavas. However, a clear diversification towards basanites-tephrites can be observed as the volcano developed, culminating in the terminal stages of the Upper Taburiente with the emission of more differentiated tephri-phonolitic lavas.

The Lower Taburiente sequences outcropping in the lower part of the Caldera de Taburiente show a remarkable petrographic uniformity, predominantly olivine-pyroxene basalts. Outcrops in the slopes and deep barrancos of the northern shield are frequently aphasic trachytoid basalts.

The Upper Taburiente volcano lava sequences are more complex, with abundant ol-cpx, ol-cpx-plg and amphibole basalts. Phonolitic tephrites and phonotephrites are the typical terms in the differentiated lavas of the terminal stages of the Upper Taburiente volcano. A representative lithologic section is the northern wall of the Bco. Jurado, where the volcanic sequence is made from bottom to top of ol-px basalts—ol-px-plg basalts—amphibolic basalts—mafic haüyne tephrites. The latter outcrop as well along the Caldera de Taburiente rim (see geological map), with diverse mineralogical and textural characteristics giving place to different typologies (mafic tephrites, phono-tephrites and trachyphonolites) .

An interesting type of rock is related to the hydromagmatic eruptive vent of La Galga, north of Puntallana, a welded-tuff type of ignimbrite, with abundant subrounded clasts of basalts; fragments of inclusions of pyroxene and clinopyroxene crystals, oxidized olivine and opaque minerals; and juvenile crystals of biotite and amphibole. The ensemble is cemented by a hypo-microcrystalline groundmass with abundant vesicles filled with zeolite and carbonates.

Geochemical features of the Taburiente volcano. The analytical data from representative lavas of the Taburiente volcano, shown in Tables 2-3 to 2-5, indicate the nearly primary character (Mg# > 60, Ni (>200 ppm) of the Lower Taburiente lavas, in contrast with the consistently more evolved and differentiated characteristics of the Upper Taburiente ones. These features are consistent with the uniform trends observable for the entire sequence in the elemental variation vs. MgO% plots of Fig. 40, with the only exception of an interruption in the range of ~ 8% MgO, very similar to that described for the Garafía volcano. The evident drop in Cr and Ni content in the range of MgO < 6% may reflect the important role of olivine and clinopyroxene fractionation. The major elements show a general decrease in these diagrams in SiO_2 vs. MgO%, in contrast with the general positive trends in the remaining major elements (CaO/Al_2O_3), Fe_2O_3t, TiO_2 and P_2O, even for MgO < 6%. These features suggest fractionation of clinopyroxene and Fe-Ti oxides in the entire sequence for MgO < 6%, possibly associated to apatite segregation in the more differentiated tephri-phonolite lavas.

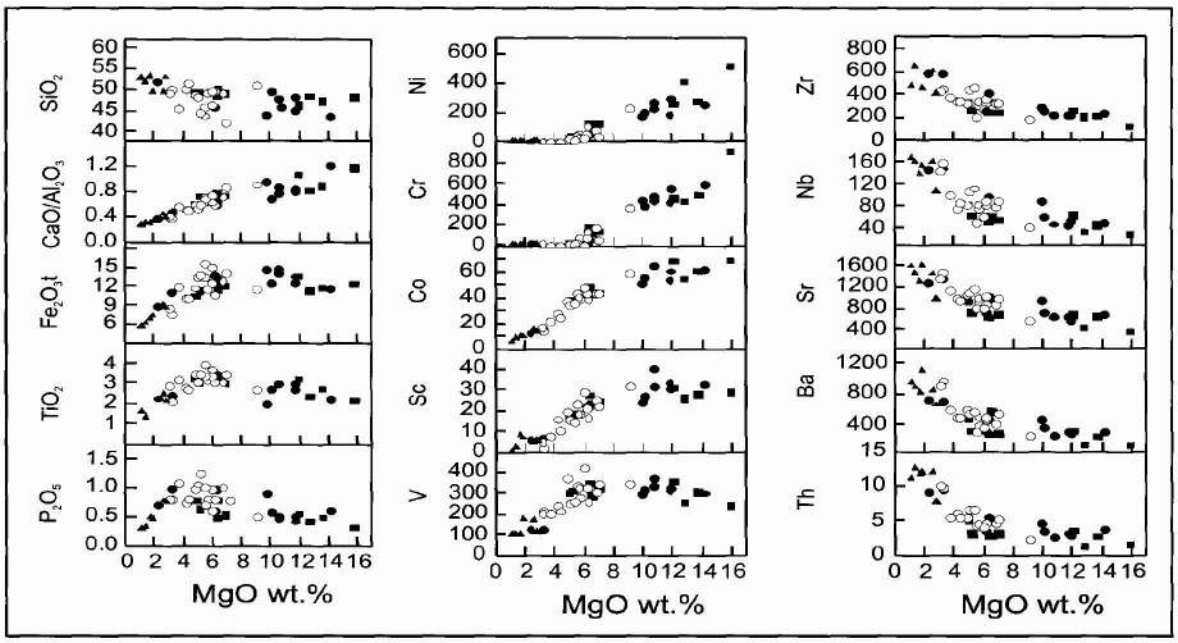

Fig. 40.—Variation diagrams for major, trace and REE elements for the Garafía and Taburiente volcano. Symbols as in Figs. 39 A and 41.

The TAS diagrams of Fig. 41A evidence these compositional variations in the entire Taburiente volcano. The Lower Taburiente volcano lavas plot mainly in the basalt field, with deviations towards the subsaturated basanitic terms in the sequences of the lower part of the Caldera de Taburiente wall and lesser representation of more differentiated trachybasalt and phono-tephrite lavas. The Upper Taburiente lavas overlap this succession, with a distinct tendency towards the basanite-tephrite fields. The more differentiated samples group in the phono-tephrite and tephri-phonolite fields, corresponding, as mentioned, with the terminal differentiated eruptions of the northern shield. Similar tendencies towards progressive differentiation in the Taburiente volcano can be concluded from the sequential overlapping of the normalized diagrams in Fig. 41B. The Lower Taburiente lavas show normalized values, Sun and McDonough (1989), with similar subparallel trends to the St. Helena and significantly higher than those corresponding to the Garafía volcano (see Fig. 39B).

The terminal eruptions of the late stages of development of the Taburiente volcano seem to be, therefore, the culmination of the differentiation process of a period of continued magmatism along the entire construction of the northern shield. This conclusion is consistent with the homogeneity of the geochemical features and the geological observations. Initial ol ± cpx ± mt-ti crystal fractionation and apatite segregation, in the more differentiated lavas, seem the main processes involved, resulting in a progressive increment in the more incompatible elements.

The Bejenado volcano. As described before, this stratovolcano developed extremely rapidly, nested in the embayment originated in the collapse of the Taburiente volcano. The patterns of differentiation observed during the entire construction of the northern shield are presented here in a very short time, probably less than about 50 ka. In this period the sequence evolved from initial basanitic rocks to differentiated lavas in the latest stages.

The bulk of the stratovolcano is made of olivine-pyroxene and pyroxene-amphibole basalts, with typical porphyritic textures. In contrast, the terminal differentiated vents erupted mainly tephrites and mafic haüyne phonolites, with subordinate haüyne-nepheline foidites. Textures are typically porphyritic, with dominant mafic minerals and less abundant feldspar —feldspathoids in a hypo— to microcrystalline groundmass with flowage patterns. The tephrites with foiditic trends are scant, and show an association of large nepheline phenocrystals, microcrystals of haüyne and abundant inclusions, in a hypocrystalline groundmass of clinopyroxene, opaque minerals and subidiomorfic feldspathoids.

The dykes and sills outcropping in the summit of the Bejenado volcano show the most evolved rocks of the entire volcano, typically mafic phonolites with predominant feldspar phenocrysts and subordi-

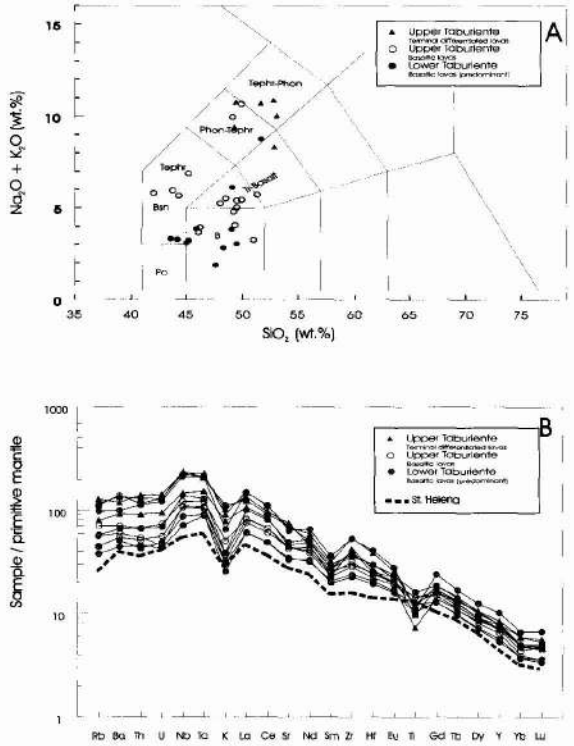

Fig. 41.—A) Total alkali vs. silica (TAS) diagram for the Taburiente volcano. Boundaries from Le Bas et al. (1986). B) Primitive mantle normalized diagram (Sun and McDonough, 1989), for incompatible trace elements for the Taburiente volcano. The data of a primitive basalt from St. Helena are taken from Sun and McDonough (1989).

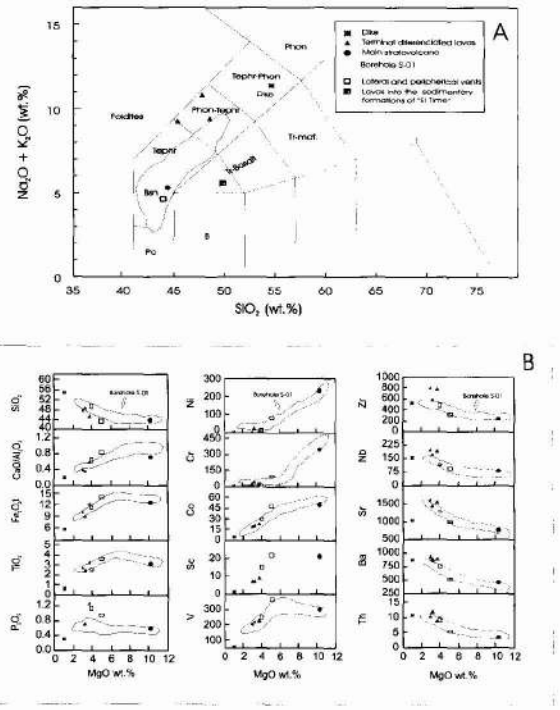

Fig. 42.—A) TAS diagram from lavas and dykes of the Bejenado volcano and adventive vents. Boundaries from Le Bas et al. (1986). B) Variation diagrams for major, trace and REE elements from lavas and dykes of the Bejenado volcano and adventive vents. The borehole S-01 limit for major, trace and REE elements is from Drury et al. (in progress). Symbols as in Fig. 42 A.

nate mafic minerals, including accessory apatite microcrystals. The hypocrystalline groundmass is made of needlelike microlites of feldspar with flow patterns embedded in a hyalopilitic glass.

Adventive vents of the Bejenado volcano emitted the lava flows that outcrop at both sides in the walls of the Bco. de Las Angustias interbedded in the El Time sediments. These lavas are primarily olivine-pyroxene and pyroxene-amphibole basalts.

The most significant geochemical feature of the Bejenado volcano is the absence of alkali basalts in comparison with the pre- and post-collapse Taburiente volcanics. Most Bejenado lavas are basanites and tephri-phonolites, as reported by Drury et al. (in progress). The plotting of the analytical data (Table 2-6) in the diagram of Fig. 42A shows a distinct separation of the basanites of the main stratovolcano from the more differentiated lavas of the terminal vents and sills. Representative samples of borehole S-01, located in the flank of the Bejenado and crossing the entire volcano to the seamount basement (Carracedo et al., 1999 a; Drury et al., in progress) show a greater petrological dispersion, from tephri-phonolites at the upper part, to tephrites and basanites at the bottom. Similar evidence is indicated by the variation diagram of Fig. 42B), where the content in SiO_2 vs. MgO% show inverse relations, a tendency clearly illustrated in the sequence of borehole S-01 by Drury et al. (in progress). The CaO/Al_2O_3, Fe_2O3t and TiO_2 vs. MgO% provide evidence of the role of mineral fractionation in the evolution of the Bejenado volcano. The positive correlation of CaO/Al_2O_3 vs. MgO% in the range of MgO < 6 % indicates significant clinopyroxene and ferromagnesian fractionation. Subparallel variation trends shown by Fe_2O3t and TiO_2 and positive correlations of Ni, Cr, Co, Sc and V vs. MgO% confirm the increasing fractionation of Fe-Ti oxides in the more differentiated lavas. In contrast, incompatible elements such as Zr, Nb, Sr, Ba and Th present increasingly negative correlations towards the more evolved tephri-phonolitic terms, with an end-point in the sills at the top of the volcano.

The normalized plots of Fig. 43A show a positive anomaly for the Ba, Nb and Ta in the basanites of the

main stratovolcano (Sun and McDonough, 1989). The differentiated lavas appear clearly enriched in all the elements except Ti, with positive anomalies Nb, Ta, Zr and LREE. Lavas from the adventive vents show similar trends, as shown in the diagrams of Fig. 43B.

In general, the main geochemical features of the Bejenado volcano suggest a distinct crystal fractionation of olivine, clinopyroxene and spinel, and the crystallization of amphibole in the more differentiated terminal phases. Contrarily, significant fractionation of plagioclase seems absent, as evidenced by the lack of Eu anomaly, with the probable exception of the sills crossing the top of the volcano.

Modelling and characterization of the isotopic heterogeneity of the original mantle source is detailed in Drury et al. (in progress).

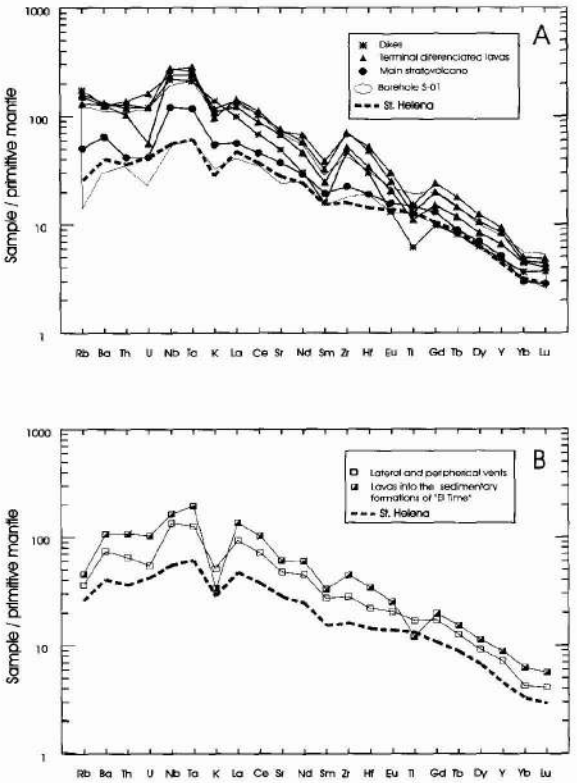

Fig. 43.—A) Primitive mantle normalized diagram for incompatible trace elements from lavas and dykes of the Bejenado Edifice. The borehole S-01 limit is from Drury et al. (in progress). B) Primitive mantle normalized diagram (Sun and McDonough, 1989), for incompatible trace elements of adventive vents of the Bejenado volcano. The data of a primitive basalt from St. Helena are taken from Sun and McDonough (1989).

The Cumbre Vieja volcano

Cliff- and Platform-forming eruptions. The last activity in La Palma, located exclusively in the Cumbre Vieja rift volcano (Carracedo, 1994; Carracedo et al., 1997, 1998, 1999a,b, 2001b; Guillou et al., 1998, 2001), shows an ample petrologic diversity (Klügel et al., 1999), with predominance of basanitic, tephritic and phono-tephritic lavas and phonolitic and tephri-phonolitic intrusives (domes and lava domes). The most significant feature is the existence of repetitive cycles in which basaltic (principally basanitic) lavas are largely predominant, with minor derivations to tephritic and phono-tephritic eruptions (Carracedo et al., 1977a,b). In general, the petrological characteristics of the Cumbre Vieja volcano are distinctly different from those of the preceding subaerial volcanoes (the Garafía, Taburiente and Bejenado volcanoes).

As described in Section II.3, two main stratigraphic units –cliff-forming and platform-forming eruptions– have been defined in the Cumbre Vieja volcano, separated by the isochrone of about 20 ka, the approximate time of occurrence of the last maximum glacial (Carracedo et al., 1997a,b, 1998).

The cliff-forming eruptions include a sequence of lava flows and intrusive rocks in the form of phonolitic domes and lava domes. Hausen (1969) and Hernández Pacheco and De La Nuez (1983) have defined the petrologic characteristics of the phonolitic intrusions. As already mentioned, these authors believed all the phonolitic intrusions in the Cumbre Vieja volcano being of the same age (Mid-Pleistocene) and forming the basement of the Cumbre Vieja rift. However, radiometric dating of these rocks shows them to form independent intrusive events along the entire volcanic history of the Cumbre Vieja volcano (Carracedo et al., 1997a,b; Guillou et al., 1998, 2001). The conclusion of the latter authors is consistent with the diverse composition of the different domes. The phonolitic tephrites of the Los Campanarios, El Cabrito and Mendo domes are the more basic and frequent terms, but mafic phonolites also abound, as in the Roque de la Fuente, Pino de La Virgen, Dña. María and Roque Niquiamo. Finally, the Roque Teneguía and other domes, cryptodomes and lava domes in the cliff near the Teneguía volcano are formed by phonolites, more alkaline and differentiated than the former. Trachytic phonolites are rare, the only outcrop being the dome of Mña Enrique, a rock made of subidiomorphic sanidine phenocrystals, euhedral microcrystals of haüyne and scant mafic minerals in a feldspatic groundmass. The rock is deeply weathered and dating has been unfeasible.

The petrological characteristics of the lava sequences of the cliff-forming unit correspond predominantly to olivine-clinopyroxene and clinopyroxene-amphibole basalts. Plagioclase basalt lavas are

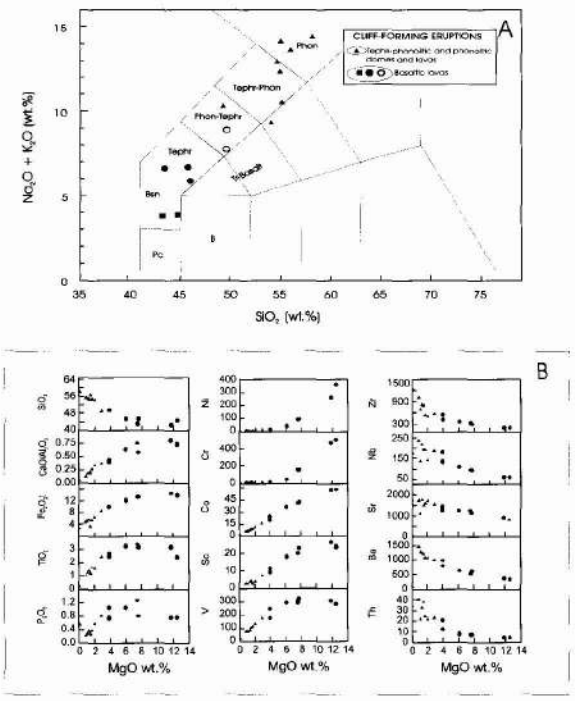

Fig. 44.—A) TAS diagram for basaltic lavas and phonolitic domes of the Cumbre Vieja volcano (cliff-forming eruptions). Boundaries from Le Bas et al. (1986). B) Variation diagrams for major, trace and REE elements from basaltic lavas and phonolitic domes of the Cumbre Vieja volcano (cliff-forming eruptions). Symbols as in Fig. 44 A.

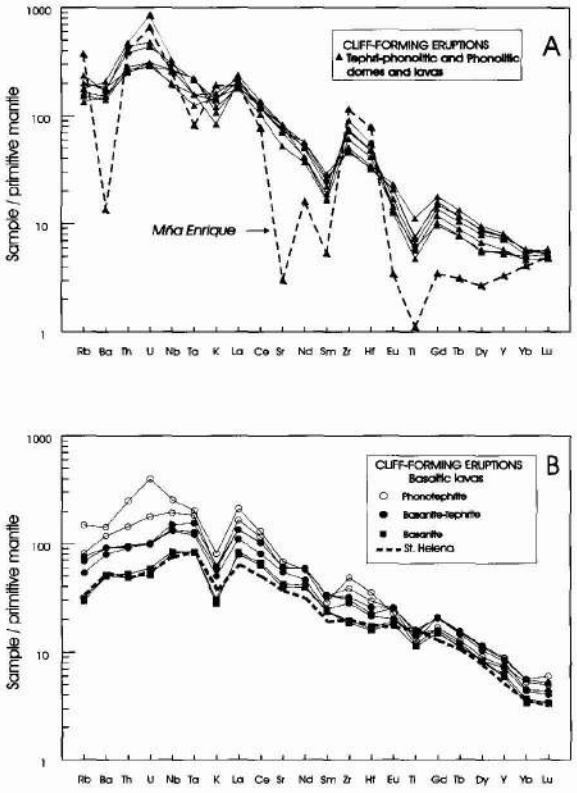

Fig. 45.—A) Primitive mantle normalized diagram (Sun and McDonough, 1989), for incompatible trace elements of tephri-phonolitic and phonolitic domes and lavas of the Cumbre Vieja volcano (cliff-forming eruptions). B) Idem of basaltic lavas of the Cumbre Vieja volcano (cliff-forming eruptions). The data of a primitive basalt from St. Helena are taken from Sun and McDonough (1989).

constrained to the pahoe-hoe lava field near Tigalate, in the SE flank of the rift.

The geochemical data and main characteristics of this unit are shown in Tables 2-7 and 2-8, and Fig. 44A. As shown in the TAS plot of Fig. 44A, most cliff-forming basaltic lavas are basanites and tephrites, with a secondary trend towards picritic basalts, probably in relation to accumulative processes, while the more differentiated lavas are phono-tephrites. The phonolitic domes show a wider dispersion, ranging from phono-tephrites similar to the more differentiated lavas, to phonolites s.s. The major element vs. MgO% diagram of Fig. 44B confirms the overlap of the more evolved basaltic lavas and the less evolved intrusions evidenced in the TAS plot. These trends are suggested in the negative correlation of SiO_2 and the positive correlation of CaO/Al_2O_2 vs. MgO%, possibly in response to clinopyroxene fractionation. The Fe_2O_3t and TiO_2 vs. MgO% correlations suggest a significant fractionation in the range of MgO < 6% in the more differentiated lavas. A similar tendency is observed in the P_2O_5 possibly in relation to apatite fractionation in the phono-tephrite lavas. The minor element variations of Fig. 44B confirm the features described, as well as in the normalized plots of Fig. 45A, where the enrichment in highly incompatible elements (Rb, Ba, Th and U) and LREE reaches a peak in the tephri-phonolitic and phonolitic domes and lava domes, with the clear exception of the trachytic phonolite dome of Mña Enrique. The basaltic cliff-forming lavas elemental trends (Fig. 45B) show basanite normalized values similar to those of St. Helena (Sun and McDonough, 1989), clearly separated from the values of the differentiated tephri-phonolitic lavas. The most noticeable feature is the marked Th-U positive anomaly, not observed in the lavas of the Taburiente and Bejenado volcanoes (see Figs. 41B and 43A). In contrast, the Nb-Ta anomalies are present in these northern shield volcanoes and in the basanite cliff lavas of the Cumbre Vieja volcano.

In summary, the distinct compositional divergences of the cliff-forming lavas of Cumbre Vieja and the associated intrusives evidence a significant geochemical break. A possible explanation, as suggested by

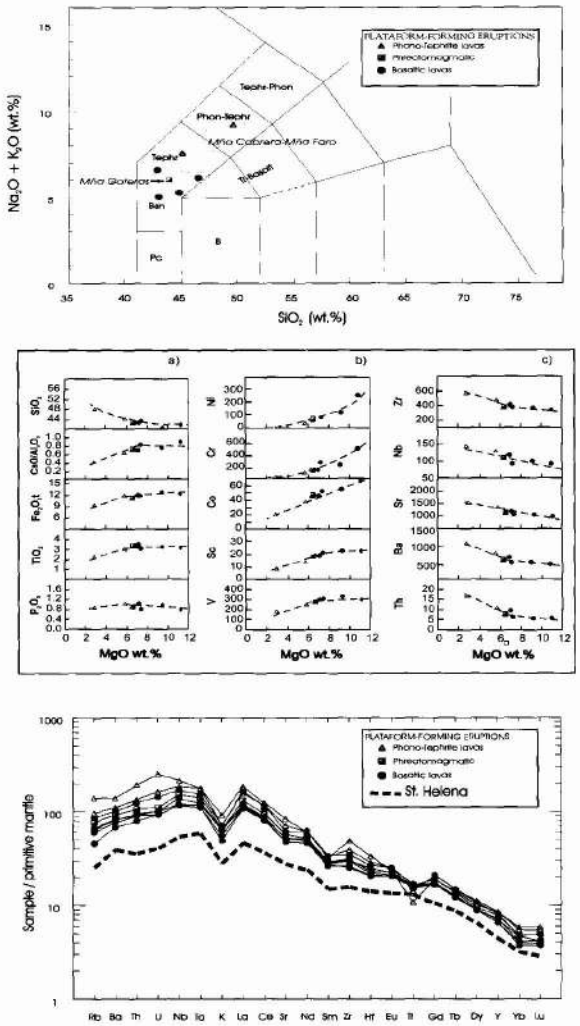

Fig. 46.—A) TAS diagram for lavas of the Cumbre Vieja volcano (platform-forming eruptions). Boundaries from Le Bas et al. (1986). B) Variation diagram for major, trace and REE elements for lavas of the Cumbre Vieja volcano (platform-forming eruptions). Symbols as in Fig. 46A. C) Primitive mantle normalized diagram (Sun and McDonough, 1989), of incompatible trace elements for lavas of the Cumbre Vieja volcano (platform-forming eruptions). Symbols as in Fig. 46A. The data of a primitive basalt from St. Helena are taken from Sun and McDonough (1989).

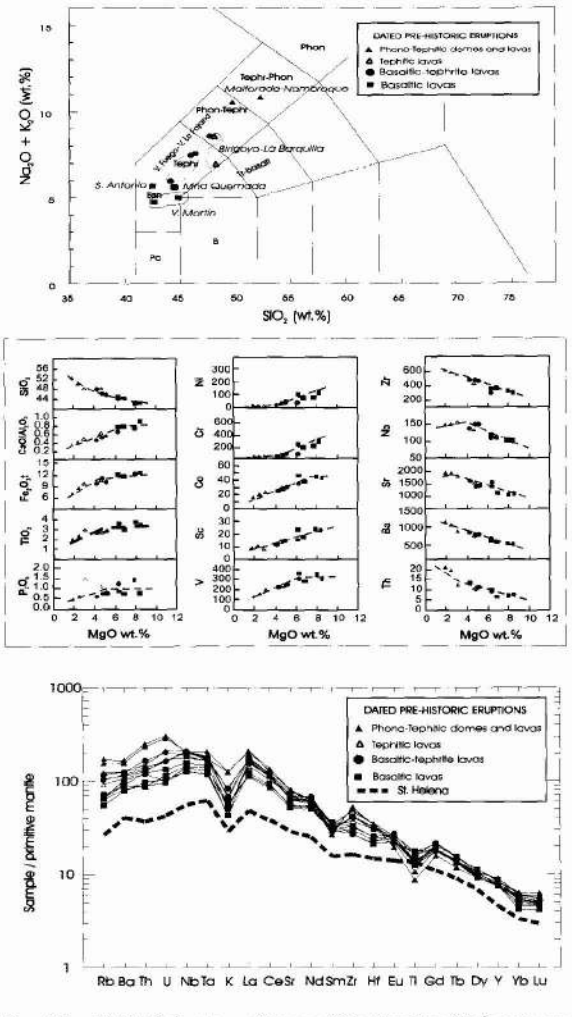

Fig. 47.—A) TAS diagram of lavas of the Cumbre Vieja volcano (dated prehistorical eruptions). The limits are from Yllescas (1977), Hernández Pacheco and Vals (1982), and De Vicente Mingarro (1986). The boundaries from Le Bas et al. (1986). B) Variation diagram for major, trace and REE elements of lavas of the Cumbre Vieja volcano (dated prehistorical eruptions). Symbols as in Fig. 47A. C) Primitive mantle normalized diagram (Sun and McDonough, 1989), of incompatible trace elements for lavas of the Cumbre Vieja volcano (dated prehistorical eruptions). Symbols as in Fig. 47A. The data of a primitive basalt from St. Helena are taken from Sun and McDonough (1989).

Klügel et al. (1999), is the role of fractionation/crystallization of mafic minerals (ol ± cpx ± amphib), feldspar, oxides and apatite in the magmatic evolution of this stage of growth of the Cumbre Vieja volcano.

The separation of the platform-forming eruptions has been useful in the definition of the volcanostratigray and in the geological maps of the Cumbre Vieja volcano, as already mentioned and described in detail in Section II-4. However, this stratigraphic division does not have a correlation in the petrological or geochemical characteristics (Table 2-9 and Fig. 46), that appear to be very similar to those of the cliff-forming eruptions. Similar trends are observed in the prehistorical lavas and intrusives dated (Table 2-10 and Fig. 47), analysed separately for comparison.

The petrological characteristics of the platform-forming lava sequences correspond predominantly to olivine-clinopyroxene and clinopyroxene-amphibole

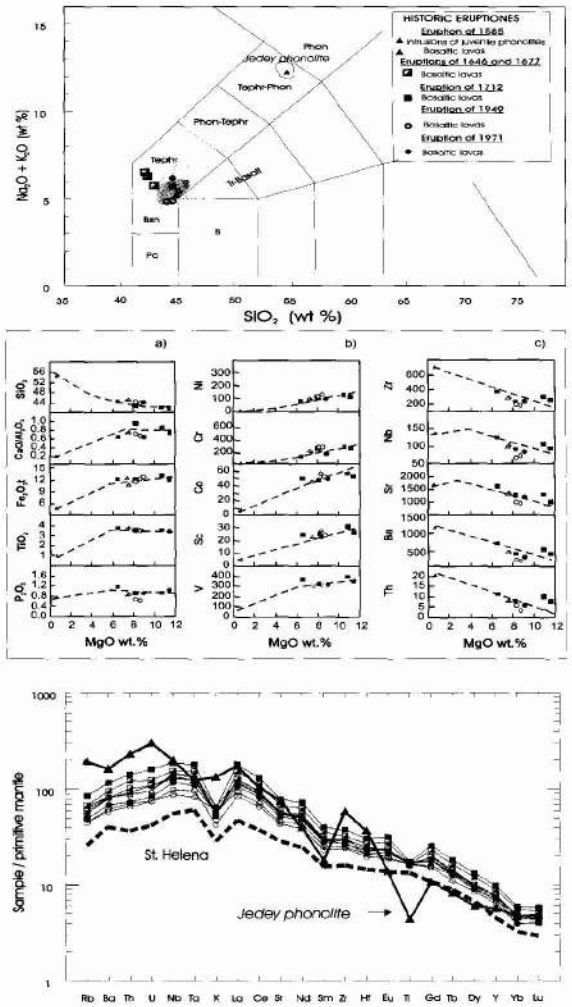

Fig. 48.—A) TAS diagram of lavas of the Cumbre Vieja volcano (historical eruptions). The limits are from Hernández Pacheco and Vals (1982), De Vicente Mingarro (1986) and Klügel et al. (1999). The boundaries from Le Bas et al. (1986). B) Variation diagrams for major, trace and REE elements of lavas of the Cumbre Vieja volcano (historical eruptions). Symbols as in Fig. 48A. C) Primitive mantle normalized diagram (Sun and McDonough, 1989), of incompatible trace elements of lavas of the Cumbre Vieja volcano (historical eruptions). The shadowed area corresponds to the 1949 eruption (Klügel et al., 1999). Symbols as in Fig. 48A. The data of a primitive basalt from St. Helena are taken from Sun and McDonough (1989).

basalts, with phono-tephrites in the more differentiated lavas (Mña Cabrera-Faro and Fuego volcano). The domes and lava domes are characteristically tephri-phonolitic (Malforada-Nambroque), their geochemical characteristics showing similar trends to the cliff-forming eruptions. The normalized plots (Figs. 46, 47), show significantly higher values than those corresponding to St. Helena (Sun and McDonough, 1989).

Historical eruptions. Although the separation of the eruptive activity of the island in the last 500 years has no stratigraphical, petrological or geochemical meaning, these historical eruptions have been traditionally analysed separately from the remaining eruptions of Cumbre Vieja volcano, because they have detailed eye-witness accounts and are easily separated in the geological maps. Petrological and geochemical data of the different historical eruptions of La Palma have been described and analysed by Hernández Pacheco and Valls (1982), De Vicente Mingarro (1986), Praegel (1986), Elliot (1919), Klügel, et al. (1999) and Carracedo et al. (2001b).

The historical lavas are consistently basaltic, with the only mentioned exception of the juvenile haüyne tephri-phonolite lavas and intrusives of the 1585 (Jedey) eruption. The predominant lithologies are ol-cpx basalts and ol-cpx basalts with amphibole. Klügel et al. (1999) quotes three typologies (basanites, tephrites and phono-tephrites) in the 1949 eruption. The last eruption (Teneguía volcano, 1971) emitted clinopyroxene-amphibole basalts, with subordinate olivine in the initial stages, while at the end of the eruption the composition changed to ol-cpx basalts with subordinate amphibole.

The geochemical characteristics of the historical eruptions shown in Table 2-11 and Fig. 48 confirm the general features described for the Cumbre Vieja volcano and evidence the homogeneity of volcanism along the entire volcanic history of the volcano, with the afore-mentioned preponderant role of fractionation/crystallization of mafic minerals (ol ± cpx ± amphib), feldspars, oxides and apatite, similar to the process proposed by Klügel et al. (1999) for the 1949 eruption.

Structural geology

The island of La Palma is an excellent scenario to analyse the main structural features developed in the shield stage of oceanic islands: dyke swarms, rift zones and gravitational landslides.

Dyke swarms

The majority of dykes in La Palma outcrop inside the Caldera de Taburiente, the Cumbre Nueva collapse scarp and the erosional windows at the headwalls of the deepest northern barrancos. In the remainder of the northern shield and the Cumbre Vieja volcano dykes are scarce (black lines in Fig. 49). However, the abundant *galerías* excavated in the northern shield (SPA-15, 1975; Coello, 1987) allowed the observation in the subsoil of the number and direction of dykes (grey in Fig. 49).

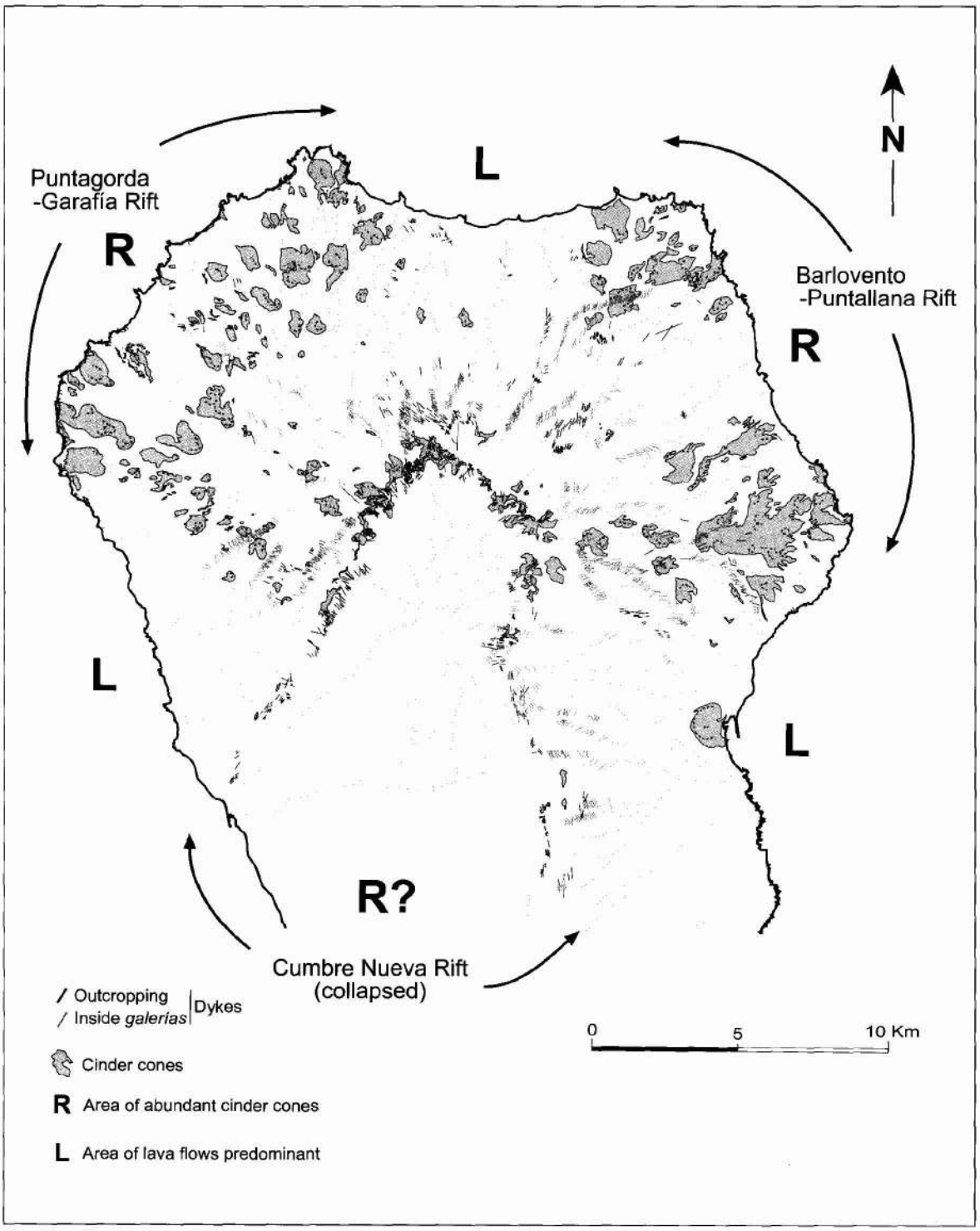

Fig. 49.—Distribution of zones where eruptive vents predominate (incipient, incompletely defined rift zones) and zones with predominance of lava flows (R and L, respectively). Dykes crossed in galerías are shown in grey, outcropping dykes in black.

A detailed geochronological study combining geomagnetic polarity and radiometric determinations in the dykes would allow the correlation of these intrusions with the corresponding volcanostratigraphic units. Until this work is carried out, only three main groups of dykes can be defined in the northern shield of La Palma:

1. Dykes and sills associated to the seamount. They are rotated about 50° and do not cross the subaerial formations.
2. Dykes associated to the Garafía volcano, with radial directions in general and NW to NE in the outcrops, as reported by Coello in 1987.
3. Dykes associated to the Taburiente volcano, also with a general radial distribution but with three, poorly defined, predominant trends (see Fig. 49): NW (Punta Gorda to Garafía), NE (Barlovento to Puntallana) and N-S (El Time to the Cumbre Nueva collapse scarp).

There are no *galerías* in Cumbre Vieja, because of the poor quality of volcanic gas-contaminated groundwater. Therefore, only a few, E-W trending dykes have been observed in the cliffs of this volcano. However, a densely packed dyke swarm can be expected to cluster along the axis of the Cumbre Vieja rift in a N-S trend.

Rift zones

Dyke directions and vent alignments are not the only features to define volcanic rifts. Vents can show considerable dispersion even in well-defined rifts, as clearly evidenced in Cumbre Vieja, where historical vents frequently align in directions oblique to the main axis of the rift, probably due to slope effects. The rift zones are best defined by the grouping of eruptive centres in preferred trends and zones, to form ridges or dorsals (Walker, 1992; Carracedo, 1994, 1996; Carracedo et al., 1998).

The volcanic evolution of La Palma offers a unique opportunity to analyse the development of a juvenile shield volcano from the seamount stage, as well as the structural changes giving place to development of rifts. As mentioned before, a reorganization of the eruptive centres took place during the construction of the northern shield. The initially dispersed eruptions in the Garafía and Lower Taburiente volcanoes, progressively grouped from about 0.8 ma in three areas of predominant cinder cones, separated by zones of predominant lava flows (R and L, respectively, in Fig. 49). The areas of concentration of emission centres form an incipient rift or dorsal, manifested by the protuberance they form in the coast, where abundant subvertical dykes outcrop at the coastal cliffs. Contrarily, cinder cones, interbedded pyroclast layers and dykes are very few or absent in the areas of predominant lavas (L), even in the deeply incised barrancos.

The relatively poor definition of rifts in the northern shield of La Palma in comparison with Cumbre Vieja, El Hierro or central Tenerife may simply reflect the fact that volcanism ceased in La Palma before the rifts were completed. Contrarily, volcanic activity remained essentially stationary in El Hierro and Tenerife for long periods and with high eruptive rates and volumes, giving place to successive overlapping volcanoes and allowing the development of well-defined rift zones. Conversely, in the northern shield, volcanism initiated a continuous southward migration in the late stages of the Upper Taburiente. Most of the volcanism was located in this period in the southern Cumbre Nueva rift, which grew steep and unstable and collapsed. The remainder of the shield had only residual activity since the Cumbre Nueva collapse and finally became extinct at about 0.4 ma. We can speculate with the hypothesis that if the abundant volcanism involved in the building of the Cumbre Nueva and Cumbre Vieja rifts had remained focused and capped the northern shield, as occurred in El Hierro or central Tenerife, well-defined rifts might have developed to completion.

Although only a fraction of the southern Cumbre Nueva rift remains, the major part collapsed, eroded or capped by the Cumbre Vieja volcano. Its approximate geometry can be inferred from the dyke swarms outcropping in the western wall of the Caldera at El Time and the Cumbre Nueva collapse scarp, trending NE-SW and N-S, respectively (see Fig. 49). The axis of the southern rift may have been located between both directions, fossilized at present by the Bejenado and Cumbre Vieja lavas (Carracedo et al., 1999 a, b).

The Cumbre Vieja rift is an interesting example of the evolution of a rift from the initial stages to a well-defined, progressively steep and unstable configuration. This rapid structural change has been modelled by Walker (1992) and Carracedo (1994, 1996), as reflecting the continuous increase in anisotropy and thermal memory in the rifts in response to dyke intrusion, favouring concentration of emission centres along the axis of the rifts. The evolution of the Cumbre Vieja volcano, from the initial stages of significantly disperse eruptive vents (see Fig. 23) to a steep, N-S trending dorsal (Fig. 24), has been explained by Carracedo and co-workers (1997 a, b, 1998, 1999 a, b) and Day and co-workers (1999) as reflecting the development of the Cumbre Vieja volcano attached to the flank of the northern shield, which acted as an effective supporting buttress and forced the southward growth of the volcano and the progressive predominance of the N-S trending rift.

The swath bathymetry coverage around the island of La Palma showed the presence of a group of seamounts forming the offshore prolongation of the Cumbre Vieja rift (Urgelés et al., 1999; Masson et al., 2002). A dredging campaign of the German oceanographic vessel Poseidon in 2001 found that most of these are recent eruptive vents, several of them corresponding to very recent submarine eruptions (Hastings et al., 2001; Gee et al., 2001).

Gravitational flank collapses

Although several gravitational flank collapses in the northern shield have been reported (Ancochea et al., 1994; Masson et al., 2002), we have only found geological evidence for the two main events mentioned, the Garafía and Cumbre Nueva giant landslides.

The available geochronological, stratigraphic and structural data constrain the occurrence of the Garafía collapse at about 1.2 ma (Fig. 8), as first described by Ancochea and co-workers (1994). A several hundred-metres-thick breccia overlying the seamount in the E and SE of the Caldera de Taburiente has been interpreted by Carracedo and co-workers (2001 a) as debris avalanche deposits, and may correspond to the Garafía collapse. The geometry of the collapsed block and embayment of the Garafía landslide has been approximately reconstructed from these data and observations inside the numerous *galerías* excavated for groundwater in the northern shield. These data agree remarkably well with the extension offshore of the corresponding debris avalanche deposits shown in Fig. 50 (Urgelés et al., 1999; Masson et al., 2002), with some significant discrepancies.

Masson et al. (2002) dated the Garafía landslide, which they named Playa de La Veta debris avalanche complex, at between 1-0.8 ma. However, there is no geochronological or stratigraphical evidence of any major landslide taking place in the northern shield between 1.2 and about 0.5 ma. These authors locate the western limit of their Playa de La Veta debris avalanche complex north of this beach, supporting this assumption in a personal communication of a supposed major tectonic discordance observed from the sea in the cliff behind this beach. However, onshore observation showed this feature to be a local unconformity, possibly the filling of a palaeobarranco, since the entire cliff sequence corresponds to the Upper Taburiente, the top lavas being dated at 0.4 ma (Guillou et al., 2001). The actual border is located east of Bco. de Jieque, very close to the present western cliff of the Caldera. In fact, lavas of the pre-collapse Garafía volcano outcrop in this barranco at about 1500 m asl. The eastern limit of this landslide is more difficult to infer from onshore geological observations. It may

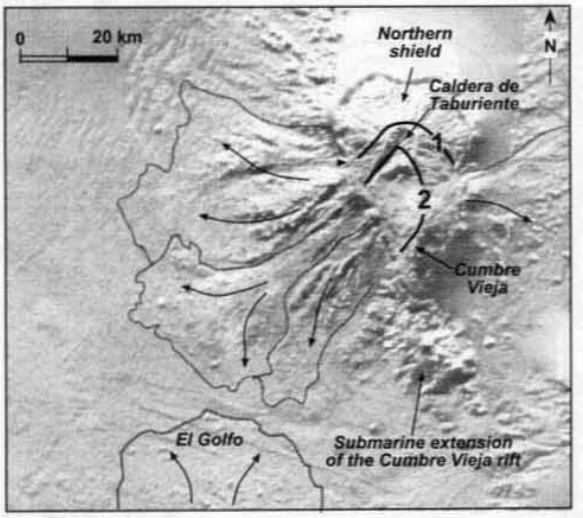

Fig. 50.—Shaded relief image of the debris avalanche deposits from different gravitational landslides in the submarine flanks of La Palma. Image from Masson et al., 2002.

correspond to the debris avalanche reported by Urgelés et al., (1999) and Masson et al. (2002), north of Santa Cruz de La Palma, which these authors associate to another collapse older than 0.9 ma, of which there is no geological evidence onshore.

The Cumbre Nueva giant landslide has been anticipated by Machado (1963) and described by Ancochea et al. (1994), Carracedo (1994) and Carracedo et al. (1999 a, b). This event is an important feature in the geology of La Palma, initiating the Caldera de Taburiente and the Valle de Aridane depressions, a geomorphologic divide between the northern shield and the southern Cumbre Vieja volcano.

The southwards migration of volcanism in the late stages of development of the Taburiente volcano favoured the growth of the southern Cumbre Nueva rift towards instability (1 in Fig. 51 A). The western flank of the rift collapsed at about 530-566 ka (2 in 37 A). As described above, the growth of the Bejenado volcano nested in the collapse embayment forced the progressive incision of the Bco. de Las Angustias, and retrogressive erosion at the headwall of the barranco originated the present Caldera de Taburiente (2 and 3 in Fig. 51A). Subsequently, the Cumbre Vieja volcano partially filled the embayment overlying the Bejenado lavas, and developed southwards attached to the remainder of the Cumbre Nueva rift. The geometry and extension of the collapsed block can be estimated from the observation of the cores of boreholes drilled in the Valle de Aridane for hydrogeological research. From these data and other observations the pre-collapse elevation of the Cumbre Nueva rift can be estimated in about 2.500 m asl, and

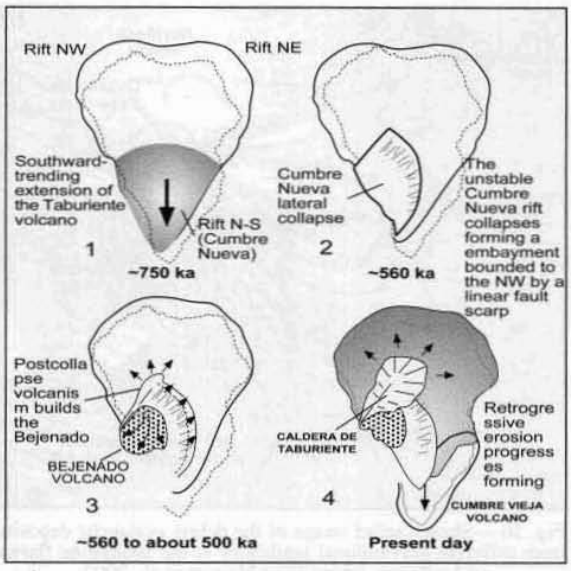

Fig. 51.—A) Cartoon illustrating the growth and collapse of the Cumbre Nueva rift. B) Inferred disposition of the slide planes of the successive gravitational flank collapses in the northern shield.

the volume of the collapsed block or blocks in about 180-200 km^3 (Carracedo et al., 1999 a, b).

Surprisingly, neither the earlier Garafía landslide nor this late collapse, nor the erosive enlargement of the Caldera de Taburiente seems to have exhumed lava sequences of the Garafía volcano, which outcrops 1000 m above the Caldera floor only a few kilometres to the north (see Fig. 16). A plausible explanation is sketched in Fig. 51 B, which shows the approximate disposition of the successive Garafía and Cumbre Nueva giant landslides, the latter cutting at a steeper angle the lava sequence filling the embayment of the former. The occurrence of these recurrent, nested giant landslides may reflect the process described by

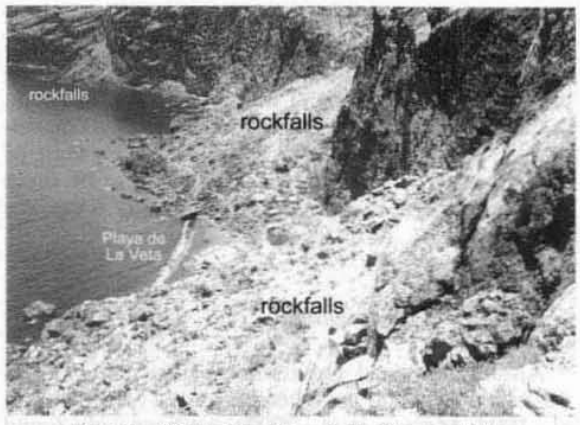

Fig. 52.—View of the Playa de La Veta rockfalls.

Siebert (1984) and quoted by Ancochea et al. (1994). Weathered debris avalanche and post-collapse sediments form a plastic layer favouring subsequent landsliding of the lava sequences filling the previous collapse embayment, giving place to successive nested calderas. This process was anticipated by Bravo (1962) who named this plastic formation «fanglomerate», although this author interpreted the sediments as weathered volcanic formations preceding and not resulting from an earlier giant landslide.

Faults, fissures and rockfalls

No important faults or regional fractures have been observed in La Palma. As already discussed, some features interpreted as major fractures or collapse scarps appear to be, in fact, local unconformities, probably fossilized palaeobarrancos. Tensional fractures close to and parallel to the cliff edges are relatively abundant, apparently precursors of the numerous rockfalls observed at the foot of the coastal cliffs of the northern shield and in the walls of the Caldera de Taburiente. They are activated by marine erosion of the base of the cliffs and show different stages of fragmentation, occasionaly preserving large blocks in which the collapsed volcanic formations can be easily recognized, as in the Fajana de Los Hombres and Playa de La Veta rockfalls (Fig. 52). Rockfalls in the walls of the Caldera de Taburiente are very frequent, some very large and recent, such as the Risco Liso, at the centre of the western wall. They drastically modify the drainage system inside the Caldera.

Bonelli Rubio (1950) first described the 2.5 km long, en echelon faults or fractures that opened during the 1949 eruption (Fig. 53). These fractures, with vertical jumps exceeding 5 metres in some places, apparently connected the vents of the 1949

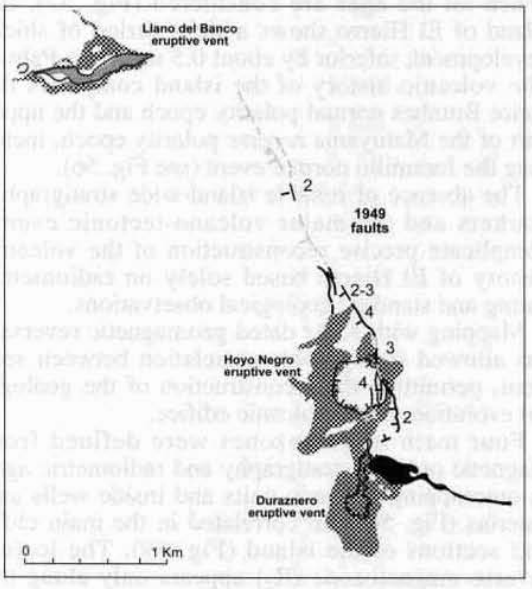

Fig. 53.—Faults that opened during the 1949 eruption (photo Bonelli Rubio). B) Map of the 1949 eruptive vents and faults. Numbers indicate observed or inferred vertical jump.

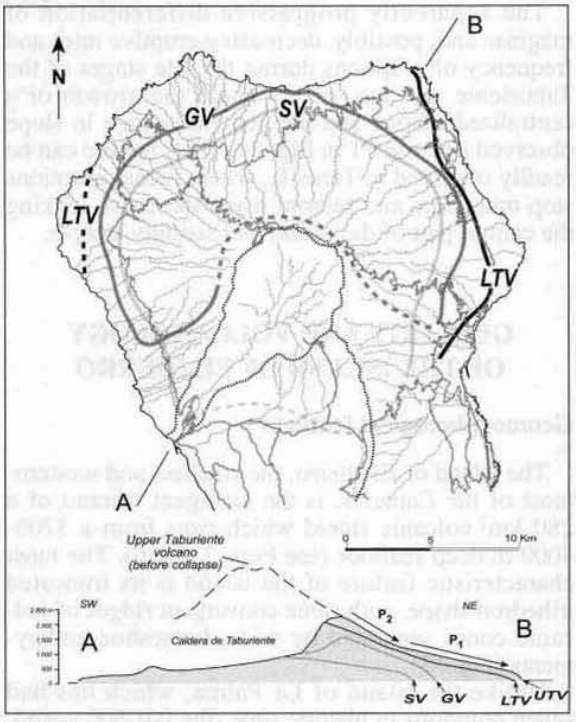

Fig. 54.—Estimated extension of the successive volcanoes forming the northern shield of La Palma: The cross section illustrates how the sequential volcanoes resurface and enlarge the island, forming extended coastal platforms in each cycle.

eruption (Fig. 53 B). Carracedo (1994), Carracedo et al. (1999 a, b) and Day et al. (1999) analysed their potential association with a detached block at the western flank of the Cumbre Vieja volcano, of which these faults could be the surficial manifestation However, the lack of seismicity and ground deformation (Moss et al., 1999) seems to point to an inactive shallow feature, that should be, notwithstanding, fully investigated and monitored.

Main patterns in shield growth

The disposition of the successive volcanoes that coalesced to form the northern shield is a good example of how these juvenile shields evolve. As shown in Fig. 54, there is a progressive increase in the extension and elevation of the island as the successive volcanoes aggregate. Each volcano undergoes a succession of constructive and destructive phases, with enlargement and mass wasting (marine and meteoric erosion and gravitational collapses), respectively. As shown in the cross sections, each volcano resurfaced the island, and lava flows fossilized the cliffs and formed new coastal platforms.

The apparently progressive differentiation of magmas and, possibly, decreasing eruptive rates and frequency of eruptions during the late stages of the Taburiente volcano, may explain the growth of a centralized edifice and the general change in slope observed (P2 and P1 in Fig. 54). This feature can be readily observed in Tenerife, where recent eruptions stop mid-slope and seldom reach the coast, making the central part of the island increasingly steeper.

GEOLOGY AND VOLCANOLOGY OF THE ISLAND OF EL HIERRO

Geomorphological features

The island of El Hierro, the smallest and westernmost of the Canaries, is the emergent summit of a 280 km^2 volcanic shield which rises from a 3700-4000 m deep seafloor (see Figs. 1 and 6). The most characteristic feature of the island is its truncated trihedron shape, with three convergent ridges of volcanic cones separated by wide, horseshoe embayments (Fig. 55).

Unlike the island of La Palma, which has had seven eruptions in historic time (the last 500 years), there are only questionable records of a single eruption (Lomo Negro volcano, 1793) in El Hierro (Hernández Pacheco, 1982), although most probably this event may have been an offshore eruption which produced the seismicity felt in that year. A sample from a group of recent emission vents on the central plateau, near the village of San Andrés (Mña. Chamuscada-Mña. Entremontañas volcanic group), yielded a ^{14}C age of 2,500 ± 70 years BP.

Previous work on El Hierro itself is relatively scarce. Hausen (1964) and Bravo (1968) made general descriptions of the geology of the island. The former provides interesting data on the subsurface structure of the El Golfo embayment and the latter suggests for the first time a possible tectonic origin for the El Golfo embayment. Abdel Monem and co-workers (1972), and Fúster et al. (1993) provided the first (whole rock) K-Ar ages, recently revised by Guillou et al. (1996), using an unspiked technique on microcrystalline groundmass separates and combining the radiometric dating with the magnetic stratigraphy. Pellicer (1977, 1979) carried out the first comprehensive geological and petrological study of El Hierro, including a schematic geological map, revised by Carracedo et al. (1997 c) and in this work.

Offshore studies by Masson (1996), Urgelés et al. (1997), and Masson et al. (2002) based on swath bathymetry coverage, detected debris deposits on the island slopes and adjacent ocean floor, clear evidence of recent landslide activity in the island. Submarine prolongation of the active rifts has been clearly outlined by these oceanographic data (see Fig. 5).

Age of volcanism

About 16 radiometric (K/Ar and ^{14}C) ages have been published from volcanics of El Hierro by Abdel Monem et al., 1972 (5 ages) and Fúster et al., 1993 (11 ages). Guillou and co-workers (1996) approached the dating of El Hierro volcanism with the same technique described for La Palma, with stringent constraints in the sampling, replicating measurements and using geomagnetic reversals and sections to control the consistency of the ages. These authors obtained 1 ^{14}C and 18 K/Ar ages, and, recently, another 9 new K/Ar ages, to complete the geochronology of the island (Table 3 and Fig. 56).

As discussed in Guillou et al. (1996), the previous ages were notably inconsistent, ranging from 3.05 ± 3 to 0.19 ± 0.01 (Abdel-Monem et al., 1972) or from 0.80 ± 0.06 to less than 0.05 ma (Fúster et al., 1993). The age of 3.05 ma of the former authors proved to be a grossly excess single age, whereas the assumption of the latter authors that the island was developed entirely in the Brunhes epoch is not consistent with the reverse polarity volcanic units identified in a preliminary study (Carracedo, 1994), later confirmed by Guillou and co-workers (1996). When all the ages are considered (Fig. 57), the island of El Hierro shows a short period of shield development, inferior by about 0.5 ma to La Palma. The volcanic history of the island comprises the entire Brunhes normal polarity epoch and the upper part of the Matuyama reverse polarity epoch, including the Jaramillo normal event (see Fig. 56).

The absence of reliable island-wide stratigraphic markers and the major volcano-tectonic events complicate precise reconstruction of the volcanic history of El Hierro based solely on radiometric dating and standard geological observations.

Mapping with K-Ar dated geomagnetic reversals has allowed stratigraphic correlation between sections, permitting the reconstruction of the geological evolution of this volcanic edifice.

Four main magnetozones were defined from magnetic polarity stratigraphy and radiometric ages in outcropping volcanic units and inside wells and galerías (Fig. 58) and correlated in the main cliffs and sections of the island (Fig. 59). The lowest reverse magnetozone (R_2) appears only along the NE side of the island, generally in lavas dipping steeply (30-35°) towards the sea from the NE ridge. R_2 lavas were also detected in galleries and boreholes in this part of the island. The oldest age,

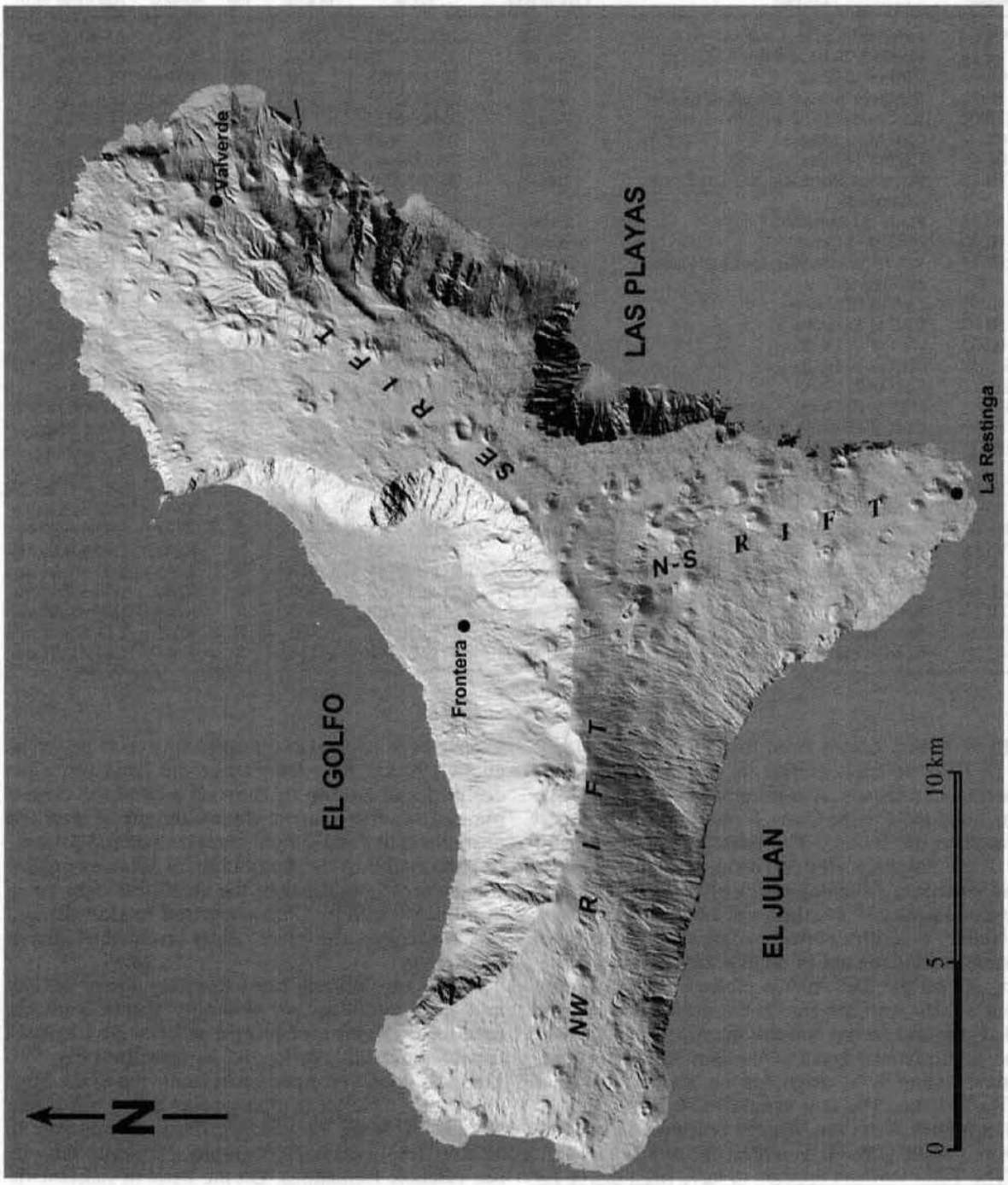

Fig. 55.—Shaded relief image of El Hierro showing the main geomorphological features (image GRAFCAN).

Table 3.—**Location, type of rock, geomagnetic polarity and age of volcanics from El Hierro (Ages from Guillou et al., 1996, and Szérémeta et al., 1999)**

Sample	Locality	Type of rock	UTM	m a.s.l.	Pol	Method	Age mean value
LPC14-1	Lavas from Mña. Chamuscada	Basalt	2098/30762	1,050	N	^{14}C	2.5 ± 0.07 ka
CI HI 16	Borehole S-10, at a depth of 23 m	Basalt	2019/30732	160	N	K/Ar	12 ± 7 ka
SJ 03	Cliff of El Julan	Basalt	2011/30658	120	N	K/Ar	15 ± 2 ka
CI HI 11	Borehole S-16, at a depth of 68 m	Basalt	2032/30732	190	N	K/Ar	15 ± 2 ka
CI HI 07	Borehole S-16, at a depth of 266 m	Basalt	2019/30732	15	N	K/Ar	21 ± 3 ka
SJ 02	Cliff of El Julan	Basalt	2007/30661	80	N	K/Ar	31 ± 2 ka
SJ 01	Cliff of El Julan	Basalt	2005/30660	20	N	K/Ar	41 ± 2 ka
CI HI 15	Rift lavas cascading into Las Playas embayment	Basalt	2081/30701	205	N	K/Ar	44 ± 3 ka
CI HI 13	Punta del Guincho	Basalt	2115/30715	80	N	K/Ar	76 ± 6 ka
CI HI 40	Cliff of El Golfo	Basalt	2065/30787	740	N	K/Ar	134 ± 4 ka
CI HI 14	Rift lavas cascading into Las Playas embayment	Basalt	2088/30702	95	N	K/Ar	145 ± 4 ka
CI HI 01	Cliff of El Golfo	Basalt	2064/30785	650	N	K/Ar	158 ± 4 ka
CI HI 02	Cliff of El Golfo	Trachyte	2064/30784	600	N	K/Ar	176 ± 3 ka
CI HI 03	Cliff of El Golfo	Basalt	2064/30783	510	N	K/Ar	261 ± 6 ka
EG 16	Cliff of El Golfo	Basalt	2062/30780	460	N	K/Ar	275 ± 6 ka
EG 22	Cliff of El Golfo	Basalt	2061/30778	420	N	K/Ar	331 ± 6 ka
EG 40	Cliff of El Golfo	Basalt	2060/30776	395	N	K/Ar	347 ± 6 ka
CI HI 04	Cliff of El Golfo	Basalt	2059/30775	370	N	K/Ar	442 ± 5 ka
CI HI 27	Cliff of El Golfo, at the end of galería Los Tincos	Basalt	2053/30748	280	N	K/Ar	543 ± 8 ka
CI HI 05	Cliff of El Golfo	Basalt	2048/30758	100	N	K/Ar	545 ± 11 ka
CI HI 06	Valverde	Basalt	2128/30796	640	R	K/Ar	882 ± 13 ka
CIHI-100	Barranco del Balón	Basalt	2118/30752	405	R	K/Ar	1.03 ± 0.02 ka
CI HI 18	El Toril	Basalt	2103/30760	980	N	K/Ar	1.04 ± 0.01 ma
CI HI 12	Crater of Mña. Ventejís	Basalt	2114/30785	910	R	K/Ar	1.04 ± 0.02 ma
CIHI-101	Barranco de Tiñor	Basalt	2126/30769	400	R	K/Ar	1.04 ± 0.02 ma
CI HI 08	Barranco de Tiñor	Basalt	2126/30769	400	R	K/Ar	1.05 ± 0.02 ma
CI HI 10	Barranco del Balón	Basalt	2124/30748	160	R	K/Ar	1.11 ± 0.01 ma
CI HI 09	Road to Puerto de La Estaca, Km 1	Basalt	2139/30768	110	R	K/Ar	1.12 ± 0.02 ma

1.12±0.02 ma, comes from the steep dipping lavas of El Tiñor volcanic edifice (R_2 magnetozone) near Puerto de La Estaca. A similar age of 1.11± 0.01 ma was obtained for the same formation 2.5 km apart (Barranco del Balón). The latest emission vents of El Tiñor volcanic edifice corresponding to the R_1 magnetozone, from samples collected near Tiñor, gave two ages of 1.05±0.02 and 1.04±0.02 ma.

Normal polarities corresponding to the N_2 magnetozone were detected in subhorizontal lavas overlying R2 on the San Andrés plateau. Some of these lavas spilled over the rim of the central plateau and filled canyons carved into the steep dipping R_2 lavas. The subhorizontal lavas of the San Andrés plateau, corresponding to N_2 magnetozone, yielded an age of 1.04±0.01 ma. The late xenolith-rich lavas from El Tiñor edifice, from the Ventejís volcanic (R_1 magnetozone) vents, gave the youngest age of 882 ±13 ka.

The Tiñor volcano appears to have been active for a period of at least 0.20-0.27 ma, taking into account the uncertainties in the ages. However, the main parts of the edifice, the steeply dipping lavas, seem to have been emitted in a surprisingly short period of about 100 ka. At a later stage the emission rates declined and erosion of canyons around the central plateau resulted in the development of marked unconformities and a more complex outcrop pattern.

This control of the distribution of lavas by erosional features is unusual in the shield-building stage of volcanic activity (i.e.: compared to Hawaii) and perhaps reflects the lower rate of eruption of lava in El Hierro.

A few xenolith-rich lavas (forming a very distinct unit since xenoliths are generally absent from the lavas of El Hierro), of reverse polarity (R_1), unconformably overlie both R_2 and N_2 lavas (see Fig. 59). These R_1 lavas correspond to a late event of the Ventejís group, a cluster of cinder cones to the NW of the town of Valverde. They flow towards the sea over an already deeply eroded topography, carved on the earlier volcanic formations. On the basis of radiometric age data we assigned R_1 and R_2 to the Matuyama reverse epoch and N_2 to the Jaramillo normal-polarity event within that epoch (Figs. 56 and 59).

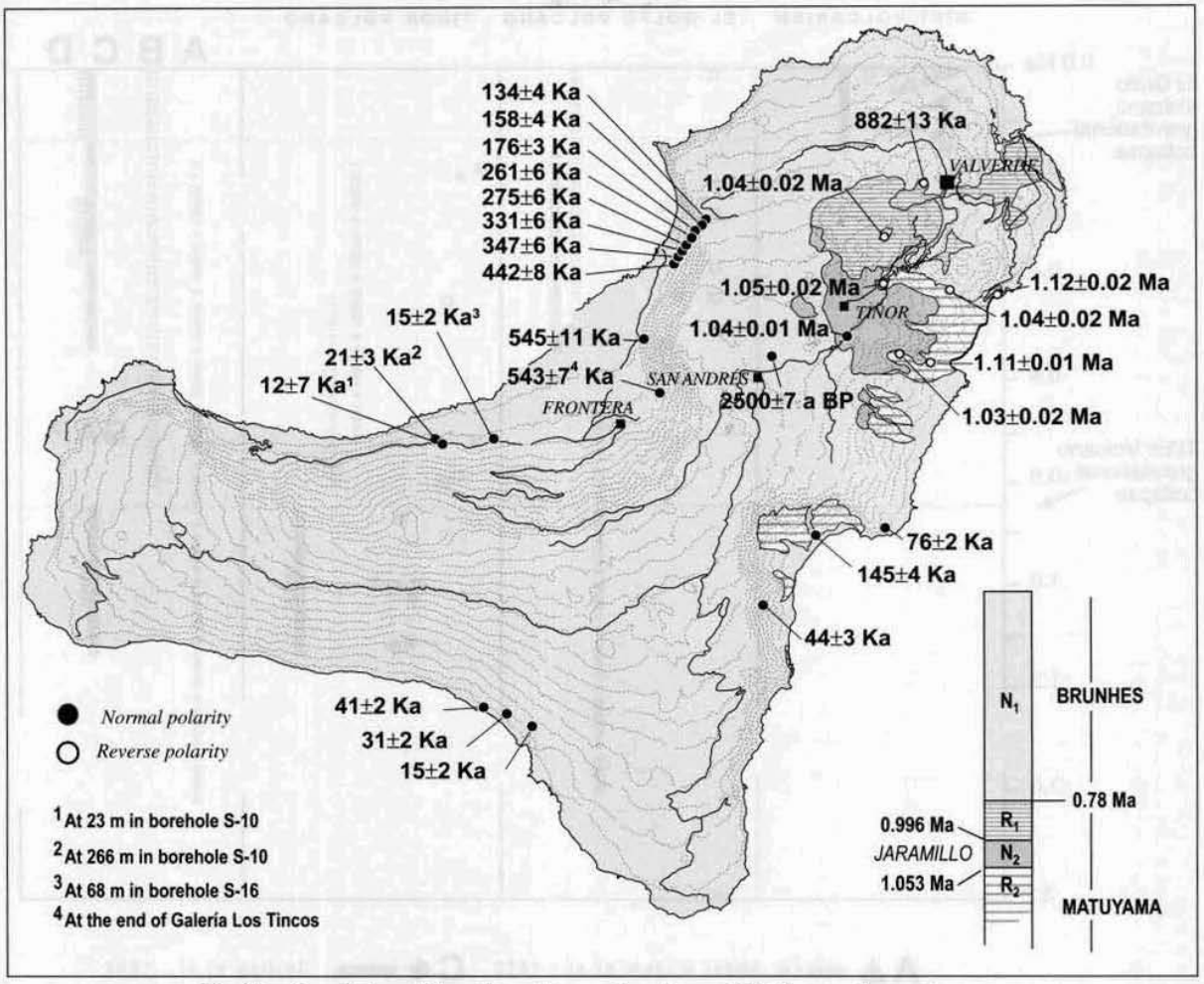

Fig. 56.—Correlation of the radiometric ages from lavas of El Hierro and magnetozones.

Finally, lava flows and cinder cones of normal polarity unconformably overlie R_1 volcanics. These normal-polarity rocks continue up without intervening reverse-polarity intervals, although a number of discordances are present, to lavas of subhistoric age. On the basis of radiometric ages discussed below we assigned the whole of this sequence to the Brunhes normal polarity chron (Figs. 56 and 59).

These youngest (N_1) normal polarity rocks form the bulk of El Hierro, including all the rocks in the south and west of the island, and form very thick sequences. Magnetic polarity profiles in the 1100-m vertical escarpment of El Golfo are entirely composed of normal polarity volcanics (Figs. 59 and 60). Normal lavas likewise partly fill the El Golfo embayment, as evidenced by samples from a 280 m-deep borehole located inside the embayment. The *galerías* located at the foot of the El Golfo escarpment also cut consistently normal polarity lava flows and dykes.

The limited outcrop of reverse polarity lavas in the NE of the island, the presence of the Jaramillo normal-polarity lavas, and the catastrophic disruption of the island by several giant lateral collapses may explain the difficulties encountered by previous researchers in their reconstructions of the volcanic history of El Hierro.

Main stratigraphic units and volcanoes of El Hierro

The radiometric and magnetostratigraphic evidence allows the division of the subaerial rocks of El Hierro into three main volcanic units that correspond to successive volcanic edifices:

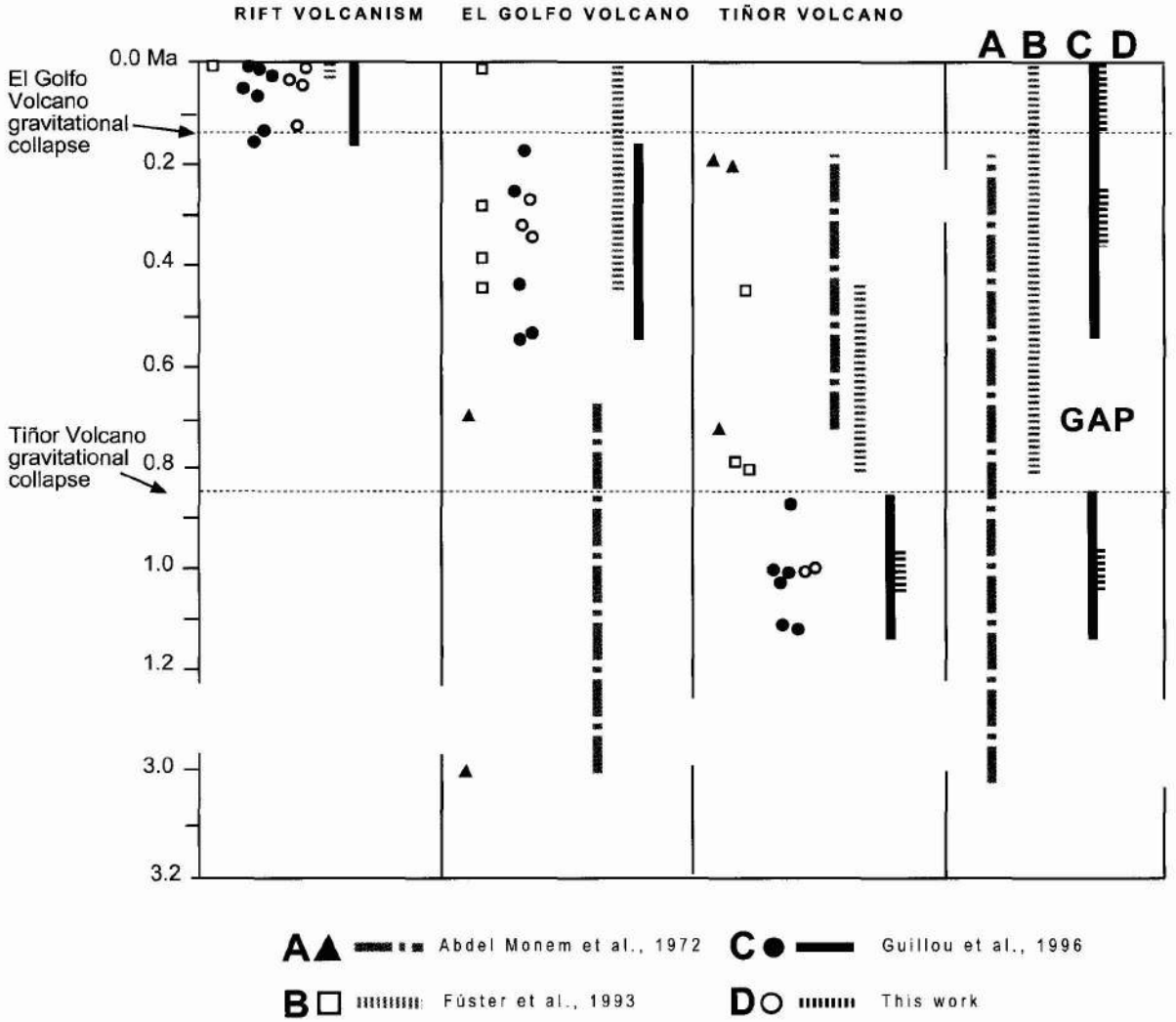

Fig. 57.—Comparison of the ages published from volcanics and intrusives of El Hierro.

1) The first subaerial edifice, the Tiñor volcano (the seamount stage does not outcrop in El Hierro); 2) The El Golfo edifice; 3) The rift volcanism which forms a relatively thin sequence with emission vents distributed in three volcanic rift branches that have not as yet produced a topographically distinct edifice (see Fig. 56 and the geological map). These main volcanoes are separated, as in La Palma, by major tectonic events (gravitational collapses).

Although the main geological and geomorphological features of El Hierro are very similar to those of La Palma, both islands being similar in age and magmatic components, their final shape and morphology are remarkably different. As discussed below, this feature may reflect the differences in the stability of the magmatic plumbing, that is stationary in El Hierro and southward migrating in La Palma.

Geological and volcanological description of the stratigraphic units and volcanoes of El Hierro

Tiñor volcano

Tiñor volcano forms the first stage of subaerial growth of El Hierro. Its present outcrop is confined to the NE flank of the island and inside the Las Pla-

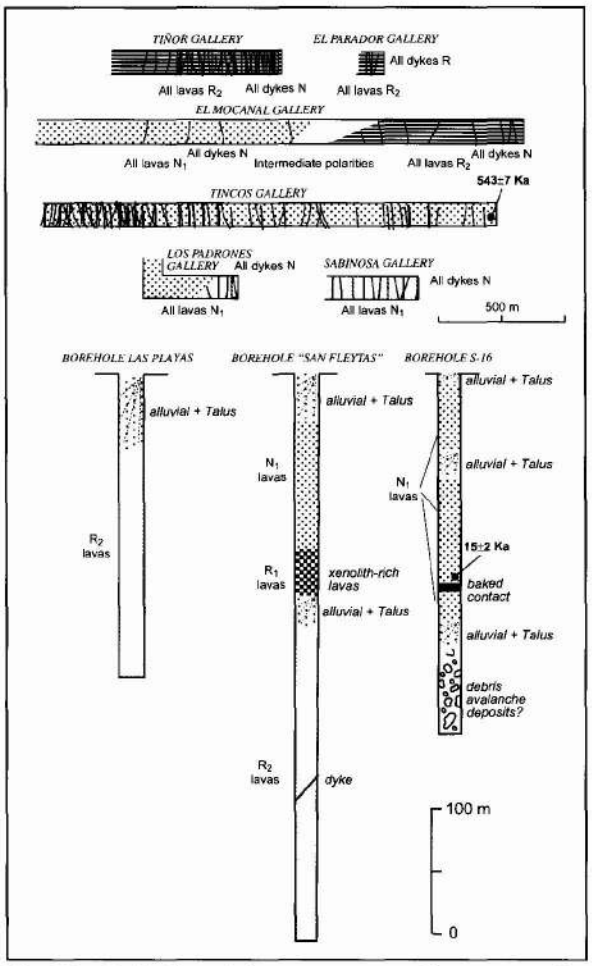

Fig. 58.—Definition of the magnetozones in representative sections of El Hierro.

yas embayment (see Figs. 56 and 60, and the geological map and cross sections). This is the result of the destruction of the NW part of the volcano by a giant collapse, as discussed below, and partial covering of the volcano during the later stages of growth of the island.

Tiñor volcano developed very rapidly and there is no consistent compositional variation with time that can be mapped in the field. However, there are several differences between units that may reflect the morphological evolution of the developing edifice: 1) a basal unit of relatively thin, steeply-dipping flows, probably corresponding to the initial stages of growth of the volcano, with steep flanks. 2) An intermediate unit of thicker lavas, that progressively trend to subhorizontal flows in the centre of the edifice, probably reflecting the lower slopes of this mature stage of growth of the volcano, but which fill canyons on the flanks, and 3) A group of emission vents with well-preserved wide craters (the Ventejís volcano group) and lavas occupying valleys and canyons carved into the older rocks. The flows of the Ventejís unit are very easily identifiable by their significant xenolith content: in contrast with the lavas of La Palma, most El Hierro flows are xenolith-poor.

These three units have different geomagnetic polarities, corresponding to magnetozones R_2, N_2 and R_1, respectively, as already discussed.

The Ventejís eruptions may have been a terminal explosive stage, as suggested by the morphology of the vents and the high xenolith content of the lavas. This explosive stage may have immediately preceded the collapse of the NW flank of Tiñor volcano, as discussed below.

Cross sections in Fig. 60 show the relative stratigraphic position of Tiñor and the subsequent volcanoes. The limited extent of Tiñor volcano towards the S and W is evident in sections 1 and 5 of this figure and in Fig. 61.

The El Golfo volcano

After Tiñor volcano collapsed a new volcanic edifice (El Golfo volcano) developed (see Fig. 61 E), filling the NW-facing collapse embayment and finally spilling lavas towards the E coast overlying Tiñor volcano (see section 4 in Fig. 60 and G in Fig. 61).

El Golfo volcano developed entirely in the Brunhes period. One of the lowest lavas filling the El Golfo embayment gave an age of 545 ka. Therefore, an important break in the activity of El Hierro may have taken place between Tiñor and El Golfo volcanoes, probably coinciding in time with the period of rapid growth of the Cumbre Nueva volcanic rift zone in the nearby island of La Palma (see discussion in section III-1 and Fig. 72).

The radial dips of the lava flows indicate that the El Golfo edifice was centred near the town of Frontera, inside the later collapse embayment. The summit region may have been as much as 1500-2000 metres high!. Two sub-units may be identified in this volcano from morphological differences and from the local development of unconformities: 1) a basal unit, predominantly composed of strombolian and surtseyan pyroclastics (cinder cones and tuff rings), with subordinate lava flows, and 2) an upper unit predominantly composed of lava flows. The lower unit is cut by numerous dykes which form NE-, ESE- and WNW- trending swarms that match the present volcanic vent systems and indicate that a triple rift system was an important feature of the El Golfo edifice. In contrast, the relatively small number of exposed fee-

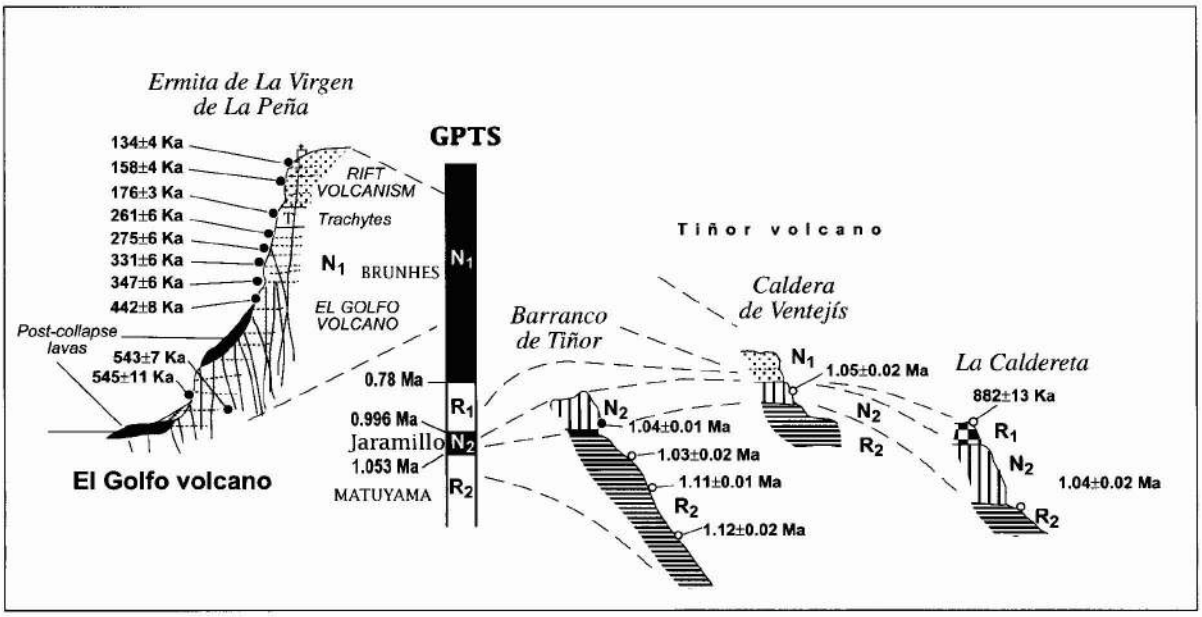

Fig. 59.—Disposition and extension of the magnetozones in *galerías* and boreholes in El Hierro.

der dykes in the Upper El Golfo unit indicates that the lavas which make this up mainly originated from near the summit of El Golfo volcano, although some flank vents are spectacularly exposed in the El Golfo cliffs. This central concentration of volcanic vents is in marked contrast with the younger rift series volcanism. The upper El Golfo unit is topped by several differentiated (trachybasalts, trachytes) lava flows and block-and-ash deposits. We interpret these volcanic differentiates as the terminal stages of activity of El Golfo volcano, prior to the establishment of the Rift volcanism (see below), similar to the central differentiated volcano developed at the late stages of the Taburiente volcano in La Palma.

The duration of the growth of El Golfo volcano can be estimated to be about 360-380 ka as indicated by the lower age of 545 ka and the age of the trachytic lavas (176 ka) in the collapse scarp section (see section 2 in Fig. 47).

The Rift volcanism

Although a multiple rift system was present in the El Golfo volcano, and may also have controlled the development of the NE - trending Tiñor volcano, we define the rift volcanism as the late stage of growth of the island when the three arms of the rift have been simultaneously active. The rift series lavas are broadly conformable on El Golfo lavas in much of the island, but striking local unconformities are present especially near the old coastlines. As a result of this wide distribution of vents a relatively thin layer of basic lavas has covered much of the island. These lavas have largely filled the El Julan collapse embayment and partially the El Golfo embayment (see sections 1, 4 and 5 in Fig. 47 and the geological map).

The maximum age of these eruptions is constrained by the differentiated emissions topping El Golfo volcano (134 ka).

Radiometric ages from 145 to 2.5 ka (K-Ar ages from 145 ka to 11 ka (Guillou et al., 1996); ^{14}C-ages of 6.74 ka (Pellicer, 1977) and 2.50 ka (Guillou et al., 1996) indicate that activity in this late volcanic stage is continuing, although the eruptive rates are relatively moderate. As yet the rift-series volcanism has not, therefore, produced a well-defined volcanic edifice comparable to the Tiñor and El Golfo volcanoes. This may be the consequence of the migration of volcanic activity to the nearby island of La Palma, where the very active Cumbre Vieja volcano developed in this period (see section III.1 and Fig. 72).

Petrology and geochemistry

The recent reconstruction of the volcanic history of the island of El Hierro by Guillou et al. (1996), applying palaeomagnetic stratigraphy and accurate

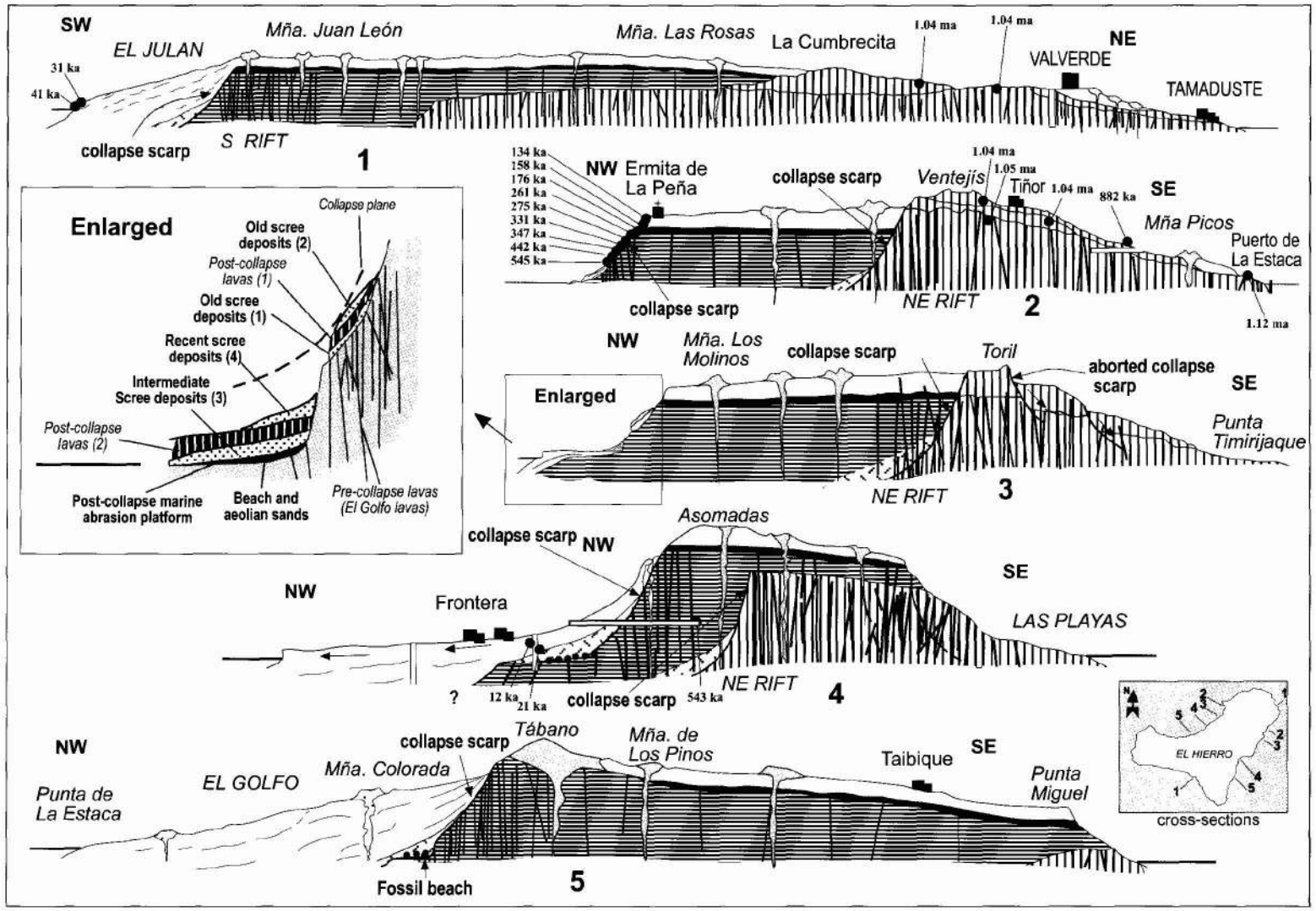

Fig. 60.—Geological cross-sections of El Hierro.

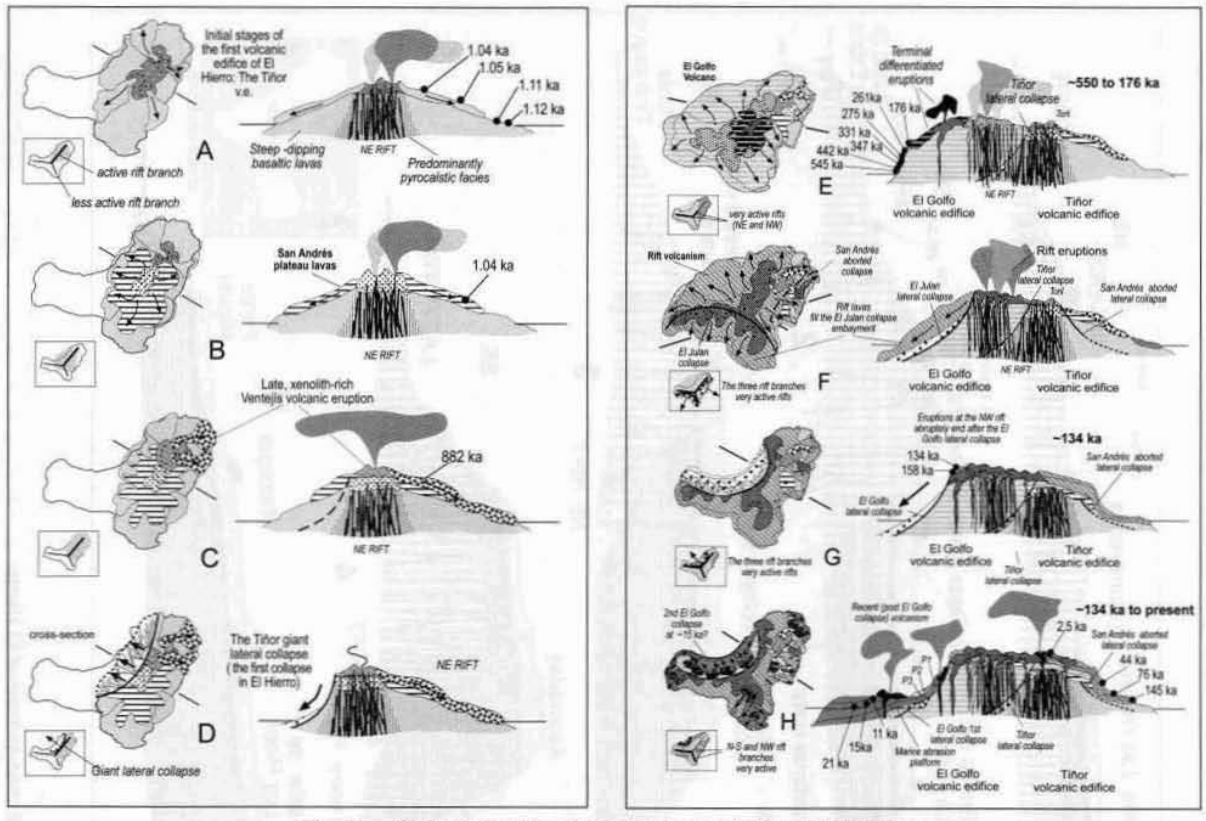

Fig. 61.—Cartoon sketching the geological evolution of El Hierro.

K/Ar dating, allows the petrological and geochemical analysis of representative samples of the volcanostratigraphic units defined (Table 4). This approach aims to define the trends of petrographical and chemical variation of the magmatism in this early stage of the island's development, as well as modelling the genesis and the nature of the El Hierro magmatic source.

Samples of the oldest Tiñor volcano are possibly the most representative of the initial magmatism of the island, while the continuous lava sequence observed at the 1500 m vertical scarp of the collapsed El Golfo volcano evolved from basalts to trachytes. Finally, the last eruptive cycle, related to volcanic activity at the triple-armed rift structure, spread over the entire island, does not show a significant temporal gap with the final stages (trachytes) of the El Golfo volcanic edifice.

The major, trace and REE elements were determined by ICP, at the Centre de Recherches Petrographiques et Geochimiques (Nancy, France), with techniques evolved by Gorvindaraju and Mevelle (1987).

Petrographical features

Tiñor volcano

The oldest subaerial lavas of El Hierro (sample CIHI-09) outcrop at the base of the Tiñor volcanic edifice, at the SE coast near Puerto de La Estaca. These massive oceanitic lavas are typical mafic basalts (see Fig. 62) with phenocrystals such as euhedral olivine and augite and several ore minerals. The groundmass has a porphyric texture with microcrystals of plagioclase, clinopyroxene and Fe-Ti oxides. These lavas are not altered and only some crystals of olivine present slight «iddingsite rims». Other flows inside the late Ventejís xenolith-rich lavas, of the same volcanic edifice, such as sample CIHI-08, are rich in phenocrystals of olivine, some with pressure shadows and partial resorption, indicating their xenolithic origin. The remaining samples (CIHI-10 and CIHI-18) from the Tiñor edifice are subaphyric hawaiite flows, with scarce phenocrystals of clinopyroxene in a cryptocrystalline matrix and some phenocrystals of plagioclase,

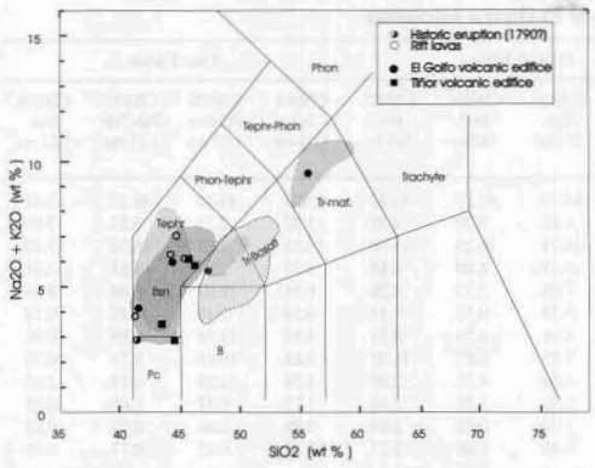

Fig. 62.—Alkalis vs. silica plot for El Hierro volcanism. The field limits are taken from Brandle et al. (1984) and Le Bas et al. (1986). The shaded areas correspond to the analytical data of Pellicer (1977, 1979).

similar to those observed in the upper lavas of the Tiñor volcano.

El Golfo volcano

The lower lava sequence of El Golfo volcano is formed by massive lava flows with petrographical characteristics similar to those of the Tiñor volcano, with olivine-augite basalts at the base of the escarpment (sample CIHI-05). Microcrystals of plagioclase, clinopyroxene and oxide microlites, and small crystals of chlorite form the groundmass. The sequence evolves to more microcrystalline lavas, some subaphyric hawaiites (sample CIHI-03), with scarce micro-phenocrystals of clinopyroxene and olivine in a cryptocrystalline matrix with plagioclase, clinopyroxene and ore minerals, and trachybasalts (sample CIHI-04), with some isolated olivine in a near crystalline matrix with microcrystals of clinopyroxene, oxide olivine and ore minerals. The more evolved lavas of the El Golfo edifice are trachytes, well represented by sample CIHI-02, with abundant phenocrystals of plagioclase feldspars, aegirine-augite and ore minerals. The amphibol hornblende appears in isolated phenocrystals with strong corrosion rims. The matrix is typically trachytic, with a network of feldspars and clinopyroxene.

The Rift volcanism

The recent rift lavas present varied compositional and textural characteristics. Some massive hawaiite lava flows, such as those filling the El Golfo embayment (sample CIHI-1) show a cryptocrystalline matrix and an almost total absence of clinopyroxene phenocrysts, in contrast with the oceanitic flow, olivine-clinopyroxene rich lavas of the NE rift at Las Lajas and Punta de El Guincho (sample CIHI-13), with evident resorption processes in some olivine crystals. The recent lavas of the NW rift at Lomo Negro, Hernandez-Pacheco (1982), show a spectacular abundance of clinopyroxene-olivine phenocrysts and ore minerals (sample CIHI-30).

Geochemical features

The geochemical composition, major and trace elements of samples representative of the three eruptive cycles are presented in Table 4. The total alkali vs. SiO_2 diagram (TAS) of Fig. 62 indicates a significant range of variation in composition, from picrite basalts to mafic trachytes, with abundant intermediate terms. The shaded areas show, for comparison, the analytical data published by Pellicer (1979). The increase in alkalinity is clearly apparent along the entire volcanic evolution of El Hierro, with normative nepheline consistently present in all the lavas sampled (see Table 4).

The Tiñor volcano shows a relatively limited range of compositions, from mafic basanite (Bsn) and picrite (Pc) lavas with high Mg numbers (Mg# 65-70), to more evolved tephrite (Tph) and trachybasalt (TrB) lavas with lesser Mg numbers (Mg# 48-50). The lavas of the El Golfo volcano show a wider compositional range, with the most basic basanites (Bsn) corresponding to the early stages of the volcano (sample CIHI-05). The Mg number (Mg# 58) and Ni content of 147 ppm indicates a relative more evolved character than the basanite-picrite lavas of the Tiñor volcano. The El Golfo sequence continues with the emission of trachybasalts (sample CIHI-04) and mafic trachytes (TM), (sample CIHI-02), probably indicating the latest phase of activity of El Golfo volcano (Guillou et al., 1996). The younger rift volcanism comprises some basanite-picrite (Bs-Pc) lavas (samples CIHI-13 and CIHI30), in consonance with their aforementioned high content in olivine-clinopyroxene phenocrystals. Part of the rift volcanism is characterised by more differentiated tephrites (Tph).

Major and trace element variation

Changes in significant major and trace elements, especially the transitional trace and incompatible elements, in relation with the MgO (Fig. 63) shows

Table 4.—**Analytical data of El Hierro volcanism**

	Historic	Fissural Rift Volcanism				El Golfo Edifice				Tiñor Edifice			
Sample	CIHI30	CIHI11	CIHI15	CIHI13	CIHI01	CIHI02	CIHI03	CIHI04	CIHI05	CIHI18	CIHI08	CIHI10	CIHI09
Rock type	PC-Bsn	Tph	Tph	Bsn	Tph	Tr	Tph	Tr-B	Bsn	Tph	PC-Bsn	Tph-TrB	Bsn
Ages	1790 ?	15 ka	44 ka	76 ka	158 ka	176 ka	261 ka	442 ka	545 ka	1.04 ma	1.05 ma	1.11 ma	1.12 ma
wt %													
SiO_2	41.33	44.64	44.16	41.19	45.30	55.61	44.30	47.27	41.45	45.67	44.46	46.17	43.41
TiO_2	4.07	4.00	3.88	4.26	3.65	1.24	3.83	3.20	4.25	3.92	2.71	3.55	3.07
Al_2O_3	9.82	16.37	15.21	11.03	16.03	19.02	16.79	16.30	13.09	16.55	12.09	16.58	13.10
Fe_2O_3	5.70	6.48	4.81	4.66	3.48	3.53	5.15	6.40	4.65	4.51	2.84	4.67	4.41
FeO	9.01	4.43	7.78	9.51	8.35	2.34	7.08	5.33	9.26	6.91	10.07	6.40	8.69
MnO	0.17	0.18	0.20	0.17	0.20	0.28	0.20	0.18	0.19	0.19	0.18	0.19	0.18
MgO	14.21	4.77	5.47	12.00	5.07	1.31	4.98	4.76	8.31	4.61	13.16	4.80	10.91
CaO	11.42	9.94	10.07	11.89	9.76	5.65	9.85	8.67	11.01	9.88	10.46	9.71	10.79
Na_2O	2.04	5.01	4.52	2.81	4.51	7.13	4.66	4.37	2.98	4.38	2.29	4.19	2.63
K_2O	0.84	2.02	1.76	1.02	1.61	2.39	1.32	1.25	1.16	1.72	0.57	1.65	0.88
P_2O_5	0.52	1.20	1.22	0.68	1.04	0.40	1.02	0.85	1.04	0.96	0.46	0.93	0.63
H_2O+CO_2	0.56	0.49	0.50	0.43	0.60	0.49	0.45	1.09	2.27	0.34	0.42	0.77	0.99
Mg #	68.8	50.5	49.8	65.8	49.2	34.3	48.3	48.5	57.6	48	69.6	49.8	65.4
nef (CIPW)	7.1	14.9	12.5	11.6	10.1	8.2	11.4	3.7	7.8	9.2	2.1	7.1	5.2
Ppm													
Cr	733	6.75	40.3	571	63.1	1.97	1.51	33.6	242	1.59	760	19	537
Ni	365	27.5	39.5	307	35.8	6.32	8.47	32.2	147	23.5	389	31.7	269
Co	69.7	28.4	34.7	64.3	30.4	3.71	29.7	27.8	49.3	31.1	63.5	29.7	55.2
Sc	27.6	13.8	16	25.2	14.8	5.9	14.8	15	21.2	15.8	23.7	15.6	23.3
V	365	277	282	365	248	34.6	230	201	316	263	263	248	327
Cu	86.6	39.9	48.2	130	44.3	10.3	18.5	38.2	122	30.8	78.9	37.8	95.2
Zn	127	138	164	133	151	186	140	138	156	132	116	131	121
Rb	19.8	50.5	45.5	21.5	36.7	68.4	27.9	27.5	27.9	38.6	12.6	38.7	19.4
Ba	197	549	450	258	394	801	416	346	336	410	155	389	198
Sr	522	1,369	1,219	734	1,070	2,099	1,124	780	952	1,056	467	994	569
Ga	21.5	29.2	30.4	23	27.5	32.9	25.2	27.5	26.5	27.6	19.4	26.5	21.2
Be	0.96	1.67	3.12	0.94	2.27	4.95	1.33	1.6	2.31	1.89	0.85	1.55	1.14
Nb	37.9	108	92.8	49.6	85.5	172	82.5	71.9	71.7	79.8	31.9	74.8	41.5
Zr	241	505	541	281	475	857	334	351	392	426	186	412	267
Y	22.2	42.2	43.4	25.5	39.9	58.5	38.5	36.8	35.3	39	22.8	34.5	25.5
Th	2.74	9.07	6.89	3.23	6.19	14.9	5.14	4.93	5.76	5.95	2.21	6.37	2.89
La	29.03	84.98	76.26	39.7	69.01	150.7	64.7	52.99	61.01	63.27	25.52	57.78	33.66
Ce	64.81	170.8	162.6	88.29	144.4	305.2	136	114.2	130.4	138.1	53.95	123.6	73.59
Pr	8.91	20.15	20.48	11.14	17.87	36.23	16.48	14.16	16.24	16.88	6.83	15.07	9.29
Nd	40.88	81.82	83.5	46.73	74.57	139	68.3	58.26	67.73	70.29	30.57	65.35	41.15
Sm	8.57	16.22	16.64	9.92	14.57	24.53	13.79	12.54	14.02	14.27	7.04	13.03	8.02
Eu	2.68	5.09	5.14	3.11	4.5	6.91	4.17	3.77	4.26	4.38	2.25	4.05	2.7
Gd	7.13	12.83	12.73	7.79	11.28	17.02	10.9	10.14	10.75	11.47	5.99	10.67	6.98
Tb	0.99	1.76	1.86	1.14	1.64	2.3	1.53	1.32	1.47	1.54	0.88	1.44	1.06
Dy	5.09	8.81	9.25	5.71	8.42	11.99	8.06	7.29	7.8	7.92	4.8	7.46	5.33
Ho	0.91	1.65	1.74	0.99	1.61	2.41	1.55	1.49	1.51	1.65	0.92	1.34	0.97
Er	1.89	3.64	3.79	2.17	3.56	5.34	3.43	3.2	3.01	3.48	2.05	3.04	2.22
Tm	0.23	0.5	0.5	0.29	0.5	0.71	0.47	0.46	0.44	0.48	0.27	0.42	0.32
Yb	1.4	3	3.11	1.69	2.87	4.52	2.75	2.6	2.34	2.88	1.77	2.53	1.88
Lu	0.21	0.41	0.44	0.22	0.42	0.63	0.37	0.39	0.3	0.39	0.26	0.4	0.28

a characteristic bend at values of about 6-7%, possibly reflecting the transition from basanites (Bsn-Pc) to more evolved terms (Tph, Tr-B, TM). This feature points to a significant degree of control of ferromagnesian minerals, such as olivine, clinopyroxene, and ore minerals, in the differentiation process. Furthermore, the maximum values of MgO are observed in the basanites-picrites (Bsn-Pc) of the Tiñor volcano and the rift volcanism. Contrarily, basanites from the lower sequences of El Golfo volcano show intermediate values, the end-terms being related to the trachytes (TM). Samples of the successive flows lavas overlap in the range of 5% MgO, a clear indication of the wide range of compositions in the volcanism of the island.

The SiO_2 vs. MgO plot (Fig. 63a) shows positive correlation trends in basanite-picrite lavas, and negative in the more evolved lavas corresponding to

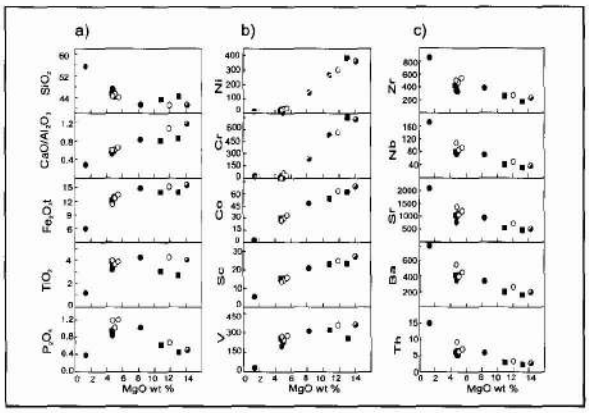

Fig. 63.—MgO variation diagrams for major oxides (wt%) and trace elements (ppm) of lavas of El Hierro. See text for discussion. Symbols as in Fig. 62.

the El Golfo and Rift volcanism. The CaO/Al_2O_3 vs. MgO variations, with positive correlation trends in all compositions, may reflect olivine and clinopyroxene segregation along the entire sequence and especially in the more evolved terms (Tph-TrB-TM). The trends observed in the variations of total $Fe2O_3$ and TiO_2, practically identical in the range MgO < 6%, differ for higher values, suggesting that the fractionating of Fe-Ti oxides is constrained to the evolved terms. Finally, P_2O_5 vs. MgO variations show negative correlation in the basic lavas, with significant evidence of apatite fractionation in the differentiated lavas.

The more compatible elements with respect to olivine and clinopyroxene, such as Ni and Cr (Fig. 63 b), show a significant decrease at values of MgO > 6%. The other transitional metals such as Co, Sc and V show general positive correlation trends, corresponding to fractionating of ferromagnesian components. The trachytes (TM), nearly totally depleted in these transitional elements, constitute the end-term of the series, in agreement with their eruption in the final stages of differentiation.

The content in trace elements such as Zr, Nb, Sr, Ba and Th with respect to MgO has been analysed for the three main volcanic units (Fig. 63 c). A tendency towards negative correlation clearly predominates with these highly incompatible elements, with progressive enrichments ranging from basanite-picrites (Bsn-Pc), intermediate terms: tephrites-trachybasalts (Tph-TrB), to trachytes (TM). The samples of the three main eruptive phases overlap in the range of 5% MgO.

The geochemical trends observed point to a certain degree of continuity or systematic differentiation in the lavas emitted in the Tiñor and El Golfo volcanoes. The oldest lavas of the former edifice (sample CIHI-09, 1.12 ma) have compositional characteristics close to those of primary materials, with high contents in MgO and compatible trace elements Ni, Cr, Co and Sc, but low contents in incompatible elements such as Zr, Nb, Sr, Ba, and Th. The lavas of the El Golfo edifice are more evolved, with decreasing values of compatible elements, while the values of incompatible elements overlap with the more evolved terms of the Tiñor volcano. The trachytes of the El Golfo volcano show the maximum enrichment in incompatible elements. Finally, the lavas related to the rift volcanism, the late stage of volcanic activity in El Hierro, with eruptions spread over the entire island, present diverse compositions, from basanite-picrite to more evolved tephritic terms.

The overlapping compositions observed suggest that lavas evolved parallel to the volcanic growth of El Hierro. The abundance ratios involving elements of similar incompatibility have been proposed by Chen et al. (1991) and Frey et al. (1994) as defining temporal changes in the Hawaiian volcanoes. In the island of El Hierro, ratios such as Nb/La (1.2 ± 0.12), La/Ce (0.47 ± 0.01), Sm/Nd (0.20 ± 0.01), Sr/Nd (14.8 ±1.1) and P/Nd (63 ± 3) are relatively constant, pointing to a homogeneous source and, likely, a comagmatic origin of the lava sequence.

Fractional crystallization

The systematic enrichment observed in the abundance of incompatible trace elements seems to be primarily controlled by crystal fractionation, inducing segregation of mafic mineral phases such as olivine, clinopyroxene and ore minerals, that constrain the variations observed in the content in MgO and transition metals.

The best-suited lava to represent a theoretical «parent magma» is possibly sample CIHI-09, from the lower sequences of the Tiñor volcano. This is the oldest lava sampled and does not present xenocrystals or accumulative processes. The calculations of the simulated fractional crystallization process were carried out with the program CRYSTAL (Barca et al., 1993). The results obtained are shown in Table 5 and plotted in Fig. 64 (see for comparison the analytical values of Table 4). The incompatible element abundance normalized to primordial mantle values (Sun and McDonough, 1989) fit, in general, with the calculated values. In summary, the greater part of the more evolved lavas from the island of El Hierro may be derived from a primary magma, represented by sample CIHI-09 from the initial eruptions of the Tiñor volcano, by

Table 5.—**Trace Element Crystal Fractional Model of El Hierro volcanism**

								Mineral phase subtracted (wt%)					Residual Melt	
PARENT	Type and Location samples	Age	MgO %	DAUGHTER	Type and Location sample	Age	MgO %	Ol	Cpx	Ox	Fsp	Ap	F %	STD
RIFT VOLCANISM														
CIHI-05	Bsn El Golfo. base escarpment (85 m)	545 ka	8.31	CIHI-11	Tph flow filling El Golfo	15 ka	4.80	30.6	61.4	7.9	—	—	68.4	0.16
CIHI-09	Bsn Puerto Estaca (Tiñor)	1.12 ma	10.91	CIHI-15	Bsn Las Playas	44 ka	5.47	61.4	32.6	6.0	—	—	46.7	0.20
CIHI-09	Bsn Puerto Estaca (Tiñor)	1.12 ma	10.91	CIHI-01	Bsn End flow lavas 650 m	158 ka	5.07	57.1	36.0	7.0	—	—	52.5	0.17
THE EL GOLFO VOLCANIC EDIFICE														
CIHI-05	Bsn El Golfo base escarpment	545 ka	8.31	CIHI-02	Tr Trachytes 585 m	176 ka	1.31	45.6	25.3	26.5	2.2	0.4	40.9	0.21
CIHI-09	Bsn Puerto Estaca (Tiñor)	1.12 ma	10.91	CIHI-03	Tph Flow lavas 505 m	261 ka	4.98	55.0	37.7	7.4	—	—	57.5	0.23
CIHI-09	Bsn Puerto Estaca (Tiñor)	1.12 ma	10.91	CIHI-04	Tr-B Flow lavas 295 m	442 ka	4.76	48.3	40.4	11.2	—	—	64.3	0.14
CIHI-09	Bsn Puerto Estaca (Tiñor)	1.12 ma	10.91	CIHI-05	Bsn El Golfo. base escarpment 85 m	545 ka	8.31	63.3	34.7	2.1	—	—	62.4	0.22
THE TIÑOR EDIFICE														
CIHI-09	Bsn Puerto Estaca (Tiñor)	1.12 ma	10.91	CIHI-18	Tph El Toril	1.04 ma	4.61	54.5	39.7	5.8	—	—	53.7	0.17
CIHI-09	Bsn Puerto Estaca (Tiñor)	1.12 ma	10.91	CIHI-10	Tph- Bco del Balón	1.11 ma	4.80	46.9	46.5	6.6	—	—	56.6	0.19

means of a continued process of fractional crystallization, with segregation of ferromagnesian mineral phases and Fe-Ti oxides. However, the origin of the trachytes from the final activity of the El Golfo volcano and the more tephritic flows filling the El Golfo embayment require a more evolved parent magma, similar in composition to the basanites at the lower part of the sequence of the El Golfo escarpment (sample CIHI-05). This is particularly evident for the derivation of the trachytic lavas (sample CIHI02), which requires the addtion of new mineral phases such as feldspar and augite for the postulated fractionated crystallization model. A distinct and consistent enrichment in regard to the more primary lavas is evident in the three main eruptive phases (Fig. 64), although the patterns relative to a primitive mantle composition are similar.

In summary, the fractional process induces a general enrichment in incompatible elements, evidenced by the uniform trend of enrichment in light REE (LREE) vs. heavy REE (HREE) elements in the $(La/Yb)_N$ variations of Fig. 65 a. The plotting of $(La/Yb)_N$ vs. MgO and $(La/Yb)_N$ vs. $(La)_N$, shows the lesser significance of basanitic-picritic terms in the Tiñor volcano when compared with the subsequent El Golfo and Rift volcanism. These values increase towards the more differentiated lavas (tephrites-trachybasalts), that overlap in the range of 5% MgO. The process reaches the maximum in the end terms (mafic trachytes).

Partial melting

Since the composition of the mantle source is unknown, a quantitative evaluation of partial melting is unfeasible. However, a semi-quantitative approach to the characteristics of the source can be inferred from the samples of relatively more primary composition, by application of the method proposed by McKenzie and O'Nions (1991) for deriving melt distribution from inversion REE data, similarly to the evaluation of the rate of plume melt production in Hawaiian volcanism (Watson and McKenzie, 1991), or the modelling of the composition of basaltic magmas of oceanic islands (McKenzie and O'Nions, 1996). As shown by Thirlwall et al. (1994), this requires the definition of the paragenesis of the source, since these features constrain significantly the applicability of the inversion method (Watson, 1993).

Plotting of La/Y vs. Zr/Nb and La/Yb vs. Dy/Yb variations, from representative primary samples, as proposed by Thirlwall et al. (1994, 2000) and Baker et al. (1997) helps in the characterization of the paragenesis of the source. In El Hierro, the lavas

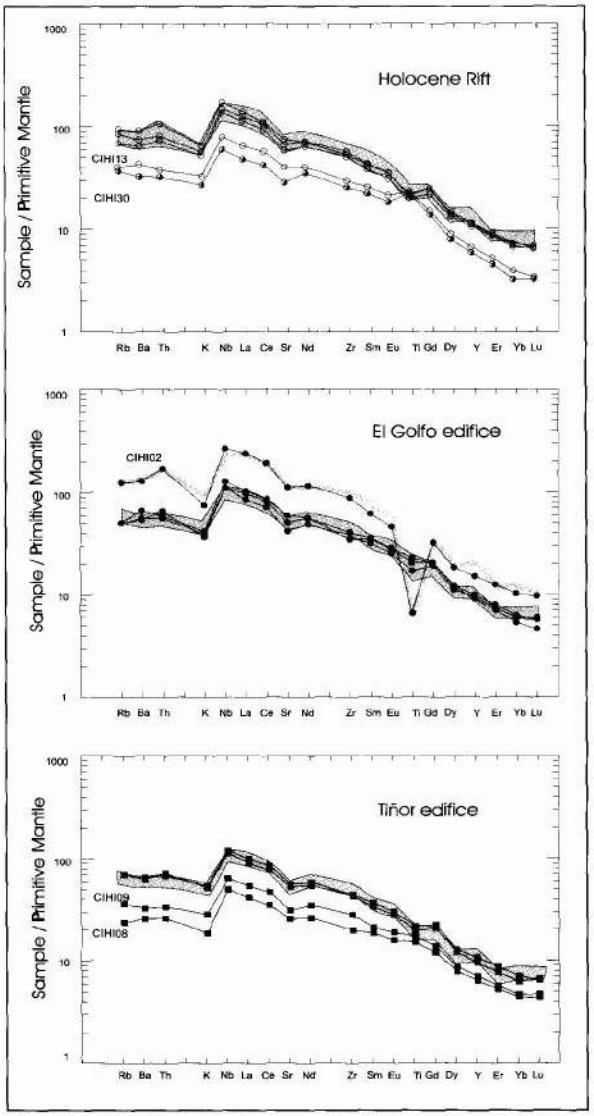

Fig. 64.—Primitive mantle normalized plots (Sun and McDonough, 1989) for the different volcanoes of El Hierro. The shaded area corresponds to the fractional crystallization model calculated from data of Table 5. See text for discussion. Symbols as in Fig. 62.

selected from the Tiñor edifice (samples CIHI-08 and CIHI-09) may be considered to be near primary (Mg# 65-70), as well as some rift volcanism lavas (samples CIHI-13 and CIHI-30), as indicated in Fig. 65 b. The Zr/Nb-La/Y diagram (Thirlwall et al., 2000) of these samples shows them to be constrained to garnet-facies melting trajectories, in intermediate position with Gran Canaria and La Palma. The basanitic-picritic terms are clearly separated from the more evolved lavas. Likewise, the $(Dy/Yb)_N$-

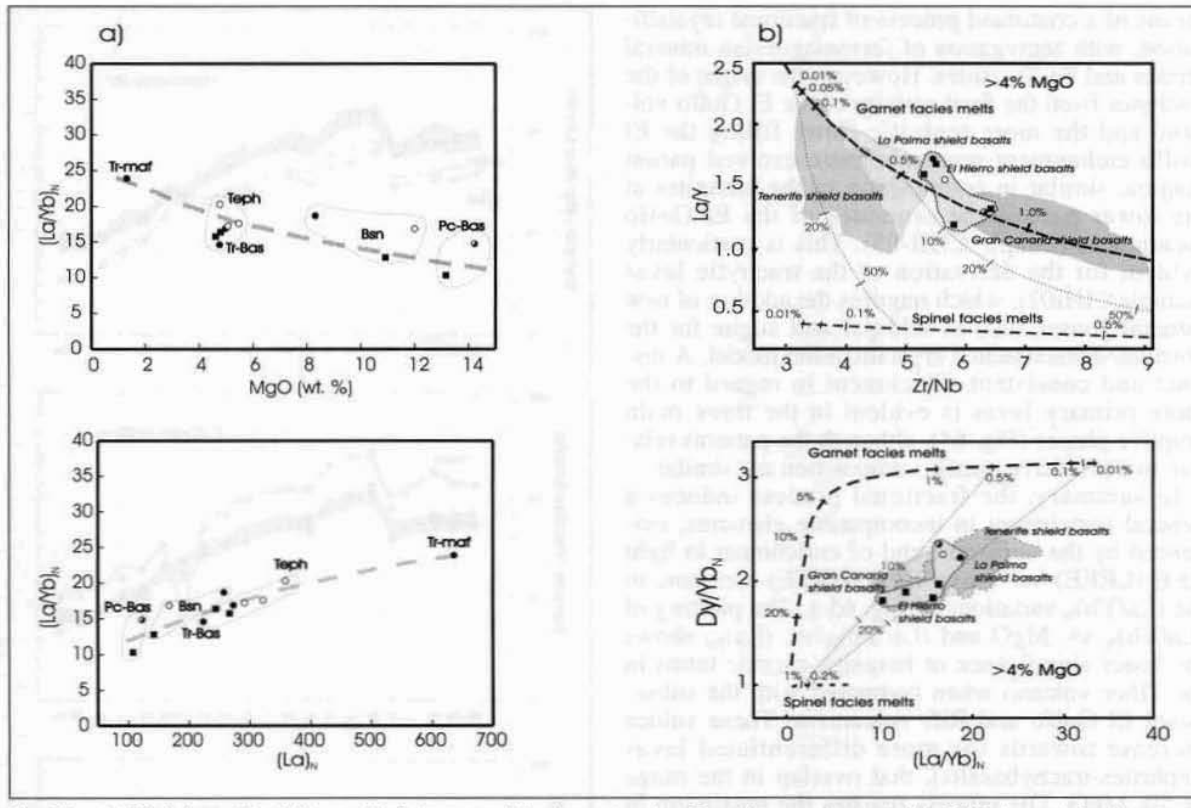

Fig. 65.—(a) Variation of $(La/Yb)_N$ vs. MgO (a compatible element) and vs. La_N (the most incompatible REE element) for the successive volcanoes of El Hierro. (b) La/Y vs. Zr/Nb and Dy/Yb_N vs. La/Yb_N diagrams, similar to those proposed by Thirlwall et al. (2000) to evaluate the source of basalts from the shield stage of Tenerife. See text for discussion. Symbols as in Fig. 62.

$(La/Yb)_N$ diagram (Thirlwall et al., 2000) shows the samples from El Hierro bound between Gran Canaria and Tenerife, and overlapping La Palma. Lavas from the Tiñor volcano group in the field of low $(Dy/Yb)_N$ when compared with the succeeding El Golfo and Rift volcanism. Dispersion of $(La/Yb)_N$ values may reflect fractionating of clinopyroxene.

If the composition of the source is assumed to be of a homogeneous nature, and the volcanics of the different eruptive phases of El Hierro are presumed to be cogenetic, the modelling by inversion of REE data, as McKenzie and O'Nions (1991) proposed, will be feasible. In this assumption, it must be accepted that the initial magmatism presents compositional characteristics close to those of the above-mentioned primitive lavas, whereas the remaining more differentiated magmas would be derived by possible fractionation under lower pressure. The result of the extraction melt obtained by inversion from the depleted upper mantle used for the normalization (Fig. 66 a) shows the element concentration REE ratios in remarkable agreement with the mean values considered to be the primary subaerial volcanism of the island. The best fit calculated melt distribution (Fig. 66 b) conforms to the decompression melting of depleted mantle after the extraction of a melt originated at 80-108 km, and increasing melt fraction in the garnet-spinel transition zone between 81-93 km. The maximum values of melt fraction would be in the range of ~1.16, with an upper limit of 2.2 %, after correction for 24% fractionation. As depicted in Fig. 66 c, the best fit of the model requires a relative enrichment in rare earth elements by a factor of ~1.5 with respect to the depleted upper mantle, possibly in response to changes in the source of the shield stage lavas (McKenzie and O'Nions, 1991; Watson, 1993).

Geochemical evolution of El Hierro

The island of El Hierro, the westernmost of the Canary Archipelago, presents a simple geochemical evolution, possibly in consonance with rapid tem-

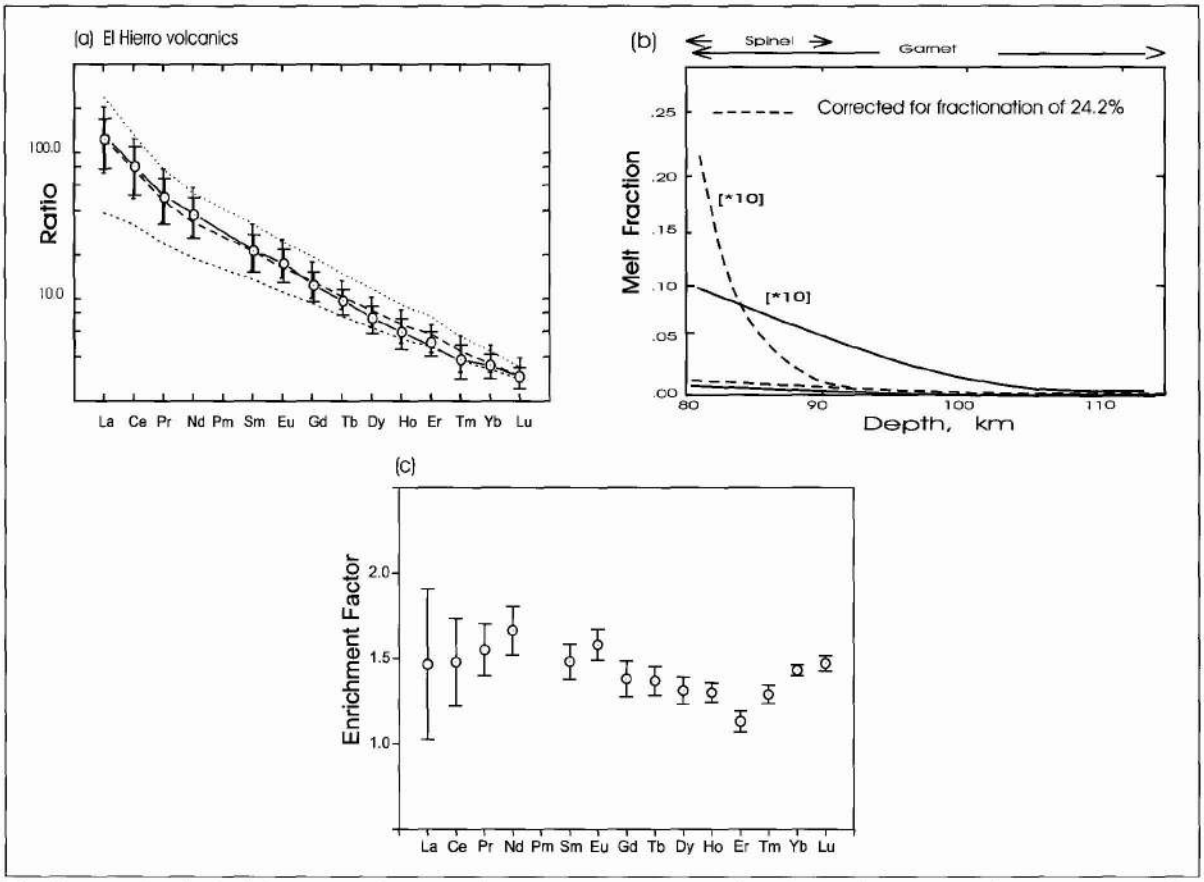

Fig. 66.—Results obtained after application to samples of El Hierro of the REE inversion model of McKenzie and O'Nions (1991): (a) Observed and calculated elemental concentration ratios and standard deviation for basalts from El Hierro in relation with the depleted upper mantle source. (b) Variation of melt fraction distribution with depth obtained by the inversion model. (c) Enrichment ratios required in the source region melts in relation to the depleted upper mantle.

poral growth. This can be related to the activity of the Canarian hotspot, presumably located at present under this island. As established by Guillou et al. (1996), the first subaerial eruptive cycle gave place to the Tiñor edifice, characterized by more primary or less evolved lavas. The lavas of the ensuing volcanic cycle, that constructed the El Golfo edifice, show more evolved geochemical characteristics, with highly differentiated final term trachytes. However, overlapping is evident in the intermediate terms of the Tiñor and El Golfo edifices.

The last eruptive cycle, corresponding to widespread eruptions distributed along a triple-armed rift system, is characterized by the wide compositional variance of the lavas. The trace-element data suggest that the eruptive cycles seem to be connected by the same stationary magmatic source. They seem to be related to fractional crystallization processes leading to a systematic enrichment in incompatible elements correlative to the evolution of the island. The contents in REE in the more primary lavas of the island (Tiñor edifice) suggest that this alkali magmatism may have originated in the garnet facies mantle at about the 12 km garnet-spinel transition zone, by a relatively low proportion of melting (1.16-2.2 %) of depleted mantle apparently enriched in REE by a factor of ~1.5.

The more primary volcanics of El Hierro show relatively low ratios of highly incompatible elements, Ba/Nb and higher La/Nb ratios (Fig. 67), in comparison with other oceanic island volcanoes (Weaver et al., 1987; Weaver, 1991 a,b; Sun and McDonough, 1989). The plot reveals that the mean values of La Palma are projected close to the limits of the island of St. Helena. In contrast, El Hierro appears in theoretical continuity to the normal

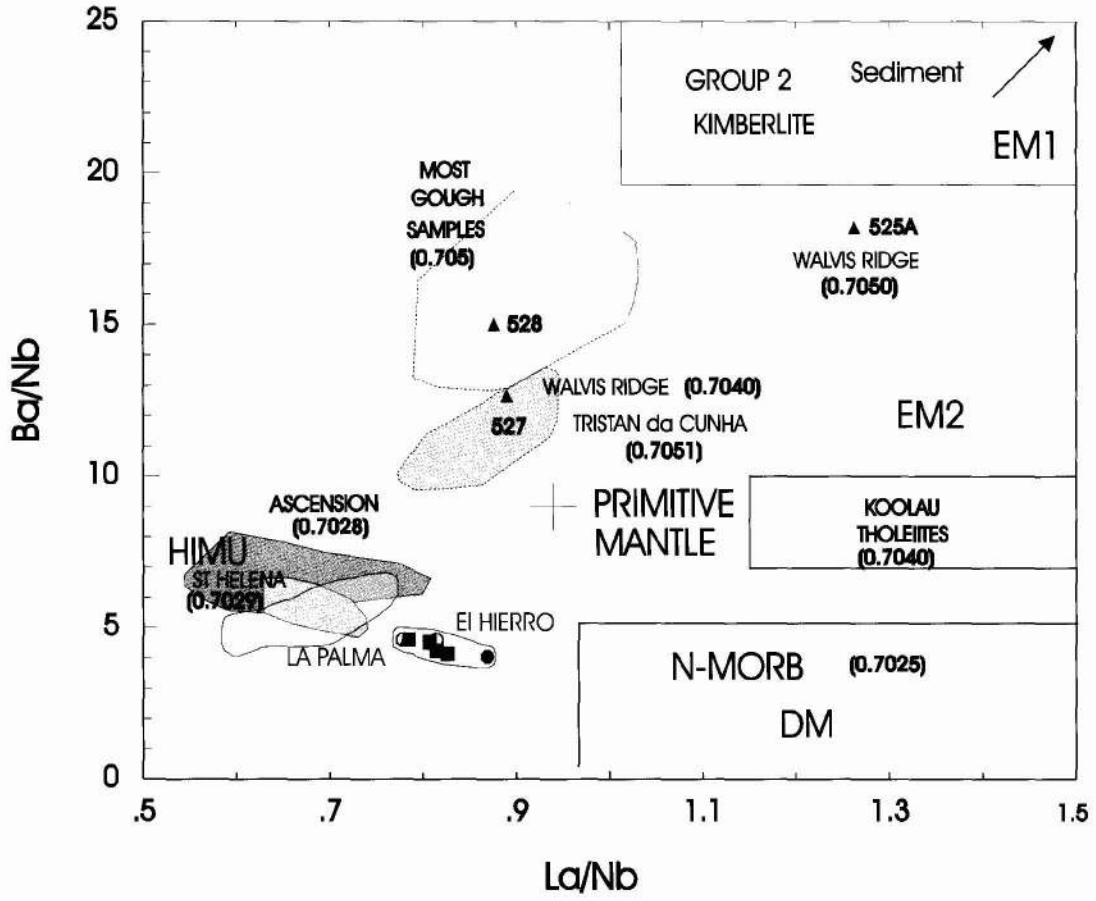

Fig. 67.—Ba/Nb vs. La/Nb diagrams. OIB mean values of South Atlantic islands from Weaver et al. (1987) and Sun and McDonough (1989). Data of the different volcanoes of El Hierro and La Palma are plotted for comparison. See text for discussion. Symbols as in Fig. 62.

MORB component, with clearly lower values in comparison with the islands of Ascension and St. Helena.

On the basis of the above-mentioned ratios, and until more accurate isotopic determinations are available, it can be postulated that the more primary materials of the island of El Hierro provide evidence of the interaction of the plume HIMU OIB source with a depleted source of normal mid-ocean ridge basalts (MORB). These results coincide with the inversion model proposed, and with those reported earlier by Hoernle et al. (1991) for the western Canary Islands (La Palma and El Hierro) on the basis of Sr-Nd-Pb isotopic data. The interpretation of these authors is based in the interaction of the Canary hotspot (HIMU-like) and the asthenosphere depleted mantle with minor amounts of enriched mantle material (DM + EM). In a more recent model by Hoernle and Schmincke (1993) the basanite magmas in the two youngest and westernmost islands of the Canary archipelago would be related to a «blob-type» process.

Structural geology

Rift zones

Rift development played a major part in the configuration of the island of El Hierro, as clearly shown in Fig. 55. Since rifts were, as well, a principal force triggering and confining giant landslides, they can be considered to be a key feature in the geological and geomorphological evolution of the island.

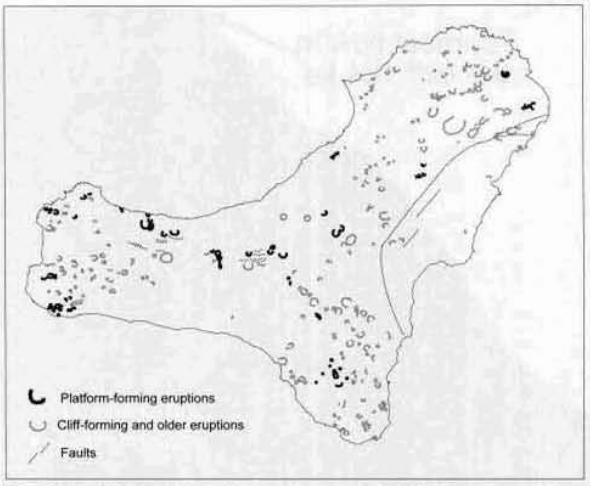

Fig. 68.—Distribution of eruptive vents in El Hierro, outlining a well-defined regular triple-armed rift system.

Fig. 69.—View of the San Andrés fault.

Rifts are defined by concentration of eruptive vents (Carracedo, 1979, 1984, 1994, 1996, 1999). The clustering of vents along three main tecto-volcanic lineaments is clearly apparent in Fig. 68. Vents appear tightly grouped at the upper part of the island and spread downslope. Observation of submarine vent distribution in a Poseidon dredging campaign in 2000 shows this dispersion to increase at the lower flanks of the island. This feature may correspond to the higher anisotropy, thermal memory and gravitational stresses at the apical part of the island edifice, correlative to the greater eruptive concentration, as discussed in Section III-3 and Fig. 73.

Rift lavas ensued after the central, differentiated emissions that ended the building of the El Golfo volcano at about 176 ka. These rift eruptions continued, with relatively low eruptive frequency and volumes, from about 158 ka to 1000 years before present, from the three arms of the rift system (see Fig. 56 and the geological map). There is no evidence of historical eruptions in the island.

Gravitational flank collapses

The volcanic history of El Hierro clearly exemplifies the intense interaction between volcano growth and lateral collapse episodes in the very early stages of subaerial development of an oceanic island. At least four main flank collapses have been clearly identified from on- and offshore observations. In this island outcrops an extensive and well-preserved fault scarp related to a detached block from an incomplete flank collapse.

Catastrophic collapses generated the submarine debris avalanche deposits observed at the flanks of El Hierro (see Fig. 5) as reported by Holcomb and Searle (1991), Urgelés et al. (1997) and Masson et al. (2002).

The present-day island of El Hierro is therefore a fraction of the three successive volcanoes accreted onto earlier, partially destroyed edifices. The present subaerial volume of the island is probably less than a third of the volcanic products erupted, which gives an idea of the difficulties encountered in these islands in the evaluation of magma production and eruptive rates.

The Tiñor giant collapse

Probably soon after the late explosive episodes of the Tiñor volcano activity (the xenolith-rich, Ventejís eruptions about 882 ka ago of Figs. 46 and 48 C), the volcanic edifice collapsed towards the NW, producing the first giant landslide of El Hierro (Figs. 47 and 48 D). This collapse may have removed more than half of the volumes of the subaerial part of the Tiñor edifice (see sections in Fig. 47).

The evidence for this giant collapse is shown in the cross sections 2-4 of Fig. 47. Section 4 of this figure shows a *galería* excavated in the El Golfo embayment scarp and progressing towards the lavas of the Tiñor volcano. At the end of the tunnel, the El Golfo lavas of 543 ka and normal (Brunhes) polarity are at the same level as gently east-dipping lavas more than 1.04 ma old and of reverse polarity (Matuyama pre-Jaramillo), which are exposed at the surface and in *galerías* to the east.

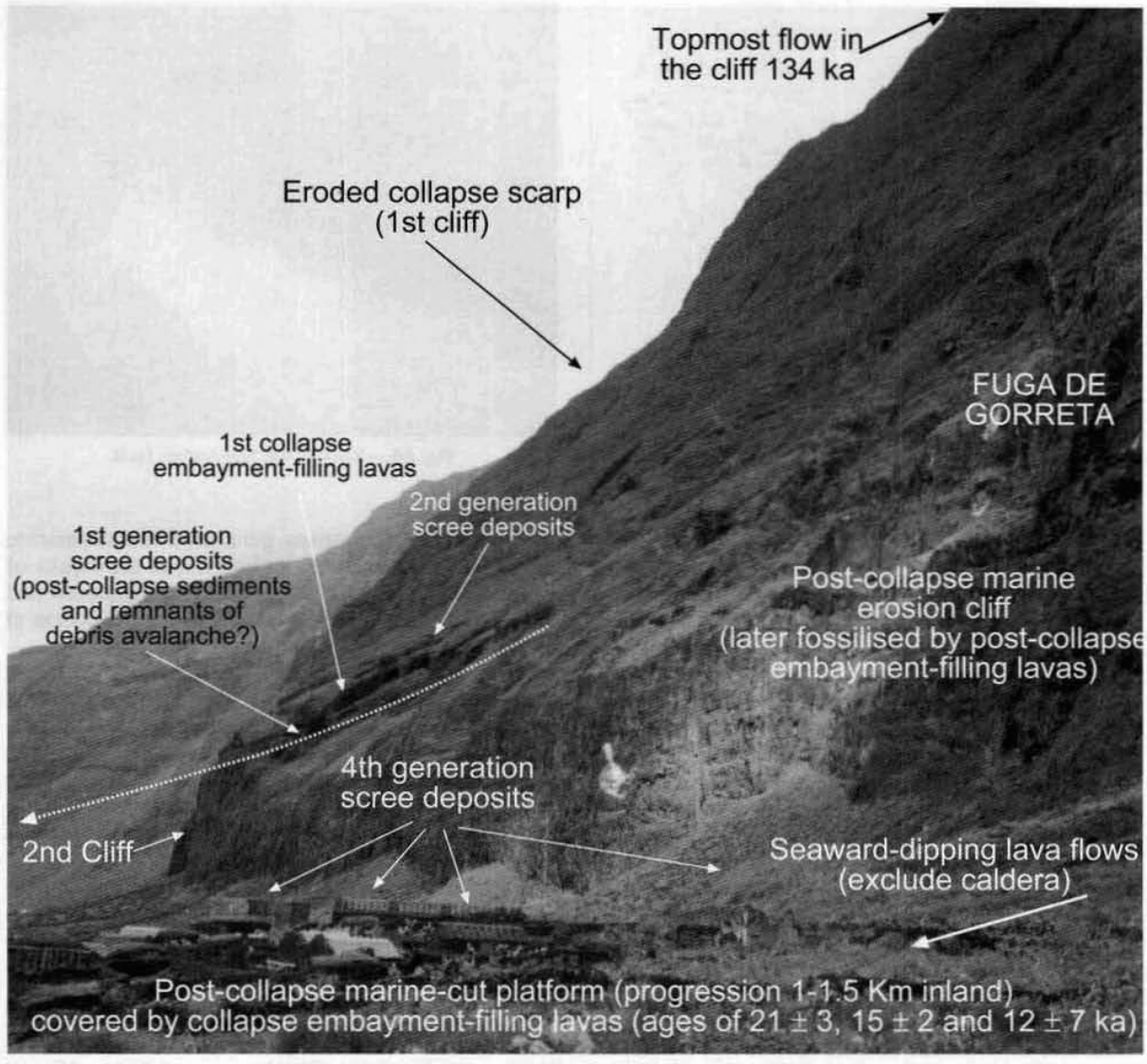

Fig. 70.—Complex sequence of cliff- and scree-forming events in the El Golfo escarpment inconsistent with the 13-17 ka dating by Masson (1996) and Masson et al. (2002) of the El Golfo collapse. See text for explanation.

The El Julan giant collapse

This feature was identified in 1991 by Holcomb and Searle, and considered older than the El Golfo collapse. The lack of outcrops of the collapse scarp makes the dating of this event from onshore evidence difficult. Water *galerías* in the El Julan collapse embayment cross part of the filling lavas, belonging to the Rift volcanism. This constrains the minimum age of the collapse in about 150 ka. The lava flows that fill the embayment have been dated at the SW coast at between 41 and 31 ka (Figs. 43 and 47-1). The El Julan collapse, which destroyed the SW flank of the El Golfo volcano, probably occurred when this volcano was well developed.

The San Andrés giant slump

The SE flank of the island is a detached block bounded by a system of faults (the San Andrés fault of Carracedo et al., 1997 c, and Day et al, 1997) parallel to the coast and with downthrows up to 300 m towards the coast (Figs. 42 and 55).

This fault (Fig. 69) is a relatively young (developed between 545 and about 261-176 ka), although inactive lateral collapse structure, constrained between the last emissions of El Golfo volcano at about 176 ka and the rift lavas cascading down the collapse scarp dated at 145 ka (Guillou et al., 1996). It was interpreted as an aborted giant flank collapse by Day and coworkers (1997), but recent offshore evidence suggests that the faults are the headwall of a slump, part of which rested onland while the remainder collapsed forming the Las Playas embayment and debris avalanche reported by Masson and coworkers (2002).

The well-developed topographic fault scarp associated with the San Andrés fault system led to the hypothesis that it was an active incipient collapse structure and, therefore, a major natural hazard. However, the age relationships of the faults to lavas and other volcanic rocks which have been dated recently (Guillou et al., 1996) constrain the fault between the ages mentioned above. This relatively old and inactive structure is unlikely to be reactivated since the El Golfo giant landslide occurred after the tectonic event, without further reactivation of the San Andrés fault.

The El Golfo collapse

The El Golfo embayment is perhaps the most spectacular feature of El Hierro. It is some 15 km across from Roques de Salmor to Arenas Blancas, extends about 10 km inland from these points, and its headwall is still in excess of 1.4 km high in places. Taking into consideration the likely original height of the El Golfo edifice (about 2000 metres) the probable volume of subaerial material removed in the formation of the embayment is at least 120 km^3. In addition the available bathymetry indicates that a similar volume has been removed below sea level.

Formation of the El Golfo embayment by catastrophic lateral collapse was first proposed on the basis of the discovery of a giant debris avalanche deposit offshore to the north (Holcomb and Searle, 1991; Masson, 1996). The age of the El Golfo embayment is still in debate. Some authors proposed a single collapse that occurred between 13 and 17 ka, based on the correlation of the collapse debris avalanche deposits found offshore to the north with a turbidite in the Madeira abyssal plain. This offshore information strongly conflicts with on-shore evidence for the age of the embayment exposed at the embayment headwall (Fig. 70) and in several boreholes emplaced within the collapse embayment

The morphology of the marine abrasion platform beneath the lavas which fill the embayment is accessible through numerous boreholes drilled for underground water exploration (Guillou et al., 1996; Carracedo et al., 1997 c). These features imply a long period of post-collapse erosion prior to the emplacement of those lavas.

The embayment cliff shows a complex geomorphology, incompatible with the simple features expected from a recent and single event collapse. Multiple (at least four) generations of screes can be identified at the foot of the embayment cliff and perched on the cliffs (Fig. 70). The first scree, possibly associated with debris avalanche deposits (inaccessible), underlies the remains of rift lava flows cascading down the scarp (scree-forming lavas of Carracedo et al., 1997 a, b, 1999 a, b). The second scree covers these lavas, and the whole appears perched over a 200-m vertical marine erosion cliff (Fig. 70). The prolongation of the flow and screes profile points to a wide completely eroded platform (see Fig. 70). The marine cliff has been fossilised by subsequent platform-forming flows from vents within the collapse embayment (see Figs. 61 H and 70, and the geological map), flowing on the marine cut platform originated by the erosion of the first post-collapse lava platform. The third generation of screes underlies these late lavas, dated at least at 21 ka (Guillou et al., 1996). Finally, the late lava platform underlies the last (4th) generation of scree deposits (see inset in Fig. 60).

The details of these lines of evidence suggest that the subaerial embayment may have formed soon after the emplacement of the lavas at the top of the cliff sequence (134 ka) during the previous interglacial period (Fig. 71).

An interesting observation by Szérémeta et al. (1999) is the easterly deviation of the mean declinations of the El Golfo and Rift sequences at the El Golfo escarpment by about 5° and 15° respectively, suggesting that the section has undergone a continued clockwise rotation.

COMPARATIVE ANALYSIS OF GEOLOGICAL AND STRUCTURAL FEATURES IN THE WESTERN CANARIES

Correlation of ages and periods of growth

An interesting feature of the Canarian archipelago is the fact that the islands of La Palma and El Hierro are coetaneous in construction and form a N-S-trending dual line of island volcanoes, perpendicular to the general trend of the archipelago (Fig. 3). Large-scale distribution and age progression in

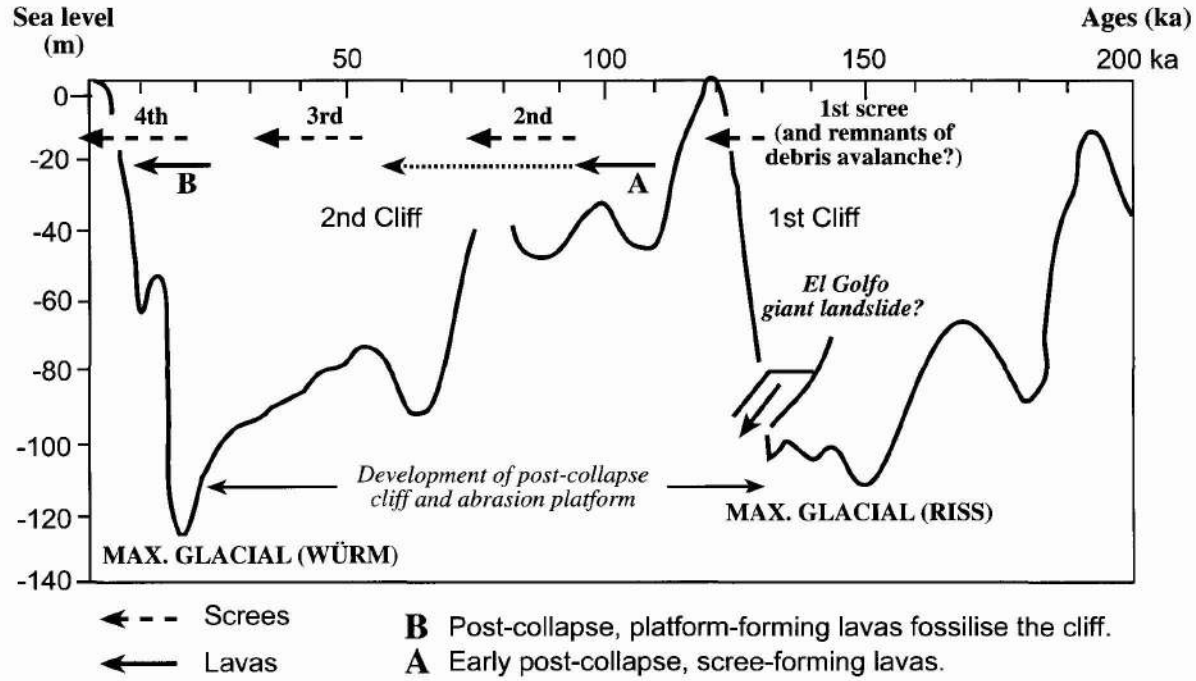

Fig. 71.—A probable correlation of the successive cliff- and scree-forming events in the El Golfo escarpment and the changes of sea level in the glaciations.

most of the oceanic island chains are well explained by the steady movement of lithospheric plates over fixed mantle plumes, yielding chains of consecutive discrete volcanoes. In this model one island starts to form when the bulk of the previous one has already developed, the inter-island distance governed by lithospheric thickness and rigidity (Voght, 1974; Ten Brink, 1991). At the initiation of an oceanic island chain the first magma cuts through unloaded pristine lithosphere. As the first island develops the volcanic load grows; increasing compressive flexural stresses eventually exceed the tensile stresses of the mantle plume, blocking magma pathways to the surface. This precludes the initiation in the vicinity of any new island volcano (Ten Brink, 1991; Carracedo 1998; Hieronymus and Bercovici, 1999).

Dual-line volcanoes, such as the Kea and Loa trends in the Hawaiian Islands, have been associated to changes in tectonic-plate motion, resulting in the location of a volcanic load off the hotspot axis. Compressive stresses related to the off-axis volcano block the formation of the next island and split the single line of volcanoes in a dual line of alternating positions of volcanoes (Hieronymus and Bercovici, 1999). However, in the Canarian chain the association of the dual line of volcanoes with a change in direction of the African plate is not clear.

In the Canaries an interesting aspect to consider is the periods of growth of the islands. Although La Palma and El Hierro developed at the same time the alternating periods of eruptive activity and quiescence are not concurrent. Most of the volcanic formations of these islands have been dated and correlated by means of extensive radiometric dating and geomagnetic reversals. When the ages are plotted and the corresponding eruptive volumes evaluated (Fig. 72), alternating periods of high eruptive rates and frequencies with intervals of lesser volcanic activity are clearly recognized. This trend suggests the switching back and forth of intense periods of growth in both islands.

The mechanism is far from clear, but the migration of volcanism from one island to the other coincides with the occurrence of giant gravitational collapses (Fig. 72).

Although El Hierro is geologically younger than La Palma, most of the volcanic activity of the western Canaries in the last 120 ka has been located in the latter, including all the historical eruptions.

A comparative analysis of rift development

The comparison of La Palma and El Hierro offers a good opportunity to analyse the processes contro-

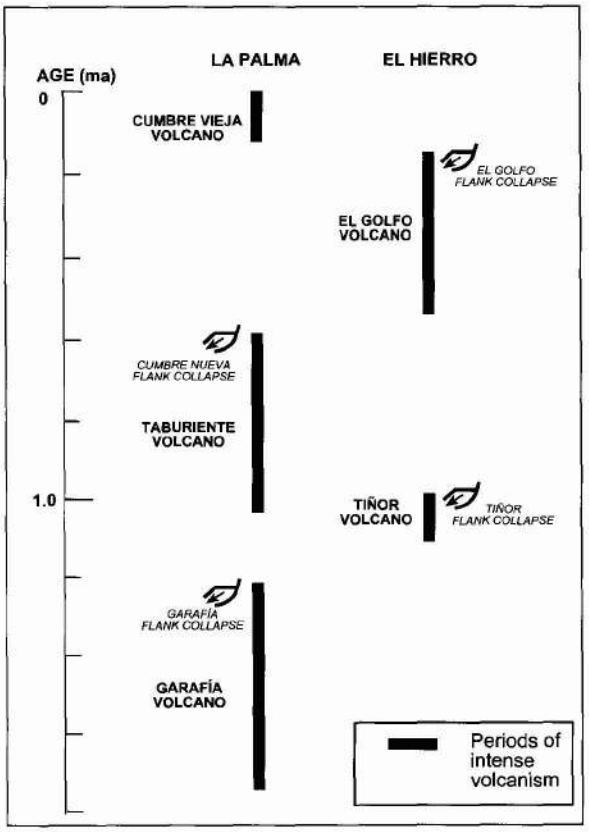

Fig. 72.—Alternation of phases of intense volcanism in La Palma and El Hierro, apparently in relation to the main gravitational landslides.

lling the development of rifts in juvenile shield volcanoes. These islands show striking differences in the evolution and geometry of rifts, notwithstanding their short period of growth. Rifts are incompletely defined in the Taburiente volcano in contrast with El Hierro and Cumbre Vieja volcano. However, in El Hierro the rift system shows a regular three-armed geometry, unlike Cumbre Vieja volcano, with a clearly predominant single arm.

As mentioned before, emission centres are dispersed throughout the early subaerial growth of La Palma (the Garafía and early Taburiente volcanoes) as evidenced by the widespread outcrops of pyroclastics. During the upper Taburiente, however, emission centres started to group in poorly-defined branches (see Figs. 19 and 49), while dyke directions tend to be spread in a radial disposition.

Eruptive vents in El Hierro started to define rifts during the growth of Tiñor and El Golfo volcanoes, and formed the distinct present three-armed rift system in the latest eruptive activity (the Rift volcanism, see Fig. 68).

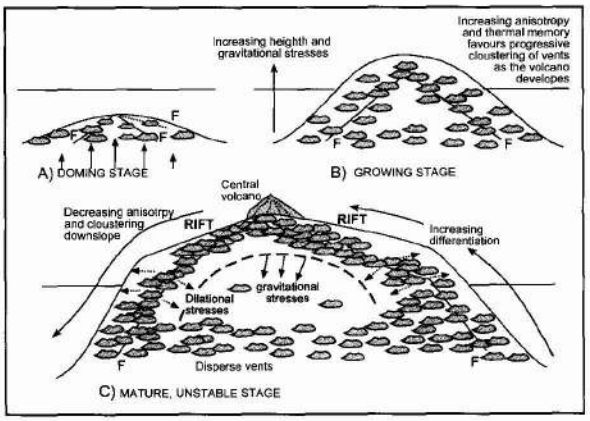

Fig. 73.—Sketch of the development of rift zones in oceanic island volcanoes.

The Cumbre Vieja volcano developed buttressed in and as a prolongation of the Taburiente volcano. During its fast growth, the initial dispersed eruptive centres rapidly grouped along a N-S trend, conforming a prominent dorsal (Figs. 21, 23 and 24). In the last 7 ka this process progressed, most of the eruptions being located in the summit region of the rift (Carracedo 1997 a, b; Day et al., 1999).

Submarine volcanoes are abundant at the flanks of La Palma and El Hierro and without any apparent grouping, as observed in a dredging campaign of the Poseidon vessel in 2001 (Hansteen et al., 2001; Gee et al., 2001). The clustering of vents increases towards the crest of the islands, to a maximum in the summit regions. Gravitational stresses seemingly could account for this grouping, but these stresses only build as the island volcano reaches a threshold elevation after a sustained period of growth. Gravitational stresses are the consequence and not the primary mechanism of rift development. Besides, these strains do not explain the regular geometry in some volcanoes. As shown in the sketch of Fig. 73, a probable mechanism is the magmatic doming and regular fracturing present from the earliest stages of island growth (Carracedo, 1994, 1996). These initial fractures will act as preferred paths for eruptions, steadily increasing the grouping of vents, anisotropy, thermal memory and, therefore, rift progression. Eruptive volumes and magmatic differentiation consistently augment with time and towards the centre of the rift system, eventually giving place to central volcanoes. Gravitational and extension (wedging) stresses build up to make the volcano progressively unstable, eventually triggering catastrophic flank collapses that consistently involve the sectors bounded by the rifts (Fig. 73 C).

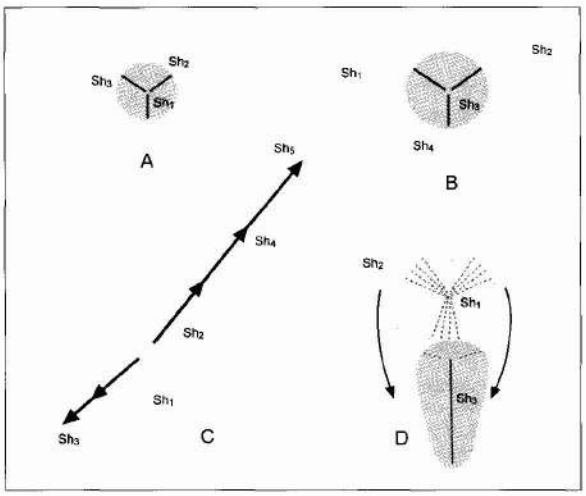

Fig. 74.—Patterns of development of oceanic islands by coalescence of successive shield volcanoes (sh_1, sh_2, etc.). Depending on the mobility magma plumbing these volcanoes may overlap concentrically in stationary magma sources (as in Central Tenerife and El Hierro) or align due to movement of the magmatic source, as in La Palma. Well-defined triple-rift systems develop only in islands where magma sources remain stationary since the early shield-building stages.

A key feature to allow these processes to develop and to explain the differences mentioned in rift development is the mobility of the islands' magmatic plumbing.

A comparative analysis of magma plumbing mobility and general patterns of island development

The Canaries and oceanic islands in general form as the result of aggregation of coalescent volcanoes with different patterns. The successive shields may overlap concentrically, as in El Hierro, La Gomera and central Tenerife (Fig. 74 A, B), or may align as independent shield volcanoes in predominant directions, as in Fuerteventura-Lanzarote and La Palma (Fig. 74 C). Only the islands formed by concentric overlapping volcanoes from persistent stationary magmatic sources may be successful in developing well-defined triple-armed rifts. The evolution of La Palma differs in that the volcanic activity migrated southwards before completion of the definition of rifts in the northern shield. On the other hand, the Cumbre Vieja volcano grew attached to the flank of the Taburiente volcano. Volcano growth on the flank of an older volcano which acts as a supporting buttress may explain the rapid change to a single-arm configuration (Fig. 74 D).

ACKNOWLEDGEMENTS

We are especially grateful to J. López Ruiz and A. Klügel for constructive review and comments, that helped greatly to improve the original manuscript.

This work has been financed by the Spanish CICYT project (PB92-0119), NATO project (NATO CRG no. 940609), by a project for the study of volcanic risks in the Canary Islands (1991-1994) financed by the Consejería de Política Territorial of the Canary Islands Government, and mainly by the MAGNA project of La Palma, financed by the Spanish Instituto Geológico y Minero. We are very grateful to the Dirección General de Medio Ambiente of the Canary Islands Government and Parques Nacionales in La Palma for permission to sample in the National and Natural Parks. To S. Day, A. Hernández Pacheco and J. Vegas for field data and collaboration during the MAGNA of La Palma. In the Laboratorio de Geoquímica and Laboratorio de Rayos-X of the Museo Nacional de Ciencias Naturales (CSIC) to M.I. Ruiz Pineda, M.A. Vallejo Haya for the analyses of major elements and R. González Martín for RX analyses of samples. The trace elements were analysed by O. Cazalla Vázquez and M.I. Moreno of the Laboratorios de ICP-MS and FRX of the Centro de Instrumentación Científica, Universidad de Granada. M. Castillejo and J.M. Hontoria (MNCN-CSIC) for the preparation of samples. E. Rodríguez Valdes for the palaeomagnetic analyses in the Estación Volcanológica de Canarias (CSIC). J.M. Cabrera Peraza in the Estación Volcanológica de Canarias (CSIC) and M.A. Vela Casado (MNCN-CSIC) for collaboration in the preparation of graphics.

We are grateful to Drs. Dan and James McKenzie, Institute of Theoretical Geophysics, Cambridge, for facilitating programs and subroutines of the «INVMEL» programs, Dr. S. Veintemillas for his assistance with compilation and application, and to Dr. D. Barca, Dipartimento di Scienze della Terra, Universita degli Studi della Calabria, for providing the «CRYSTAL» computer software.

Pauline Agnew spent many hours helping to improve the English.

References

Abdel-Monem, A.; Watkins, N.D. and Gast, P.W. (1972). Potassium-argon ages, volcanic stratigraphy and geomagnetic polarity history of the Canary Islands: Tenerife, La Palma and Hierro, *Amer. J. Sci.*, Vol. 272, 805-825.

Ancochea, E.; Fuster, J.M.; Ibarrola, E.; Cendrero, A.; Coello, J.; Hernán, F.; Cantagrel, J.M.; Jamond, C. (1990). Volcanic evolution of the Island of Tenerife (Canary Islands) in the light of new K-Ar data. *J. Volcanol. Geoth. Res.*. Vol. 44, 231-249.

Ancochea, E.; Hernán, F.; Cendrero A.; Cantagrel, J.M.; Fúster, J.M.; Ibarrola, E.; Coello, J. (1994). Constructive and destructive episodes in the building of a young Oceanic Island, La Palma, Canary Islands, and genesis of the Caldera de Taburiente, *J. Volcanol. Geoth. Res.*, 60, 3-4, 243-262.

Araña, V. (1971). Litología y estructura del edificio Cañadas, Tenerife (Islas Canarias). Estudios Geol. 27, 95-137.

Baker, J.A.; Menzies, M.A.; Thirlwall, M.F.; Macpherson, C.G. (1977). Petrogenesis of Quaternary intraplate volcanism, Sana'a, Yemen: Implication for plume-lithosphere interaction and polybaric melt hybridisation. *J. Petrology*, 38, 1359-1390.

Barca, D.; Crisci, G.M. and Ranieri, G.A. (1993). Developments of the Rayleigh Equation: «CRYSTAL» a

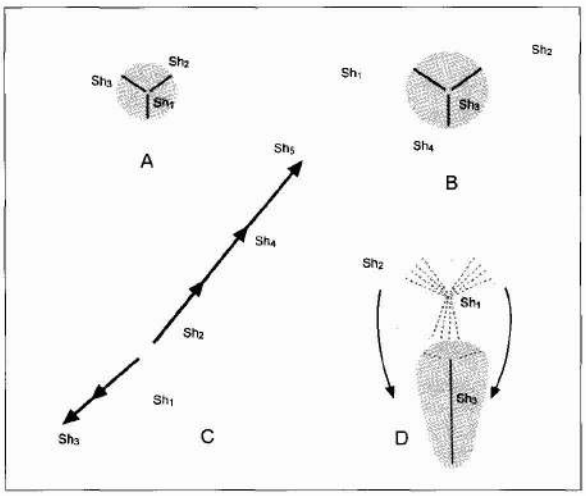

Fig. 74.—Patterns of development of oceanic islands by coalescence of successive shield volcanoes (sh_1, sh_2, etc.). Depending on the mobility magma plumbing these volcanoes may overlap concentrically in stationary magma sources (as in Central Tenerife and El Hierro) or align due to movement of the magmatic source, as in La Palma. Well-defined triple-rift systems develop only in islands where magma sources remain stationary since the early shield-building stages.

A key feature to allow these processes to develop and to explain the differences mentioned in rift development is the mobility of the islands' magmatic plumbing.

A comparative analysis of magma plumbing mobility and general patterns of island development

The Canaries and oceanic islands in general form as the result of aggregation of coalescent volcanoes with different patterns. The successive shields may overlap concentrically, as in El Hierro, La Gomera and central Tenerife (Fig. 74 A, B), or may align as independent shield volcanoes in predominant directions, as in Fuerteventura-Lanzarote and La Palma (Fig. 74 C). Only the islands formed by concentric overlapping volcanoes from persistent stationary magmatic sources may be successful in developing well-defined triple-armed rifts. The evolution of La Palma differs in that the volcanic activity migrated southwards before completion of the definition of rifts in the northern shield. On the other hand, the Cumbre Vieja volcano grew attached to the flank of the Taburiente volcano. Volcano growth on the flank of an older volcano which acts as a supporting buttress may explain the rapid change to a single-arm configuration (Fig. 74 D).

ACKNOWLEDGEMENTS

We are especially grateful to J. López Ruiz and A. Klügel for constructive review and comments, that helped greatly to improve the original manuscript.

This work has been financed by the Spanish CICYT project (PB92-0119), NATO project (NATO CRG no. 940609), by a project for the study of volcanic risks in the Canary Islands (1991-1994) financed by the Consejería de Política Territorial of the Canary Islands Government, and mainly by the MAGNA project of La Palma, financed by the Spanish Instituto Geológico y Minero. We are very grateful to the Dirección General de Medio Ambiente of the Canary Islands Government and Parques Nacionales in La Palma for permission to sample in the National and Natural Parks. To S. Day, A. Hernández Pacheco and J. Vegas for field data and collaboration during the MAGNA of La Palma. In the Laboratorio de Geoquímica and Laboratorio de Rayos-X of the Museo Nacional de Ciencias Naturales (CSIC) to M.I. Ruiz Pineda, M.A. Vallejo Haya for the analyses of major elements and R. González Martín for RX analyses of samples. The trace elements were analysed by O. Cazalla Vázquez and M.I. Moreno of the Laboratorios de ICP-MS and FRX of the Centro de Instrumentación Científica, Universidad de Granada. M. Castillejo and J.M. Hontoria (MNCN-CSIC) for the preparation of samples. E. Rodríguez Valdes for the palaeomagnetic analyses in the Estación Volcanológica de Canarias (CSIC). J.M. Cabrera Peraza in the Estación Volcanológica de Canarias (CSIC) and M.A. Vela Casado (MNCN-CSIC) for collaboration in the preparation of graphics.

We are grateful to Drs. Dan and James McKenzie, Institute of Theoretical Geophysics, Cambridge, for facilitating programs and subroutines of the «INVMEL» programs, Dr. S. Veintemillas for his assistance with compilation and application, and to Dr. D. Barca, Dipartimento di Scienze della Terra, Universita degli Studi della Calabria, for providing the «CRYSTAL» computer software.

Pauline Agnew spent many hours helping to improve the English.

References

Abdel-Monem, A.; Watkins, N.D. and Gast, P.W. (1972). Potassium-argon ages, volcanic stratigraphy and geomagnetic polarity history of the Canary Islands: Tenerife, La Palma and Hierro, *Amer. J. Sci.*, Vol. 272, 805-825.

Ancochea, E.; Fuster, J.M.; Ibarrola, E.; Cendrero, A.; Coello, J.; Hernán, F.; Cantagrel, J.M.; Jamond, C. (1990). Volcanic evolution of the Island of Tenerife (Canary Islands) in the light of new K-Ar data. *J. Volcanol. Geoth. Res.*. Vol. 44, 231-249.

Ancochea, E.; Hernán, F.; Cendrero A.; Cantagrel, J.M.; Fúster, J.M.; Ibarrola, E.; Coello, J. (1994). Constructive and destructive episodes in the building of a young Oceanic Island, La Palma, Canary Islands, and genesis of the Caldera de Taburiente, *J. Volcanol. Geoth. Res.*, 60, 3-4, 243-262.

Araña, V. (1971). Litología y estructura del edificio Cañadas, Tenerife (Islas Canarias). Estudios Geol. 27, 95-137.

Baker, J.A.; Menzies, M.A.; Thirlwall, M.F.; Macpherson, C.G. (1977). Petrogenesis of Quaternary intraplate volcanism, Sana'a, Yemen: Implication for plume-lithosphere interaction and polybaric melt hybridisation. *J. Petrology*, 38, 1359-1390.

Barca, D.; Crisci, G.M. and Ranieri, G.A. (1993). Developments of the Rayleigh Equation: «CRYSTAL» a

Pascal Program for simulating Fractional Crystallization. *Computers & Geosci.*, 19, 8, 1127-1153.
Benitez Padilla, S. (1951). La erupción de Las Manchas en la isla de La Palma y el volcanismo canario (24 Junio-31 Julio 1949). *El Museo Canario.* Las Palmas de Gran Canaria: 51-72.
Bonelli Rubio, J.M. (1950). Contribución al estudio de la erupción del Volcán Nambroque o San Juan (isla de La Palma), 24 de Junio a 4 de Agosto de 1949. *Inst. Geograf. y Catastral*, Madrid.
Brandle, J.L.; Ancochea, E. y Muñoz, M. (1984). Clasificación de las Rocas Volcánicas Españolas: El Diagrama Total Alcalis Sílice: (T.A.S.). de la I.U.G.S. I *Congreso Español de Geología.* Tomo II: 63-81.
Bravo, T. (1962). El circo de Las Cañadas y sus dependencias. *Bol. R. Soc. Esp. Hist. Nat.* (G) 60, 93-108.
Bravo, T. (1964). Estudio geológico y petrográfico de la isla de La Gomera. *Estudios Geol.* Vol. 20. Pp.1-56
Bravo, T. (1968). Hidrogeología de la isla de El Hierro. *Inst. Estudios Canarios* 11-12: 88-90.
Calvet, F.; Aguilar, A.; Carracedo, J.C.; Mangas, J.; Pérez Torrado, F.J. y Travé, A. «Beachrocks» de la Isla de La Palma, Islas Canarias. *(in press).*
Carracedo, J.C. (1979). Paleomagnetismo e historia geológica de Tenerife. *Aula Cultura Cabildo Tenerife*, 81 págs.
Carracedo, J.C. (1984). Geografía de Canarias. Edit. Interinsular Canaria.
Carracedo, J.C. (1994). The Canary Islands: an example of structural control on the growth of large oceanic island volcanoes. *J. Volcanol. Geoth. Res.*, 60, 3/4, 225-242.
Carracedo, J.C. (1996). A simple model for the genesis of large gravitational landslide hazards in the Canary Islands. In: Volcano Instability on the Earth and other Planets, McGuire, Jones and Neuberg, edts. Geological Society London Sp. Pub. 110, 125-135.
Carracedo, J.C. (1999). Growth, structure, instability and collapse of Canarian volcanoes and comparisons with Hawaiian volcanoes. J. Volcanol. Geoth. Res., 94, 1-19.
Carracedo, J.C. and Soler, V. (1995). Anomalously shallow palaeomagnetic inclinations and the question of the age of the Canarian Archipelago. Geophys. J. Int. Vol. 122, 393-406
Carracedo, J.C.; Day, S.; Guillou, H. and Rodríguez Badiola, E. (1996). The 1677 eruption of La Palma, Canary Islands. Estudios Geol., 52, 103-114.
Carracedo, J.C.; Day, S.J.; Guillou, H. and Gravestock, P. (1997a). Geological map of the Cumbre Vieja volcano. International Workshop on Volcanism & Volcanic Hazards in Immature Intraplate Oceanic Islands. La Palma, 15-18 September, 1997.
Carracedo, J.C.; Day, S.J. and Guillou, H. (1997b). La Palma, Geological Excursion Guidebook, International Workshop on Volcanism & Volcanic Hazards in Immature Intraplate Oceanic Islands. La Palma, Geological Excursion 19-21 September, 1997: 1-84.
Carracedo, J.C.; Day, S.J.; Guillou, H. and Pérez Torrado, F.J. (1997c). El Hierro, Geological Excursion Guidebook. International Workshop on Volcanism & Volcanic Hazards in Immature Intraplate Oceanic Islands. 19-21 September, 1997: 1-43.
Carracedo, J.C.; Day, S.; Guillou, H.; Rodríguez Badiola, E.; Canas, J.A. and Pérez Torrado, F.J. (1998). Hotspot volcanism close to a passive continental margin: the Canary Islands. Geol. Mag., 135(5), 591-604.
Carracedo, J.C.; Day, S.J.; Guillou, H. and P. Gravestock, (1999a). Later stages of volcanic evolution of La Palma, Canary Islands: Rift evolution, giant landslides and the genesis of the Caldera de Taburiente. G.S.A. Bulletin, 111, 755-768.
Carracedo, J.C.; Day, S.J.; Guillou, H. and Pérez Torrado, F.J. (1999b). Giant quaternary landslides in the evolution of La Palma and El Hierro, Canary Islands, J. Volcanol. Geoth. Res., 94, N° 1-4, 169-190.
Carracedo, J.C.; Rodríguez Badiola, E.; Guillou, H.; De La Nuez, J.; Hernández Pacheco, A.; Pérez Torrado, F.J.; Cabrera, M.C.; La Moneda, E.; Hansen, A. and Cueto, L. (2001a). Mapa geológico de España (MAGNA), Norte de La Palma (Memoria) y Hojas 1083-I a 1083-IV. Inst. Tecnol. GeoMin. España (ITGE), Madrid.
Carracedo, J.C.; Rodríguez Badiola, E.; Guillou, H.; De La Nuez, J.; Hernández Pacheco, A.; Pérez Torrado, F.J.; Cabrera, M.C.; La Moneda, E.; Hansen, A. and Cueto, L. (2001b). Mapa geológico de España (MAGNA), Sur de La Palma (Memoria) y Hojas 1085-I-IV a 1087-I-II. Inst. Tecnol. GeoMin. España (ITGE), Madrid
Cassignol, C.; Cornette, Y.; David, B. and Gillot, P.Y. (1978). Technologie potassium-argon. C.E.N., Saclay. Rapp. CEA R-4802, 37 pp.
Cendrero, A. (1971). Cendrero, A. (1971). Estudio geológico y petrológico del complejo basal de la isla de La Gomera (Canarias). Estudios Geol. Vol. 27, 3-73
Coello, J. (1987). Las aguas subterráneas en las formaciones volcánicas del norte de La Palma (Islas Canarias), Simposio Internacional de Recursos Hidráulicos «Canarias Agua 2000». Consejería de Obras Públicas, Gobierno de Canarias. Tenerife, Spain.
Chen, C.Y.; Frey, F. A.; Garcia, M.O.; Dairymple, G.B. and Hart, S.R. (1991). The tholeiite to alkalic basalt transition at Haleakala Volcano, Maui, Hawaii. Contrib. Mineral. Petrol., 106, 183-200.
Day, S.J.; Carracedo, J.C. and Guillou, H. (1997). Age and geometry of an aborted rift flank collapse: The San Andres fault system, El Hierro, Canary Islands. Geol. Mag. 134 (4), 231-255.
Day, S.; Carracedo, J.C.; Guillou, H. and Gravestock, P. (1999). Recent structural evolution of the Cumbre Vieja Volcano, La Palma, Canary Islands: Volcanic rift zone reconfiguration as a precursor to volcanic flank instability? J. Volcanol. Geoth. Res., Special Issue, 94, 1-4, 135-167.
Day, S.J.; Carracedo, J.C.; Guillou, H.; Pais Pais, F.J.; Rodríguez Badiola, E.; Fonseca, J.F.B.D. and Heleno, S.I.N. (2000). Comparison and cross-checking of historical, archaeological and geological evidence for the location and type of historical and sub-historical eruptions of multiple-vent oceanic island volcanoes. In: «The Archaeology of Geological Catastrophes», Geol. Soc. London Sp. Pub. 171, 281-306.
De La Iglesia, A.; Fernandez Santín, S. y Hernandez-Pacheco, A. (1996). Laumontita y Prehnita en la formación submarina del Complejo Basal de La Palma, Islas Canarias. *Rev. Soc. Geol. España*, 9 (1-2), 67-73.
De La Nuez, J. (1984). El complejo intrusivo subvolcánico de la Caldera de Taburiente, La Palma (Canarias).

Tesis Doctoral. Universidad Complutense de Madrid. 401 págs.

De La Nuez, J. (1991). Pautas estructurales en los diques de la caldera de Taburiente, La Palma (Islas Canarias). En: Homenaje al Profesor Telesforo Bravo (Tomo I), 543-557. Universidad de La Laguna (Secretariado de Publicaciones)

De Vicente Mingarro, I. (1986). Estudio geoquímico de las erupciones históricas del Archipiélago Canario. Tesis de Licenciatura, Universidad Complutense de Madrid, 79 págs.

Drury, R.M.; Nelson, B.K.; Carracedo, J.C. (in progress). Tracing mantle heterogeneities and magmatic storage: Geochemical stratigraphy of the Bejenado Volcano, La Palma. Canary Islands. <http://depts.washington.edu/~isochem/research/lapalma.html>

Elliott, T.R. (1991). Element Fractionation in the Petrogenesis of Ocean Islands Basalt. Ph. D. thesis, The Open University, Milton Keynes.

Fifton, J.G. and Upton, B.G.J. (eds.) Alkaline igneous rocks: Geol. Soc. London Sp. Pub. 30, 253-267.

Frey, F.A.; Garcia, M.O. and Roden, M.F. (1994). Geochemical characteristics of Koolan Volcano: Implications of intershield geochemical differences among Hawaiian volcanoes. Geochim. Cosmochim. Acta, 58, 5, 1441-1462.

Fúster, J.M.; Fernández Santín, S.; Sagredo, J.; (1968a). Geología y volcanología de las Islas Canarias: Lanzarote. Instituto «Lucas Mallada», C.S.I.C., Madrid, 177 págs.

Fúster, J.M.; Cendrero, A.; Gastesi, P.; Ibarrola, E.; López Ruiz, J. (1968b). Geología y volcanología de las Islas Canarias: Fuerteventura. Instituto «Lucas Mallada», C.S.I.C., Madrid, 239 págs.

Fúster, J.M.; Hernández Pacheco, A.; Muñoz, M.; Rodríguez Badiola, E. and García Cacho, L. (1968c). Geología y volcanología de las Islas Canarias: Gran Canaria. Instituto «Lucas Mallada», C.S.I.C., Madrid, 243 págs.

Fúster, J.M.; Araña, V.; Brandle, J.L.; Navarro, M.; Alonso, U.; Aparicio, A. (1968d). Geología y volcanología de las Islas Canarias: Tenerife. Instituto «Lucas Mallada», C.S.I.C., Madrid, 218 págs.

Fúster, J.M.; Hernán, F.; Cendrero, A.; Coello, J.; Cantagrel, J.M; Ancochea, E. and Ibarrola, E. (1993). Geocronologia de la isla de El Hierro (Islas Canarias). Bol. R. Soc. Esp. Hist. Nat. (sec. Geol.), 88 (1-4), 85-97.

Gee, J.; Staudigel, H.; Tauxe, L.; Pick, T. y Gallet, Y. (1993). Origin of anomalous remanence directions in the La Palma Seamount Series. Terra Nova Abstr. Suppl., 5, 85.

Gee, M.J.R.; Masson, D.G.; Watts, A.B.; Mitchell, N.C. (2001). Offshore continuation of volcanic rift zones, El Hierro, Canary Islands. *J. Volcanol. Geotherm. Res.,* 105, 107-119.

Geldmacher, J.; Hoernle, K.; van den Bogaard, P.; Zankl, G. and Garbe-Scönberg, D. (2001). Earlier history of the >70-Ma-old Canary hotspot based on the temporal and geochemical evolution of the Selvagen Archipelago and neighboring seamounts in the eastern North Atlantic. J. Volcanol. Geoth. Res. 111, 55-87.

Govindaraju, K. and Mevelle, G. (1987). Fully automated dissolution and separation methods for inductively coupled plasma atomic emission spectrometry rock analysis. Application to the determination of rare earth elements. Journal of Analytical Atomic Spectrometry 2, 615-621.

Guillou H.; Carracedo J.C.; Pérez Torrado F. and Rodríguez Badiola E. (1996) K-Ar ages and magnetic stratigraphy of a hotspot-induced, fast grown oceanic island: El Hierro, Canary Islands. J. Volcanol. Geoth. Res. 73, 141-155.

Guillou H.; Carracedo J.C. y Day S.J. (1998). Dating of the Upper Pleistocene-Holocene volcanic activity of La Palma using the unspiked K - Ar technique, J. Volcanol. Geoth. Res., 86, 1-4, 137-149.

Guillou, H.; Carracedo, J.C. and Duncan, R. (2001). K-Ar, 40Ar/39Ar Ages and Magnetostratigraphy of Brunhes and Matuyama Lava Sequences from La Palma Island. J. Volcanol. Geoth. Res., 106, 3-4: 175-194.

Hansteen, T.H.; Klügel, A.; Schmincke, H.U.; Krastel, S. (2001). Widespread volcanic activity on the submarine flanks of the western Canary Islands. *Abstract,* 2001 Margins Meeting, Kiel.

Hausen, H. (1956). Contributions to the geology of Tenerife. Soc. Sci. Fennica. Com. Phys-Math., 18-1, 247.

Hausen, H. (1958). On the geology of Fuerteventura, Canary Islands. Soc. Scient. Fennica, Comm. Physico-Mathematicae. 22-1: 1-211.

Hausen, H. (1961). Canarian calderas. A short review based on personal impressions. 1947-1957. Bull. Com. Geol. Finlande, num. 196: 179-213.

Hausen, H. (1969). Contributions to the geology of La Palma (Canary Islands) with a geologic map in 1:100.000. Com. Physico-Mathematicae. Societas Scientiarum Fennica, vol. 32. Helsinki-Helsingfors.

Hausen, H. (1964). Rasgos geológicos generales de la isla de El Hierro. Anuario de Estudios Atlánticos, 10: 547-593.

Hernández-Pacheco, A. (1971). Nota previa sobre el complejo basal de la isla de La Palma (Canarias). Estudios Geol., vol. 27, 255-265.

Hernández-Pacheco, A. (1974). Estado actual de los conocimientos geológicos, vulcanológicos y petrológicos de la isla de La Palma (Archipiélago Canario), 1ª Asamblea Nacional de Geodesia y Geofísica, 1974, 1319.

Hernández Pacheco, A. (1975). Los diques-brecha duníticos de fluidificación de la Caldera de Taburiente. La Palma (Islas Canarias). Estudios Geol., 31, 465-478.

Hernández Pacheco, A. (1982). Sobre una posible erupcion en 1793 en la isla de El Hierro (Canarias). (On a possible eruption in 1793 in the island of El Hierro, Canary Islands). Estudios Geol., 38, 15-25.

Hernández Pacheco, A. (1990). La erupción del Tahuya, en 1585 y el origen de los Roques de Jedey, La Palma, Canarias, En: Homenaje al Profesor Telesforo Bravo (Tomo I), 425-446. Universidad de La Laguna (Secretariado de Publicaciones).

Hernández Pacheco, A. y Fernández Santín, S. (1974). Las formaciones volcánicas submarinas de la Caldera de Taburiente en La Palma (Canarias) y sus transformaciones metasomáticas. Proc. Symp. Andean Antarctic Volcanol. Problems. Santiago, Chile. IAVCEI. 14 págs.

Hernández Pacheco, A. and De la Nuez J. (1983). Las extrusiones sálicas del sur de la Isla de La Palma. Estudios Geol., 39: 3-30.

Hernández Pacheco, A. and Vals, M.C. (1982). The historical eruptions of La Palma Island (Canarias). Arquipelago, Rev. Univ. Azores. Ser. C. Nat., 3: 83-94.

Hieronimus, C.F. and Bercovici, D. (1999). Discrete alternating hotspot islands formed by interaction of magma transport and lithospheric flexure. Nature, 397, 604-607.

Hoernle, K. and Schmincke, H.U. (1993). The Role of Partial Melting in the 15ma Geochemical Evolution of Gran Canaria: A Blob Model for the Canary Hotspot. J. Petrol., 34, 599-626.

Hoernle, K.; Zhang, Y.-S. and Graham, D. (1995). Seismic and geochemical evidence for large-scale mantle upwelling beneath the eastern Atlantic and western and central Europe. Nature 374, 34-39.

Hoernle, K. and Schmincke, H.U. (1993). The Role of Partial Melting in the 15-ma Geochemical Evolution of Gran Canaria: A Blob Model for the Canary Hotspot. J. Petrol., 34, 3, 599-626.

Hoernle, K.; Tilton, G.; Schmincke, H.U. (1991). Sr-Nd-Pb isotopic evolution of Gran Canaria: evidence for shallow enriched mantle beneath the Canary Islands. Earth Planet. Sci. Letters, 106: 44-63.

Holcomb, R.T. and Searle, R.C. (1991). Large landslides from oceanic volcanoes. Marine Geotechnology, 10: 19-32.

Hunter, P.M.; Searle, R.C. and Laughton, A.S. (1983). Bathymetry of the N.E. Atlantic, Sheet 5: Continental margin off N.-W. Africa. Institute of Oceanographic Sciences, UK.

Klitgord, K.D. and Schouten, H. (1986). Plate kinematics of the Central Atlantic. In: Voght, PR. and Tucholke, B.E (eds.). The Geology of North America, Vol. M, The Western North Atlantic Region. Geol. Soc. Amer Bull., 351-378.

Klügel, A. (1998). Reactions between mantle xenoliths and host magma beneath La Palma (Canary Islands): constraints on magma ascent rates and crustal reservoirs. Contrib. Mineral. Petrol., 131, 237-257.

Klügel, A.; Hansteen, T.H. and Schmincke, H.U. (1997). Rates of magma ascent and depths of magma reservoirs beneath La Palma (Canary Islands), Terra Nova, 9, N° 3, 117-121.

Klügel, A.; Hoernle, K.A.; Schmincke, H.U.; White, J.D.L. (1999). The chemically zoned 1949 eruption on La Palma (Canary Islands): Petrologic evolution and magma supply dynamics of a rift-zone eruption. J. Geophys. Res., 94, 1-4, 267-282

Le Bas, M.J.; Le Maitre, R.W.; Streckeisen, A. and Zanettin, B. (1986). A Chemical Classification of Volcanic Rocks Based on the Total Alkali Silica Diagram. *J. Petrol.*, 27, 745-750.

Lyell, C. (1865). Elements of Geology. 6th ed. London.

MacDonald, G.A. and Abbot, A. (1970). Volcanoes in the sea. The Geology of Hawaii. Honolulu: University of Hawaii Press, 441 pp.

Machado, F. (1963). Erupcöes da ilha de La Palma (Canarias). Bol. Museo Mineral. Geol. Lisboa, 1-17.

Marcantonio, F.; Zindler, A.; Elliott, T. and Staudigel, H. (1995). Os isotope systematics of La Palma, Canary Islands: Evidence for recycled crust in the mantle source of HIMU ocean islands, *Earth Planet. Sci. Letters*, Vol. 133, 3-4, 397-410.

Martel San Gil, M. (1960). El volcán de San Juan, La Palma (Canarias). Madrid, 1960, 234 pp.

Masson, D.G. (1996) Catastrophic collapse of the volcanic island of Hierro 15 ka ago and the history of landslides in the Canary Islands *Geology*, 24-3, 231-234.

Masson, D.G.; Watts, A.B.; Gee, M.J.R.; Urgelés, R.; Mitchell, N.C.; Le Bas, T.P. and Canals, M. (2002). Slope failures on the flanks of the western Canary Islands. *Earth-Scx. Reviews* 57: 1-35.

McKenzie, D. and O'Nions, R.K. (1991). Partial Melt Distribution from Inversion of Rare Earth Element Concentrations. *J. Petrology*, 32, 5, 1021-1091.

McKenzie, D. and O'Nions, R.K. (1995). The Source Regions of Ocean Island Basalts. J. Petrology, 36, 1, 133-159.

Moss, J.; McGuire, W.J. and Page, D. (1999). Ground deformation monitoring of a potential landslide at La Palma, Canary Islands. *J. Volcanol. Geoth. Res.*, 94, 1-4, 251-265.

Morgan, W.J. (1983). Hotspot tracks and the early rifting of the Atlantic. *Techtonophysics*, 94, 123-139.

Navarro, J.M. and Coello, J. (1989). Depresssions originated by landslide processes in Tenerife. ESF Meetingon Canarian Volcanism, Lanzarote, 150.

Navarro, J.M. y Coello, J. (1994). Mapa geológico del P.N. Taburiente. ICONA.

Oyarzun, R.; Doblas, M.; López Ruiz, J.; Cebriá, J.M. (1997). Opening of the central Atlantic and asymetric mantle upwelling phenomena: Implications for long-lived magmatism in western North Africa and Europe. *Geology*, 25, 727-730.

Pellicer, M.J. (1977). Estudio volcanológico de la Isla de El Hierro (Islas Canarias) (Volcanological study of the island of El Hierro (Canary Islands)). *Estudios Geol.* 33, 181-197.

Pellicer, J.M. (1979). Estudio geoquímico del vulcanismo de la isla del Hierro. Archipiélago Canario. *Estudios Geol.*, 35, 15-29.

Praegel, N.O. (1986). The petrology and geochemistry of Volcán Teneguía, La Palma, Canary Islands. Ph. D. thesis, Univ. Copenhagen.

Quidelleur, X. and Valet, J.P. (1994). Geomagnetic changes across the last reversal recorded in lava flows from La Palma (Canary Islands), Laboratorie de Paléomagnétisme. Institut de Physique du Globe de Paris, Francia.

Robertson, A.H.F.; Stillman, C.J. (1979a). Late mesozoic sedimentary rocks of Fuerteventura, Canary Islands: Implications for west african continental margin evolution. *J. Geol. Soc. Lond.* Vol. 136, 47-60.

Robertson, A.H.F.; Stillman, C.J. (1979b). Submarine volcanic and associated sedimentary rocks of the Fuerteventura basal complex, Canary Islands. *Geol. Mag.*, Vol. 116, 203-214.

Romero Ortiz, J.; Recondo, D.; Castillo, W.; Vidarte, M.; Fernández, E. (1950). La erupción del Nambroque en la isla de La Palma, *Bol. Geol. Min.* de España, Vol. 63, 3-163.

San Miguel de la Cámara, M.; Fúster Casas, J.M.; Martel, M. (1952). Las erupciones y materiales arrojados por ellas en la isla de La Palma. Junio-Julio de 1949, *Bulletin Volcanol.*, Tomo 12-13, 145-163.

Santiago, M. (1960). Los volcanes de La Palma (Islas Canarias). *El Museo Canario*, No. 75-76, 281-346.

Schiffman, P. and Staudigel, H. (1994). Hydrothermal alteration of a seamount complex on La Palma, Canary Islands: Implications for metamorphism in accreted terranes, *Geology*, Vol. 22, 151-154.

Schiffman, P. and Staudigel, H. (1995). The smectite to chlorite transition in a fossil seamount hydrothermal

system: the Basement Complex of La Palma, Canary Islands. *J. Metamorphic Geol.* 13, 487-498.

Schmincke, H.U. (1994). Geological Field Guide of Gran Canaria. *Edit. Pluto*, Germany.

Schmincke, H.U.; Sumita, M. and Funk T. (1997). Growth and destruction of Gran Canaria: Evidence from land studies, bathymetry, offshore seismic studies and drilling during ODP Leg 157. Internat. Workshop, Volcanism and Volcanic Hazards in Immature Intraplate Oceanic Islands, La Palma, Canary islands, Abstracts Vol., 10-12.

Schmincke, H.U. (1982). Volcanic and chemical evolution of the Canary Islands. In: Von Rad, U. Hinz. Eds. «Geology of the Northwest African Continental Margin». Springer Veriag. Berlin, 273-306.

Siebert, L. (1984). Large volcanic debris avalanches: characteristics of source areas, deposits, and associated eruptions. *J. Volcanol. Geoth. Res.*, 22, 163-197.

Singer, B.S.; Relle, M.K.; Hoffman, K.A.; Battle, A.; Laj, C.; Guillou, H. and Carracedo, J.C. (2002). 40Ar/39Ar ages from transitionally magnetized lavas on La Palma, Canary Islands, and the geomagnetic instability timescale. J. Geophys. Res. -Solid Earth

SPA-15 (1975). Estudio científico de los recursos de agua en las Islas Canarias (SPA/69/515). Volumen III, 2.ª parte. Minist. Obras Públ, Dir. Gral. Obr. Hidr. UNESCO. Las Palmas de Gran Canaria, Madrid. 3 vol.+ mapas.

Staudigel, H. and Schmincke, H.U. (1984). The Pliocene Seamount Series of La Palma/ Canary Islands. *J. Geophys. Res.* 89, 11195-11215.

Staudigel, H. (1981). Der basale Komplex von La Palma, submarine vulkanische prozesse, petrologie, geochemie und sekundare prozesse im herausgehobenen, submarinen Teil einer ozean-ischen Insel. Dissertation. Ruhr Universität, Bochum, Germany, 1-357.

Staudigel, H. (1997). The Pliocene Seamount Series of La Palma: A filed trip along the Barranco de Las Angustias. Internat. *Workshop on Immature oceanic islands*, La Palma, 1977. Vol. Abstr.

Staudigel, H.; Feraud, G. and Giannerini G. (1986). The history of intrusive activity on the Island of La Palma (Canary Islands). *J. Volcanol. Geoth. Res.*, 27, 299-322.

Stillman, C.J. (1987). A Canary islands dyke swarm: implications for the formation of oceanic islands by extensional fissural volcanism. In: Mafic dyke swarms (eds. H.C. Halls and W. F. Fahrig), 243-255. Geol. Assoc. of Canada Sp. Paper, 34.

Stillman, C. and Robertson, A.H.F. (1977). The dyke swarm of the Fuerteventura Basal Complex, Canary Islands. *Geol. Soc. London Newsletter*, 6, 1-8.

Stillman, C.; Furnes, H.; Le Bas, M.J.; Robertson, A.H.F. and Zielonka, J. (1982). The geological history of Maio, Cape Verde islands. *J. of the Geological Society of London*, 139, 347-361.

Sun, S.S. and McDonough, W.F. (1989). Chemical and isotopic systematics of oceanic basalts: implications for mantle composition and processes. In: *Magmatism in the Ocean Basins* (A.D. Saundres and M.J. Norry (eds). *Geol. Soc. Sp. Pub.*, 42, 313-345.

Szérémeta, N.; Laj, Guillou, H.; Kissel, K.; Mazaud, A. and Carracedo, J.C. (1999). Geomagnetic paleosecular variation in the Brunhes period, from the island of El Hierro. Earth Planet. Sci. Letters 165, 241-253.

Teneguía volcano (1974). *Estudios Geol.. Sp. vol.* 85 págs.

Ten Brink, U.S. (1991). Volcano spacing and plate rigidity. *Geology* 19, 397-400.

Thirlwall, M.F.; Upton, B.G.J. and Jenkins, C. (1994). Interaction between Continental Lithosphere and the Iceland Plume –Sr-Nd-Pb Isotope Geochemistry of Tertiary Basalts, NE Greenland. *J. Petrology*, 35, 839-879.

Thirlwall, M.F.; Singer, B.S. and Marriner G.F. (2000). ^{39}Ar-^{40}Ar ages and geochemistry of the basaltic shield stage of Tenerife, Canary Islands. Spain. *J. Volcanol. Geoth. Res.*, 103, 247-297.

Torriani, L. (1592). Descripción e historia del reino de las Islas Canarias. Wölfel, 1940. Spanish translation by A. Cioranescu, Edit. Goya, 1978 (with the map of the 1585 eruption made by Torriani).

Urgelés, R.; Masson, D.G.; Canals, M.; Watts, A.B. and Le Bas, T. (1997). Recurrent large-scale landsliding on the west flank of La Palma, Canary islands. *J. Geophys. Res.* 104, 25331-25348.

Urgelés, R. (1999). Esllavisements gegants a les illes Canaries: Les illes dEl Hierro i La Palma. Tesis doctoral. Univ. Barcelona, España.

Urgelés, R.; Masson, D.G.; Canals, M.; Watts, A.B. and Le Bas, T. (1999). Recurrent giant landslides on the west flank of La Palma. Canary Islands. *J. Geophys. Res.* 104, 25331-25348.

Vegas, J.; Hernández-Pacheco, A. y Marfil Pérez R. (1999). Los depósitos volcanoclásticos de la isla de La Palma (Canarias). Su relación con la evolución de las calderas de Taburiente y Cumbre Nueva. *Bol. Geol. Min. de España,* 110-2, 135-158.

Vogt, P.R. (1974). Volcano spacing, fractures and thickness of the lithosphere. *Earth Planet. Sci. Letters*, 21, 235-252.

Walker, G.P.L. (1990). Geology and volcanology of the Hawaiian Islands. *Pacific Science* 44, 315-347.

Walker, G.P.L. (1992). Coherent intrusion complexes in large basaltic volcanoes- a new structural model. *J. Volcanol. Geoth. Res.*, 50, 41-54.

Watson, S. and McKenzie, D. (1991). Melt Generation by Plumes: A Study of Hawaiian Volcanism. *J. Petrology*, 32, 501-537.

Watson, S. (1993). Rare Earth Element Inversions and Percolation Models for Hawaii. *J. Petrology*, 34, 763-783.

Weaver, B.L.; Wood, D.A.; Tarney J.; Joron, J.L. (1987). Geochemistry of ocean island basalts from the South Atlantic: Ascension, Bouvet, St. Helena, Gough and Tristan da Cunha. In: Fitton, J.G. and Upton B.G.J., eds., Alkaline igneous rocks: *Geol. Soc. of London Sp. Pub* 30, 253-267.

Weaver, B.L. (1991). The origin of ocean island basalts end-member compositions: trace elements and isotopic constraints. *Earth Planet. Sci. Letters.*, 104, 381-397.

Weaver, B.L. (1991). Trace element evidence for the origin of ocean-island basaits. *Geology*, 19, 123-126.

White J.D.L.; Schmincke H.U. (1999). Phreatomagmatic eruptive and depositional processes during the 1949 eruption on La Palma (Canary Islands), *J. Volcanol. Geoth. Res.*, Vol. 94, 1-4, 283-304.

Yllescas, D. (1977). La extrusión del Nambroque (isla de La Palma). Tesis de Licenciatura, Facultad de Ciencias Geológicas, Universidad Complutense, Madrid.

Recibido el 5 de febrero de 2001.
Aceptado el 20 de julio de 2001.

APPEND 1

ANALYTICAL DATA FROM SAMPLES OF THE LA PALMA VOLCANISM

NOTE

The referenced samples and analytical data are taken from the memory of La Palma Geological Map (MAGNA).

Table 2-1.—**Analytical data from samples of the Seamount**

Ref. Sample	95	105	59	96	98	109	103	104	108	102	106	107	177	178	181
Geol. Unit*	1	2	3	3	3	3	12	12	12	D	D	D	D	D	D
wt %															
SiO_2	45.67	60.84	47.50	43.53	45.44	40.19	44.53	44.68	40.97	63.59	53.20	51.69	47.34	37.65	58.69
TiO_2	3.23	0.43	3.26	3.21	2.96	4.71	1.89	1.35	3.41	1.16	1.93	1.03	2.44	0.57	1.36
Al_2O_3	14.01	17.03	16.66	9.23	7.84	15.20	7.32	7.27	12.59	19.68	17.96	20.82	14.25	2.19	17.57
Fe_2O_3	7.00	0.56	5.91	3.92	4.59	6.28	5.75	4.89	4.93	0.49	4.86	2.87	5.92	5.06	2.21
FeO	4.14	0.54	4.39	8.44	6.12	6.50	5.68	6.22	7.06	1.35	2.26	1.67	5.26	8.58	2.23
MnO	0.24	0.03	0.22	0.15	0.14	0.15	0.16	0.14	0.18	0.00	0.16	0.17	0.20	0.18	0.08
MgO	5.82	0.39	3.32	12.85	11.16	6.56	16.41	17.45	7.84	0.18	2.35	0.83	5.73	29.18	1.47
CaO	7.35	5.93	8.06	14.19	17.68	11.27	13.10	13.38	14.64	0.52	5.90	4.38	8.51	6.36	2.59
Na_2O	4.61	9.76	4.61	1.12	1.30	3.22	0.86	0.67	2.89	7.02	4.75	6.65	4.86	0.09	6.01
K_2O	1.62	0.06	2.03	0.39	0.48	1.29	0.72	0.40	1.84	3.53	2.83	3.85	1.28	0.06	4.49
P_2O_5	0.50	0.17	0.99	0.16	0.21	1.04	0.20	0.11	0.90	0.33	0.55	0.19	0.49	0.08	0.33
H_2O+CO_2	5.72	3.83	2.85	1.17	1.07	2.45	2.41	2.27	1.46	1.73	2.99	6.15	3.39	9.30	2.42
Mg #	53.0	41.0	37.9	65.7	66.0	49.0	72.9	74.5	54.9	16.9	41.8	28.3	49.10	81.8	41.3
Ppm															
Cr	58	8	8	560	480	2	1371	1545	124	8	53	8	45	1599	8
Ni	52	16	7	225	133	19	336	401	91	7	52	6	67	1209	9
Co	41	24	20	65	48	44	67	75	48	2	19	6	42	141	7
Sc	29	9	13	52	73	20	47	47	28	8	12	7	30	16	10
V	306	21	183	442	427	382	249	198	390	32	108	84	308	75	73
Cu	71	19	27	84	58	62	73	72	147	44	45	22	86	52	44
Pb	8	6	7	9	3	4	3	3	3	17	9	18	153	11	9
Zn	115	32	154	95	90	123	88	80	113	78	122	105	125	87	73
Sn	2.06	3.13	2.24	1.93	1.92	1.96	1.98	1.85	2.07	2.28	2.21	1.86	3.27	1.76	1.83
Mo	8.28	12.07	12.56	5.18	7.18	9.20	7.08	5.20	10.84	17.53	10.78	8.89	1.18	8.26	6.09
Rb	24	1.30	47	9	11	25	17	9	38	93	71	135	26	3	66
Cs	0.92	0.46	1.38	0.59	0.56	0.63	0.73	0.68	1.18	0.59	0.98	2.74	0.05	0.49	0.54
Ba	356	8.01	504	143	156	460	114	96	726	1,086	796	908	4.05	16	695
Sr	316	139	852	418	302	1,100	248	235	1,070	200	936	1,429	971	184	318
Tl	0.04	0.03	0.07	0.03	0.03	0.04	0.07	0.05	0.05	0.15	0.13	0.37	0.03	0.04	0.04
Ga	18	21.06	25	16	17	23	13	11	22	29	27	35	20	5	26
Li	6.32	4.11	15.98	8.65	8.73	9.73	9.42	9.15	10.99	5.95	14.02	22.77	6.50	7.68	8.17
Be	1.85	7.52	3.62	0.86	1.45	1.93	1.30	0.74	1.91	3.21	4.27	7.65	1.48	0.71	3.11
Ta	3.32	24.70	6.71	1.34	1.39	4.55	1.24	0.61	5.39	9.54	6.47	5.46	2.97	0.73	4.77
Nb	47	352.08	95	17	19	65	17	8	77	144	99	136	48.5	7	65
Hf	5.79	30.05	7.98	4.03	5.11	5.51	3.09	1.89	7.21	12.90	10.97	13.47	9.31	0.81	8.74
Zr	234	1,213.74	375	127	152	225	95	54	295	624	537	802	2.14	33	417
Y	28	24.08	42	15	22	34	17	11	27	34	39	21	26	4	29
Th	3.28	26.49	6.43	1.13	1.21	3.37	1.31	0.77	4.78	17.13	10.24	14.46	2.94	0.48	5.89
U	0.88	6.94	1.68	0.32	0.32	0.84	0.34	0.17	1.22	3.86	2.41	3.79	0.77	0.17	1.46
La	33.83	48.15	66.32	14.68	17.69	49.39	16.45	8.53	54.40	112.24	97.81	79.18	32.56	4.89	58.35
Ce	71.46	91.96	132.53	33.66	42.62	104.87	37.70	19.38	112.37	196.05	168.74	122.29	69.79	10.57	115.65
Pr	9.02	9.38	15.80	4.68	6.08	13.40	5.09	2.70	14.09	18.03	19.79	11.63	8.53	1.39	13.26
Nd	37.83	30.06	63.36	22.03	28.41	57.81	21.82	12.99	59.79	60.00	70.90	37.50	35.76	5.34	50.84
Sm	7.92	4.99	12.19	5.21	7.30	11.98	5.26	3.31	11.70	9.43	11.39	6.06	7.58	1.29	9.00
Eu	2.49	0.61	3.55	1.55	2.12	3.71	1.52	1.07	3.45	2.35	3.34	1.71	2.41	0.38	2.21
Gd	7.36	3.88	10.85	4.57	6.33	10.40	4.71	2.90	9.60	7.58	9.30	4.70	6.87	1.11	7.68
Tb	1.09	0.65	1.57	0.65	0.97	1.52	0.71	0.44	1.37	1.19	1.41	0.71	0.99	0.17	1.13
Dy	5.60	3.82	8.83	3.35	5.16	7.43	3.91	2.40	6.39	6.56	7.34	4.00	5.30	0.96	5.92
Ho	1.11	0.84	1.68	0.64	0.94	1.34	0.75	0.45	1.15	1.34	1.43	0.74	0.93	0.18	1.13
Er	2.76	2.53	3.98	1.42	2.20	3.08	1.76	1.11	2.40	3.60	3.72	1.91	2.28	0.43	2.69
Tm	0.37	0.49	0.59	0.20	0.29	0.41	0.25	0.15	0.30	0.53	0.55	0.30	0.34	0.06	0.41
Yb	2.32	3.46	3.45	1.21	1.60	2.37	1.39	0.85	1.84	3.30	3.17	1.88	1.85	0.37	2.33
Lu	0.30	0.53	0.50	0.16	0.22	0.31	0.20	0.12	0.25	0.46	0.45	0.27	0.26	0.05	0.34

95.—Tr-Basalt-plag. Bco. de las Angustias. MAGNA*.
105.—Trachyte fragment intrusive dome. Bco. de las Angustias. MAGNA*.
59.—Gabbro anf. Plutonic intrusive rock. (Lomo de la Juraga). MAGNA*.
96.—Gabbro px-ol. Plutonic intrusive rock. (Lomo Gazmil). MAGNA*.
98.—Gabbro px. Plutonic intrusive rock. (Barranco de Rivanceras). MAGNA*.
109.—Gabbro anf. Plutonic intrusive rock. (Barranco de Taburiente). MAGNA*.
103.—Gabbro px-ol. Plutonic intrusive rock. (Barranco del Salto del Agua). MAGNA*.
104.—Gabbro px-ol. Plutonic intrusive rock. (Barranco del Salto del Agua). MAGNA*.
108.—Gabbro alc. (px-ol-nef). Plutonic intrusive rock. (Barranco de Rivanceras). MAGNA*.
102.—Trachyte dike. Bco. Salto del Agua. MAGNA*.
106.—Mafic trachyte dyke. Lomo del Escuchadero. MAGNA*.
107.—Phonolite dyke. Bco. de Madera de Garcia. MAGNA*.
177.—Basalt dyke in the seamount. MAGNA*.
178.—Dunite breccia. MAGNA*.
181.—Syenite alcaline. MAGNA*.

(*) Carracedo et al. (2001) Mapa Geológico de España (MAGNA): Norte de La Palma, Hojas 1083-I a 1083-IV, ITGE, Madrid.

Table 2-2.—**Analytical data from samples of the Garafía volcano**

Ref. Sample	77	78	80	134	144	157	171	170	172
Geol. Unit*	5	5	5	5	5	5	5	5	5
wt %									
SiO_2	47.27	50.25	46.36	49.22	49.00	48.50	48.50	49.00	48.22
TiO_2	2.72	3.37	3.24	3.21	3.04	2.34	3.39	3.04	2.14
Al_2O_3	11.38	14.58	10.75	16.33	14.55	11.56	14.08	14.56	8.82
Fe_2O_3	2.88	1.16	4.05	3.88	4.61	4.84	4.54	6.23	4.24
FeO	8.00	9.40	8.54	5.99	6.71	5.78	7.35	4.55	7.26
MnO	0.18	0.19	0.21	0.19	0.17	0.13	0.17	0.19	0.18
MgO	13.62	6.44	11.98	4.88	6.93	12.74	6.32	5.15	15.80
CaO	10.15	9.10	11.33	9.46	10.53	9.42	10.79	10.52	10.40
Na_2O	2.41	3.25	2.00	4.06	2.65	2.34	2.43	2.51	2.02
K_2O	0.58	1.21	0.55	1.37	0.82	0.47	0.67	0.95	0.34
P_2O_5	0.48	0.78	0.56	0.78	0.54	0.41	0.49	0.63	0.31
H_2O+CO_2	0.09	0.09	0.47	0.07	0.09	0.93	0.79	2.42	0.08
Mg #	72.23	55.49	66.54	51.00	56.35	71.77	50.63	52.78	74.26
Ppm									
Cr	397	121	466	36	148	433	173	32	920
Ni	279	86	266	27	131	409	128	52	516
Co	61	44	69	36	44	54	49	37	69
Sc	28	24	31	17	25	26	28	19	29
V	310	290	363	303	330	256	351	312	242
Cu	87	88	108	38	103	76	120	89	70
Pb	2	3	3	5	3	1	4	2	1
Zn	124	126	129	133	121	117	146	117	96
Sn	1.56	2.26	1.84	3.99	3.56	3.98	5.50	4.42	3.17
Mo	1.51	6.06	2.10	3.44	1.95	1.02	1.66	1.19	0.64
Rb	17	34	27	41	25	13	31	44	9
Cs	0.19	0.72	0.34	1.06	0.22	0.71	0.68	0.61	0.04
Ba	249	577	329	484	286	149	271	334	148
Sr	653	953	699	943	700	444	637	734	381
Tl	0.02	0.04	0.03	0.03	0.01	0.02	0.01	0.08	0.01
Ga	20	23	21	25	23	19	24	22	15
Li	5.76	9.73	5.93	8.49	6.38	3.34	6.62	7.82	3.74
Be	1.62	2.23	1.91	3.46	1.70	1.37	2.09	1.76	1.24
Ta	2.79	4.87	3.90	4.60	3.25	2.07	2.95	3.71	1.80
Nb	46	65	66	85	57	34	52	64	31
Hf	5.46	7.32	6.47	7.00	5.95	5.02	5.89	5.93	3.37
Zr	217	344	266	329	258	213	250	267	134
Y	23	33	25	32	29	24	30	30	19
Th	2.73	2.82	3.67	5.20	3.25	1.36	2.73	3.19	1.64
U	0.68	0.69	1.04	1.52	0.88	0.31	0.75	0.71	0.36
La	31.84	52.96	41.99	55.74	37.45	20.15	32.95	40.15	21.29
Ce	69.22	115.01	89.77	113.47	78.80	49.67	72.61	86.28	44.66
Pr	8.65	14.34	11.02	13.51	9.97	6.91	9.11	10.55	5.51
Nd	37.14	59.92	45.35	54.44	41.42	31.21	38.88	43.14	23.14
Sm	7.78	11.78	9.38	10.59	8.62	7.36	8.81	9.65	5.42
Eu	2.49	3.50	2.91	3.30	2.76	2.29	2.68	2.84	1.73
Gd	7.04	9.88	8.03	8.98	7.86	6.66	7.76	8.73	5.28
Tb	0.97	1.38	1.10	1.24	1.13	0.91	1.15	1.18	0.76
Dy	5.07	7.00	5.42	6.33	5.85	4.97	5.91	6.11	4.19
Ho	0.92	1.36	0.96	1.14	1.09	0.95	1.07	1.15	0.77
Er	2.26	3.04	2.19	2.82	2.60	2.21	2.59	2.77	1.81
Tm	0.30	0.41	0.28	0.39	0.34	0.31	0.34	0.39	0.25
Yb	1.54	2.42	1.60	2.29	2.07	1.66	1.99	2.03	1.35
Lu	0.21	0.35	0.22	0.30	0.28	0.24	0.28	0.30	0.19

77.—Basalt. Marcos-Cordero lava flow directly over discordance at the upper spring. MAGNA*.
78.—Basalt /Tr-Basalt. Bco Los Tilos, 1,365 m (lower sping of Marcos-Cordero). MAGNA*.
80.—Basalt. Bco Franceses, of Tagamentera section. (1,920 m). MAGNA*.
134.—Tr-Basal. Garafía Volcano. MAGNA*.
144.—Basalt. Galería de los Hombres 1,650 m. MAGNA*.
157.—Basalt. Galería de Los Hombres, 2,100. MAGNA*.
171.—Basalt. Galería de Los Hombres, 1,500 m. MAGNA*.
170.—Basalt. Galería Cuevitas, 2,700 m. MAGNA*.
172.—Basalt. Galería Cuevitas, 2,000 m. MAGNA*.

(*) Carracedo et al. (2001) Mapa Geológico de España (MAGNA): Norte de La Palma, Hojas 1083-I a 1083-IV, ITGE, Madrid.

Table 2-3.—**Analytical data from samples of thee Lower Taburiente volcano**

Ref. Sample	44	48	85	148	156	167	204	217	243	263	225
Geol. Unit*	8	8	8	8	8	8	8	8	8	8	D
wt %											
SiO_2	43.59	44.20	49.09	51.70	46.28	45.20	48.30	49.50	49.00	45.00	47.60
TiO_2	2.24	2.12	2.40	2.26	3.25	3.11	2.71	2.68	3.51	2.99	3.03
Al_2O_3	11.23	12.24	17.57	18.42	16.07	12.48	11.34	12.77	14.85	12.99	11.07
Fe_2O_3	2.89	6.58	5.89	3.08	3.91	5.57	4.78	4.89	2.91	4.40	5.73
FeO	7.94	7.18	4.46	5.16	8.86	7.77	7.97	6.93	9.55	7.45	8.06
MnO	0.15	0.18	0.22	0.22	0.18	0.19	0.17	0.18	0.19	0.16	0.18
MgO	14.13	9.84	3.20	2.31	6.14	10.67	11.77	10.07	6.30	11.76	10.66
CaO	13.54	11.86	7.92	6.67	11.00	9.45	9.15	8.85	8.71	10.92	9.53
Na_2O	2.58	2.61	4.15	6.30	2.80	2.40	2.27	2.15	2.68	2.43	1.50
K_2O	0.77	0.68	1.99	2.46	1.07	0.83	0.58	0.92	1.17	0.67	0.40
P_2O_5	0.59	0.91	0.99	0.71	0.59	0.49	0.42	0.57	0.96	0.49	0.46
H_2O+CO_2	0.32	0.97	2.03	0.34	0.10	0.85	0.37	0.26	0.10	0.67	1.53
Mg #	73.1	60.3	39.9	37.1	50.1	62.8	66.0	64.3	51.2	67.6	62.0
Ppm											
Cr	602	453	8	16	28	448	563	392	57	430	485
Ni	252	179	0	5	60	274	300	210	55	189	226
Co	62	51	16	13	40	65	61	56	44	54	65
Sc	33	24	7	6	22	32	31	28	22	33	40
V	304	298	126	130	332	338	325	317	346	319	375
Cu	115	86	12	14	97	97	100	88	72	122	104
Pb	3	3	6	9	3	3	3	4	5	7	4
Zn	109	112	138	143	130	143	114	127	156	102	122
Sn	2.07	2.80	3.78	4.27	3.83	3.52	2.48	2.76	3.91	2.05	2.67
Mo	8.06	2.79	4.11	4.91	1.79	1.44	1.69	2.20	2.48	8.83	1.20
Rb	24	22	63	75	22	18	20	28	37	20	14
Cs	0.66	0.33	0.75	1.67	0.79	0.70	0.19	0.29	0.42	0.75	0.25
Ba	310	481	700	735	312	250	299	356	465	313	274
Sr	700	968	1,355	1,307	724	660	587	730	1,042	642	636
Tl	0.04	0.02	0.03	0.07	0.02	0.01	0.01	0.03	0.03	0.04	0.01
Ga	19	20	27	29	23	21	20	22	26	19	20
Li	9.43	6.70	13.69	16.46	5.75	6.55	7.49	7.82	8.83	9.80	6.15
Be	1.92	2.05	4.44	6.06	1.63	1.75	2.03	3.08	3.46	2.03	2.20
Ta	3.64	4.93	8.55	8.21	3.81	2.76	3.11	3.74	5.30	3.41	2.68
Nb	51	92	151	150	63	49	53	62	100	48	49
Hf	5.95	6.15	12.65	11.70	6.18	5.38	5.25	6.34	9.14	5.77	5.20
Zr	252	296	594	592	262	230	222	266	415	236	221
Y	24	30	46	41	30	25	24	26	36	26	24
Th	3.86	4.74	9.58	9.22	3.40	2.60	3.07	3.61	5.65	3.27	2.77
U	0.91	1.21	2.60	2.62	0.80	0.71	0.69	1.03	1.46	0.80	0.79
La	41.89	54.79	102.44	95.01	41.07	33.07	35.08	41.40	69.49	35.92	34.93
Ce	87.01	112.44	200.06	183.73	84.33	71.70	73.41	87.01	143.75	75.72	73.92
Pr	10.78	13.94	23.91	20.57	10.38	8.89	8.99	10.51	17.51	9.55	9.02
Nd	44.69	55.76	89.00	77.78	43.09	37.05	36.63	42.85	71.09	39.38	37.10
Sm	8.76	10.70	16.00	13.69	9.04	8.21	7.80	9.20	13.25	8.44	7.78
Eu	2.64	3.42	4.66	4.08	2.82	2.57	2.42	2.72	3.92	2.42	2.32
Gd	7.69	9.28	14.26	11.24	8.58	7.10	6.78	7.63	11.09	7.14	6.80
Tb	1.05	1.23	1.81	1.57	1.16	1.02	0.97	1.07	1.50	1.02	0.89
Dy	5.19	6.09	9.19	7.64	6.31	4.97	4.98	5.32	7.32	5.14	4.68
Ho	0.97	1.08	1.72	1.43	1.20	0.89	0.89	0.96	1.32	1.01	0.87
Er	2.25	2.49	4.16	3.53	2.90	2.19	2.15	2.34	3.22	2.53	2.01
Tm	0.31	0.34	0.61	0.53	0.40	0.29	0.30	0.33	0.44	0.35	0.29
Yb	1.83	2.00	3.27	3.03	2.15	1.66	1.79	1.83	2.45	2.13	1.65
Lu	0.25	0.26	0.49	0.45	0.33	0.25	0.24	0.26	0.37	0.28	0.23

44.—Basanite. Northern wall of the Caldera de Taburiente, 50 m. asl. MAGNA**.
48.—Basanite. Northern wall of the Caldera de Taburiente, 650 m. asl. MAGNA**.
85.—Tr-Basalt. Headwall of Bco. Franceses, Tagamentera trail, 2,160 m. Asl. MAGNA*.
148.—Tephrite mafic. Lower Taburiente. MAGNA*.
156.—Basalt. Lower Taburiente. MAGNA*.
167.—Basalt-Basanita. Lower Taburiente. MAGNA*.
204.—Basalt. Bco. Franceses. West of road, 450 m asl. MAGNA*.
217.—Basalt. Fajama Los Hombres, 30 m. asl. MAGNA*.
243.—Basalt. Lower Taburiente. MAGNA*.
263.—Basalt-Basanita. Bco. Los Hombres, 60 m. asl. MAGNA*.
225.—Basalt. Basaltic dyke over agglomerates, La Cumbrecita. MAGNA*.

(*) Carracedo et al. (2001) Mapa Geológico de España (MAGNA): Norte de La Palma, Hojas 1083-I a 1083-IV, ITGE, Madrid.
(**) Carracedo et al. (2001) Mapa Geológico de España (MAGNA): Sur de La Palma, Hojas 1085 I-IV a 1087 I-II, ITGE, Madrid.

Table 2-4.—**Analytical data from samples of the Upper Taburiente volcano**

Ref. Sample	76	122	125	129	130	183	184	187	188	189	202	213	240	241	245	248	267
Geol. Unit*	11	11	11	11	11	11	11	11	11	11	11	11	11	11	11	11	11
wt %																	
SiO_2	49.18	45.21	46.02	51.00	49.50	48.50	49.30	49.92	51.30	49.90	49.50	48.00	49.14	43.78	44.30	42.05	46.18
TiO_2	3.13	3.16	3.38	2.65	3.07	3.48	3.07	2.75	2.71	2.11	3.32	3.07	2.84	3.99	3.44	3.45	3.70
Al_2O_3	15.21	18.30	15.21	11.83	15.57	15.64	13.79	16.47	16.32	18.20	13.85	15.83	18.71	16.20	15.87	14.26	15.15
Fe_2O_3	3.06	5.13	5.95	0.90	1.75	4.41	1.34	6.75	5.70	2.63	2.36	4.71	3.46	4.97	9.44	4.33	3.82
FeO	7.81	6.09	8.59	9.71	8.03	6.62	10.30	3.08	3.85	4.60	9.26	7.94	4.45	7.53	3.87	8.78	10.12
MnO	0.19	0.23	0.18	0.18	0.19	0.19	0.20	0.19	0.18	0.21	0.20	0.21	0.17	0.22	0.21	0.17	0.18
MgO	5.66	3.76	5.50	9.09	6.21	4.82	6.76	4.25	4.32	3.17	6.09	5.04	3.11	5.57	5.27	7.01	5.97
CaO	9.79	10.15	10.78	10.74	9.17	9.09	9.74	8.40	8.08	6.61	8.78	8.11	7.35	10.77	9.45	12.22	11.10
Na_2O	3.83	4.68	2.89	2.67	4.10	4.60	2.94	4.00	4.19	7.28	3.74	3.81	6.96	4.78	3.79	4.93	2.93
K_2O	0.97	2.21	0.79	0.60	1.32	0.93	1.13	1.45	1.53	3.39	1.30	1.45	3.01	1.18	1.89	0.90	1.01
P_2O_5	0.80	1.08	0.71	0.49	0.82	0.97	1.00	0.75	0.79	0.80	0.97	1.06	0.80	1.01	1.24	0.87	0.62
H_2O+CO_2	0.09	0.44	0.10	0.11	0.09	0.66	0.25	1.76	0.65	1.02	0.10	0.65	0.48	0.36	1.14	0.91	0.05
Mg #	52.01	41.53	44.37	63.60	56.66	47.93	54.30	48.43	49.32	47.92	51.97	45.56	0.48	0.36	46.30	52.79	47.10
Ppm																	
Cr	74	9	23	361	128	1	171	8	9	9	74	25	12	27	15	49	8
Ni	52	0	36	237	104	20	80	7	0	4	55	28	0	28	10	49	35
Co	39	22	44	58	39	37	43	28	24	15	43	34	17	40	35	44	48
Sc	19	8	24	32	17	19	25	16	10	2	21	16	5	18	14	22	29
V	277	200	339	351	258	374	311	243	218	217	333	250	201	332	262	350	428
Cu	59	20	43	157	64	43	86	32	16	14	76	56	20	33	52	47	99
Pb	3	7	2	3	3	7	5	10	4	7	5	6	6	5	5	4	14
Zn	135	201	132	128	126	130	138	121	116	125	146	144	115	147	139	131	125
Sn	3.22	2.99	3.35	2.51	2.68	2.15	2.93	2.13	4.52	3.02	3.59	3.67	3.48	4.34	4.71	2.02	2.10
Mo	2.30	3.22	2.19	1.53	2.29	9.11	2.31	11.01	2.80	5.32	2.58	3.24	3.31	2.42	3.96	2.59	9.46
Rb	29	47	16	19	37	20	36	45	45	72	37	47	26	19	49	11	30
Cs	0.33	0.54	0.23	0.81	0.32	1.08	0.33	0.84	1.12	1.26	0.37	0.64	1.30	1.06	1.39	0.50	0.75
Ba	382	599	317	263	461	610	422	507	497	977	503	536	923	511	584	541	374
Sr	937	1142	811	583	886	1,083	900	1,008	940	1,498	1,017	1,093	1,366	999	1,171	983	802
Tl	0.03	0.05	0.02	0.01	0.05	0.04	0.05	0.04	0.03	0.05	0.03	0.04	0.05	0.01	0.03	0.03	0.05
Ga	24	24	23	21	24	24	24	24	24	27	25	27	26	24	25	23	24
Li	5.71	6.80	4.40	6.75	8.58	13.04	8.36	13.66	4.74	15.74	9.38	11.58	12.70	9.61	6.25	9.54	10.24
Be	2.35	2.94	1.49	1.99	2.69	2.69	3.16	3.25	2.72	4.55	3.69	4.70	3.63	3.93	3.58	3.66	2.55
Ta	4.27	5.84	2.75	2.60	4.74	5.71	4.41	5.32	5.05	8.54	5.22	5.87	7.55	4.45	6.54	5.08	4.24
Nb	77	103	51	45	82	83	79	78	87	160	92	108	147	83	115	89	62
Hf	6.81	7.73	5.30	4.86	7.00	7.33	7.62	7.64	7.39	7.80	8.15	9.50	7.89	7.32	9.64	7.72	6.65
Zr	318	384	217	200	332	324	332	351	354	446	369	449	441	346	469	335	276
Y	29	37	31	24	31	34	32	33	32	35	33	38	31	34	37	33	28
Th	4.36	5.58	4.27	2.48	4.59	5.54	4.59	6.02	5.68	9.81	4.83	6.73	10.15	4.60	6.63	5.32	4.20
U	1.19	1.50	1.15	0.72	1.03	1.35	0.96	1.74	1.56	2.76	1.14	1.76	2.46	1.21	1.82	1.22	1.04
La	52.32	66.91	54.60	32.05	52.97	58.46	56.70	58.54	57.38	86.28	58.47	76.32	76.54	57.13	77.79	63.70	46.96
Ce	107.90	139.04	108.88	68.20	110.79	119.85	119.01	117.42	119.16	163.71	124.63	154.32	144.23	121.05	160.17	124.12	95.44
Pr	13.10	16.33	12.81	8.45	13.18	14.75	14.46	14.08	14.03	18.31	15.25	18.14	16.07	15.04	19.16	15.50	11.73
Nd	52.25	64.49	50.23	34.43	53.60	62.07	59.48	56.71	54.73	68.33	62.48	70.95	59.38	62.04	75.48	62.60	47.89
Sm	10.26	12.43	10.17	7.83	10.66	11.88	11.43	11.06	10.92	12.16	12.74	13.51	10.86	12.28	14.56	12.02	9.78
Eu	3.16	3.76	3.13	2.39	3.24	3.63	3.39	3.25	3.33	3.75	3.65	3.77	3.43	3.58	4.19	3.68	2.78
Gd	8.91	10.59	9.32	6.89	9.11	10.40	9.71	9.23	9.56	10.21	10.77	11.13	9.33	10.44	11.95	10.05	8.44
Tb	1.20	1.45	1.28	0.99	1.24	1.49	1.35	1.30	1.27	1.37	1.40	1.47	1.29	1.46	1.57	1.39	1.17
Dy	5.97	7.42	6.43	5.15	6.29	7.38	6.76	6.66	6.52	6.73	6.98	7.39	6.33	7.11	7.82	6.86	5.83
Ho	1.11	1.37	1.17	0.88	1.18	1.37	1.20	1.26	1.21	1.21	1.18	1.32	1.11	1.27	1.39	1.24	1.09
Er	2.60	3.23	2.71	2.15	2.79	3.17	3.04	2.99	2.86	3.03	2.84	3.18	2.71	2.97	3.20	2.79	2.54
Tm	0.34	0.45	0.38	0.30	0.37	0.42	0.41	0.41	0.41	0.44	0.39	0.45	0.39	0.41	0.47	0.38	0.35
Yb	1.94	2.47	2.04	1.63	2.02	2.49	2.37	2.55	2.17	2.39	2.00	2.48	1.98	2.39	2.38	2.02	2.16
Lu	0.26	0.38	0.29	0.24	0.32	0.34	0.33	0.34	0.35	0.35	0.29	0.38	0.29	0.32	0.35	0.29	0.30

76.—Tr-Basalt. Upper Taburiente post-collapse. MAGNA*.
122.—Tephrite. Upper Taburiente- basaltic lavas. MAGNA**.
125.—Basanite. Upper Taburiente- basaltic lavas. MAGNA**.
129.—Basalt. Upper Taburiente. MAGNA*.
130.—Tr-Basalt. Upper Taburiente. MAGNA*.
183.—Tr-Basalt. Southern wall of Bco. del Jorado, 0 m. asl. MAGNA*.
184.—Basalt. Southern wall of Bco. del Jorado, 140 m. asl. MAGNA*.
187.—Tr-Basalt. Southern wall of Bco. del Jorado, 225 m. asl. MAGNA*.
188.—Tr-Basalt. Southern wall of Bco. del Jorado, 260 m. asl. MAGNA*.
189.—Phon-Tephrite. Southern wall of Bco. del Jorado, 265 m, asl. MAGNA*.
202.—Tr-Basalt. Road to Barlovento, 180 m. asl. MAGNA*.
213.—Tr-Basalt. Laguna Barlovento, 850 m. Asl. MAGNA*.
240.—Phon-Tephrite. Coast of Tijarafe - Pta. Los Gomeros, 350 m. asl. MAGNA*.
241.—Bsn/Tephr. Coast of Tijarafe - Pta. Los Gomeros, 392 m. asl. MAGNA*.
245.—Basanite. Upper Taburiente. MAGNA*.
248.—Basanite. Upper Taburiente. MAGNA*.
267.—Basalt. Road to Pico de las Nieves, 2.100 m. asl. MAGNA*.

(*) Carracedo et al. (2001) Mapa Geológico de España (MAGNA): Norte de La Palma, Hojas 1083-I a 1083-IV, ITGE, Madrid.
(**) Carracedo et al. (2001) Mapa Geológico de España (MAGNA): Sur de La Palma, Hojas 1085 I-IV a 1087 I-II, ITGE, Madrid.

Table 2-5.—**Analytical data from samples of the Upper Taburiente volcano (Terminal differentiated lavas)**

Ref. Sample	212	260	268	269	270	272
Geol. Unit*	13	13	13	13	13	13
wt %						
SiO_2	51.63	53.11	49.42	52.85	49.30	52.78
TiO_2	1.30	1.76	2.14	2.13	2.48	1.58
Al_2O_3	20.46	19.78	20.02	17.93	18.32	20.77
Fe_2O_3	5.02	2.00	0.94	1.10	2.83	2.86
FeO	1.04	4.40	5.77	6.74	5.68	2.59
MnO	0.18	0.18	0.19	0.17	0.22	0.14
MgO	1.40	1.72	1.89	2.82	2.61	1.12
CaO	5.93	5.90	6.34	6.81	7.95	5.58
Na_2O	6.85	6.79	6.98	5.98	6.66	7.72
K_2O	3.87	3.26	3.79	2.38	2.76	3.14
P_2O_5	0.32	0.48	0.47	0.76	0.78	0.30
H_2O+CO_2	1.69	0.42	1.52	0.24	0.03	1.05
Mg #	33.8	35.9	36.6	42.5	39.1	30.5
Ppm						
Cr	11	8	8	10	13	8
Ni	5	6	5	1	2	2
Co	8	10	9	13	15	5
Sc	2	8	7	6	5	1
V	99	101	177	114	166	101
Cu	13	24	23	8	18	6
Pb	11	28	10	5	9	8
Zn	115	111	119	112	129	104
Sn	2.32	2.02	1.99	2.27	2.42	2.29
Mo	4.68	20.43	14.43	4.44	4.99	5.06
Rb	99	81	92	51	82	75
Cs	1.32	1.42	1.86	0.69	1.22	1.34
Ba	880	815	1,096	646	835	947
Sr	1,468	1,293	1,597	968	1,440	1,588
Tl	0.06	0.12	0.11	0.08	0.09	0.06
Ga	29	27	27	24	27	25
Li	17.56	18.23	20.11	12.65	16.08	12.92
Be	6.73	5.14	4.67	3.12	5.11	4.32
Ta	8.15	9.85	10.78	6.28	9.32	8.51
Nb	162	139	155	106	163	169
Hf	12.22	10.75	8.05	9.23	11.95	8.34
Zr	643	566	458	403	605	470
Y	33	34	34	36	39	33
Th	12.66	11.74	11.92	7.75	11.92	11.04
U	3.57	3.05	3.01	2.00	3.02	2.76
La	99.42	101.61	90.11	73.84	103.97	93.34
Ce	183.98	186.19	166.80	148.38	196.24	171.67
Pr	18.93	20.03	18.44	17.13	22.13	18.26
Nd	66.55	72.85	67.94	66.45	81.03	62.35
Sm	10.99	11.37	12.26	12.10	13.93	10.22
Eu	3.32	3.33	3.59	3.64	4.26	3.07
Gd	8.72	9.44	9.47	10.03	11.01	8.28
Tb	1.27	1.30	1.36	1.43	1.55	1.18
Dy	6.43	6.73	7.20	7.70	7.77	6.24
Ho	1.19	1.26	1.32	1.43	1.42	1.17
Er	3.20	3.22	3.02	3.42	3.50	2.96
Tm	0.47	0.48	0.44	0.49	0.47	0.44
Yb	2.68	2.86	2.51	2.91	2.92	2.50
Lu	0.39	0.40	0.37	0.39	0.41	0.35

212.—Phonolite.- West wall of La Somada, 1,930 m. asl. MAGNA*.
260.—Tephr-Phonolite. West wall of La Caldera. MAGNA*.
268.—Tephr-Phonolite / mafic Fhonolite. Peak Piedra Llana, wall of La Caldera, 2,300 m. asl. MAGNA*.
269.—Tr-Basalt/ mafic Trachyte. Pico de Las Nieves, 2,232 m. asl. MAGNA*.
270.—Tephr-Phon. Northern of Roque Palmero, wall of La Caldera, 2,200 m. asl. MAGNA*.
272.—Tephr-Phon. Peak of La Sabina, top eastern part of La Caldera. MAGNA*.

(*) Carracedo et al. (2001) Mapa Geológico de España (MAGNA): Norte de La Palma, Hojas 1083-I a 1083-IV, ITGE, Madrid.

Table 2-6.—**Analitycal data from samples of the Bejenado volcano**

	Main stratovolcano	Adventive vents		Terminal differenciated vents			
Ref. Sample	73	45	273	72	81	82	221
Geol. Unit**	17	19	19	21	21	21	dyke
wt %							
SiO_2	44.40	49.87	43.91	47.79	45.39	48.60	54.67
TiO_2	3.20	2.63	3.70	2.75	3.26	2.38	1.33
Al_2O_3	13.39	15.59	13.92	17.36	15.21	18.66	21.68
Fe_2O_3	3.35	4.95	5.69	5.33	6.56	4.56	2.73
FeO	8.54	6.00	7.62	4.27	5.03	3.92	2.71
MnO	0.19	0.22	0.22	0.22	0.26	0.20	0.14
MgO	10.23	3.96	5.03	2.99	3.75	3.24	1.04
CaO	9.94	10.08	11.82	6.67	8.95	6.43	4.00
Na_2O	3.66	4.18	3.10	7.29	6.40	6.17	7.25
K_2O	1.66	1.01	1.55	3.53	2.89	3.28	4.15
P_2O_5	0.62	1.16	0.98	0.84	1.26	0.72	0.30
H_2O+CO_2	0.50	0.25	1.56	0.61	0.99	1.6	0.77
Mg #	64.16	43.38	44.4	40.01	40.96	44.96	28.93
Ppm							
Cr	349	8	96	12	16	36	4
Ni	234	12	81	0	0	23	0
Co	50	30	49	18	22	20	5
Sc	21	15	22	7	8	7	1
V	295	249	366	201	223	216	58
Cu	105	55	69	32	32	35	8
Pb	2	8	4	9	8	9	9
Zn	123	134	136	134	155	104	85
Sn	3.62	2.27	3.18	3.71	4.81	2.29	3.10
Mo	1.94	11.04	2.35	2.95	4.42	3.61	10.46
Rb	32	29	23	101	83	97	111
Cs	0.42	1.26	0.61	0.77	0.94	1.44	1.03
Ba	452	745	520	923	882	864	878
Sr	787	1,280	1,006	1,591	1,538	1,428	1,042
Tl	0.02	0.07	0.05	0.08	0.12	0.13	0.14
Ga	21	27	22	31	30	27	28
Li	5.84	17.10	7.70	11.53	13.19	17.06	14.31
Be	1.92	4.37	2.51	5.82	6.07	4.69	4.77
Ta	4.80	7.98	5.16	10.48	11.60	9.85	8.66
Nb	86	117	96	196	189	170	156
Hf	5.87	10.62	6.83	14.85	16.14	10.56	9.25
Zr	252	500	318	795	773	581	523
Y	23	41	33	38	42	30	22
Th	3.57	9.18	5.54	10.15	8.74	11.68	10.82
U	0.88	2.16	1.14	2.52	1.18	3.39	2.50
La	39.03	93.65	64.07	94.69	98.18	83.96	67.93
Ce	81.72	183.36	128.33	183.99	198.63	156.58	120.93
Pr	9.84	21.38	15.33	20.68	23.55	17.26	12.26
Nd	40.07	81.57	61.14	78.68	91.54	62.74	41.41
Sm	8.60	14.64	12.12	14.38	17.09	10.90	7.04
Eu	2.64	4.28	3.44	4.19	5.06	3.45	2.19
Gd	7.71	11.66	10.22	11.82	14.32	8.90	5.82
Tb	0.96	1.67	1.37	1.56	1.93	1.26	0.87
Dy	5.10	8.33	6.75	7.79	9.06	6.14	4.59
Ho	0.89	1.61	1.18	1.37	1.58	1.16	0.81
Er	2.03	3.83	2.92	3.21	3.41	2.81	2.06
Tm	0.27	0.54	0.40	0.44	0.47	0.38	0.31
Yb	1.45	3.07	2.09	2.23	2.43	2.19	1.78
Lu	0.21	0.42	0.30	0.32	0.36	0.30	0.27

73.—Basanite. Lava from Bejenado, 1,070 m. asl. MAGNA*.
45.—Tr-Basalt. Lavas from Bejenado adventive vents interbedded in sediment of El Time, 85 m. asl. MAGNA**.
273.—Basanite. Lavas from Bejenado adventive vents. MAGNA**.
72.—Tephr-Phonolite. Lava from Bejenado, 1,810 m. asl. MAGNA**.
81.—Tephite. Lava from Mña. La Yedra, an adventive vent of Bejenado. MAGNA**.
82.—Tephr-Phonolite. Lava from top of Bejenado 1,580 m. asl. MAGNA**.
221.—Phonolite.-Dyke in the top of Bejenado. MAGNA**.

(*) Carracedo et al. (2001) Mapa Geológico de España (MAGNA): Norte de La Palma, Hojas 1083-I a 1083-IV, ITGE, Madrid.
(**) Carracedo et al. (2001) Mapa Geológico de España (MAGNA): Sur de La Palma, Hojas 1085 I-IV a 1087 I-II, ITGE, Madrid.

Table 2-7.—**Analytical data from samples of the Cumbre Vieja volcano, Cliff-forming eruptions (Domes and lava domes)**

Ref. Sample	7	8	26	41	62	168	276	278
Geol. Unit**	24	24	24	24	24	24	24	24
wt %								
SiO_2	57.00	55.10	55.10	54.65	49.24	55.04	55.47	58.15
TiO_2	1.23	1.32	1.64	1.59	2.42	1.41	1.03	0.22
Al_2O_3	18.86	20.78	19.60	18.48	18.20	20.54	21.52	22.87
Fe_2O_3	1.36	3.21	1.72	4.13	3.57	3.49	3.24	1.70
FeO	1.99	1.77	3.30	2.19	4.67	1.97	1.27	0.77
MnO	0.14	0.17	0.18	0.19	0.21	0.17	0.16	0.14
MgO	1.50	1.07	1.68	2.01	2.90	1.33	0.86	0.41
CaO	3.96	3.91	5.35	6.21	6.83	3.87	2.90	1.10
Na_2O	8.68	7.97	7.30	6.54	6.72	7.61	8.48	8.77
K_2O	4.21	4.40	3.25	2.51	3.62	4.20	4.84	5.64
P_2O_5	0.28	0.30	0.38	0.58	0.81	0.37	0.23	0.54
H_2O+CO_2	0.29	0.54	0.26	0.34	0.03	0.59	0.84	0.87
Mg #	48.6	31.7	41.2	40.8	42.7	34.5	29.4	8.1
Ppm								
Cr	21	9	12	11	16	8	18	10
Ni	0	2	7	3	13	0	8	1
Co	9	6	9	11	17	8	6	1
Sc	4	2	3	4	7	4	3	2
V	102	73	110	131	176	82	75	23
Cu	19	9	11	10	25	14	12	3
Pb	27	15	18	12	16	22	23	18
Zn	87	106	101	105	113	99	95	70
Sn	3.03	1.17	3.06	1.53	3.03	2.26	2.88	2.36
Mo	9.81	8.57	9.24	7.63	6.93	12.63	13.15	11.79
Rb	149	128	103	85	97	127	113	233
Cs	1.38	1.46	1.60	1.10	1.42	1.91	2.05	2.77
Ba	1,185	1,273	1,071	1,063	982	1,225	1,451	89
Sr	1,487	1,104	1,567	1,708	1,532	1,749	1,716	59
Tl	0.22	0.13	0.10	0.04	0.07	0.16	0.94	0.34
Ga	33	29	28	26	28	31	37	41
Li	17.93	20.74	18.41	15.45	17.32	19.60	20.59	17.10
Be	8.49	6.32	5.53	5.09	5.14	6.89	10.59	16.40
Ta	6.42	5.10	9.21	6.51	9.24	8.84	6.41	3.24
Nb	195	138	191	143	187	219	235	178
Hf	14.79	12.74	9.82	10.19	10.64	14.90	17.32	23.37
Zr	807	683	543	516	569	837	1,006	1,247
Y	26	24	35	34	37	33	25	14
Th	37.62	22.10	24.17	21.47	22.54	32.70	40.32	33.80
U	9.98	6.47	6.49	6.06	6.02	9.11	17.79	13.62
La	142.60	122.92	128.96	138.36	124.79	163.11	152.57	128.01
Ce	208.69	182.74	211.54	228.49	215.81	242.61	210.98	132.00
Pr	18.61	16.45	21.39	23.12	22.78	22.13	18.71	8.84
Nd	56.43	49.83	70.49	77.15	77.88	67.87	55.30	20.53
Sm	8.35	7.31	11.23	11.81	12.82	9.81	7.67	2.21
Eu	2.41	2.23	3.47	3.49	3.87	2.83	2.11	0.53
Gd	7.09	5.71	8.99	9.48	10.63	8.13	6.09	1.92
Tb	0.95	0.82	1.25	1.26	1.43	1.12	0.83	0.31
Dy	4.94	4.24	6.55	6.38	7.02	5.81	4.04	1.83
Ho	0.90	0.88	1.24	1.21	1.32	1.06	0.81	0.39
Er	2.33	2.41	3.07	3.16	3.24	2.89	2.20	1.35
Tm	0.40	0.36	0.45	0.46	0.46	0.45	0.38	0.26
Yb	2.29	2.48	2.83	2.88	2.75	2.58	2.30	1.87
Lu	0.36	0.38	0.39	0.41	0.39	0.43	0.35	0.34

7.—Phonolite. Dome of Doña María MAGNA**.
8.—Tephr-Phonolite. Lava dome of Roque de Fuente Pino de La Virgen. MAGNA**.
26.—Tr-Phonolite. Lava dome of Don Mendo. MAGNA**.
41.—Phonolite. Lava from dome of los Campanarios. MAGNA**.
62.—Tephri-Phonolite from Cabrito. MAGNA**.
168.—Phonolite. Roque Niquiomo. MAGNA**.
276.—Phonolite. Roque Teneguia. MAGNA**.
278.—Phonolite. Montaña Enrique. MAGNA**.

(*) Carracedo et al. (2001) Mapa Geológico de España (MAGNA): Norte de La Palma, Hojas 1083-I a 1083-IV, ITGE, Madrid.
(**) Carracedo et al. (2001) Mapa Geológico de España (MAGNA): Sur de La Palma, Hojas 1085 I-IV a 1087 I-II, ITGE, Madrid.

Table 2-8.—**Analytical data from samples of the Cumbre Vieja volcano, Cliff-forming eruptions (Basaltic lavas)**

Ref. Sample Geol. Unit** wt %	4 25	9 25	13 25	14 25	15 25	19 25	118 25
SiO_2	44.92	43.11	46.00	49.62	46.00	49.60	43.37
TiO_2	2.46	3.19	3.29	2.76	3.23	2.55	3.47
Al_2O_3	12.19	12.37	15.09	17.81	14.73	16.43	14.42
Fe_2O_3	3.73	5.49	4.24	3.65	5.59	4.30	8.33
FeO	9.27	8.40	7.31	5.83	7.00	5.26	4.50
MnO	0.19	0.18	0.20	0.17	0.18	0.19	0.19
MgO	12.53	11.78	5.98	3.89	7.67	3.87	7.46
CaO	9.19	10.16	9.77	7.13	8.89	7.12	10.97
Na_2O	3.06	3.00	4.80	5.95	4.37	6.59	4.88
K_2O	0.92	0.84	1.86	1.81	1.51	2.43	1.76
P_2O_5	0.78	0.79	1.08	1.07	0.81	0.77	1.28
H_2O+CO_2	0.10	0.09	0.08	0.06	0.08	0.06	0.15
Mg #	66.74	64.11	52.09	46.33	56.32	46.16	55.71
Ppm							
Cr	508	468	59	14	159	15	159
Ni	361	258	43	0	96	19	90
Co	59	57	36	20	42	25	41
Sc	24	26	18	10	23	11	20
V	281	304	287	174	319	241	298
Cu	104	84	58	18	85	46	61
Pb	3	2	4	6	5	13	4
Zn	120	115	122	125	123	127	124
Sn	2.82	1.88	3.94	4.17	3.05	2.77	2.64
Mo	3.44	2.89	4.31	7.27	4.47	11.61	4.13
Rb	19	20	44	52	48	95	34
Cs	0.23	0.20	0.52	0.53	0.60	1.08	0.34
Ba	350	361	638	828	641	999	556
Sr	832	896	1,265	1,241	1,155	1,443	1,296
Tl	0.02	0.03	0.04	0.05	0.05	0.09	0.03
Ga	19	20	23	26	23	29	23
Li	5.26	6.31	8.06	9.09	8.67	14.13	6.97
Be	1.51	2.00	2.80	3.15	2.59	4.42	2.54
Ta	3.41	3.44	6.42	7.58	4.98	8.37	5.26
Nb	59	60	108	139	94	183	97
Hf	4.90	5.14	7.96	9.14	6.58	10.92	6.93
Zr	207	216	358	432	315	544	340
Y	27	28	39	40	32	34	37
Th	4.14	4.48	8.13	12.24	7.84	21.18	7.76
U	1.07	1.24	2.11	3.74	2.07	8.32	2.11
La	54.62	57.16	92.65	114.44	75.53	146.08	92.69
Ce	111.99	117.03	183.09	206.54	143.64	231.82	180.89
Pr	13.23	13.90	21.09	22.01	16.25	23.26	20.78
Nd	53.25	55.46	80.18	80.44	62.66	77.83	78.92
Sm	10.46	10.65	14.85	14.54	11.05	12.68	14.97
Eu	3.07	3.25	4.31	4.20	3.36	3.78	4.22
Gd	8.97	9.02	12.49	12.46	9.48	9.97	12.23
Tb	1.20	1.22	1.64	1.68	1.29	1.37	1.58
Dy	6.07	6.13	8.23	8.48	6.11	6.70	7.72
Ho	1.05	1.10	1.48	1.51	1.15	1.19	1.35
Er	2.33	2.47	3.52	3.68	2.69	3.11	3.02
Tm	0.33	0.32	0.50	0.51	0.35	0.44	0.42
Yb	1.66	1.81	2.74	2.77	2.16	2.59	2.21
Lu	0.25	0.25	0.38	0.44	0.30	0.37	0.32

4.—Basanite.-Early lava of Cumbre Vieja volcano. MAGNA**.
9.—Basanite.-Lava of Cumbre Vieja, Bco. de Torres. MAGNA**.
13.—Tephrite. Lava from Montaña Cosme (Los Chumasquinos). MAGNA**.
14.—Tephr-Phonolite/Tr-Basalt. Lava from the cliff of El Puertito de Tigalate. Pahoe-hoe lavas of Monte de Luna. MAGNA**.
15.—Tephrite/Tr-Basalt. Lava from the cliff of Puerto Tigalate, 80 m. asl. Playa del Rio. MAGNA**.
19.—Tephr-Phonolite. Lava from Llanos de Tazacorte, cliff of Tazacorte. MAGNA**.
118.—Bsn/Tephr. Cliff Teneguia. MAGNA**.

(*) Carracedo et al. (2001) Mapa Geológico de España (MAGNA): Norte de La Palma, Hojas 1083-I a 1083-IV, ITGE, Madrid.
(**) Carracedo et al. (2001) Mapa Geológico de España (MAGNA): Sur de La Palma, Hojas 1085 I-IV a 1087 I-II, ITGE, Madrid.

Table 2-9.—**Analytical data from samples of the Cumbre Vieja volcano, Platform-forming eruptions**

	Mña. Dioquen	Mña. Cabrera-Faro	Mña. Goteras	Other basaltic lavas of platform-forming eruptions				
Ref. Sample	2	112	264	36	66	84	113	143
Geol. Unit*	28	28	28	28	28	28	28	28
wt %								
SiO_2	45.10	49.64	43.68	44.81	43.90	43.00	41.68	41.99
TiO_2	3.09	2.34	3.53	3.27	3.61	3.39	3.46	3.58
Al_2O_3	15.97	18.13	16.08	13.94	14.77	12.71	14.94	10.97
Fe_2O_3	4.55	3.90	4.38	5.58	6.89	3.82	2.65	3.84
FeO	7.19	5.37	7.06	6.52	5.45	8.44	9.96	9.24
MnO	0.21	0.21	0.22	0.19	0.21	0.20	0.20	0.18
MgO	5.81	2.95	6.56	7.36	7.07	11.10	9.35	12.29
CaO	9.39	6.81	11.24	11.24	10.00	11.07	11.05	12.73
Na_2O	5.39	6.45	4.36	3.36	3.95	3.38	4.64	3.06
K_2O	2.18	2.78	1.98	1.93	2.15	1.67	1.96	1.48
P_2O_5	0.97	0.85	0.91	0.84	1.02	0.80	0.94	0.89
H_2O+CO_2	0.08	0.06	0.08	0.07	0.06	0.09	0.11	0.10
Mg #	51.0	40.2	54.7	56.3	55.1	65.4	61.9	66.2
Ppm								
Cr	95	19	149	253	140	472	222	460
Ni	44	10	85	101	82	271	130	306
Co	32	20	40	44	39	54	46	58
Sc	15	9	22	25	22	27	27	28
V	254	191	301	320	310	317	345	331
Cu	46	28	72	88	65	162	91	92
Pb	6	11	4	5	6	4	8	4
Zn	122	135	124	114	126	109	267	124
Sn	4.18	2.83	2.93	1.95	4.54	3.53	2.52	2.82
Mo	8.03	6.94	5.11	4.19	5.48	3.68	3.20	4.12
Rb	61	89	49	41	55	38	43	29
Cs	0.82	1.70	0.59	0.53	0.64	0.46	0.51	0.34
Ba	777	977	651	573	708	534	583	477
Sr	1,504	1,776	1,215	1,109	1,295	1,009	1,090	1,007
Tl	0.05	0.06	0.02	0.04	0.05	0.03	0.05	0.03
Ga	25	28	23	22	24	20	23	21
Li	9.22	15.66	8.48	8.36	7.39	6.64	7.41	5.82
Be	3.40	6.08	3.11	2.76	2.63	2.48	2.61	2.28
Ta	7.31	7.30	5.84	4.83	6.35	4.55	5.10	4.57
Nb	132	154	109	86	121	84	98	83
Hf	8.90	10.41	7.21	7.70	8.30	6.47	6.83	6.31
Zr	440	548	346	337	389	294	332	284
Y	39	39	36	32	37	30	33	30
Th	11.46	16.42	9.09	8.11	10.57	7.73	7.74	6.75
U	3.46	5.32	2.33	2.13	3.05	1.96	2.16	1.96
La	108.66	127.48	90.43	77.87	112.73	76.83	81.55	74.05
Ce	206.66	221.23	169.08	151.78	208.09	147.83	156.61	144.33
Pr	22.76	23.64	18.91	17.93	22.73	16.71	17.58	16.36
Nd	84.19	83.15	70.87	69.91	84.72	62.75	66.93	63.77
Sm	14.57	14.34	13.11	12.60	15.11	11.75	12.39	12.26
Eu	4.26	3.94	3.79	3.69	4.23	3.44	3.54	3.46
Gd	12.33	11.19	11.32	10.27	12.54	9.96	10.48	10.29
Tb	1.63	1.54	1.48	1.38	1.60	1.31	1.34	1.34
Dy	8.20	7.47	6.96	6.63	7.88	6.54	6.57	6.48
Ho	1.48	1.33	1.26	1.21	1.40	1.16	1.18	1.13
Er	3.49	3.41	3.04	2.83	3.15	2.54	2.70	2.50
Tm	0.50	0.51	0.42	0.40	0.43	0.34	0.37	0.34
Yb	2.71	2.88	2.36	2.30	2.36	1.96	2.03	1.83
Lu	0.40	0.44	0.37	0.31	0.36	0.29	0.31	0.28

2.—Tephrite. Mña. Dioquen. Punta del Banco. MAGNA*.
112.—Tephrite-Phonolite, Tephritic lava from Mña. Cabrera. MAGNA*.
264.—Basanite. Mña. Goteras. MAGNA*.
36.—Bsn/Tephr. Lava from Laderas del Gallo. MAGNA*.
66.—Bsn/Tephr. Lava from Los Valentines. MAGNA*.
84.—Basanite. Platform-forming lava from Cumbre Vieja. MAGNA*.
113.—Basanite. Basaltic lava from Mña. Pelada. MAGNA*.
143.—Basanite. Platform-forming lava from Cumbre Vieja. MAGNA*.

(*) Carracedo et al. (2001) Mapa Geológico de España (MAGNA): Sur de La Palma, Hojas 1085 I-IV a 1087 I-II, ITGE, Madrid.

Table 2-10.—**Analytical data from samples of the Cumbre Vieja volcano, dated prehistoric eruptions**

	Birigoyo-La Barquilla		S.Antonio	Volcán Fuego-Volcán de La Fajana				Malforada y Nambroque		Mña. Quemada y Volcán Martín		
Ref. Sample	37	279	277	6	16	17	18	61	71	20	63	274
Geol. Unit*	31	31	33	33	33	33	33	30	30	33	33	33
wt %												
SiO_2	48.26	48.15	42.52	44.20	46.42	45.98	48.03	49.80	52.30	44.50	42.69	45.38
TiO_2	2.70	2.97	3.82	3.40	2.79	2.91	2.71	2.28	1.86	3.04	3.57	3.72
Al_2O_3	15.79	17.54	14.65	15.54	17.26	17.12	17.29	18.28	19.27	14.32	13.40	13.82
Fe_2O_3	6.05	5.46	5.03	4.69	4.35	2.72	3.31	4.02	3.73	4.77	4.15	6.17
FeO	4.57	4.28	7.22	7.51	6.66	7.23	6.24	4.37	3.30	6.92	8.31	6.08
MnO	0.21	0.22	0.23	0.20	0.19	0.18	0.19	0.23	0.20	0.19	0.21	0.21
MgO	4.71	3.09	7.95	6.36	4.82	5.17	4.21	2.50	1.91	6.88	8.48	6.67
CaO	9.77	8.16	11.40	10.63	8.69	9.53	7.78	6.78	5.99	11.87	12.87	11.25
Na_2O	4.59	6.09	3.94	4.64	5.58	5.40	6.01	6.74	7.03	3.86	3.44	3.51
K_2O	2.36	2.47	1.71	1.31	2.00	2.07	2.56	3.83	3.80	1.73	1.30	1.53
P_2O_5	1.20	1.57	1.53	1.38	0.84	0.90	0.75	0.72	0.55	0.88	0.91	0.98
H_2O+CO_2	0.10	0.05	0.08	0.08	0.07	0.08	0.07	0.05	0.04	0.15	0.09	0.07
Mg #	48.8	40.5	57.8	52.3	48.0	51.9	48.0	38.8	36.7	55.4	58.7	53.7
Ppm												
Cr	23	13	185	59	48	62	19	15	0	164	271	210
Ni	19	8	86	41	35	42	22	10	13	81	124	102
Co	30	22	47	37	29	31	25	18	13	41	46	50
Sc	15	9	28	18	16	18	14	12	10	20	27	28
V	258	209	363	322	245	268	239	172	145	298	325	376
Cu	45	26	83	56	49	65	46	38	32	66	102	105
Pb	6	9	5	4	7	6	8	13	13	23	3	6
Zn	134	146	130	124	123	125	118	119	113	135	116	149
Sn	2.67	3.45	3.04	3.29	2.43	1.93	2.82	2.09	2.15	3.23	3.15	4.08
Mo	4.10	6.33	4.52	3.80	4.43	4.07	6.41	44.48	30.92	3.64	5.09	6.88
Rb	59	77	40	42	66	65	74	98	109	46	35	42
Cs	0.76	1.29	0.46	0.49	0.75	0.73	0.95	1.55	1.78	0.50	0.41	0.83
Ba	748	884	573	714	805	824	882	1,083	1,158	627	552	643
Sr	1,440	1,629	1,098	1,465	1,338	1,353	1,514	1,719	1,701	1,177	1,146	1,353
Tl	0.05	0.06	0.03	0.03	0.12	0.07	0.09	0.11	0.14	0.03	0.03	0.02
Ga	26	29	24	22	26	26	25	28	28	23	22	25
Li	11.15	14.40	8.99	8.20	12.01	10.76	12.66	20.89	22.91	9.61	6.70	9.66
Be	3.53	5.91	3.66	2.89	4.08	3.86	3.91	5.16	5.97	2.95	2.47	3.64
Ta	7.03	7.37	4.83	5.24	7.19	7.34	6.74	8.49	7.06	5.77	4.91	5.94
Nb	125	153	92	100	147	148	134	147	144	103	91	112
Hf	9.42	10.68	7.22	6.71	10.06	9.92	9.30	10.66	10.52	7.74	6.53	7.81
Zr	417	530	331	299	466	455	469	559	588	369	303	359
Y	39	41	34	40	35	35	36	37	34	35	34	40
Th	10.85	12.67	7.57	10.12	11.17	11.88	14.14	19.99	21.25	7.42	8.28	10.40
U	3.61	4.44	2.05	2.10	3.43	3.46	4.27	6.11	6.47	2.42	2.19	2.82
La	99.90	118.70	76.86	108.85	113.18	122.97	115.17	143.25	141.94	79.16	85.63	108.18
Ce	186.62	211.29	150.37	208.41	199.17	214.72	202.86	241.31	228.73	158.01	163.23	201.45
Pr	21.51	23.06	17.37	24.15	21.29	23.09	21.97	24.92	22.65	18.43	18.33	22.83
Nd	82.25	85.65	67.93	91.42	77.04	81.65	77.93	84.98	75.86	72.52	70.60	87.00
Sm	14.73	15.28	12.77	15.51	13.08	13.66	13.23	13.48	11.82	13.03	13.10	16.10
Eu	4.42	4.32	3.68	4.59	3.96	4.01	3.93	3.81	3.25	3.91	3.74	4.43
Gd	12.12	12.08	10.93	12.97	10.45	11.04	10.61	10.99	9.37	10.96	10.85	12.62
Tb	1.64	1.65	1.43	1.66	1.43	1.51	1.44	1.52	1.27	1.44	1.49	1.67
Dy	8.18	7.61	6.69	8.09	7.13	7.65	6.85	7.33	6.69	7.12	7.11	8.17
Ho	1.48	1.40	1.27	1.48	1.30	1.33	1.29	1.31	1.26	1.28	1.25	1.40
Er	3.64	3.61	2.95	3.43	3.16	3.26	3.21	3.31	3.18	3.19	2.88	3.31
Tm	0.49	0.51	0.41	0.44	0.44	0.44	0.43	0.49	0.48	0.41	0.38	0.45
Yb	2.94	2.97	2.27	2.55	2.68	2.63	2.78	3.12	2.91	2.40	2.08	2.63
Lu	0.40	0.43	0.33	0.34	0.36	0.38	0.38	0.46	0.43	0.34	0.30	0.35

37.—Tephrite. Terminal lava flow of Birigoyo. MAGNA*.
279.—Tephrite-Phonolite. Lava flow of Birigoyo. MAGNA*.
277.—Basanite. San Antonio. MAGNA*.
6.—Bsn/Tephrite. East lava flow of Volcán Fuego. MAGNA*.
16.—Tephrite. West lava flow of Volcán Fuego (Coladas al Oeste). MAGNA*.
17.—Tephrite. Lavas Volcanes de la Fajana. MAGNA*.
18.—Tephr-Phonolite. East lava flow of Volcán Fuego. MAGNA*.
61.—Tephr-Phonolite. Lava flow of La Malforada. MAGNA*.
71.—Phonolite. Northern lava flow of Nambroque. MAGNA*.
20.—Basanite. Mña. Quemada (prehistoric). MAGNA*.
63.—Basanite (ol-cpx). Pre historic lava flow of Martín volcano. MAGNA*.
274.—Bsn/Basalt (cpx-anf). Pre historic lava flow of Martín volcano. MAGNA*.

(*) Carracedo et al. (2001) Mapa Geológico de España (MAGNA): Sur de La Palma, Hojas 1085 I-IV a 1087 I-II, ITGE, Madrid.

Table 2-11.—**Analytical data from samples of the Cumbre Vieja volcano, historical eruptions**

	XVI Century			XVII Century			XVIII Century	XX Century		
	Coladas de Jedey		Fon de Jedey	Tigalate (1646)		1677	El Charco	San Juan	Duraznero	Teneguia
Ref. Sample	28	33	280	132	275	121	24	110	60	119
Geol. Unit*	35	35	36	38	38	38	41	44	44	44
wt %										
SiO_2	45.04	44.86	54.56	42.37	42.96	42.15	44.50	44.00	44.50	44.50
TiO_2	3.75	3.59	0.95	3.56	3.63	3.43	3.78	3.50	3.55	3.55
Al_2O_3	14.12	13.93	21.62	12.38	13.02	13.11	14.64	14.62	14.22	13.95
Fe_2O_3	4.27	4.00	3.04	4.66	4.26	4.35	4.05	2.82	4.15	4.24
FeO	6.19	8.24	1.65	8.36	7.95	7.59	8.06	9.39	7.52	8.43
MnO	0.19	0.18	0.15	0.18	0.19	0.19	0.19	0.19	0.17	0.19
MgO	7.58	7.44	0.71	10.74	8.17	11.40	6.48	8.60	8.22	8.94
CaO	10.95	10.71	4.32	11.19	13.17	10.14	10.04	10.46	10.95	9.78
Na_2O	3.48	3.48	8.21	4.74	4.02	4.87	3.77	3.56	3.06	4.51
K_2O	1.99	1.75	4.02	1.58	1.73	1.64	1.93	1.29	1.82	1.67
P_2O_5	0.84	0.81	0.77	0.90	0.90	0.99	1.09	0.68	0.71	0.90
H_2O+CO_2	0.69	0.09	0.36	0.09	0.09	0.70	0.80	0.10	0.80	0.09
Mg #	60.4	56.0	24.7	63.4	58.4	66.7	52.8	59.3	59.6	59.6
Ppm										
Cr	206	230	11	296	274	272	147	296	289	181
Ni	93	95	4	130	116	121	78	129	112	102
Co	42	42	7	53	44	49	47	49	52	46
Sc	22	23	3	33	26	27	25	25	29	24
V	297	301	86	394	326	348	370	302	311	315
Cu	75	81	10	122	97	90	93	87	102	86
Pb	4	4	14	7	3	6	6	3	4	5
Zn	122	122	107	215	119	143	156	117	118	175
Sn	3.42	1.98	2.30	6.31	4.03	4.08	6.76	1.62	2.10	2.93
Mo	4.39	3.43	9.41	5.94	4.34	5.45	6.76	3.26	11.85	4.43
Rb	43	41	123	44	36	38	54	29	28	31
Cs	0.50	0.50	1.91	0.50	0.43	1.14	0.67	0.40	0.74	0.37
Ba	586	575	1,140	674	569	571	817	411	435	482
Sr	1,180	1,146	1,585	1,415	1,154	1,200	1,653	907	955	1,079
Tl	0.02	0.05	0.16	0.06	0.04	0.04	0.05	0.04	0.04	0.04
Ga	22	22	30	26	22	24	28	22	23	23
Li	8.50	8.83	21.07	8.63	6.48	9.34	9.49	7.70	11.39	6.88
Be	2.74	2.53	7.42	3.16	2.45	3.48	3.80	2.21	2.89	2.20
Ta	5.65	5.59	5.15	6.31	5.18	5.15	7.41	3.98	3.41	4.52
Nb	103	99	142	110	92	95	133	70	63	83
Hf	7.54	7.69	11.31	8.28	6.93	7.10	9.36	6.06	6.48	6.48
Zr	339	331	657	363	302	328	421	270	277	308
Y	35	34	26	41	34	36	45	29	31	33
Th	7.48	7.52	19.59	10.34	8.61	7.85	12.03	5.59	6.05	6.24
U	2.04	2.04	6.30	2.63	2.30	2.31	3.39	1.58	1.60	1.77
La	82.62	79.66	119.62	105.17	87.14	88.27	124.85	58.15	64.26	73.87
Ce	158.73	154.77	184.46	200.43	166.81	168.46	233.91	116.53	126.25	147.10
Pr	18.46	17.87	16.81	22.48	18.99	19.40	26.02	13.66	15.01	16.64
Nd	70.09	68.36	53.28	85.93	72.08	74.73	98.47	53.43	59.41	65.35
Sm	12.83	12.60	7.94	15.70	13.06	13.42	17.79	10.24	11.21	12.32
Eu	3.75	3.74	2.30	4.67	3.93	3.99	5.27	3.16	3.26	3.65
Gd	10.60	10.65	6.31	13.62	11.41	11.71	15.17	8.98	9.27	10.51
Tb	1.47	1.42	0.88	1.78	1.49	1.55	1.97	1.20	1.38	1.38
Dy	7.00	7.10	4.38	8.83	7.30	7.35	9.70	6.24	6.60	6.78
Ho	1.29	1.24	0.86	1.55	1.30	1.26	1.72	1.07	1.26	1.17
Er	3.02	3.11	2.36	3.46	2.87	3.01	3.96	2.63	2.85	2.76
Tm	0.41	0.42	0.37	0.50	0.41	0.42	0.55	0.37	0.39	0.37
Yb	2.36	2.39	2.29	2.74	2.23	2.32	2.90	1.92	2.37	1.95
Lu	0.32	0.32	0.36	0.39	0.31	0.34	0.42	0.30	0.32	0.29

28.—Basanite.(cpx-anf). Lava from upper vent of 1585. MAGNA*.
33.—Basanite (cpx-ol). Lava from lower vent of 1585. MAGNA*.
280.—Phonolite. Juvenile phonolite flow of 1585. MAGNA*.
132.—Basanite (cpx-ol). Basaltic flow of 1646. MAGNA*.
275.—Basanite (cpx-ol). Basaltic flow of 1646. MAGNA*.
121.—Basanite (cpx-ol). Basaltic flow of 1677. MAGNA*.
24.—Basanite (cpx-ol-anf). Lava from second upper vent of 1712. MAGNA*.
110.—Basanite (cpx-ol). Basaltic flow of 1949 (Llano del Banco). MAGNA*.
60.—Basanite (cpx-ol). Basaltic flow of 1949 (Duraznero). MAGNA*.
119.—Basanite. Basaltic flow of Volcán Teneguia, 1971. MAGNA*.

(*) Carracedo et al. (2001) Mapa Geológico de España (MAGNA): Sur de La Palma, Hojas 1085 I-IV a 1087 I-II, ITGE, Madrid.

APPEND 2

GEOLOGICAL MAP

La Palma
El Hierro

GEOLOGICAL CROSS-SECTIONS OF LA PALMA

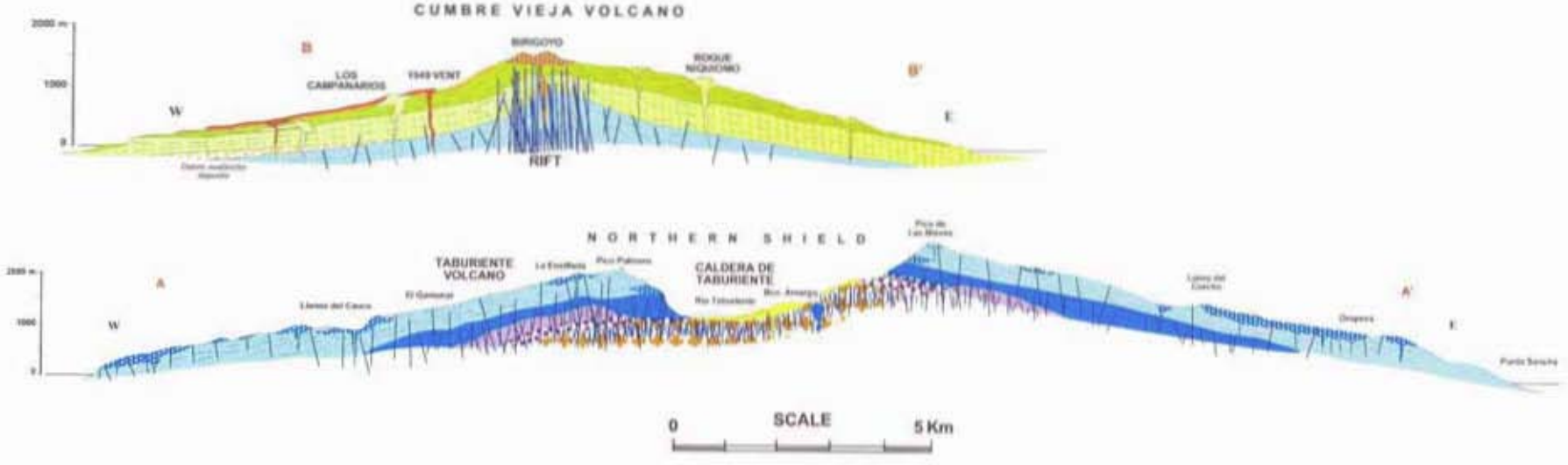

GEOLOGICAL MAP OF LA PALMA (CANARY ISLANDS)

J.C. Carracedo[1*], H. Guillou[2], E.R. Badiola[3], J. de La Nuez[4] and F.J. Pérez Torrado[5]

[1]Estación Volcanológica de Canarias, IPNA-CSIC, Tenerife, Spain *carracedo@ipna.csic.es [2]Laboratoire des Sciences du Climat et de l'Environnement, CEA-CNRS, Gif-sur-Yvette, France [3]Museo Nacional de Ciencias Naturales, CSIC, Madrid, Spain
[4]Universidad de La Laguna, Tenerife, Spain [5]Universidad de Las Palmas de Gran Canaria, Spain (with data from A. Hernández Pacheco for the submarine banks of the Caldera de Taburiente and S. Day of the 1585 and 1949 eruptions)

VOLCANIC FORMATIONS

GEOMAGNETIC POLARITY TIME-SCALE

QUATERNARY

HOLOCENE

PLEISTOCENE

PLIOCENE

NEOGENE

BRUNHES

MATUYAMA

JARAMILLO

OLDUVAI

CUMBRE VIEJA VOLCANO

PLATFORM-FORMING ERUPTIONS

HISTORIC ERUPTIONS

Historic Volcanism

PRE HISTORIC ERUPTIONS

OTHER PLATFORM-FORMING ERUPTIONS

CLIFF-FORMING ERUPTIONS

BEJENADO VOLCANO

SUBAERIAL DIFFERENTIATED VENTS

LATERAL AND PERIPHERAL VENTS

MAIN STRATOVOLCANO

Taburiente discordance (lateral collapse)

TABURIENTE VOLCANO

UPPER TABURIENTE

LOWER TABURIENTE

Taburiente discordance (lateral collapse)

GARAFIA VOLCANO

ANGULAR AND ANGULAR DISCORDANCE (ERODIVE GAP, UPLIFT AND TILT)

SEAMOUNT

SCALE

0 5 Km

CONTOUR INTERVAL 50 m (Topography ICMC)

UTM WGS 84, REGCAN 95

SEDIMENTARY FORMATIONS

HOLOCENE SEDIMENTS

PLEISTOCENE SEDIMENTS

SYMBOLS

A digital version of this map map can be downloaded from http://www.ipna.csic.es or obtained from jcarracedo@ipna.csic.es

(Partially financed by the Instituto Geológico y Minero de España, IGME)

With data of S. Day, A. Hernández Pacheco and J. Vegas

EL HIERRO, CANARY ISLANDS

J.C. Carracedo[1*], H. Guillou[2], E.R. Badiola[3], F.J. Pérez Torrado[4] and S. Day[5]

[1]Estación Volcanológica de Canarias, CSIC, La Laguna, Tenerife, Spain

[2]Laboratoire des Sciences du Climat et d l'Environnement, CEA-CNRS, Giff- sur-Yvette, France

[3]Museo Nacional de Ciencias Naturales, Madrid, Spain

[4]Departamento de Física, Universidad de Las Palmas de Gran Canaria, Spain

[5] University College London, UK

Scale

0 5 km

Contour interval 25 m
(Topography GRAFCAN)
UTM WGS 84, REGCAN 95
See geological cross-sections in Fig. 60

SEDIMENTARY FORMATIONS

- Alluvial fill
- Recent piedmont (4th generation)
- 3rd generation
- 2nd generation
- 1st generation

Pre-platform-forming eruptions

VOLCANIC FORMATIONS

RIFT VOLCANISM

Post-date maximum glacial: Pyroclasts, Lavas — Platform-forming eruptions

Pre-date maximum glacial: Pyroclasts, Phreatomag., Lavas — Cliff-forming eruptions

EL GOLFO VOLCANO

- Differentiated lavas (trachybasalts, trachytes)
- Basaltic eruptions

TIÑOR VOLCANO

- Ventejís late, xenolith-rich lavas
- Pyroclasts
- Horizontal lavas
- Dipping lavas

0.78 ma

0.97 ma

Jm

1.11ma

Mt

? MATUYAMA NORMAL

SYMBOLS

- Levees
- Front of lava flows
- Direction of flows
- Dip of flows
- Crater
- Fault: outcropping / buried
- Tensional fractures
- Basaltic dykes

A digital version of this map map can be downloaded from http://www.ipna.csic.es or obtained from jcarracedo@ipna.csic.es